Forty new specimens of *Ichthyornis* provide unprecedented insight into the postcranial morphology of crownward stem group birds

Juan Benito[1,2], Albert Chen[1,2], Laura E. Wilson[3], Bhart-Anjan S. Bhullar[4,5], David Burnham[6] and Daniel J. Field[2,7]

[1] Department of Biology & Biochemistry, Milner Centre for Evolution, University of Bath, Bath, United Kingdom
[2] Department of Earth Sciences, University of Cambridge, Cambridge, Cambridgeshire, United Kingdom
[3] Fort Hays State University, Sternberg Museum of Natural History and Department of Geosciences, Hays, Kansas, United States
[4] Yale Peabody Museum of Natural History, New Haven, Conneticut, United States
[5] Department of Earth & Planetary Sciences, Yale University, New Haven, Conneticut, United States
[6] University of Kansas, Biodiversity Institute and Natural History Museum, Lawrence, Kansas, United States
[7] University Museum of Zoology, Cambridge, United Kingdom

Corresponding authors
Juan Benito, jb2284@cam.ac.uk
Daniel J. Field, djf70@cam.ac.uk

ABSTRACT

Ichthyornis has long been recognized as a pivotally important fossil taxon for understanding the latest stages of the dinosaur–bird transition, but little significant new postcranial material has been brought to light since initial descriptions of partial skeletons in the 19th Century. Here, we present new information on the postcranial morphology of *Ichthyornis* from 40 previously undescribed specimens, providing the most complete morphological assessment of the postcranial skeleton of *Ichthyornis* to date. The new material includes four partially complete skeletons and numerous well-preserved isolated elements, enabling new anatomical observations such as muscle attachments previously undescribed for Mesozoic euornitheans. Among the elements that were previously unknown or poorly represented for *Ichthyornis*, the new specimens include an almost-complete axial series, a hypocleideum-bearing furcula, radial carpal bones, fibulae, a complete tarsometatarsus bearing a rudimentary hypotarsus, and one of the first-known nearly complete three-dimensional sterna from a Mesozoic avialan. Several pedal phalanges are preserved, revealing a remarkably enlarged pes presumably related to foot-propelled swimming. Although diagnosable as *Ichthyornis*, the new specimens exhibit a substantial degree of morphological variation, some of which may relate to ontogenetic changes. Phylogenetic analyses incorporating our new data and employing alternative morphological datasets recover *Ichthyornis* stemward of Hesperornithes and *Iaceornis*, in line with some recent hypotheses regarding the topology of the crownward-most portion of the avian stem group, and we establish phylogenetically-defined clade names for relevant avialan subclades to help facilitate consistent discourse in future work. The new information provided by these specimens improves our understanding of morphological evolution among the

crownward-most non-neornithine avialans immediately preceding the origin of crown group birds.

INTRODUCTION

Ichthyornis is a key taxon in the history of avian palaeontology. First described by Marsh in 1872, early specimens of *Ichthyornis* provided some of the first known fossil evidence documenting the evolutionary origins of birds, thereby bolstering evolutionary theory in the late 19th Century (*Marsh, 1872a*). Indeed, "Darwin's Bulldog", Thomas Henry Huxley, declared—presumably in partial reference to *Ichthyornis* and *Hesperornis*—that:

"*There is nothing in any way comparable . . . for their scientific importance, to the series of fossils which Professor Marsh has brought together.*" (*Rieppel, 2019*).

And Darwin himself complimented Marsh by writing:

"*Your work on these old birds, & on the many fossil animals of N. America has afforded the best support to the theory of evolution, which has appeared within the last 20 years.*" (*Burkhardt, 2021*).

Now, almost 150 years later, *Ichthyornis* remains a key taxon for understanding the morphological transitions that gave rise to crown bird anatomy—or, as O.C. Marsh put it, "to break down the old distinction between Birds and Reptiles" (*Marsh, 1873b*), and it has been consistently recovered in a phylogenetic position close to the origin of the avian crown group (*e.g.*, *Clarke, 2004*; *Field et al., 2018b*).

Previous research on *Ichthyornis*

Fossil remains attributable to *Ichthyornis* have been commonly recovered from Late Cretaceous deposits of the Western Interior Seaway of North America, usually from the middle to late Santonian rocks of the Niobrara Formation in Kansas, USA (*Marsh, 1872a*, *1880*; *Clarke, 2004*; *Field et al., 2018b*) and from the early Campanian deposits of the Mooreville Chalk in Alabama, USA (*Wetmore, 1962*; *Olson, 1975*; *Field et al., 2018b*). Additional material has been recovered from the Cenomanian of Saskatchewan, Canada (*Tokaryk, Cumbaa & Storer, 1997*; *Sanchez, 2010*) and Kansas (*Shimada & Wilson, 2016*), the Turonian of Alberta, Canada (*Fox, 1984*), Kansas (*Shimada & Fernandes, 2006*), and New Mexico, USA (*Lucas & Sullivan, 1982*), the Campanian of Texas, USA (*Parris & Echols, 1992*) and the Coniacian–Campanian of Coahuila, Mexico (*Porras-Múzquiz, Chatterjee & Lehman, 2014*). *Ichthyornis* long remained the only named and well-known member of Ichthyornithes, until the recent description of *Janavis finalidens* from the latest Maastrichtian of Belgium (*Benito et al., 2022*), which had previously been described as a possible ichthyornithine (*Dyke et al., 2002*). Fragmentary fossil material showing similarities to *Ichthyornis* has additionally been recovered from the Cenomanian of Russia (*Zelenkov, Averianov & Popov, 2017*) and Egypt (*Mohesn et al., 2020*), and the

Maastrichtian of the US (*Longrich, Tokaryk & Field, 2011*), but the precise phylogenetic relationships of these remains have yet to be assessed in detail.

Eight different species of *Ichthyornis* have been erected in the past on the basis of specimens from the Niobrara and Mooreville Formations (*Marsh, 1872a*, *1872b*; *1873a*, *1876*, *1880*; *Wetmore, 1962*). However, despite the substantial geographic and temporal distribution of *Ichthyornis* (ranging in age from 95 to 83.5 MYA), *Clarke (2004)* found no discrete morphological differences among the YPM *Ichthyornis* specimens to substantiate their designation as distinct species, and therefore synonymized five of the eight previously named species into *Ichthyornis dispar* in addition to providing a detailed definition and diagnosis of this taxon. One of the remaining species was separated into its own genus, *Guildavis*, while the specimens belonging to *I. celer*, already assigned to their own genus, *Apatornis*, by *Marsh (1880)*, were separated into two distinct taxa, *A. celer* and *Iaceornis marshi*.

The comprehensive study by *Clarke (2004)* reevaluated all of the 19th Century specimens of *Ichthyornis* housed at the Yale Peabody Museum (YPM), greatly updating our understanding of the taxon and clarifying its morphological differences with respect to more stemward Mesozoic avialans and the avian crown group. However, the fragmentary nature of many YPM specimens seriously hinders our understanding of *Ichthyornis* postcranial anatomy, particularly in key skeletal regions such as the sternum, pelvis, and hindlimbs. Unfortunately, only a small fraction of the YPM material was clearly figured in *Clarke (2004)* in order to avoid duplicating many illustrations of specimens that were initially figured by *Marsh (1880)*. However, *Clarke (2004)* noted several inaccuracies in these 19th Century illustrations; thus, the relative dearth of unambiguous images of *Ichthyornis* postcranial morphology limits the availability of anatomical data on this key taxon for comparative morphological studies.

A substantial amount of new cranial material belonging to *Ichthyornis* has recently been described (*Field et al., 2018b*; *Torres, Norell & Clarke, 2021*), with recent work on *Ichthyornis* predominantly targeting questions related to jaw morphology, the origin of the neornithine beak, and brain architecture (*Gingerich, 1972*; *Martin & Stewart, 1977*; *Dumont et al., 2016*; *Field et al., 2018b*; *Brocklehurst & Field, 2021*; *Torres, Norell & Clarke, 2021*). By contrast, postcranial material reported since the original descriptions of *Ichthyornis* in the 19th Century is limited, consisting mostly of several isolated humeri and other highly fragmentary elements (*e.g.*, *Olson, 1975*; *Fox, 1984*; *Porras-Múzquiz, Chatterjee & Lehman, 2014*; *Shimada & Wilson, 2016*). As a result, our knowledge of the postcranial osteology of *Ichthyornis* still primarily rests on the material originally described by *Marsh (1872a*, *1880)* and redescribed by *Clarke (2004)*, housed in the collections of the YPM.

Importantly, the postcranial anatomy of *Ichthyornis* has yet to be reinvestigated in light of a surge of crownward euornithean discoveries over the last two decades. Since the redescription of *Ichthyornis* by *Clarke (2004)*, a wealth of recently described taxa, mainly from the Early Cretaceous of China has shed much needed light on the diversity and morphology of Mesozoic avialans, and particularly on Euornithes, the avialan subclade including crown birds (Neornithes) and their closest relatives (*Pittman et al., 2020a*,

2020b). These discoveries have documented the gradual evolutionary acquisition of crown-bird-like postcranial anatomy, revealing an increasingly complex picture of euornithean evolution, and affirming the phylogenetic position of *Ichthyornis* as among the most crownward Mesozoic avialans yet known. Newly-recognized euornitheans that have been described since the last substantial work on *Ichthyornis* postcranial morphology include clades such as Hongshanornithidae (*Zhou & Zhang, 2005*; *O'Connor, Gao & Chiappe, 2010*; *Chiappe et al., 2014*; *Wang, Zhou & Zhou, 2016*), Songlingornithidae (or Yanornithidae; Fig. 1; *Zhou & Zhang, 2001*; *Clarke, Zhou & Zhang, 2006*; *Zheng et al., 2014*; *Wang et al., 2013a*, *2019*, *2020c*, *2021*), and Schizoouridae (*Zhou, Zhou & O'Connor, 2012*; *Wang et al. 2020d*). Of particular relevance are taxa such as *Gansus* (*You et al., 2006*; *Wang et al., 2016*) and *Iteravis* (*Liu et al., 2014*; *Zhou, O'Connor & Wang, 2014*; *O'Connor et al., 2015*; *Wang et al., 2018*), which have been recovered in phylogenetic positions close to *Ichthyornis* along the most crownward portion of the avialan stem lineage. In light of these recent discoveries, renewed investigations into the morphology of *Ichthyornis* may provide important insights into key morphological transitions immediately preceding the origin and diversification of the avian crown group, as well as the refinement of powered flight capacity among Mesozoic avialans (*Pittman et al., 2020c*).

Recently, the description of a substantial amount of new skull material from *Ichthyornis*, aided by high-resolution μCT imaging, revealed a striking mosaic of crown bird-like and plesiomorphic avialan features (*Field et al., 2018b*; *Torres, Norell & Clarke, 2021*). This transitional cranial architecture departs in important ways from earlier, largely hypothetical reconstructions of the *Ichthyornis* skull on the basis of poorly preserved, incomplete remains (*e.g.*, *Marsh, 1880*). Despite this recent advance in our understanding of its skull and jaws, much about the postcranial morphology of *Ichthyornis* remains unknown. Here, we investigate the postcranial morphology of numerous new *Ichthyornis* specimens, including those whose cranial material was previously described by *Field et al. (2018b)*. The new information revealed here has enabled us to reconstruct the postcranial skeletal morphology of *Ichthyornis* in unprecedented detail, leaving only a small number of minor skeletal components unknown for this taxon.

Phylogenetic interrelationships of Cretaceous euornitheans

The exact phylogenetic position of *Ichthyornis* with respect to Neornithes and other Ornithurae (the most exclusive clade uniting Ichthyornithes, Hesperornithes, and Neornithes; see below for full phylogenetic definitions) remains controversial (*Pittman et al., 2020a*), but *Ichthyornis* has been consistently recovered in a phylogenetic position close to the origin of crown group birds (*Clarke, Zhou & Zhang, 2006*; *O'Connor, Chiappe & Bell, 2011*; *O'Connor, Wang & Hu, 2016*; *Huang et al., 2016*; *Wang et al., 2016*, *2017*, *2020a*, *2020c*, *2020d*; *Atterholt, Hutchison & O'Connor, 2018*; *Field et al., 2018b*; *Zheng et al., 2018*; *Torres, Norell & Clarke, 2021*). A few additional taxa, such as *Apsaravis* (*Clarke & Norell, 2002*), *Ambiortus* (*Kurochkin, 1985*; *O'Connor & Zelenkov, 2013*), *Hollanda* (*Bell et al., 2010*) and *Patagopteryx* (*Chiappe, 1996*, *2002*) have occasionally been recovered within Ornithurae, close to *Ichthyornis* and Hesperornithes, but these results have not been consistently recovered in most studies (*O'Connor & Zelenkov, 2013*; *Field et al., 2018b*;
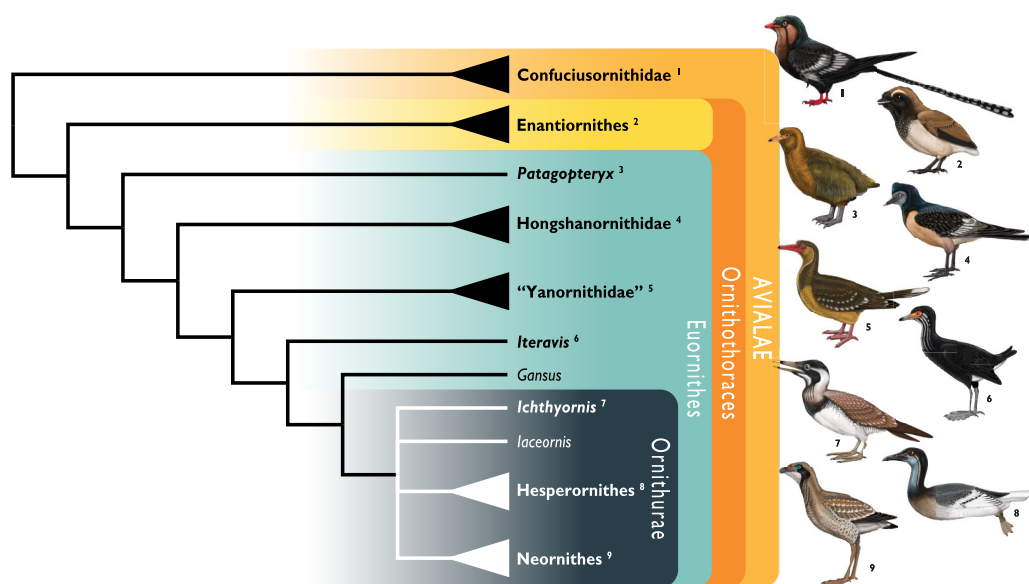
Figure 1 Simplified cladogram showing the most commonly recovered phylogenetic positions of *Ichthyornis* and relevant Mesozoic avialans. White branches highlight phylogenetic uncertainty within the major clade Ornithurae, which includes *Ichthyornis*, Hesperornithes, and the bird crown group (Neornithes). Taxa in bold are figured, superscript numbers indicate the corresponding illustration. For Confuciusornithidae, the illustration corresponds to *Eoconfuciusornis zhengi*; for Enantiornithes, the illustration corresponds to *Cathayornis yandica*; for Hongshanornithidae the illustration corresponds to *Hongshanornis longicresta*; for "Yanornithidae" the illustration corresponds to *Abitusavis lii*; for Hesperornithes the illustration corresponds to *Brodavis varneri*; for Neornithes the illustration corresponds to *Asteriornis maastrichtensis*. Quotation marks associated with "Yanornithidae" reflect the fact that this clade has not been consistently recovered in several recent phylogenetic analyses, including the present study. Illustrations courtesy of R. Olivé, used with permission.

Pittman et al., 2020a; *Wang et al., 2020c*, *2020d*). Recent analyses have recovered alternative phylogenetic positions for *Ichthyornis* with respect to the diving Hesperornithes, which have been recovered in a position either slightly crownward of (*O'Connor, Chiappe & Bell, 2011*; *O'Connor et al., 2020*; *Wang et al., 2017*, *2019*; *Atterholt, Hutchison & O'Connor, 2018*; *Field et al., 2018b*), slightly stemward (*Chiappe, 2002*; *Clarke, 2004*; *You et al., 2006*; *Huang et al., 2016*; *Wang et al., 2020c*; *Torres, Norell & Clarke, 2021*) or in an unresolved polytomy (*Wang et al., 2021*) with *Ichthyornis* (Fig. 1). The relative position of both groups is highly sensitive to both the dataset and the methods used in phylogenetic analyses (*Wang et al., 2017*; *Field et al., 2018b*; *Pittman et al., 2020a*). Moreover, numerous postcranial character states have been impossible or very difficult to score with accuracy for *Ichthyornis*, due to a lack of suitably complete and well-preserved material, highlighting the need for additional data on *Ichthyornis* in order to recover a more consistent phylogenetic topology for the most crownward portion of the avian stem lineage. Other than Hesperornithes, very few Mesozoic euornithean stem-birds have been recovered in a phylogenetic position crownward of *Ichthyornis*. Such taxa, such as *Guildavis, Apatornis*, and *Iaceornis* (*Clarke, 2004*), as well as *Limenavis* (*Clarke & Chiappe, 2001*), are generally based on highly fragmentary material, which limits their
informativeness and complicates the assessment of phylogenetic interrelationships among the crownward-most stem birds.

Reconstructing the morphology of the earliest crown birds

The origin of the bird crown group is well-established to have occurred during the Cretaceous Period (*Jarvis et al., 2014*; *Prum et al., 2015*; *Berv & Field, 2018*), but the scarcity of Late Cretaceous crown bird material complicates our understanding of the early morphology and evolutionary history of the group (*Chatterjee, 1989*, *2000*; *Clarke et al., 2005*, *2016*; *Longrich, Tokaryk & Field, 2011*; *Field et al., 2020a*, *2020b*). Given this significant gap in the crown bird fossil record, work attempting to understand aspects of the ecology, biology, and morphology of the earliest crown birds must rely on inferences based on extant birds and the most crownward-known stem birds (*Zheng et al., 2014*, *2018*; *Berv & Field, 2018*; *Field et al., 2018a*; *Wang et al., 2018*; *O'Connor, 2019*; *O'Connor & Zhou, 2015*, *2020*; *Torres, Norell & Clarke, 2021*). Thus, an improved understanding of the morphology of the closest relatives of crown birds from the Late Cretaceous is pivotal for reconstructing the nature of the earliest Neornithes. Unfortunately, despite their abundance and their crownward position among Mesozoic Ornithurae, Hesperornithes were secondarily flightless, exhibiting highly specialized, autapomorphic postcranial features including greatly reduced wings, strongly modified hindlimbs for foot-propelled diving, and osteosclerotic skeletons. These specialized features preclude the use of many aspects of hesperornithean postcranial osteology as a reliable source for reconstructions of the plesiomorphic condition of the avian crown group (*Bell & Chiappe, 2016*). By contrast, *Ichthyornis* was obviously less ecologically specialized than hesperornitheans, and easily falls within the size range of extant volant marine birds. These features suggest that the morphology of *Ichthyornis* provides a more useful approximation of the ancestral condition of the crown bird postcranium (*Clarke, 2004*; *Field et al., 2018b*), with some aspects of *Ichthyornis* postcranial morphology hypothesized to fall within the range of variation of extant bird diversity (*Mayr, 2017a*). Given the scarcity of Mesozoic fossil material recovered crownward of *Ichthyornis* and Hesperornithes, the postcranial morphology of *Ichthyornis* may be more representative of the ancestral condition of crown birds than that of any other known Mesozoic avialan; thus, its study has crucial implications for understanding morphological evolution immediately preceding the great radiation of the avian crown group.

Focus of the present study

Despite the substantial number of well-preserved Mesozoic euornitheans that have recently been described, its crownward phylogenetic position continues to render *Ichthyornis* a key taxon in our understanding of avian evolution, and the abundance of its remains makes it almost unique in its potential for revealing important insights into avialan intraspecific variation (*Clarke, 2004*). Here, we substantially advance our understanding of the morphology of this pivotal taxon by describing three-dimensional μCT scans of the postcranial morphology of 40 new specimens of *Ichthyornis*, including four substantially complete partial skeletons with recently-described cranial remains (*Field*
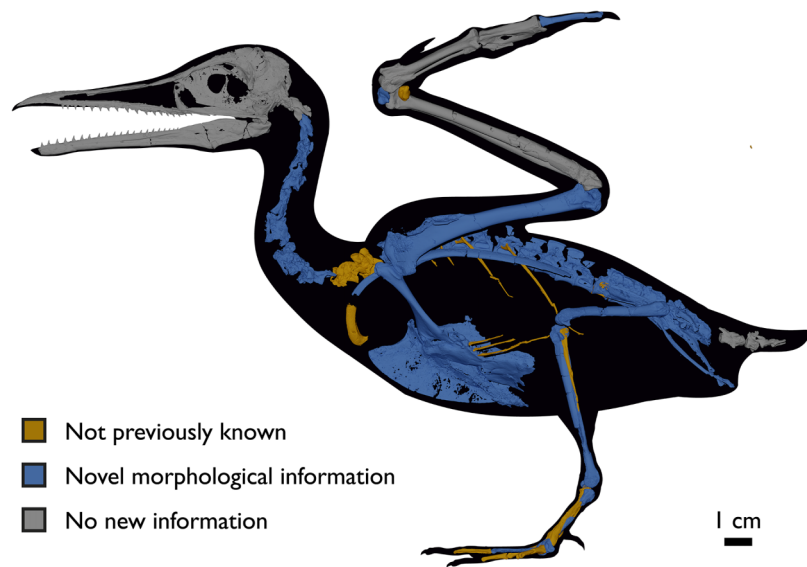
Figure 2 Reconstruction of the skeleton of *Ichthyornis dispar*, showing elements described in the present study that exhibit novel morphological information for *Ichthyornis*. Elements in yellow correspond to those skeletal elements not previously known or described for *Ichthyornis*, while elements in blue indicate those skeletal elements that were known for *Ichthyornis* but for which novel morphological information is provided by the specimens described in this study. Elements in grey correspond to those for which little novel information is provided by the specimens described here. The reconstructed skeleton is a composite incorporating multiple specimens described in this study (see Table 1). All specimens are scaled to the dimensions of the FHSM VP-18702 specimen.

et al., 2018b). The new material includes several skeletal elements that have not previously been described for *Ichthyornis*, including the radial carpal and the fibula, as well as significantly better-preserved examples of elements previously known from highly fragmentary remains, such as the sternum, the furcula, the pelvis, the tibiotarsus, and the foot (Fig. 2). Many of the new specimens are exceptionally well-preserved in three dimensions, exceeding the completeness and degree of preservation of much of the classic YPM material. Together, the new material offers a nearly complete view of *Ichthyornis* postcranial osteology (Fig. 3), facilitating a detailed reinvestigation of the phylogenetic position of *Ichthyornis* among Mesozoic Avialae.

MATERIAL AND METHODS

Specimens studied

The present work is based on the study of a series of previously undescribed postcranial specimens referred to *Ichthyornis*, with the cranial material of several of these specimens previously described in *Field et al. (2018b)*. The most complete specimens included in the study are FHSM VP-18702 (a partial skeleton from a single fossil block, including cranial material, the pectoral girdle and forelimbs, and the synsacrum and hindlimbs); KUVP 119673 (a partial skeleton from a single block filled with radiopaque inclusions, preserving cranial material, most cervical and anterior thoracic vertebrae, the pectoral girdle, a partial forelimb, the pelvic girdle and partial hindlimb); ALMNH:Paleo:3316 (a partial skeleton
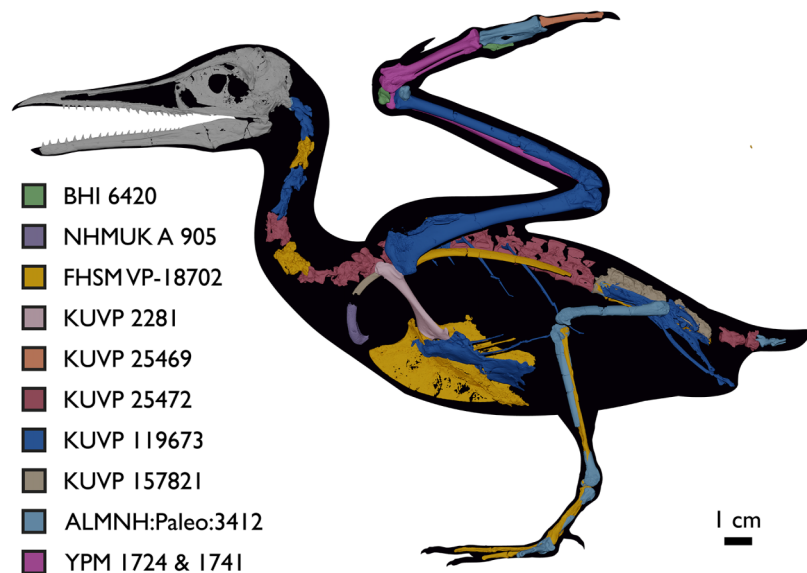
Figure 3 Reconstruction of the skeleton of *Ichthyornis dispar*, showing elements that are described here for the first time. The reconstructed skeleton is a composite incorporating numerous new specimens described in this study (see colour-coded legend and Table 1). All specimens are scaled to the dimensions of FHSM VP-18702.

including cranial material, thoracic, sacral, and caudal vertebrae, a partial forelimb and complete hindlimb); and BHI 6420 (preserving the complete pectoral girdle and forelimb). Thirty-six additional undescribed specimens that are less complete are also described here for the first time—see Table 1 for the complete list of material. In addition to this substantial amount of new material, several skeletal elements from YPM specimens previously described by *Marsh (1880)* and *Clarke (2004)* have been incorporated into this study: the *Ichthyornis dispar* holotype YPM 1450 (ulna), 1724 (carpometacarpus), 1733 (coracoid), 1740 (ulna) and 1741 (radius).

All specimens studied come from middle to late Santonian rocks of the Niobrara Formation in Kansas (US), and from the early Campanian deposits of the Mooreville Chalk in Alabama (US), the same localities that produced the majority of the classic *Ichthyornis* material (*Marsh, 1880*; *Clarke, 2004*; *Field et al., 2018b*). See Table 1 and the Supplemental Information for available information on the provenance of each specimen.

The newly described specimens were referred to *Ichthyornis dispar* based on the presence of multiple autapomorphies, previously described by *Clarke (2004)*. Where no diagnostic features were preserved, specimens were referred to *Ichthyornis* based on their morphological similarity to specimens preserving autapomorphies. See Table 1 for a full list of the diagnostic features preserved in each specimen.

Methods

CT-scanning

The specimens were scanned at the Cambridge Biotomography Centre, the University of Texas High-Resolution CT Facility (UTCT), and the Center for Nanoscale Systems at Harvard. Scan parameters and details for each specimen are provided in the Supplemental

Table 1 List of specimens included in this study. All specimens, with the exception of those from the YPM collections and the skull of FHSM VP 18702, are newly described in the present study. The elements preserved in each specimen are listed; see description and Supplemental Information for additional information. Synapomorphies diagnosing *Ichthyornis* from *Clarke (2004)* that are recognizable in each specimen are indicated. Where none of these apomorphies are preserved, specimens were identified based on morphological similarity with other diagnosed *Ichthyornis* specimens. Synapomorphies: (1) a single large pneumatic foramen situated on the anteromedial surface of the quadrate, (2) amphicoelous cervical vertebrae, (3) free caudal vertebrae exhibiting well-developed and elongated prezygapophyses, (4) scapula exhibiting an extremely diminutive acromion process, (5) pit-shaped fossa on the distal end of the bicipital crest of the humerus, (6) ulnar trochlear surface equal in length across its caudal and distal surfaces, (7) oval scar located on the caudoventral surface of the distal radius, (8) large tubercle developed close to the articular surface of phalanx II:1 in the carpometacarpus and (9) presence of an internal index process on the distal end of manual phalanx II:1.

Specimen number	Elements represented	Origin	Age	Discrete synapomorphies supporting referral to *Ichthyornis*
ALMNH: Paleo:1043	Proximal humerus & bone fragment	Mooreville Fm, Alabama	Early Campanian	5
ALMNH: Paleo:1310	Distal tarsometatarsus	Mooreville Fm, Alabama	Early Campanian	-
ALMNH: Paleo:1311	Distal tarsometatarsus	Mooreville Fm, Alabama	Early Campanian	-
ALMNH: Paleo:1314	Distal femur	Mooreville Fm, Alabama	Early Campanian	-
ALMNH: Paleo:1319	Proximal femur	Mooreville Fm, Alabama	Early Campanian	-
ALMNH: Paleo:1677	Proximal tarsometatarsus	Mooreville Fm, Alabama	Early Campanian	-
ALMNH: Paleo:1786	Proximal humerus	Mooreville Fm, Alabama	Early Campanian	5
ALMNH: Paleo:1944	Possible pedal phalanx	Mooreville Fm, Alabama	Early Campanian	-
ALMNH: Paleo:3316	Partial skeleton. Premaxilla, maxillae, mandible, 8 vertebrae, rib, coracoid, omal furcula fragment, distal ulna, ulnar carpals, carpometacarpus, manual phalanges, femur, tibiotarsus, tarsometatarsus & pedal phalanx	Mooreville Fm, Alabama	Early Campanian	6,8,9
ALMNH: Paleo:3412	Distal tibiotarsus	Mooreville Fm, Alabama	Early Campanian	-
BHI 6420	Partial skeleton. Scapulae, coracoids, omal furcula fragment, humeri, radius, proximal ulna, radial carpal, carpometacarpus, manual phalanges	Niobrara Fm, Kansas	Middle Santonian	4,5,8,9
BHI 6421	Partial skeleton. Mandibles, quadrate, 3 thoracic vertebrae, distal humerus, distal ulna, manual phalanx & distal tibiotarsus	Niobrara Fm, Kansas	Middle Santonian	5,9
FHSM VP-18702	Largely complete skeleton. Partial skull, lower jaws, 2 cervical vertebrae, synsacrum, ribs, sternum, scapula, coracoids, partial humeri, ulna, radii, radial carpals, ulnar carpal, carpometacarpus, manual phalanx, femur, distal tibiotarsus, fibula, tarsometatarsus & pedal phalanges	Niobrara Fm, Kansas	Middle Santonian	1,2,4,5,7,8,9
KUVP 2281	Scapula & coracoid	Niobrara Fm, Kansas	Middle Santonian	4
KUVP 2284	Coracoid, humerus, ulna, radius, ulnar carpal, manual phalanx	Niobrara Fm, Kansas	Middle Santonian	Lacks 9
KUVP 2300	Humerus	Niobrara Fm, Kansas	Middle Santonian	5
KUVP 25469	Distal humerus & manual phalanx	Niobrara Fm, Kansas	Middle Santonian	-

(Continued)

Specimen number	Elements represented	Origin	Age	Discrete synapomorphies supporting referral to *Ichthyornis*
KUVP 25471	Fragmentary vertebra & humerus	Niobrara Fm, Kansas	Middle Santonian	5
KUVP 25472	17 vertebrae (cervical, thoracic & caudal), radius & proximal ulna	Niobrara Fm, Kansas	Middle Santonian	2,3
KUVP 119673	Partial skeleton. Quadrate, jugal, mandible, 13 vertebrae (cervical, thoracic & caudal), synsacrum, sternum, ribs, coracoid, scapula, humeri, radii, ulnae, pelves, femur, distal tibiotarsus & fibula	Niobrara Fm, Kansas	Middle Santonian	1,2,3,4,5,6
KUVP 123459	Partial carpometacarpus & distal ulna	Niobrara Fm, Kansas	Middle Santonian	8
KUVP 157821	Synsacrum, omal furcula fragment, distal radius & carpometacarpus	Niobrara Fm, Kansas	Middle Santonian	7
MSC 2841	Distal carpometacarpus	Mooreville Fm, Alabama	Early Campanian	8
MSC 3394	Distal carpometacarpus	Mooreville Fm, Alabama	Early Campanian	8
MSC 5794	Proximal humerus	Mooreville Fm, Alabama	Early Campanian	-
MSC 5895	Distal humerus, proximal radius & manual phalanx	Mooreville Fm, Alabama	Early Campanian	9
MSC 5916	Proximal ulna	Mooreville Fm, Alabama	Early Campanian	-
MSC 5937	Partial coracoid	Mooreville Fm, Alabama	Early Campanian	-
MSC 6200	Proximal radius & distal ulna	Mooreville Fm, Alabama	Early Campanian	6
MSC 6201	Manual phalanx	Mooreville Fm, Alabama	Early Campanian	9
MSC 6202	Carpometacarpus	Mooreville Fm, Alabama	Early Campanian	8
MSC 7841	Omal coracoid, humeri & distal ulna	Mooreville Fm, Alabama	Early Campanian	5,6
MSC 7842	Partial humerus	Mooreville Fm, Alabama	Early Campanian	-
MSC 7844	Distal humerus	Mooreville Fm, Alabama	Early Campanian	-
MSC 13214	Partial tarsometatarsus	Mooreville Fm, Alabama	Early Campanian	-
MSC 13868	Fragmentary pedal phalanx	Mooreville Fm, Alabama	Early Campanian	-
MSC 34426	Distal carpometacarpus	Mooreville Fm, Alabama	Early Campanian	8
MSC 34427	Partial coracoid, distal ulna & partial carpometacarpus	Mooreville Fm, Alabama	Early Campanian	6,8
NHMUK A 905	Sternum, medial portion of furcula, coracoids, scapulae, humeri & proximal radius	Niobrara Fm, Kansas	Middle Santonian	4,5

Specimen number	Elements represented	Origin	Age	Discrete synapomorphies supporting referral to *Ichthyornis*
YPM 1450	Partial skeleton. Partial skull, mandibles, 4 vertebrae, synsacrum, partial sternum, ribs, coracoid, humerus, ulna, radius, carpometacarpus, femur & tibiotarsus. This study includes only scans of its sternum & ulna	Niobrara Fm, Kansas	Middle Santonian	Holotype. 2,5,6,7,8
YPM 1461	Sternum, ribs, coracoid & humerus. This study includes only scans of its sternum.	Niobrara Fm, Kansas	Middle Santonian	-
YPM 1724	Carpometacarpus	Niobrara Fm, Kansas	Middle Santonian	8
YPM 1733	Partial skeleton. 10 vertebrae, synsacrum, coracoid, scapula, humerus, radius & partial ilium. This study includes only scans of its coracoid.	Niobrara Fm, Kansas	Middle Santonian	2,4
YPM 1740	Ulna	Niobrara Fm, Kansas	Middle Santonian	6
YPM 1741	Coracoid, humerus & radius. This study includes only scans of its radius	Niobrara Fm, Kansas	Middle Santonian	7

Information. The scans were assembled and digitally segmented using VG Studio Max 3.3 (Volume Graphics, Heidelberg, Germany), from which 3D surface meshes of individual elements were extracted and exported. Skeletal models of each specimen in anatomical connection were built in Autodesk Maya 2020.

Anatomical comparisons

The main references for comparative morphological information on *Ichthyornis* were descriptions of the classic *Ichthyornis* specimens from the YPM collections by *Marsh (1880)* and *Clarke (2004)*. Comparisons with other fossil euornithean taxa were based on available literature (*e.g.*, *Zhou, O'Connor & Wang, 2014*; *Wang et al., 2016*, *2020c*). Comparisons with extant taxa were based on specimens from the University of Cambridge Museum of Zoology (UMZC). Osteological and myological nomenclature follows that of *Baumel & Witmer (1993)* and *Baumel & Raikow (1993)*, with additional nomenclature from *Livezey & Zusi (2007)* and *Mayr (2014*, *2016)*. We acknowledge the complicated developmental identities of the free carpal bones (*Botelho et al., 2014*), and how these may be at odds with the traditional usage of the terms ulnare and radiale. For clarity, in light of *Botelho et al. (2014)*, we have decided to refer to these elements as the ulnar carpal and radial carpal, respectively. We use standard terminology for morphological orientation (medial/lateral, dorsal/ventral, *etc.*), and preferentially apply the terms cranial/caudal instead of anterior/posterior, except for cases where disambiguation is required (*e.g.*, anterior caudal vertebrae).

Phylogenetic analyses

We tested the phylogenetic position of *Ichthyornis* by re-scoring it in updated versions of the morphological matrices from *Torres, Norell & Clarke (2021)* and *Wang et al. (2020c)*. Taxa were also added and re-scored from *Wang & Zhou (2020)*, *Wang et al. (2020d)* and *O'Connor et al. (2020)*. With the exception of *O'Connor et al. (2020)*, these studies did not
incorporate the additional five characters and character re-scorings from *Field et al. (2018b)*. We produced a new dataset by combining the matrices from *Wang et al. (2020c)*, including updates from *Field et al. (2018b)*, with the matrix from *O'Connor et al. (2020)*. The *Torres, Norell & Clarke (2021)* matrix was found to contain multiple scoring errors, affecting at least six characters, including several characters scored for more states than described. Several of these problems were inherited from previous versions of that dataset (*Huang et al., 2016*; *Li et al., 2014*), but these errors were not present in *Clarke (2004)* or *Clarke, Zhou & Zhang (2006)*. These issues were corrected for the present study, but an exhaustive overhaul of that dataset would be beyond the scope of this study. Therefore, we recommend caution in future investigations employing the *Torres, Norell & Clarke (2021)* morphological matrix. Some taxa were re-scored based on published literature, such as *Gansus* (*Wang et al., 2016*) and *Iteravis* (*Zhou, O'Connor & Wang, 2014*). A complete list of scoring changes and corrections to published matrices is provided in the Supplemental Information.

Given the presence of several morphological differences among the specimens described here (see morphological descriptions), well-represented specimens were initially included as distinct operational taxonomic units (OTUs) in our phylogenetic analyses. In all cases, these were recovered either within an exclusive clade including the *Ichthyornis* holotype, or in a polytomy comprising the holotype of *Ichthyornis* and the clade formed by Hesperornithes + crown birds (see Supplemental Trees in the Supplemental Information). Based on these results, all specimens were treated as a single, combined OTU for *Ichthyornis dispar* in subsequent analyses.

We performed phylogenetic analyses under both parsimony and Bayesian analytical frameworks in order to account for differences introduced by alternative optimality criteria. As found by *Field et al. (2018b)*, *Apsaravis* was identified as a wildcard taxon, and alternative analyses were performed including and excluding it. Its removal yielded better-resolved relationships and higher node support values within Euornithes. Parsimony analyses were conducted using TNT 1.5 (*Goloboff & Catalano, 2016*, made available with the sponsorship of the Willi Hennig Society). An unconstrained heuristic search with equally weighted characters was performed, with 1,000 replicates of random stepwise addition using the tree bisection reconnection (TBR) algorithm. Ten trees were saved per replicate, and all most parsimonious trees (MPTs) were used to calculate a strict consensus. Bremer support values were calculated in TNT using TBR from existing trees. Bootstrap analyses were performed using a traditional search and 1,000 replicates, with outputs saved as absolute frequencies. Our Bayesian analyses followed the same protocol as *Field et al. (2020a)*. We conducted Bayesian analyses with MrBayes (*Ronquist et al., 2012*) using the CIPRES Science Gateway (*Miller, Pfeiffer & Schwartz, 2010*), and data were analysed under the Mkv model (*Lewis, 2001*). Gamma-distributed rate variation was assumed in order to allow for variation in evolutionary rates across different characters. Analyses were conducted using four chains and two independent runs, with a tree sampled every 4,000 generations and a burn-in of 25%. Analyses were run for 30,000,000 generations, and analytical convergence was assessed using standard diagnostics provided in MrBayes (average standard deviation of split frequencies <0.02, potential scale reduction

factors = 1, effective sample sizes >200). Results obtained from independent runs of the same analyses were summarized using the sump and sumt commands in MrBayes. Morphological synapomorphies of recovered tree topologies were optimized under parsimony, by exporting the recovered trees into TNT.

Clade definitions

To facilitate consistent phylogenetic nomenclature in the present and in future work on crownward stem birds, we establish definitions for the following clade names in accordance with rules outlined by the *International Code of Phylogenetic Nomenclature* (*PhyloCode*) (*de Queiroz & Cantino, 2020*). All names and definitions have been registered in the online database RegNum (*Cellinese & Dell, 2020*).

Avialae *Gauthier, 1986*, converted clade name

Registration number. 552

Definition. The largest clade containing *Vultur gryphus Linnaeus, 1758* (Aves *sensu Clarke et al., 2020* or Neornithes) but not *Dromaeosaurus albertensis Matthew & Brown, 1922* (Dromaeosauridae) and *Saurornithoides mongoliensis Osborn, 1924* (Troodontidae). This is a maximum-clade definition.

Abbreviated definition. Max ∇ (*Vultur gryphus Linnaeus, 1758* ~ *Dromaeosaurus albertensis Matthew & Brown, 1922* & *Saurornithoides mongoliensis Osborn, 1924*).

Reference phylogeny. Figure S1A in *Pei et al. (2020)* should be considered the primary reference phylogeny. Figure 3 in *Cau (2018)* may be regarded as a secondary reference phylogeny.

Composition. In addition to Euornithes (which includes the crown clade Neornithes; see below), taxa that are typically recovered as members of Avialae by recent phylogenetic analyses include Enantiornithes, Jinguofortisidae, Confuciusornithiformes, *Sapeornis*, Jeholornithiformes, and often *Alcmonavis* and *Archaeopteryx* (*O'Connor, Chiappe & Bell, 2011*; *Turner, Makovicky & Norell, 2012*; *Foth, Tischlinger & Rauhut, 2014*; *Huang et al., 2016*; *O'Connor, Wang & Hu, 2016*; *Mayr, 2017a*; *Wang et al., 2017*; *Cau, 2018*; *Field et al., 2018b*; *Chiappe & Bell, 2020*; *Cordes-Person et al., 2020*; *O'Connor et al., 2020*; *Pei et al., 2020*; *Pittman et al., 2020a*, *2020b*; *Wang & Zhou, 2020*; *Wang et al., 2020a*, *2020b*). Other taxa for which avialan affinities have been supported by some phylogenetic analyses include *Zhongornis*, *Rahonavis*, *Balaur*, Anchiornithinae, and Scansoriopterygidae, but their assignment to this clade remains controversial (*Foth, Tischlinger & Rauhut, 2014*; *Cau, Brougham & Naish, 2015*; *Mayr, 2017a*; *Cau, 2018*; *Hartman et al., 2019*; *Pittman et al., 2020a*).

Diagnostic apomorphies. Character states optimized as synapomorphies of Avialae by *Pei et al. (2020)* include a transition in caudal vertebra morphology towards longer centra with reduced transverse processes anterior to the seventh caudal, the nasal and lacrimal forming the dorsal border of the antorbital fossa in lateral view, the distalmost mediolateral width

of the tibia being approximately equal to the width of the tibial shaft, a caudally curved pubic shaft with a convex cranial surface, a long axis of the external naris approximately equal in length to the long axis of the antorbital fenestra, and an acromion process of the scapula that surpasses the articular surface for the coracoid cranially. The analyses of *Pei et al. (2020)* recovered anchiornithines as the most stemward avialans. For a topology in which scansoriopterygids were also resolved as avialans, *Cau (2018)* reported relatively shortened nasals, a marked reduction in the number and size of anterior caudal neural spines, a humeral shaft subequal in thickness to the femur, a caudally concave ischium, a reduced cnemial crest, and the penultimate phalanx of pedal digit III not shorter than the preceding phalanges as synapomorphies of Avialae.

Comments. Avialae was originally coined by *Gauthier (1986)* for maniraptorans more closely related to Ornithurae (including crown birds) than to Deinonychosauria. A minimum-clade definition for Avialae was also proposed by *Wagner & Gauthier (1999)*, referring to the last common ancestor of *Archaeopteryx* and crown birds, and all of its descendants, whereas *Gauthier & de Queiroz (2001)* later redefined Avialae as an apomorphy-based clade, referring to the clade characterized by feathered wings used in powered flight homologous with those of *Vultur gryphus*. However, a maximum-clade definition similar to that of *Gauthier (1986)* is followed by most recent authors (*e.g.*, *Maryańska, Osmólska & Wolsan, 2002*; *Padian, 2004*; *Xu et al., 2011*; *Turner, Makovicky & Norell, 2012*; *Godefroit et al., 2013*; *Cau, Brougham & Naish, 2015*; *Hendrickx, Hartman & Mateus, 2015*; *Hartman et al., 2019*; *Field et al., 2020a*; *O'Connor et al., 2020*; *Pei et al., 2020*; *Pittman et al., 2020a*), and this is accordingly reflected by our proposed definition. In the interest of stability, a maximum-clade definition with the sole internal specifier anchored on a crown bird is further preferable to the aforementioned minimum-clade and apomorphy-based definitions considering the occasionally labile position of *Archaeopteryx* (*Xu et al., 2011*; *Hartman et al., 2019*) and uncertainty over the presence and homology of powered flight capabilities among early paravians (*Hartman et al., 2019*; *Pei et al., 2020*).

    In the findings of *Gauthier (1986)* and many subsequent studies (*e.g.*, *Turner, Makovicky & Norell, 2012*; *Hartman et al., 2019*; *Pei et al., 2020*), Deinonychosauria includes the clades Dromaeosauridae and Troodontidae. However, some analyses have recovered Troodontidae as more closely related to crown birds than to Dromaeosauridae (*e.g.*, *Godefroit et al., 2013*; *Foth, Tischlinger & Rauhut, 2014*; *Cau, Brougham & Naish, 2015*; *Cau, 2018*). As a result, some proposed definitions of Avialae include both dromaeosaurid and troodontid representatives as external specifiers (*e.g.*, *Maryańska, Osmólska & Wolsan, 2002*; *Xu et al., 2011*; *Turner, Makovicky & Norell, 2012*; *Godefroit et al., 2013*; *Cau, Brougham & Naish, 2015*; *Hendrickx, Hartman & Mateus, 2015*; *Field et al., 2020a*; *O'Connor et al., 2020*; *Pei et al., 2020*). Given that the scope of Avialae as coined by *Gauthier (1986)* was likely intended to exclude all taxa known at the time that were more distantly related to crown birds than *Archaeopteryx*, this decision is followed here. Although the type genus of Troodontidae is *Troodon*, its holotype consists only of an isolated tooth, which may be non-diagnostic with respect to other troodontids known from the Upper Cretaceous of North America (*van der Reest & Currie, 2017*; *Cullen et al., 2021*).

In recognition of this possibility, we instead use *Saurornithoides mongoliensis* as a representative of Troodontidae in our proposed definition, as it is known from more complete remains than *Troodon*, had been described prior to *Gauthier (1986)*, is frequently included in phylogenetic analyses, and is universally recovered as a member of Troodontidae (*e.g.*, *Xu et al., 2011*; *Turner, Makovicky & Norell, 2012*; *Godefroit et al., 2013*; *Foth, Tischlinger & Rauhut, 2014*; *Cau, Brougham & Naish, 2015*; *Hartman et al., 2019*; *Pei et al., 2020*).

Euornithes *Sereno, 1998*, converted clade name

Registration number. 553

Definition. The largest clade containing *Vultur gryphus Linnaeus, 1758* (Aves or Neornithes) but not *Enantiornis leali Walker, 1981* (Enantiornithes) and *Cathayornis yandica Zhou, Jin & Zhang, 1992* (Enantiornithes). This is a maximum-clade definition.

Abbreviated definition. Max ∇ (*Vultur gryphus Linnaeus, 1758* ~ *Enantiornis leali Walker, 1981* & *Cathayornis yandica Zhou, Jin & Zhang, 1992*).

Reference phylogeny. Figure 31 in the present study should be considered the primary reference phylogeny. Figure S1 in *Wang & Zhou (2020)* may be regarded as a secondary reference phylogeny.

Composition. Recent studies often recover the internal topology of Euornithes as a pectinate series of largely monotypic lineages successively more closely related to the crown clade Neornithes (*e.g.*: *Huang et al., 2016*; *Field et al., 2018b*; *Pittman et al., 2020a*; *Wang & Zhou, 2020*). An exhaustive list of these lineages is beyond the scope of this article, but well-studied taxa that are consistently recovered as members of Euornithes include Ornithurae (which includes Neornithes; see below), *Gansus*, *Iteravis*, *Yanornis*, *Yixianornis*, Hongshanornithidae, *Patagopteryx*, *Schizooura*, and *Archaeorhynchus*.

Diagnostic apomorphies. In the present study, character states optimized as synapomorphies of Euornithes include a sternal carina near or rostral to the cranial border of the sternum; a furcula exhibiting tapered omal ends and lacking a hypocleideum; a procoracoid process present on the coracoid; a globe-shaped and craniocaudally convex humeral head; the midline of the proximal end of the humerus projecting further proximally than its dorsal edge; metacarpals II and III with a similar proximal extension; a flat and craniocaudally expanded manual phalanx II-1; distal end of pubis not flared—straight and subequal in proportion with rest of the pubis; femur lacking a caudal trochanter; tibiotarsus twice the length of the tarsometatarsus or longer; metatarsal IV of approximately the same mediolateral width as metatarsals II and III; and metatarsal II exhibiting approximately the same trochlear width as metatarsals III and/or IV. *Cau (2018)* also recovered a relatively enlarged premaxilla, a furcula lacking a hypocleideum, a relatively elongate sternum with a caudally extended sternal keel, and elongate

intermediate trabeculae (caudomedial processes) on the sternum forming two pairs of sternal incisures as synapomorphies of Euornithes.

Comments. Euornithes was coined by *Sereno (1998)* with a maximum-clade definition, referring to the clade including all taxa more closely related to crown birds than to Enantiornithes. Although use of the name Ornithuromorpha *Chiappe et al. (1999)* for an equivalent clade has become prevalent in recent literature (*e.g.*, *O'Connor, Chiappe & Bell, 2011*; *O'Connor, Wang & Hu, 2016*; *Mayr, 2017a*; *Wang et al., 2017*; *Cau, 2018*; *Chiappe & Bell, 2020*; *Cordes-Person et al., 2020*; *Wang & Zhou, 2020*; *Wang et al., 2020a, 2020b*), the earliest phylogenetic definition proposed for Ornithuromorpha was a minimum-clade definition, referring to the last common ancestor of *Patagopteryx*, *Vorona*, and Ornithurae, and all of its descendants (*Chiappe, 2001*). An explicit redefinition of Ornithuromorpha with a maximum-clade definition equivalent to that of Euornithes was not proposed in technical literature until *O'Connor, Wang & Hu (2016)*. Given that Euornithes was the first name to be defined for this clade, has nominal priority over Ornithuromorpha, and has never fallen into disuse (*e.g.*, *Elzanowski, Paul & Stidham, 2000*; *Senter, 2006*; *Longrich, 2009*; *Godefroit et al., 2013*; *Tanaka, Zelenitsky & Therrien, 2015*; *Smith-Paredes et al., 2018*; *Pei et al., 2020*; *Pittman et al., 2020a*; *Xu et al., 2020*; *Foth et al., 2021*), we favour its application here. Establishing the name Ornithuromorpha for a different (but potentially taxonomically similar) clade remains feasible for future work.

The name Enantiornithes is derived from the genus *Enantiornis*, thus we designate the type and only species of *Enantiornis* as an external specifier. Although the validity of *Enantiornis* is not in dispute, this genus is known only from partial pectoral girdle and forelimb bones (*Walker & Dyke, 2009*), and is often excluded from recent phylogenetic analyses (*e.g.*, *O'Connor, Chiappe & Bell, 2011*; *O'Connor, Wang & Hu, 2016*; *Wang et al., 2017*; *Field et al., 2018b*; *Bailleul et al., 2019*; *Cordes-Person et al., 2020*; *O'Connor et al., 2020*; *Pittman et al., 2020a*; *Wang & Zhou, 2020*; *Wang et al., 2020a, 2020b*). As a result, we have chosen to include *Cathayornis yandica* as a second external specifier, as it is known from more complete remains than *Enantiornis*, had been described prior to *Sereno (1998)*, is frequently included in phylogenetic analyses, and is universally recovered as a member of Enantiornithes (*e.g.*, *O'Connor, Chiappe & Bell, 2011*; *Turner, Makovicky & Norell, 2012*; *Foth, Tischlinger & Rauhut, 2014*; *O'Connor, Wang & Hu, 2016*; *Wang et al., 2017*; *Field et al., 2018b*; *Bailleul et al., 2019*; *Hartman et al., 2019*; *Cordes-Person et al., 2020*; *O'Connor et al., 2020*; *Pei et al., 2020*; *Pittman et al., 2020a*; *Wang & Zhou, 2020*; *Wang et al., 2020a, 2020b*).

Before *Sereno (1998)*, the name Euornithes had been independently coined by several authors, including *Stejneger (1885)*, *Dementjev (1940)*, and *Sanz & Buscalioni (1992)*, each assigning it a different taxonomic scope (*Sereno, 2005*). However, none of these other proposed applications of Euornithes saw wide use in later literature, and *Sereno (1998)* coined Euornithes without reference to these previous authors. The name Euornithes as used here is thus attributed to *Sereno (1998)*, per *PhyloCode* Note 9.15A.2.

Ornithurae *Haeckel, 1866*, converted clade name

Registration number. 554

Definition. The smallest clade containing *Ichthyornis dispar Marsh, 1872a*, *Hesperornis regalis Marsh, 1872b*, and *Vultur gryphus Linnaeus, 1758* (Aves or Neornithes). This is a minimum-clade definition.

Abbreviated definition. Min ∇ (*Ichthyornis dispar Marsh, 1872a* & *Hesperornis regalis Marsh, 1872b* & *Vultur gryphus Linnaeus, 1758*).

Reference phylogeny. Figure 31 in the present study should be considered the primary reference phylogeny. Figure S1 in *Wang & Zhou (2020)* may be regarded as a secondary reference phylogeny.

Composition. In addition to the crown clade Neornithes, well-studied representatives of Ornithurae include *Ichthyornis* and Hesperornithes. *Antarcticavis*, *Guildavis*, *Apatornis*, *Iaceornis*, and *Limenavis* may also belong to this group, but are only known from fragmentary specimens, hampering confident phylogenetic placement (*Clarke & Chiappe, 2001*; *Clarke, 2004*; *Cordes-Person et al., 2020*). Other taxa for which ornithuran affinities have been supported by some phylogenetic analyses include *Apsaravis*, *Hollanda*, and *Patagopteryx*, though their assignment to this clade is controversial (*Huang et al., 2016*; *O'Connor, Wang & Hu, 2016*; *Mayr, 2017a*; *Cau, 2018*; *Field et al., 2018b*; *Hartman et al., 2019*; *Wang et al., 2020b*).

Diagnostic apomorphies. In the present study, character states optimized as synapomorphies of Ornithurae include a sternum exhibiting costal facets and lacking a xiphoid process; the presence of caudally projected medial and/or lateral processes in the sternum; a cranially projected deltopectoral crest in the humerus; ulnar carpal with well-developed rami (U-shaped to V-shaped); a shelf-shaped distal articulation of metacarpal I with phalanx I; ischium less than two-thirds the total length of the pubis; subparallel ischium and pubis with a caudally directed and mediolaterally compressed pubis; distinct fossa for the capital ligament in the femur; two proximal vascular foramina on the tarsometatarsus; and a well-developed and globose tarsometatarsal intercotylar eminence. *Cau (2018)* also recovered the presence of an intermetacarpal process, a caudoventral orientation of the pubic peduncle of the ilium, a relatively enlarged ischial peduncle of the ilium, the absence of a pubic symphysis, the presence of a distinct obturator flange on the ischium, a pedal digit IV subequal in length to pedal digit II, and a relatively small pedal ungual IV as synapomorphies of Ornithurae.

Comments. Ornithurae was coined by *Haeckel (1866)* for a group uniting all extant birds to the exclusion of *Archaeopteryx*, but the name was largely abandoned by subsequent authors in favour of Neornithes *Gadow, 1892* (which is now widely used for the avian crown group) (*Gauthier, 1986*). However, Ornithurae was later adopted in palaeontological literature for a group including crown birds, Hesperornithes, and *Ichthyornis* (*Martin, 1983*). *Gauthier (1986)* was the first to propose a phylogenetic

definition for Ornithurae, a maximum-clade definition referring to all taxa more closely related to crown birds than to *Archaeopteryx*. *Chiappe (1991)* suggested a minimum-clade definition, referring to a less inclusive clade composed of the last common ancestor of Hesperornithes and crown birds, and all of its descendants, whereas *Gauthier & de Queiroz (2001)* advocated for an apomorphy-based definition, referring to the clade characterized by a tail shorter than the femur, with an upturned, ploughshare-shaped pygostyle composed of fewer than six segments and shorter than the free part of the tail, homologous with that of *Vultur gryphus*.

Both the maximum-clade (*Sereno, 1998*; *Longrich, 2009*) and apomorphy-based (*Clarke, 2004*; *Huang et al., 2016*) definitions of Ornithurae have been used in recent literature. The majority of recent authors, however, apply the name to a clade similar in scope to that circumscribed by the minimum-clade definition of *Chiappe (1991)* (*e.g.*, *O'Connor, Chiappe & Bell, 2011*; *Mayr, 2017a*; *Cau, 2018*; *Cordes-Person et al., 2020*; *Pittman et al., 2020a*; *Wang et al., 2020a*), though *Ichthyornis* is often stated or implied to be a member of Ornithurae by definition (*e.g.*: *Padian, 2004*; *O'Connor et al., 2015*; *Dumont et al., 2016*; *O'Connor, Wang & Hu, 2016*; *Buffetaut & Angst, 2019*; *Chiappe & Bell, 2020*), even under topologies where it is found stemward of Hesperornithes. Given the apparent utility of having a name for the least inclusive clade containing crown birds, *Ichthyornis*, and Hesperornithes, the prevailing usage of the name Ornithurae, and the absence of alternative names that have been previously defined for the same group, we have chosen to establish Ornithurae as corresponding to this clade. Additionally, due to ongoing disagreement regarding the interrelationships among *Ichthyornis*, Hesperornithes, and crown birds, this definition of Ornithurae will likely allow the group to remain more stable in scope compared to a definition anchored solely on Hesperornithes and crown birds.

Ichthyornithes *Marsh, 1873b*, converted clade name

Registration number. 555

Definition. The largest clade containing *Ichthyornis dispar Marsh, 1872a* but not *Hesperornis regalis Marsh, 1872b* and *Vultur gryphus Linnaeus, 1758* (Aves or Neornithes). This is a maximum-clade definition.

Abbreviated definition. Max ∇ (*Ichthyornis dispar Marsh, 1872a* ~ *Hesperornis regalis Marsh, 1872b* & *Vultur gryphus Linnaeus, 1758*).

Reference phylogeny. Figure 31 in the present study should be considered the primary reference phylogeny. Figure ED6 (Extended Data 6) in *Benito et al. (2022)* and Fig. S1 in *Wang & Zhou (2020)* may be regarded as secondary reference phylogenies.

Composition. At present, *Ichthyornis dispar* and the recently described *Janavis finalidens* (*Benito et al., 2022*) are the only well-corroborated named taxa within Ichthyornithes. However, fragmentary remains that may represent distinct, currently unnamed species within this clade have been identified by previous studies (*e.g.*, *Nessov, 1992*; *Bell &*

Everhart, 2011; *Longrich, Tokaryk & Field, 2011*; *Porras-Múzquiz, Chatterjee & Lehman, 2014*; *Zelenkov, Averianov & Popov, 2017*).

Diagnostic apomorphies. Synapomorphies shared by *Ichthyornis dispar* and *Janavis finalidens* include amphicoelous cervical vertebrae, an acromion process projected less cranially than the scapular articulation surface for the coracoid and the presence of an internal index process on manual phalanx II:1 (*Benito et al., 2022*). In the present study these are instead recovered as autapomorphies of *Ichthyornis*, as *Janavis* was not included.

Comments. Due to its monotypic status until the recent description of *Janavis* (*Benito et al., 2022*), the name Ichthyornithes has only been occasionally used in recent literature. However, when it is used, it generally denotes a lineage that includes *Ichthyornis* and excludes crown birds and Hesperornithes (*e.g.*: *Longrich, Tokaryk & Field, 2011*; *Zelenkov, Averianov & Popov, 2017*), and a maximum-clade definition for Ichthyornithes was proposed by *Clarke (2004)*, referring to all taxa more closely related to *Ichthyornis* than to crown birds. We have followed this proposal here, though we additionally include *Hesperornis* as an external specifier. A clade uniting *Ichthyornis* and Hesperornithes to the exclusion of crown birds has not been supported by most recent analyses, but cannot be entirely rejected at this time (*Hartman et al., 2019*). In the event that such a clade is recovered by future studies, a name for the lineage more closely related to *Ichthyornis* than to Hesperornithes would likely find utility, and Ichthyornithes would be suited to this purpose given its current usage.

SYSTEMATIC PALAEONTOLOGY
Avialae *Gauthier, 1986*
Ornithurae, *Haeckel, 1866*
Ichthyornithes *Marsh, 1873b* *sensu* *Clarke, 2004*
Ichthyornis dispar *Marsh, 1872a*

Holotype: YPM 1450, a partial skeleton consisting of portions of the skull, mandible, most of the axial elements, pectoral girdle, wings and hindlimbs. The specimen was illustrated and described most recently by *Clarke (2004)*, with additional elements identified and described by *Field et al. (2018b)*.

Locality and horizon: YPM 1450 was collected from sediments of the Smoky Hill Chalk Member, Niobrara Formation, near the Solomon River in Section 1, Township 6, Range 19, in Rooks County (*Marsh, 1880*; *Brodkorb, 1967*; *Clarke, 2004*).

Referred specimens in this study: ALMNH:Paleo:1043, 1310, 1311, 1314, 1319, 1677, 1786, 3316, 3412; BHI 6420, 6421; FHSM VP-18702; KUVP 2281, 2284, 2300, 25469, 25471, 25472, 119673, 123459, 157821; MSC 2841, 3394, 5794, 5895, 5916, 5937, 6200, 6201, 6002, 7841, 7842, 7844, 13214, 13868, 34426, 34427; NHMUK A 905; YPM 1461, 1724, 1733, 1740, 1741. See Table 1 for summaries of the material associated with each specimen.

Diagnosis: Following *Clarke (2004)*, *Ichthyornis dispar* shows the following autapomorphies: a single large pneumatic foramen located on the craniomedial surface of the corpus of the quadrate, amphicoelous or biconcave cervical vertebrae, anterior free caudal vertebrae with well-developed prezygapophyses clasping the dorsal surface of the preceding vertebra, an extremely diminutive acromion process of the scapula, a pit-shaped fossa for muscle attachment at the distal end of the humeral bicipital crest, the length of the trochlear surface along the caudal surface of the distal ulna approximately equal to the width of the trochlear surface, an oval scar on the caudoventral surface of the distal radius, a large turbercle close to the articular surface for phalanx II:1 in the carpometacarpus, and the presence of an internal index process on manual phalanx II:1 (*Clarke, 2004*). Three of these (amphicoelous cervical vertebrae, diminutive acromion process of the scapula and an internal index process on manual phalanx II:1) were found to be present in the recently described Maastrichtian ichthyornithean *Janavis finalidens*, and were recovered as synapomorphies of Ichthyornithes instead (*Benito et al. 2022*).

ANATOMICAL DESCRIPTION

Presacral vertebrae

Seven of the newly described specimens preserve some vertebral material. Three of them—KUVP 25472, KUVP 119673, and ALMNH:Paleo:3316—preserve a significant portion of the axial series (Figs. 4–7), although no complete vertebral columns are yet known for *Ichthyornis*. BHI 6421 preserves three isolated thoracic vertebrae, with two of which are extremely fragmentary. FHSM VP-18702 preserves two complete but severely distorted cervical vertebrae, as well as a complete but poorly preserved synsacrum. KUVP 157821 preserves a complete synsacrum, and KUVP 2471 preserves only a single very fragmentary thoracic vertebra.

KUVP 25472 preserves the highest presacral vertebral count yet known for *Ichthyornis*, with five cervical (Figs. 4 and 5) and nine thoracic vertebrae (Figs. 6 and 7), most of them in an exceptional state of preservation, as well as three caudal vertebrae. Of these, only two posterior thoracic and two of the caudal vertebrae are articulated. KUVP 119673 preserves the highest total vertebral count of any *Ichthyornis* specimen known to date, with eight cervical vertebrae, three anterior thoracic vertebrae, a complete synsacrum, and three caudal vertebrae. KUVP 119673 is remarkable as well for being the only specimen known to preserve a significant portion of its vertebral column in articulation, with at least seven of the cervical vertebrae and the anterior thoracic vertebrae preserved in anatomical connection, although five of the posterior cervical vertebrae are badly distorted and crushed against one-another (Fig. 4). ALMNH:Paleo:3316 preserves the axis, two fragmentary posterior cervical vertebrae (Fig. 4), two anterior and two posterior thoracic vertebrae, and a partial synsacrum.

The wealth of axial material preserved among the new specimens included in this study contrasts with the limited number of vertebrae previously described for *Ichthyornis*, although both *Marsh (1880)* and *Clarke (2004)* extensively described and illustrated the limited YPM axial material. Of the previously described specimens, only four, including the holotype (YPM 1450), preserve axial material (*Marsh, 1880*; *Clarke, 2004*). YPM 1733
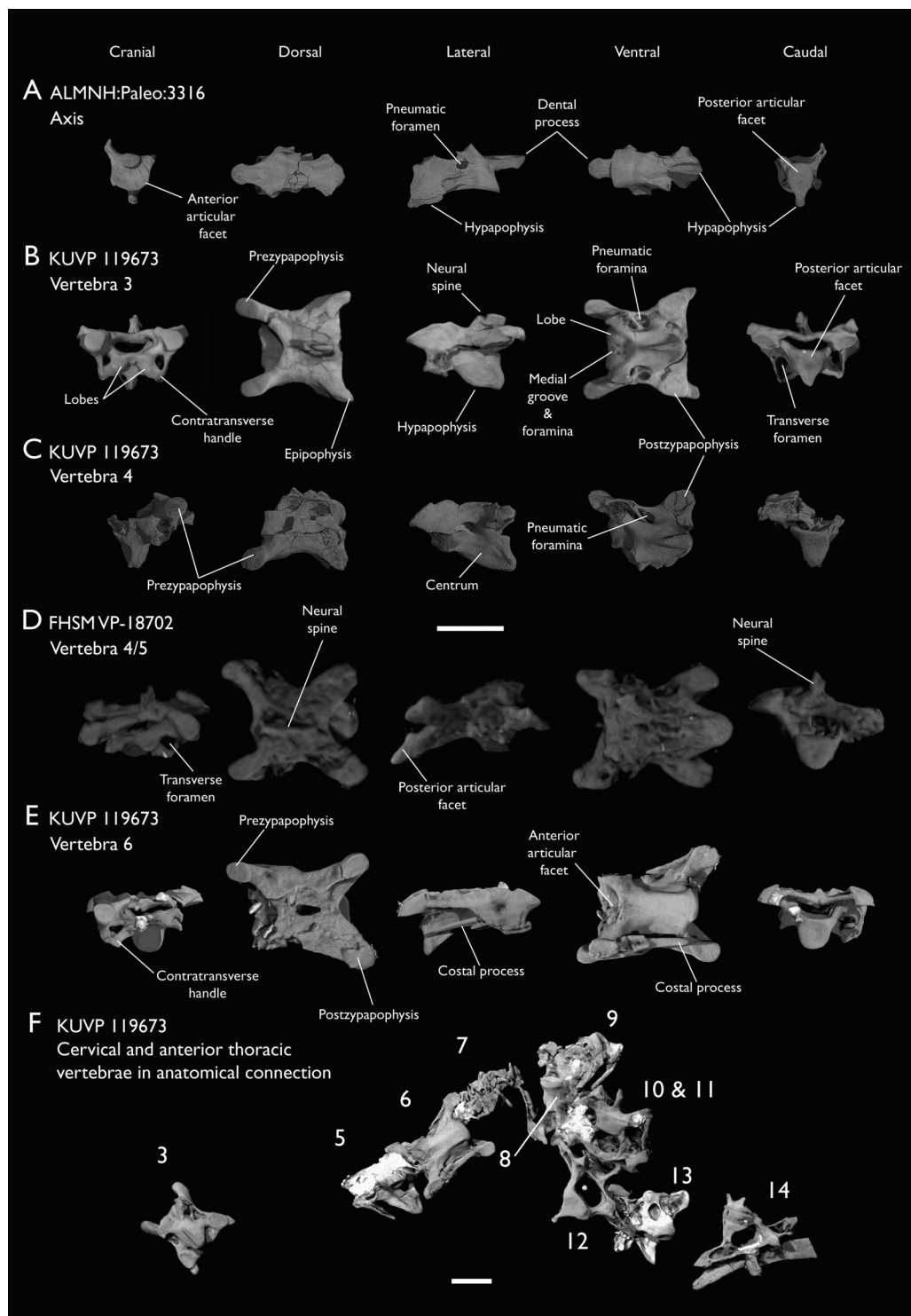
Figure 4 Anterior cervical vertebrae of *Ichthyornis*. (A) ALMNH:Paleo:3316 axis, (B) KUVP 119673 3rd cervical, (C) KUVP 119673 4th cervical, (D) FHSM VP-18702 possible 4th or 5th cervical, and (E) KUVP 119673 6th cervical, in cranial, dorsal, lateral, ventral, and caudal views. (F) KUVP 119673, cervical and anterior thoracic vertebrae in anatomical connection as preserved in the specimen, with probable vertebral numbers indicated. Scale bar equals 5 mm.
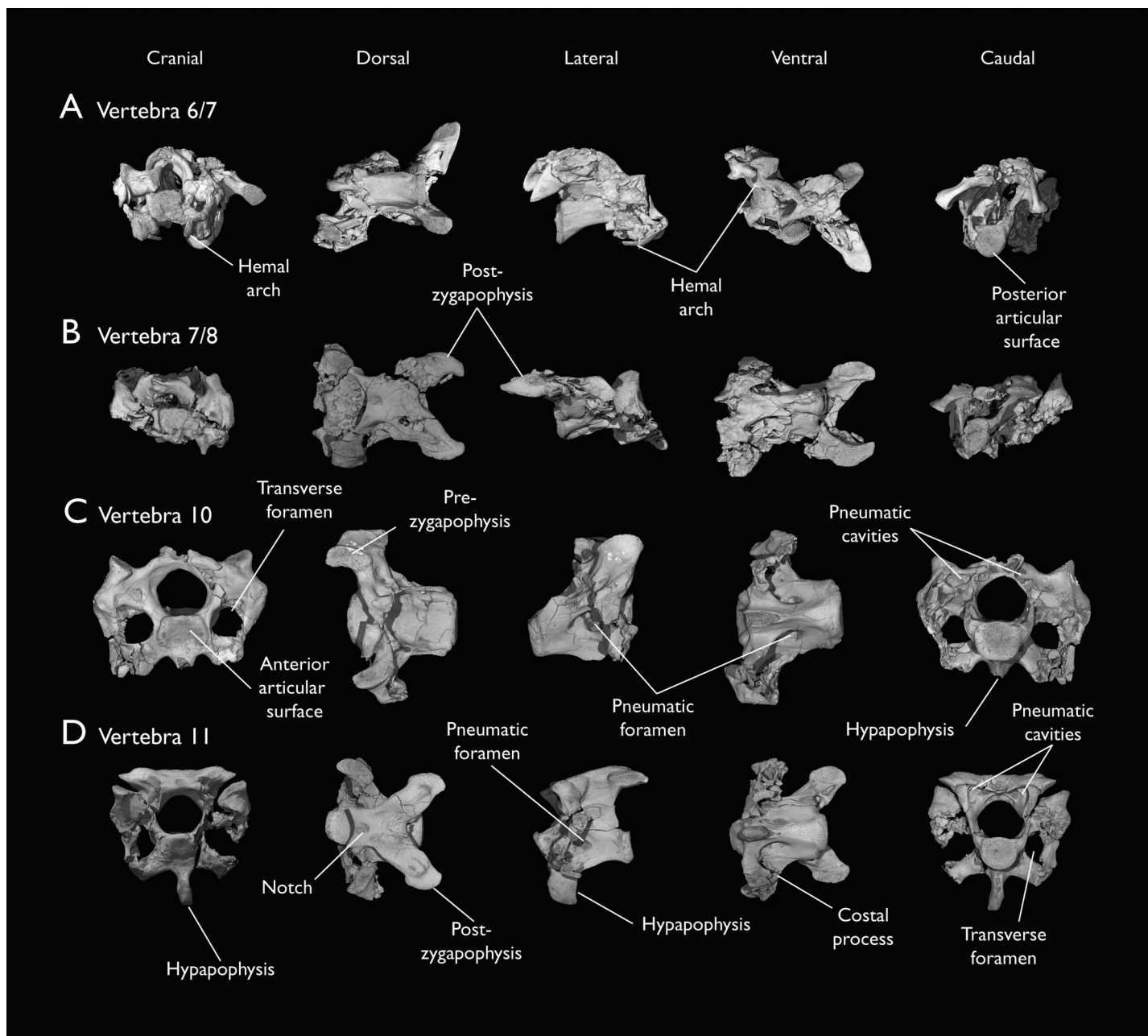
Figure 5 Mid and posterior cervical vertebrae of *Ichthyornis* specimen KUVP 25472. (A) 6th or 7th cervical vertebra, (B) 7th or 8th cervical vertebra, (C) 10th cervical vertebra and (D) 11th cervical vertebra; in cranial, dorsal, lateral, ventral, and caudal views. Scale bar equals 5 mm.

exhibits the highest vertebral count among the YPM specimens, with four cervical vertebrae and six thoracic vertebrae, as well as a complete synsacrum. In total, the YPM material includes 19 presacral vertebrae, three synsacra and possibly six caudal vertebrae, while the new specimens preserve 38 presacral vertebrae, four partial or complete synsacra, and six caudal vertebrae.
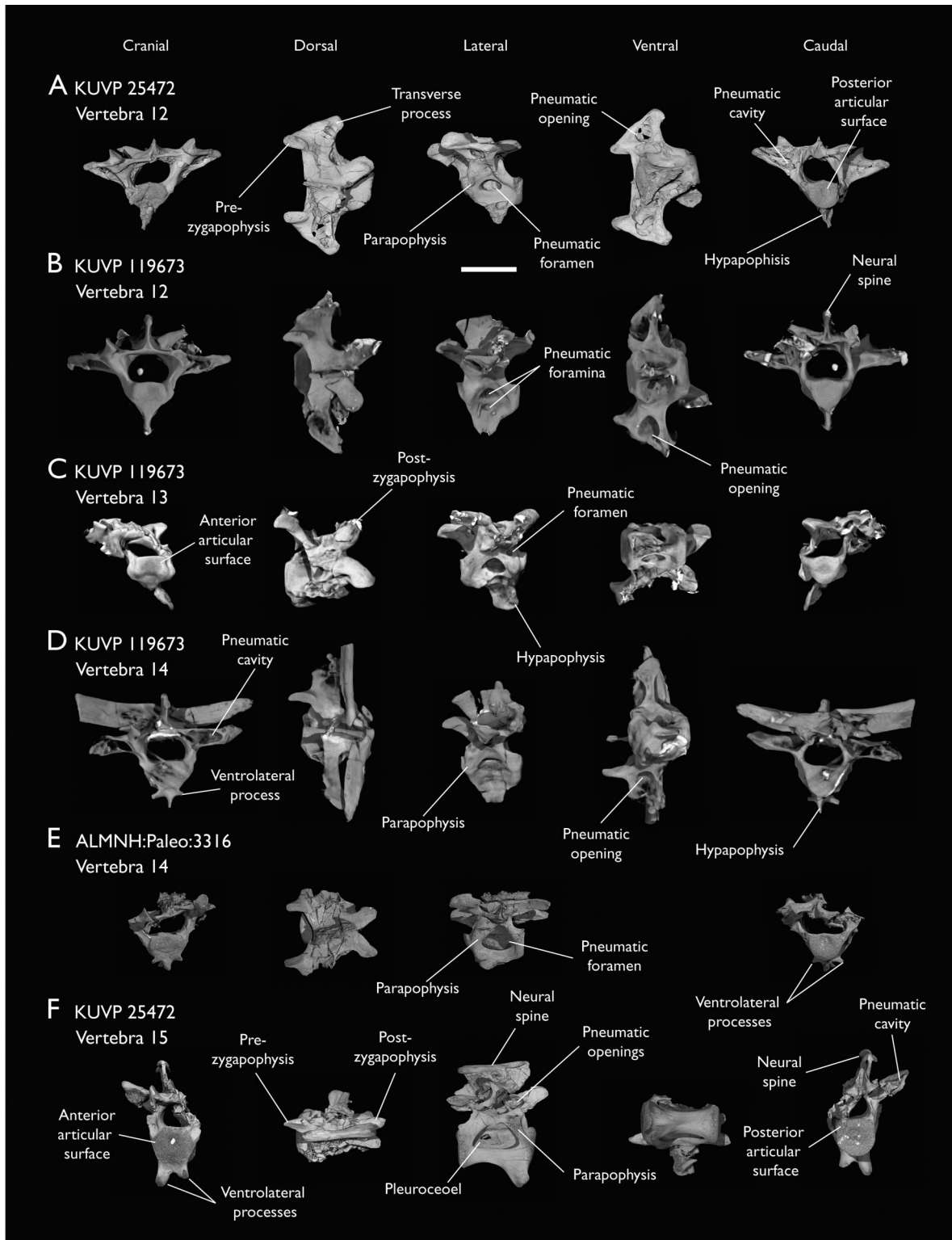
Figure 6 Anterior thoracic vertebrae of *Ichthyornis*. (A) KUVP 25472 12th vertebra, (B) KUVP 119673 12th vertebra, (C) KUVP 119673 13th vertebra, (D) KUVP 119673 14th vertebra, (E) ALMNH:Paleo:3316 13th vertebra, and (F) KUVP 25472 15th vertebra, in cranial, dorsal, lateral, ventral, and caudal views. Scale bar equals 5 mm.
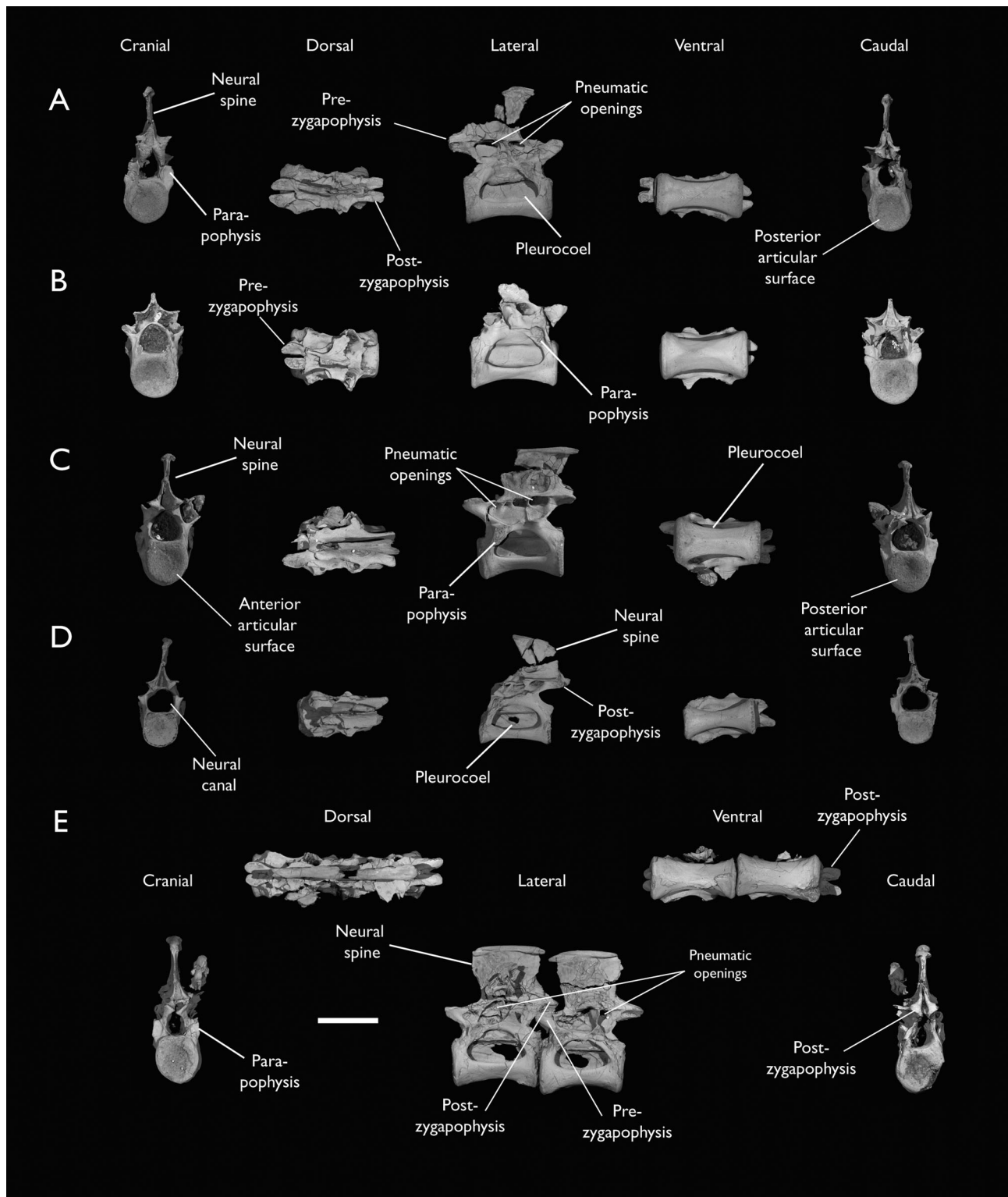
Figure 7 Mid-to-posterior thoracic vertebrae of *Ichthyornis* specimen KUVP 25472. (A) Indeterminate mid thoracic vertebra 1, (B) indeterminate mid thoracic vertebra 2, (C) indeterminate mid thoracic vertebra 3, (D) indeterminate posterior thoracic vertebra 1, (E) 2 mid-thoracic vertebrae in anatomical connection; in cranial, dorsal, lateral, ventral, and caudal views. Scale bar equals 5 mm.

In spite of the considerable amount of new vertebral material, it is currently impossible to establish a precise total vertebral count for *Ichthyornis*, although the new specimens offer a much better opportunity for estimating this figure, enabling comparisons with other Mesozoic avialans. The vertebrae preserved in KUVP 25472 and 119673 indicate a minimum number of 21 presacral vertebrae, with at least eleven cervical vertebrae (including the axis and atlas) and ten thoracic vertebrae. This estimate is the same as that of *Marsh (1880)*, who based his estimate on the axial skeleton of the extant tern *Sterna maxima*, although he considered the incompletely fused first sacral vertebra of *Ichthyornis* (YPM 1732) the caudal-most thoracic vertebra (*Clarke, 2004*). Although it is not possible to verify this vertebral count without additional, more complete specimens, similar presacral counts have been described for the few Mesozoic euornitheans preserving sufficiently complete vertebral columns, such as *Yixianornis* with 22 presacral vertebrae (12 cervical and 10 thoracic; *Clarke, Zhou & Zhang, 2006*), and the hesperornitheans *Hesperornis* and *Parahesperornis*, both with 23 presacral vertebrae, although in Hesperornithes the relative count of cervical vertebrae is notably higher (17 cervical and six thoracic; *Marsh, 1880*; *Bell & Chiappe, 2020*).

The abundance of new vertebral material described here, and especially the quality of preservation of the articulated presacral series in KUVP 119673, allow a more precise estimate of the relative position of each vertebra than was previously possible based on the more fragmentary YPM material (*Clarke, 2004*), although establishing the absolute position of each vertebra remains impossible. Thus, each vertebra will henceforth be referred to by its most probable position or positions (*e.g.*, "8th or 9th cervical vertebra") instead of the alphabetical system used by *Clarke (2004)*, which, although appropriate for the lower vertebral counts preserved among the YPM specimens, is unnecessary in view of the improved completeness of the new material.

Cervical vertebrae

The axis of *Ichthyornis* was previously known from YPM 1733, where it is attached to the atlas, and YPM 1755, where it is isolated (*Clarke, 2004*). A fragmentary and poorly preserved axis is also known from AMNH FARB 32773 (*Torres, Norell & Clarke, 2021*). The morphology exhibited by ALMNH:Paleo:3316 is mostly congruent with that described by *Marsh (1880)* and *Clarke (2004)*. The axis of ALMNH:Paleo:3316 is missing its neural arch, preserving most of the centrum with the exception of the costal processes, which are broken at their bases (Fig. 4A). The corpus of the axis is elongated and exhibits a single large pneumatic foramen on either side, ventrally bounded by the caudally directed costal processes. The atlanteal articulation surface is completely preserved: it is round and moderately concave, with a large and well-developed dental process (processus odontoideus; *Livezey & Zusi, 2006*). No remains of the atlanteal centrum are preserved attached to the axis of ALMNH:Paleo:3316, in contrast to the otherwise similarly preserved axis of YPM 1755, in which a portion of the atlas is co-ossified to the anterior articular surface, separated by a clear suture, and to YPM 1733 in which both vertebrae are completely fused with no suture visible, perhaps indicating an earlier developmental stage for ALMNH:Paleo:3316. The hypapophysis or ventral crest (crista ventralis corporis;

Baumel & Witmer, 1993) of the axis was described by *Clarke (2004)* as being prominent though incomplete, missing its tip in both YPM specimens. However, this structure appears complete in ALMNH:Paleo:3316 (Fig. 4A), and its shape is virtually indistinguishable from that illustrated for YPM 1755, revealing that the axial hypapophysis of *Ichthyornis* was robust and proportionally short, exhibiting a very limited ventral expansion and a flat and broad ventral margin, extending further caudally than the posterior articular surface of the axis. The preservation of the axis is uncommon amongst Mesozoic euornitheans, but the condition of the hypapophysis in *Ichthyornis* appears better developed than the condition in *Parahesperornis* (*Bell & Chiappe, 2020*). In contrast, the hypapophysis of many crown birds is substantially more ventrally extended, as in *Anser albifrons* (Anseriformes) and *Sterna hirundo* (Laridae). The posterior articular surface of the axis is laterally compressed and subtriangular in caudal view (Fig. 4A), and, as described by *Marsh (1880)* and *Clarke (2004)*, exhibits an incipient heterocoelous condition, with a slightly laterally and ventrally convex articular surface becoming concave medially.

The third cervical vertebra is only preserved in KUVP 119673 (Fig. 4B), in which it is mostly undistorted, exhibiting only minor dorsoventral compression, and its morphology is virtually indistinguishable from that of YPM 1733 (*Clarke, 2004*) and AMNH FARB 32773 (*Torres, Norell & Clarke, 2021*), although it is more complete, exhibiting both pre- and postzygapophyses. The vertebra is strongly heterocoelous, with a short and laterally compressed centrum and a broad neural arch. As noted by *Clarke (2004)*, the anterior articular surface of the third cervical is unique amongst all surveyed crown and stem avialans, with a cranially displaced articular surface. The anterior facet is angled dorsoventrally, exhibits a flat dorsal margin, and in contrast with the clearly concave articular surface in all other surveyed taxa, is composed of two lobes separated by a medial groove, which is pierced by four tiny holes, likely corresponding to nutrient foramina (Fig. 4B). These lobes extend ventrolaterally onto the robust and ventrally projected costotransverse handle (ansa costotransversaria, *Baumel & Witmer, 1993*), which bound the minute transverse foramina, and do not extend into caudally directed costal processes. No pneumatic foramina pierce the lateral surfaces of the centrum, although extensive pneumatic excavations are present in the lateral neural laminae and ventral surfaces of the neural arch just caudal to the transverse foramina. The posterior articular facet is high, strongly laterally compressed, and subtriangular in shape, similar to that of the axis, but slightly mediolaterally broader, and its articular surface is flat to moderately concave. The articular surface is continuous with the caudal and ventral edges of the robust and high hypapophysis (Fig. 4B). The neural arch is mediolaterally broad, with a mostly flat dorsal surface and a highly concave anterior margin and large and cranially displaced ovoid prezygapophyses. The posterior margin of the neural arch is mostly flat, with a medial notch, and is coplanar with the posterior articular surface. The neural spine is short craniocaudally but moderately high dorsoventrally, with a slightly hooked posterior edge. The postzygapophyses have broad and rounded ventral articular surfaces, and minute and caudally directed epipophyses extend from their posterior end (Fig. 4B).

Although establishing the absolute position of the rest of cervical vertebrae is presently impossible, the preservation of seven articulated contiguous cervical vertebrae in KUVP 119673 (Fig. 4F) is of key importance for reconstructing the order of the cervical vertebrae. This specimen reveals a continuous degree of variation in the shape of the posterior articular facets, which are laterally compressed and subtriangular in the anterior cervicals (Figs. 4A–4C), subquadrangular halfway through the series (Figs. 4D, 4E and 5A), and mostly round in the posterior cervicals (Figs. 5B–5D). Thus, by examining the variation in articular shape between the isolated third cervical of KUVP 119673, an additional isolated cervical from the same specimen (here interpreted as the fourth) and the first vertebra of the articulated series, we interpret that only one cervical vertebra is currently missing, and that the articulated vertebrae in KUVP 119673 (Fig. 4F) extend from the sixth to the thirteenth, including the three first thoracic vertebrae. All of the cervical vertebrae preserved in FHSM VP-18702, KUVP 25472 and ALMNH:Paleo:3316 can be matched to one of these vertebrae in KUVP 119673, although in many cases it remains difficult to establish their precise position, especially in light of the poor state of preservation of the seventh to tenth vertebrae of KUVP 119673 (Fig. 4F).

The middle to posterior portion of the cervical vertebral series, extending from the fourth to the ninth vertebrae, are well represented amongst the new specimens, particularly in KUVP 119673 (fourth, and six to ninth; Figs. 4C, 4E and 4F), but also in FHSM VP-18702 (fourth/fifth and seventh/eighth; Fig. 4D), and in KUVP 25472 and ALMNH:Paleo:3316 (with three and two vertebrae respectively, in both cases falling between positions six to eight; Figs. 5A and 5B). In contrast, only a single vertebra from this cervical region has been previously described: YPM 1733D of *Clarke (2004)*, which *Marsh (1880)* interpreted as the tenth cervical, but here is interpreted as either the eighth or ninth vertebra. The morphologies of these vertebrae are very similar across the whole series, with continuous variation in the shape of the different vertebral features extending caudally. These vertebrae are craniocaudally long and, at least in comparison with the posteriormost cervicals, dorsoventrally low (Figs. 4D and 4E). Their centra lack hypapophyses, and instead exhibit robust and arched carotid processes (processus caroticus; *Baumel & Witmer, 1993*) extending ventrally from their contratransverse handles (Fig. 5A). These carotid processes are smaller on the anterior vertebrae and become progressively more pronounced caudally across the series. The cranial articular surfaces are strongly caudoventrally angled, with a robust dorsal margin in the anterior vertebrae, and progressively more ventrally extended lateral margins in the posterior vertebrae, defining a flat to concave articular surface which is unbounded ventrally (Figs. 4E, 5A, 5C and 5D). The contratransverse handles define proportionally small transverse processes, and extend caudally into costal processes (resulting from the fusion of the cervical ribs), which, when complete, reach the posterior articular surface of the vertebra (Fig. 4E). The centrum is strongly angled ventrally in the anterior vertebrae of the series (most notably, in the fourth, Fig. 4C), but become progressively straighter moving caudally across the series. No pneumatic foramina pierce the centrum in these mid to posterior cervical vertebrae, but as in the third vertebra, numerous pneumatic openings are found between the neural laminae and the ventral surface of the neural arch (Figs. 4B and 4C), with one major

foramen just anterior to the transverse foramen and another one just posterior to it, both opening into the internal trabecular structure of the neural arch, and more minute foramina surrounding them. The posterior articular surface, as described above, ranges from subtriangular, to quadrangular, to mostly round across the series, being flat to moderately concave in all cases. Both the cranial and caudal margins of the neural arch are concave, in contrast to the third cervical, which exhibits a straight caudal margin (Fig. 4B). Both pre- and postzygapophyses extend substantially beyond the cranial and caudal extent of the centrum, and although these appear to be more rounded in the anterior vertebrae and more pointed in the posterior ones, they are distorted in most of the studied cervical vertebrae. No epipophyses are present, in contrast to the condition in the third cervical vertebra. The caudoventral surface of the postzygapophyses is extensively excavated by pneumatic cavities and openings (Figs. 5A and 5B), although this region is compressed in all the new specimens. By contrast, this region is well preserved in YPM 1733, and was extensively figured and discussed by *Clarke (2004)*. No dorsal processes are completely preserved across this region of the cervical series.

The posterior cervical vertebrae exhibit a distinct morphology as noted by both *Marsh (1880)* and *Clarke (2004)* and are here identified as the tenth and eleventh vertebrae (Figs. 5C and 5D). These were both previously represented only in the *Ichthyornis dispar* holotype, YPM 1450, although in that specimen they are badly distorted and incomplete (*Clarke, 2004*). These were interpreted by *Marsh (1880)* as the 12th and 14th vertebrae, and as likely more cranially situated by *Clarke (2004)*. Both the tenth and eleventh vertebrae are preserved in KUVP 119673 (although they are badly crushed into each other; Fig. 4F), and in KUVP 25472 (where they are in exceptional condition; Figs. 5C and 5D). These vertebrae are comparatively craniocaudally short and dorsoventrally high. Their anterior articular surfaces are moderately concave, similar to those of the preceding vertebrae, with broad and robust dorsal and lateral margins, which are more pronounced in the tenth (Fig. 5C) than in the eleventh vertebra (Fig. 5D). Unlike in the preceding vertebrae, a large hypapophysis extends ventral to the articular surface, which is narrow and bladelike in the tenth vertebra (Fig. 5C) and more robust and broader in the eleventh, with a flat and slightly bifurcated ventral margin (Fig. 5D), as described by *Clarke (2004)*. Very large and round transverse foramina are delimited by the contratransverse handles, which extend caudally into broad but short costal processes (Figs. 5C and 5D). Very large pneumatic openings pierce the lateral surfaces of the centrum on both vertebrae; these are asymmetrical between both sides and expose the internal trabecular structure of the centrum. The caudal articular surface is round and slightly concave, with a flat dorsal surface. The neural arch is high and delimits a very large neural canal. The neural arch is moderately arched and dorsally convex in the tenth vertebra, whereas it is mostly flat in the eleventh, with a tear-shaped shallow groove on its anterior edge (Fig. 5D). The prezygapophyses are ovoid in shape and extend only moderately beyond the anterior surface of the centrum; these are ventromedially inclined in the tenth vertebra and flat in the eleventh, coplanar with the dorsal surface of the neural arch. The postzygapophyses are broad and caudolaterally oriented, and, as in the preceding vertebrae, show extensive

caudoventral pneumatic excavations and openings, which are best preserved in the eleventh cervical of KUVP 25472 (Fig. 5D).

The cervical series tends to be poorly preserved and heavily distorted in most known Mesozoic avialans (this is especially true for euornitheans), complicating comparisons with *Ichthyornis*. Members of Hesperornithes preserve extensive axial remains, and in general their cervical vertebrae are more craniocaudally elongated, lower dorsoventrally, and narrower lateromedially, with proportionally shorter pre- and postzygapophyses (*Marsh, 1880*; *Bell & Chiappe, 2020*). However, their main difference with *Ichthyornis* is in the shape of the vertebral articular surfaces, which in Hesperornithes are markedly heterocoelous, concave on the anterior surface and strongly convex on the posterior one, as in most crown group birds (*Clarke, 2004*). As described above, the condition in *Ichthyornis* ranges from moderately heterocoelous in the anterior cervical vertebrae to amphicoelous or biconcave across the axial series. Heterocoelous cervical vertebrae are present in most euornitheans such as *Patagopteryx* (*Chiappe, 1996*, *2002*), *Apsaravis* (*Clarke & Norell, 2002*), *Khinganornis* (*Wang & Zhou, 2020*), *Piscivoravis* (*Zhou, O'Connor & Wang, 2014*), and *Iteravis* (*Zhou, O'Connor & Wang, 2014*). An intermediate condition similar to that of *Ichthyornis* has been described only in *Yixianornis* (*Clarke, Zhou & Zhang, 2006*), but the flattened preservation of known *Yixianornis* specimens complicates an accurate reconstruction of its vertebral morphology, and a partially amphicoelous cervical series is currently only well-supported in *Ichthyornis*, optimizing as an autapomorphy for this taxon (see Phylogenetic Results).

Thoracic vertebrae

The thoracic vertebrae, distinguished by the absence of fused ribs and the presence of clear costal articulation facets, are well represented amongst the new specimens, with KUVP 119673 preserving the articulated cervicothoracic transition, including the first three thoracic vertebrae (12th to 14th presacrals; Fig. 4F), KUVP 25472 preserving the first, second and fourth thoracic vertebrae (12th, 13th and 15th presacrals; Figs. 6A and 6F) and six mid-to-posterior thoracic vertebrae (Fig. 7), ALMNH:Paleo:3316, perserving the first three thoracic vertebrae and two indeterminate mid-thoracic vertebrae in a fragmentary state, and BHI 6420 preserving three indeterminate mid-thoracic vertebrae. Although no specimen appears to preserve the complete thoracic series, the new specimens show that *Ichthyornis* had at least ten thoracic vertebrae, including four anterior vertebrae with distinct morphologies spanning the cervicothoracic transition, which can be matched in several of the studied specimens, and at least six morphologically homogeneous mid-to-posterior thoracic vertebrae, as shown by KUVP 25472 (Fig. 7).

The three anteriormost thoracic vertebrae (12th to 14th presacrals) are distinct from the rest of the series and share several morphological features with the posteriormost cervical vertebrae, being craniocaudally short and dorsoventrally high, and exhibiting extensive pneumatization and well-developed hypapophyses (Figs. 6A–6E). The anterior articular surface is, as in the posterior cervicals, moderately caudoventrally angled and slightly concave, becoming progressively less angled across the series, being almost flat and coplanar with the posterior articular surface in the third thoracic. The dorsolateral margins

of the anterior articular surface are bounded by large and marked ovoid parapophyses (eminentia costolateralis; *Baumel & Witmer, 1993*) for the articulation with the ribs; these are low and do not extend much from the surface of the centrum (Figs. 6A–6E). As in the posteriormost cervical vertebrae, the centrum is extensively pneumatized, with large openings occupying much of the centrum lateral surface exposing the interior trabecular structure of the centrum. These openings are irregularly sized and vary between well-defined ovoid openings to large cavities containing multiple small foramina, even between both sides of the same vertebra, as in the second thoracic of KUVP 25472 (Fig. 6A). Additional smaller pneumatic foramina are found in the centrum of some of the anterior thoracic vertebrae, but these vary in number and position between specimens and individual vertebrae. Both the first and second thoracic vertebrae of ALMNH:Paleo:3316 and the second thoracic of KUVP 25472 and 119673 exhibit small pneumatic foramina craniodorsally to the main pneumatic openings, just caudal to the parapophyses (Fig. 6C). A similarly sized foramen is found ventral to the main pneumatic opening, close to the base of the hypapophysis in the first thoracic of KUVP 25472 and 119673 (Fig. 6B), though this is absent in the equivalent vertebra in ALMNH:Paleo:3316. The caudal articular surfaces of the three anteriormost thoracic vertebrae are mostly round and moderately concave with flattened dorsal margins, being laterally and ventrally bounded by a thickened rim.

All three anterior thoracic vertebrae exhibit large and marked hypapophyses extending ventrally from their centra. These are thin and bladelike and are continuous with the anterior articular surface of the vertebrae, extending just cranial to the posterior articular surface. The hypapophyses of the first two thoracic vertebrae are as tall as the centrum, and are subtriangular to quadrangular in lateral view (Figs. 6A–6C). In contrast, the third thoracic has a low and more robust hypapophysis, half the height of the centrum in KUVP 119673, which exhibits two small tubercle-like ventrolateral processes extending from its anterior end, giving it a triradiate appearance (Figs. 6D and 6E). This triradiate morphology was described by *Marsh (1880)* and *Clarke (2004)* in the YPM 1733E and YPM 1733F vertebrae, which Marsh interpreted as the 15th and a posterior presacral, respectively. Both KUVP 119673 and ALMNH:Paleo:3316 exhibit a single vertebra with a triradiate morphology, whose articular surfaces approach the level of amphicoely of the posterior thoracic vertebrae, such that we consider it unlikely that more than one triradiate thoracic vertebra was present in the full axial series of *Ichthyornis*. Whether the presence of two such vertebrae in YPM 1733 is genuine can only be clarified by new specimens preserving this region in articulation.

All three anterior thoracic vertebrae sport broad neural arches which extend craniolaterally into large and wing-like transverse processes, as in *Hesperornis, Parahesperornis* (*Marsh, 1880*; *Bell & Chiappe, 2020*) and most crown group birds (*Baumel & Witmer, 1993*; *Livezey & Zusi, 2006*). These processes include ovoid prezygapophyses on their anterior margins. The anterior margins of these processes are flat to moderately concave, and the processes are caudally extended, defining hooked and strongly concave caudal margins (Figs. 6A and 6B). The transverse processes lack any clear articulation facets for the rib costal tubercles, exhibiting large and round pneumatic openings on their

ventral surfaces, and deep pneumatic cavities on their caudomedial surfaces (Figs. 6A, 6B and 6D). The neural spines are broken in most of the preserved vertebrae, with the exception of the second thoracic of KUVP 119673, in which the spine is thin and bladelike, similar in height to the ventral hypapophysis. The spine exhibits a straight anterior margin, and decreases in height caudally. The postzygapophyses are short and laterally flared, only extending slightly beyond the centrum caudally, defining a wedged caudal margin. Their posterior surfaces show moderate pneumatic excavations, which in no cases approach the extensive pneumatisation of the equivalent structures in the posteriormost cervicals.

The fourth thoracic vertebra (15th presacral) is only preserved in KUVP 25472 (Fig. 6F), which shows a transitional morphology between that of the anterior thoracic and the mid-to-posterior thoracic vertebrae, as reported by *Clarke (2004)* based on the equivalent vertebra of YPM 1450, which was interpreted as the 16th presacral vertebra by *Marsh (1880)*. The centrum, in contrast with that of the preceding vertebrae, is elongated and strongly mediolaterally constricted halfway through its length, giving it an hourglass-like appearance in ventral view (Fig. 6F). The anterior articular surface is moderately concave and bounded by a thickened rim, and is not caudoventrally inclined as in the anterior thoracic vertebrae, being instead vertical and coplanar with the posterior articular surface, giving the vertebra an authentic amphicoelous or biconcave appearance. Just ventral to the anterior articular surface, there are two large and robust lateroventral processes which are moderately craniolaterally directed. These are divided by a deep medial groove, and no medial hypapophysis is present, unlike in the preceding third thoracic vertebra (Fig. 6F). Large ovoid parapophyseal facets for the thoracic ribs are present just caudal to the dorsal edge of the anterior articular surface. The lateral surfaces of the centrum exhibit very large and deep concavities, cranially bounded by the parapophyses. These concavities do not perforate the surface of the bone, and are therefore not truly pneumatic in nature (Fig. 6F). As such, these openings are best interpreted as pulmonary fossae (*O'Connor, 2006*) or pleurocoels (*Mayr, 2021*), which in extant birds accommodate lung tissue or air sac diverticula, but do not pneumatize the interior cavities of the vertebra (*Mayr, 2021*). Such structures are widespread in the thoracic vertebrae of living charadriiforms and procellariiforms, but are absent in taxa possessing pneumatic vertebrae, which instead exhibit smaller lateral foramina more similar to those of the anterior thoracic vertebrae of *Ichthyornis* (*Mayr, 2021*). Similar lateral pleurocoels appear to be the norm among Mesozoic euornitheans, being present in all taxa with well-preserved thoracic vertebrae (*Mayr, 2021*), with the exception of Hesperornithes (*Bell & Chiappe, 2020*). The caudal articular surface of the fourth thoracic is mostly round and moderately concave, essentially identical to the anterior articular surface. The neural arch is distorted in KUVP 25472, but it exhibits short and broad prezygapophyses and very short postzygapophyses that differ from those of the preceding vertebrae in their very limited lateral extension. In contrast with the apneumatic centrum, the neural arch exhibits extensive pneumatic openings and cavities exposing its internal trabecular structure; these are most apparent on the lateral surface of the arch, just caudal to the prezygapophyses. The neural spine is completely preserved in KUVP 25472: it is quadrangular in lateral view and very tall, as dorsoventrally high as the centrum or the rest of the neural arch. The dorsal edge of the neural spine is

thickened, exhibiting very marked and hooked lateral edges which extend slightly beyond the rest of the crest caudally, giving it a "T" shape in caudal view.

The transition between single hypapophyses in the anterior thoracic vertebrae to paired ventrolateral processes, with an intermediate triradiate condition, is mirrored to an extent by several extant taxa, such as the larids *Sterna hirundo* and *Chroicocephalus novaehollandiae*, and the procellariiforms *Puffinus lherminieri* and *Pelagodroma marina*. By contrast, this pattern is absent in most other surveyed taxa such as *Crypturellus tataupa*, *Anseranas semipalmata, Charadrius vociferus* or *Jynx torquilla*, in which the number of hypapophyses/lateroventral processes remains constant across the cervicothoracic transition. The presence of strongly developed hypapophyses in the cervicothoracic transition has been documented in multiple aquatic crown group birds and has been suggested to be an adaptation for a strong underwater use of the neck (*Baumel & Witmer, 1993*), but the functional significance of the morphology found in *Ichthyornis* and in comparable extant marine soaring birds remains unclear.

The mid-to-posterior thoracic vertebrae are very similar in shape to the fourth thoracic vertebra, being truly amphicoelous, and exhibiting mediolaterally constricted centra with large apneumatic lateral pleurocoels, and marked ovoid parapophyses, though they lack any ventrolateral processes (Fig. 7). Their neural arches show very reduced pre- and postzygapophyses with no lateral deviations, likely due to the reduced mobility of this part of the axial skeleton, a condition which is widespread among the crown group birds surveyed. The lateral surfaces of the neural arch are also deeply excavated by pneumatic openings and cavities which puncture the bone surface (Fig. 7C); these openings extend from the caudal end of the prezygapophyses to the cranial end of the postzygapophyses. The neural spines are well preserved in several thoracic vertebrae of KUVP 25472, and, as in the fourth thoracic, are quadrangular in lateral view and very tall, with a thickened dorsal edge (Figs. 7A, 7C and 7E). Despite being the most numerous presacral vertebral group, with at least six being present in KUVP 25472, the mid-to-posterior thoracic vertebrae exhibit very little variation, and it is difficult to establish their order and any patterns of morphological variation throughout the series (Fig. 7). The relative size and shape of their articular surfaces remains constant across the different vertebrae in this region, contrary to the condition in the cervical vertebrae, and although the level of mediolateral constriction of the centrum varies, no clear relationship can be established between this feature and vertebral position. The two mid-to-posterior thoracic vertebrae in ALMNH:Paleo:3316 are noticeably more mediolaterally constricted than any of the vertebrae in KUVP 25472, but whether this corresponds to a specific region within the thoracic series or is an example of intra- or interspecific variation is currently unclear.

The moderately amphicoelous to completely amphicoelous thoracic vertebrae of *Ichthyornis* are unlike those of any crown group birds, with even taxa which otherwise exhibit very similar thoracic vertebral morphologies, such as larids and procellariiforms, showing heterocoelous thoracic vertebrae with concave anterior and convex posterior articular surfaces. Fully heterocoelous thoracic vertebrae are also found in Hesperornithes (*Marsh, 1880*; *Bell & Chiappe, 2020*, *2022*), *Apsaravis* (*Clarke & Norell, 2002*), and in *Khinganornis* (*Wang & Zhou, 2020*), in which they are opisthocoelous, and in

Table 2 Measurements of the synsacrum of *Ichthyornis* specimens. Maximum length corresponds to the total craniocaudal length of the ankylosed or fused vertebrae, not including disassociated sacral vertebrae. Acetabulum width is measured from the total width of the complete acetabulum transverse processes. Maximum width and height are provided for the cranialmost and caudalmost fused sacral vertebrae. Asterisks (*) denote measurements that might be unreliable due to breakage or distortion, but are included for completeness. All measurements are in mm. – = not measurable.

Specimen	Max. length	Acetabulum width	Cranial centrum width	Cranial centrum height	Caudal centrum width	Caudal centrum height
ALMNH:Paleo:3316	–	–	–	–	2.78	1.42
FHSM VP-18702	44.30	–	4.08	1.94*	2.70	1.50*
KUVP 119673	31.64	17.12	4.06	2.61	2.32	–
KUVP 157821	43.01	–	4.03	4.70*	2.59	2.43*

Patagopteryx (*Chiappe, 2002*), in which they are procoelous, but the detailed morphology of the vertebral articular surfaces is difficult to reconstruct for most fossil avialans due to poor preservation. A condition with amphicoelous thoracic vertebrae similar to that of *Ichthyornis* seems to be widespread among Mesozoic euornitheans, and has been inferred in *Yixianornis* (*Clarke, Zhou & Zhang, 2006*), *Piscivoravis* (*Zhou, O'Connor & Wang, 2014*), *Iteravis* (*Zhou, O'Connor & Wang, 2014*) and *Gansus* (*You et al., 2006*; *Wang et al., 2016*), but reconstructing the extent of this condition across Mesozoic euornitheans remains challenging.

Sacral vertebrae

The synsacrum is represented in four of the studied specimens, of which three preserve virtually the entire element: FHSM VP-18702, KUVP 119673, and KUVP 157821. The synsacrum of ALMNH:Paleo:3316 is divided into two matching fragments but appears to be missing the cranialmost sacral vertebrae. The preservation of FHSM VP-18702 is fairly poor, preventing the discernment of several salient morphological details, such as the morphology of most transverse processes and the clear delineation of several individual vertebrae. Despite the breakage of the transverse processes and several missing parts, both KUVP 157821 and ALMNH:Paleo:3316 show very little distortion, and the sacral vertebrae are easily distinguishable. KUVP 119673 is dorsoventrally flattened, and many of its morphological features are obscured by radiopaque inclusions. Nonetheless, this specimen shows minimal breakage and preserves most of the vertebral transverse processes. Synsacral measurements are provided in Table 2.

The number of fused sacral vertebrae varies among the studied specimens; the same was reported by *Clarke (2004)* in reference to the two complete synsacra in the YPM collection. YPM 1450 preserves ten vertebrae, but YPM 1732, a larger specimen, preserves twelve. They also differ in terms of which vertebra bears the perpendicular costal processes attaching to the acetabular area: this was reported to be the seventh vertebra in YPM 1450, and the ninth in YPM 1732 (*Clarke, 2004*). An additional *Ichthyornis* synsacrum was recently described by *Torres, Norell & Clarke (2021)*, including at least eight fused sacral vertebrae; however, the specimen is poorly preserved and crushed, complicating the identification of individual vertebrae. Both FHSM VP-18702 and KUVP 157821, the largest specimens investigated here, include twelve ankylosed vertebrae (Figs. 8A and 8C),
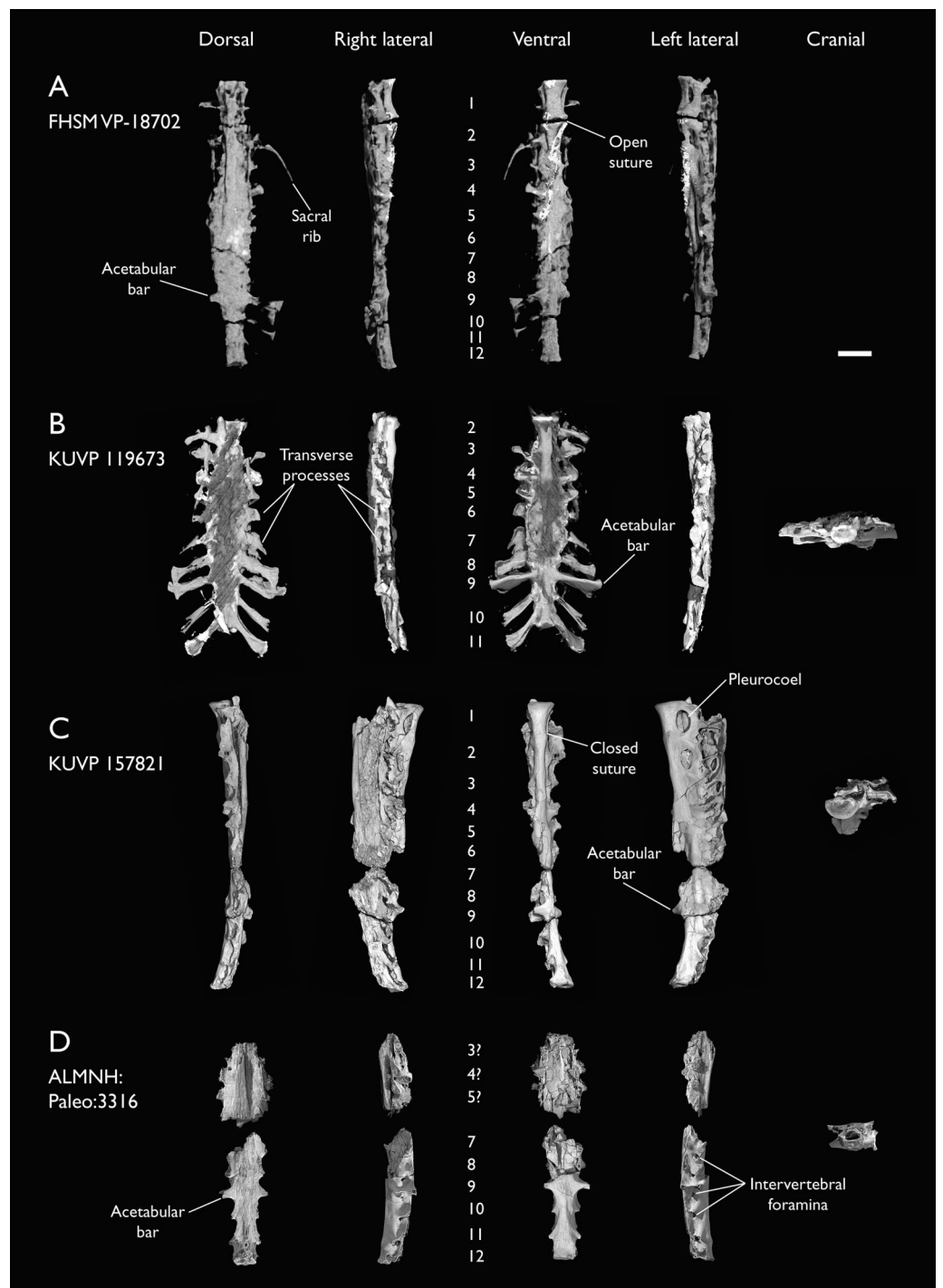
Figure 8 Synsacra of *Ichthyornis*. (A) FHSM VP-18702, (B) KUVP 119673 (C) KUVP 157821 and (D) ALMNH:Paleo:3316 in dorsal, right lateral, ventral, left lateral and cranial views. Numbers indicate sacral vertebral order. The 1st sacral vertebra in FHSM VP-18702 is incompletely fused, and the 1st and 11th sacral vertebrae in KUVP 119673 are unfused and not pictured here. Scale bar equals 1 cm.

although the poor preservation of FHSM VP-18702 makes it difficult to differentiate individual vertebrae. The first sacral of FHSM VP-18702, much larger than the second, is poorly ankylosed, connected only by ossified tendons dorsally, with a noticeable gap between its centrum and that of the second sacral (Fig. 8A). The same vertebra is fully fused in KUVP 157821, and no suture is visible (Fig. 8C). An intermediate condition seems to be present in YPM 1732, in which the first sacral is fully ankylosed to the second but a suture is clearly visible (*Clarke, 2004*). The acetabular bar is present in both specimens on the ninth vertebra. KUVP 119673, the smallest synsacrum, preserves only ten fused sacral vertebrae, with the acetabular bar on the eighth vertebra (Fig. 8B). Interestingly, a large, isolated vertebra with a dorsoventrally compressed centrum is preserved for KUVP 119673, which, given the size of its caudal articular surface, probably sits just cranial to the first fused sacral. The morphology and proportions of this vertebra match those of the first sacral of FHSM VP-18702 and KUVP 157821. Thus, this element probably represents the first sacral of KUVP 119673, even though it is unfused. From this point onwards, this element will be referred as the first sacral of this specimen. KUVP 119673 also differs from all other specimens in the number of postacetabular fused sacrals, exhibiting two distinguishable vertebrae instead of three. ALMNH:Paleo:3316 is incomplete, preserving ten vertebrae; however, given its size (which is comparable to that of KUVP 157821) and the presence of three postacetabular vertebrae, it is probably missing the two cranialmost sacrals (Fig. 8D).

The new specimens, therefore, bridge a gap between the YPM synsacra, revealing a pattern of vertebral fusion in which an additional sacral is added at both the cranial and caudal ends of the synsacrum. Given that the larger specimens are those with twelve fused vertebrae (Table 2), as well as the absence of a suture between the first and the second sacrals in KUVP 157821, we consider it likely that the differences among these specimens and the YPM synsacra are ontogenetic in nature. The largest specimens, KUVP 157821 and FHSM VP-18702, are respectively only 16.2% and 16.7% longer than KUVP 119673 (including the unfused first sacral and excluding the presumably missing last unfused postacetabular sacral), suggesting a late ontogenetic acquisition of complete bone fusion, as all specimens probably represent adults or subadults. A reduced number of fused sacral vertebrae in hatchlings and juveniles has been reported in Enantiornithes, with several immature specimens preserving variably five, six, or eight fused sacrals, with eight sacrals being the normal condition amongst adults (*Chiappe, Shu'An & Qiang, 2007*; *Knoll et al., 2018*). Developmental variability in the number of fused sacrals is less well-known in stemward euornitheans, and probable ontogenetic variation in sacral fusion has only been described in *Archaeorhynchus*, where early-stage juveniles exhibit completely unfused sacrals (*Foth et al., 2021*), with at least four of the seven sacrals fused in subadults (*Zhou, Zhou & O'Connor, 2013*) and a maximum of seven completely fused in fully-grown adults (*Zhou & Zhang, 2006*). The total number of fused sacrals varies among Mesozoic euornitheans, with seven in *Archaeorhynchus*, eight in *Zhongjianornis* (*Zhou & Li, 2010*) and *Abitusavis* (*Wang & Zhou, 2020*), nine in *Schizooura* (*Zhou, Zhou & O'Connor, 2012*), *Mengciusornis* (*Wang et al., 2020d*), *Patagopteryx* (*Chiappe, 2002*), *Similiyanornis*, *Yanornis* and *Yixianornis* (*Zhou & Zhang, 2001*; *Clarke, Zhou & Zhang, 2006*; *Wang &*

Zhou, 2020), ten in *Apsaravis* (*Clarke & Norell, 2002*) and *Gansus* (*You et al., 2006*; *Wang et al., 2016*), eleven in *Chaoyangia* (*O'Connor & Zhou, 2013*) and *Changmaornis* (*Wang et al., 2013b*), twelve in *Juehuaornis* (*Wang, Wang & Hu, 2015*), and, although unclear, between ten and fourteen in Hesperornithes (*Bell & Chiappe, 2016*, *2020*). This evidence suggests the possibility of a general crownward trend towards an increase in the number of fused sacrals across euornithean phylogeny. Although variation in sacral number and degree of sacral fusion is poorly characterized among crown birds, a greater degree of fusion in the posterior sacral vertebrae in more mature or older specimens has been reported in Anatidae (*Woolfenden, 1960*). The total number of fused sacral vertebrae shows a moderate degree of intraspecific variation among Anatidae (*Verheyen, 1955*; *Woolfenden, 1960*), Cuculiformes (*Berger, 1956*), and Gruiformes (*Hiraga et al., 2014*), with variation in total fused sacral count of up to two vertebrae documented. Although variation in the total number of documented sacral vertebrae has been suggested to be related differing counting approaches, this variation is considered to be genuine (*Berger, 1956*). However, the relationship between total number of fused vertebrae in the synsacrum and ontogenetic stage is poorly studied and deserves research attention.

The cranial articular surfaces of the first sacral in KUVP 157821 and FHSM VP-18702 are taphonomically compressed dorsoventrally (Figs. 8A and 8C). The unfused first sacral of KUVP 119673 reveals that the articular surface is dorsoventrally shortened with respect to the thoracic vertebrae, but is similarly moderately concave. The caudal articular surface is broken and obscured by radiopaque inclusions in KUVP 119673 and barely appreciable in FHSM VP-18702, but seems to be smaller than the cranial articular surface, matching with the substantial size and dorsoventral height reduction between the first and second sacrals in KUVP 157821. The vertebra bears small but elongate prezygapophyses, which are triangular in dorsal view. A small gap is present between the first two sacrals in FHSM VP-18702, and a suture is visible between them in YPM 1732, but no equivalent suture is visible in KUVP 157821, in which only a moderate ventrolateral tubercle or ossification is present (Fig. 8C). Only the first two sacral vertebrae in KUVP 157821 and FHSM VP-18702 show large and deeply excavated lateral pleurocoels, which are probably non-pneumatic (*O'Connor, 2006*; *Mayr, 2021*), similar to those of the thoracic vertebrae; in KUVP 119673 these are only observable in the first isolated sacral, as they are obscured by radiopaque inclusions caudally (Fig. 8B). Similar lateral excavations or pleurocoels in the anterior sacral vertebrae have only been rarely reported for Mesozoic euornitheans, although they occur in a possible ornithuran synsacrum from the Maastrichtian of Madagascar (*O'Connor & Forster, 2010*). The first fused sacral of KUVP 119673 bears minute prezygapophyses that barely extend beyond the cranial articular surface of the vertebra. These are presumably fused or ankylosed with the postzygapophyses of the first sacral in the other specimens. The third sacrals of KUVP 157821 and FHSM VP-18702 show lateral concave depressions, but these are not fenestrated nor deeply excavated, and therefore seem apneumatic. A similar condition is present in the first preserved sacral of ALMNH:Paleo:3316, here assumed to represent the third sacral (Fig. 8C). Only the first sacral of each specimen preserves clear parapophyses or articular surfaces for the sacral ribs similar to those of the thoracic vertebrae; the equivalent positions in the second, third
and fourth sacrals show a shallow concavity pierced by numerous minute foramina. The transverse processes of the first three vertebrae are thin and craniocaudally compressed in FHSM VP-18702 and KUVP 157821 (Figs. 8A and 8C)—in which they are fused to a portion of the iliac preacetabular wing, but in contrast, they are proportionally more robust in KUVP 119673, in which they extend into wide, caudolaterally directed wing-like structures similar to those preserved in several thoracic vertebrae (Fig. 8B). The fourth vertebra shows no lateral excavations, and its transverse processes are much more robust than those of the preceding vertebrae in all specimens. The transverse processes are dorsolaterally oriented and extend along the entire dorsoventral extent of the centrum. The ventral portion of each transverse process is short and wide, and meets the subtriangular, flange-like and laterally oriented dorsal portion, which is only preserved in KUVP 119673, forming a marked cranial cavity (Fig. 8B). The centra of these first four vertebrae are short and circular in cross-section, and, following the pronounced reduction in size between the first and second sacrals, become progressively narrower caudally. A moderate ventrolateral expansion marks the suture between the centra of each vertebra.

The following three sacral vertebrae are dorsoventrally flattened, with laterally expanded centra forming a plate-like surface in ventral view, from which it is difficult to distinguish individual vertebrae. Their transverse processes are only well preserved in KUVP 119673 (Fig. 8B). The transverse processes of the fifth sacral are similar in morphology to those of the 4th sacral, but with a thinner and craniocaudally compressed ventral portion and a shorter dorsal flange. The transverse processes of the sixth and seventh sacrals show minimal dorsoventral extension, and flat dorsal and slightly concave ventral surfaces. These processes are short, subquadrangular and laterally oriented on the sixth sacral vertebra, but longer and caudolaterally oriented on the seventh, with a caudal subtriangular expansion. The eighth sacral shows massively laterally expanded and elongate transverse processes, which lack any kind of ventral expansion. These are flat on both their dorsal and ventral surfaces, and are caudolaterally oriented and rectangular in shape, with a moderate caudolateral expansion at their lateral end, which contacts the processes of the ninth sacral caudally. Both the seventh and eighth sacral vertebrae show minute but deep lateral perforations just caudal to their transverse processes in ALMNH: Paleo:3316 (Fig. 8D), distinct from the large pleurocoels present in the anterior sacral vertebrae of KUVP 157821 and FHSM VP-18702 and those from the thoracic vertebrae, but these are either not preserved or not distinguishable in any of the other specimens. These likely correspond to the intervertebral foramina (Foramina intervertebralia; *Baumel & Witmer, 1993*), which allow the innervation of the neural canal and are often open in immature birds (*Baumel & Witmer, 1993*). While such foramina are not often preserved amongst fossil avialans, they are apparent in the synsacra described by *O'Connor & Forster (2010)*. The ninth sacral shows the largest and most laterally expanded transverse processes, which attach in the acetabular area and form robust acetabular bars. These are only completely preserved in KUVP 119673 (Fig. 8B), with the rest of the specimens preserving only the base of the processes. They show a dorsoventral expansion similar to those of the fourth and fifth sacrals, with the ventral portion of each process extending along the entire height of the centrum. The ventral portion is laterally oriented and

perpendicular to the main axis of the synsacrum; it is craniocaudally compressed and widens slightly on its ventral margin. Laterally, it expands into a flat and rounded articular facet for the ilium. The dorsal portions of the processes are similar in shape to those of the eighth sacral vertebra, and, in contrast to the ventral portions, are caudolaterally directed. A thin continuous sheet of bone extends dorsoventrally between both portions of the process in KUVP 119673, but this sheet is fenestrated in ALMNH:Paleo:3316. The extent of the fenestration varies between the right and left processes, with the fenestra constituting a small round hole in the middle of the sheet on the left process, and a significantly larger opening on the right process, to the extent that it appears to that the bone sheet is almost entirely absent (Fig. 8D). Similar to the previous two sacral vertebrae, ALMNH:Paleo:3316 shows tiny but deep intervertebral foramina in the ninth sacral, absent in the other specimens.

Caudal to the ninth sacral, the number of fused vertebrae varies among the specimens investigated here, with two vertebrae in KUVP 119673 (Fig. 8B) and three in the rest (Figs. 8A–8C). The tenth sacral is craniocaudally elongated, similar to the ninth, but the eleventh and twelfth are craniocaudally compressed. Their centra are narrow, with a low ridge running craniocaudally along their ventral surface. The contact between the eleventh and twelfth sacral vertebrae shows two moderately developed tubercles on its ventral surface, situated on either side of the aforementioned ridge. The caudal articular surface of the twelfth sacral is dorsoventrally short and almost quadrangular in shape, with a slightly concave caudal surface. The bases of the postzygapophyses seem to be present in ALMNH: Paleo:3316, although these are broken. As in the previous sacral vertebrae, the eleventh and the twelfth sacrals of ALMNH:Paleo:3316 exhibit intervertebral foramina on their lateral surfaces (Fig. 8D). Only KUVP 119673 preserves the complete transverse processes for the tenth and the eleventh vertebrae, although their bases are well-preserved in ALMNH: Paleo:3316. The shapes of the transverse processes of the tenth and eleventh sacrals are similar to those of the ninth sacral; this is particularly true for the eleventh, which shows a great dorsoventral extension, in contrast to the tenth, which is dorsoventrally short. The processes are more caudally oriented than those of the preceding sacral vertebrae. The dorsal portions of the processes are flat and craniocaudally narrow; the distal end is broken in the tenth sacral vertebra, but a large, rounded expansion is visible on the distal end of the processes of the eleventh.

The internal morphology of the *Ichthyornis* synsacrum is obscured by imperfect preservation of the specimens, which, as mentioned, show variable degrees of flattening, distortion, and/or presence of radiopaque inclusions. Despite significant dorsoventral crushing cranially, the fragmentary synsacrum of ALMNH:Paleo:3316 shows an enlarged neural canal towards the middle region of the synsacrum, congruent with an enlarged spinal cord and similar to the condition in the probable euornithean Maastrichtian synsacrum reported by *O'Connor & Forster (2010)*. Although the presence of circumferential lumbosacral canals related to the balance-maintenance system (*Necker, 2006*) is difficult to verify in any of the specimens, circumferential indentations on the dorsal interior surface of ALMNH:Paleo:3316 are congruent with the presence of such

canals, constituting the second apparent occurrence of a lumbosacral sensory system in stem euornitheans (*O'Connor & Forster, 2010*).

Guildavis and *Apatornis*, represented exclusively by sacral remains, were differentially diagnosed from *Ichthyornis* by *Clarke (2004)* on the basis of only a few sacral characters. *Clarke (2004)* differentiated *Guildavis* from *Ichthyornis* based on the presence of a parapophysis on the left side of the first sacral vertebra, which was missing in YPM 1450 and 1732. These are well preserved in both KUVP 157821 and KUVP 119673, and are apparent in FHSM VP-18702 (Figs. 8A–8C); therefore, their absence in the YPM specimens may be taphonomic. *Apatornis* was diagnosed as distinct from *Ichthyornis* based on the different number of fused sacral vertebrae (at least eleven), the number of mid-sacrals bearing dorsally directed transverse processes (four), and the lack of ossified tendons on the dorsal surface of the synsacrum. All of these characters are exhibited by one or more of the new specimens. As discussed above, the total number of fused sacral vertebrae varies among the studied specimens, presumably as a result of ontogenetic change. Both FHSM VP-18702 and KUVP 157821 exhibit four mid-sacrals with dorsally directed transverse processes, while KUVP 119673 exhibits only three such vertebrae. Both KUVP 119673 and ALMNH:Paleo:3316 lack clear ossified tendons on their dorsal surfaces, while these are difficult to verify in FHSM VP-19702.

All the studied synsacra derive from specimens diagnosable as *Ichthyornis* on the basis of multiple apomorphic features (Table 1), and therefore it appears that the supposed diagnostic features of both *Guildavis* and *Apatornis* may fall within the range of variation of *Ichthyornis*. A more detailed reassessment of the preserved material of *Guildavis* and *Apatornis* will be necessary to confidently assess their taxonomic validity.

Caudal vertebrae

Very few caudal vertebrae are preserved among the new specimens, with one isolated and two articulated caudal vertebrae in KUVP 25472 and two isolated vertebrae in KUVP 119673 (Figs. 9A and 9B). The complete free caudal vertebral count in *Ichthyornis* remains unknown. No known *Ichthyornis* specimen preserves more than five caudal vertebrae (YPM 1732; *Clarke, 2004*), and an articulated caudal series has yet to be discovered. However, more complete euornitheans preserve five free caudals, such *Yixianornis* (*Clarke, Zhou & Zhang, 2006*) and *Apsaravis* (*Clarke & Norell, 2002*); five or six, as in *Iteravis* (*Zhou, O'Connor & Wang, 2014*); or seven, as in *Gansus* (*Wang et al., 2016*), so it is likely that *Ichthyornis* exhibited a similar number of free caudal vertebrae.

The morphology of the newly reported caudal vertebrae is indistinguishable from that described by *Clarke (2004)* for the YPM specimens. The vertebrae are craniocaudally short, with a dorsoventrally flattened centrum and amphicoelous articular surfaces. The neural arch is subtriangular in cranial/caudal view, and bears narrow and pointed cranially directed prezygapophyses. As illustrated by the two articulated caudal vertebrae in KUVP 25472, these wrap around the caudal edges of the neural arch of the preceding vertebrae, which lacks postzygapophyses, in a reversal of the usual relation between pre- and postzygapophyses. This feature has been considered autapomorphic for *Ichthyornis* (*Clarke, 2004*). Neural spines were previously unknown from any of the YPM caudal
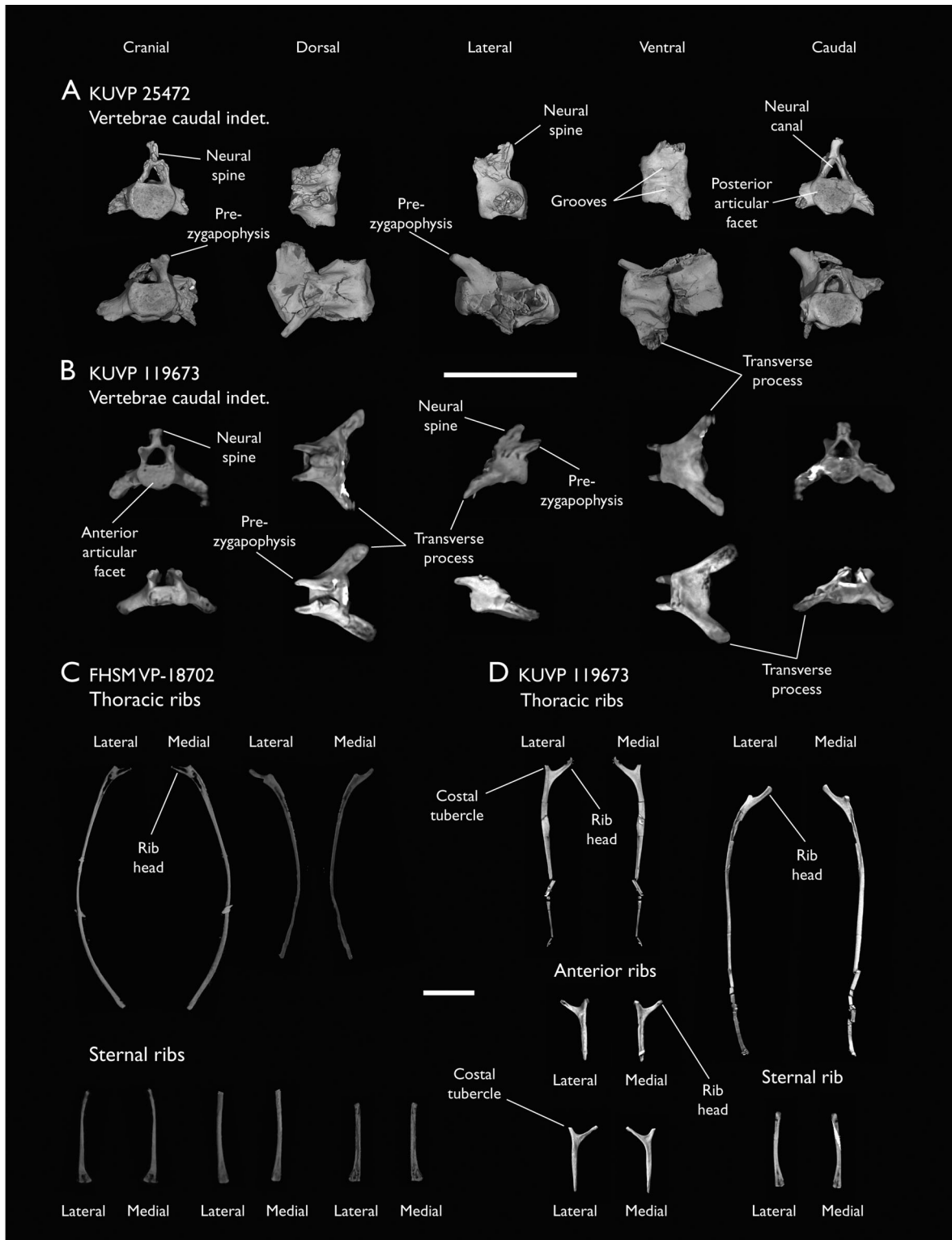
Figure 9 Caudal vertebrae and ribs of *Ichthyornis*. (A) KUVP 25472, caudal vertebra indeterminate, (B) KUVP 119673, caudal vertebrae indeterminate; in cranial, dorsal, lateral, ventral and caudal views; (C) FHSM-VP 18702, thoracic and sternal ribs and (D) KUVP 119673 anterior, thoracic, and sternal ribs, in lateral and medial views. Scale bar equals 1 cm.

vertebrae, but one is preserved on one of the isolated caudals of KUVP 119673 (Fig. 9B). The spine is caudally angled and hooked, with a broad and expanded dorsal margin that does not appear bifurcated, although poor preservation precludes a confident assessment of this feature. *Clarke (2004)* discussed the distribution of bifid caudal neural spines in Hesperornithes and crown group birds, speculating that it might constitute a synapomorphy of a Hesperornithes + Neornithes clade. The poor preservation of this feature in *Ichthyornis* complicates the evaluation of the distribution of this feature.

Two very long and broad transverse processes, as craniocaudally long as the vertebral body, extend from the lateral surfaces of the centrum and are lateroventrally directed. No haemal arches or chevrons are preserved in association with the caudal vertebrae, as in the YPM specimens, although as noted by *Marsh (1880)*, the grooves and ridges on the ventral surface of the centra (Fig. 9A) might be evidence of the articulation of these structures.

No pygostyle is preserved in any of the new specimens nor in any of the YPM specimens, since the identification of this element in YPM 1755 is considered dubious (*Clarke, 2004*), and, in light of the new material described herein, this element constitutes the largest remaining gap in our knowledge of the postcranial skeleton of *Ichthyornis*.

Ribs

FHSM VP-18702 and KUVP 119673 both preserve several isolated vertebral and sternal ribs spread around other skeletal elements (Figs. 9C and 9D). NHMUK A 905 preserves a single rib in association with the sternum (Fig. 9C), but comparison with the sternal ribs preserved in the other two specimens, and the shape of the sternal costal facets, reveal that it does not represent an articulated sternal rib.

No vertebral rib seems to be entirely complete, though most of the identifiable ribs preserve the proximal region. The ribs exhibit a flat and broad lateral surface but become progressively cylindrical in cross-section distally. KUVP 119673 preserves two floating ribs; these are short and lack the flat lateral surface seen in the other vertebral ribs (Fig. 9D). The sternal ribs are short and wide, with a flattened caudal surface and a broad sternal articulation facet. They vary in length, with the shorter ones exhibiting wider sternal ends, matching the cranial sternal costal facets. The broad sternal end is caudally depressed and perforated by many small foramina. An element from FHSM VP-18702 described by *Field et al. (2018b)* as the palatine is reinterpreted here as a rib fragment. Although flattened and distorted, the size, proportions, and general morphology of this element agree with those of the proximal region of the preserved ribs (Fig. 9C). The palatine of *Ichthyornis* was illustrated by *Torres, Norell & Clarke (2021)*, and is notably different from that reported by *Field et al. (2018b)*.

No uncinate processes, fused or unfused, are found in any of the studied specimens, and they seem to be absent in all of the YPM specimens (*Clarke, 2004*). These elements are found in both *Hesperornis* and *Parahesperornis* (*Marsh, 1880*; *Bell & Chiappe, 2020*) and in several closely related euornitheans, like *Gansus* (*Wang et al., 2016*) and *Iteravis* (*Wang et al., 2018*). While the absence of these elements could be preservational, the fact that several of the known *Ichthyornis* specimens preserve numerous costal remains without any

recognizable uncinate processes perhaps points to their genuine absence, a lack of (or incomplete) ossification of these processes, or at least a lack of fusion between the ribs and uncinate processes even in mature individuals, as seen in extant kiwis (Apterygiformes) and penguins (Sphenisciformes) (*Codd, 2010*). Whereas uncinate processes are present in most extant birds, they are absent in screamers (Anseriformes: Anhimidae; *Codd, 2010*). Uncinate processes are integral to the mechanics of ventilation in modern birds, and their length appears to be functionally important and related to locomotor mode (*Tickle et al., 2007*). However, the functional significance of the absence of uncinate processes in screamers, and potentially, in *Ichthyornis*, remains obscure (*Codd, 2010*).

Sternum

Three of the studied specimens preserve sterna in varying levels of completeness (Fig. 10). FHSM VP-18702 preserves a nearly complete, three-dimensional sternum, with the left side virtually undistorted from its original shape (Fig.10A). This is similar to the skull associated with that specimen, in which the left side, preserved downward in the sediment, appears virtually undistorted, whereas the right side is mostly crushed flat (*Field et al., 2018b*). KUVP 119673 preserves a partial, dorsoventrally flattened sternum missing most of its right side but preserving the complete caudal portion of the element (Fig. 10B). Despite the excellent general preservation of KUVP 119673, much of the cranial portion of the sternum is infilled with radiopaque inclusions, which complicates the observation of several morphological features. NHMUK A 905, previously figured by *Clarke (2004)*, exhibits a partial sternum, including the left side of the element and much of the sternal keel (Fig. 10C). Additionally, we CT-scanned and studied the two previously reported *Ichthyornis* sterna, those of the YPM 1450 and YPM 1461, which are considerably more fragmentary, but preserve clear pneumatic foramina (Fig. 11). The specimens described here reveal the complete morphology of the sternum for the first time, including the first information on the caudal portion of this element. Measurements of the sternum from the most complete specimens are provided in Table 3. The three new specimens were previously used as a case study for a new reconstruction workflow combining retrodeformation and retopology, which produced a complete three-dimensional reconstruction of the sternum of *Ichthyornis* (*Demuth et al., 2022*), yet they have not been formally described before.

The rostral region of the sternum is well preserved in FHSM VP-18702 and NHMUK A 905, and as both *Marsh (1880)* and *Clarke (2004)* previously described, exhibits asymmetrical crossed coracoid sulci, in which the right coracoid sulcus lies ventral to the left, crossing at the midline (Figs. 10A and 10C; Figs. 11A and 11B). This condition is widespread among Neornithes, and is exhibited by numerous taxa such as Musophagidae, certain Gruidae, Phoenicopteridae, Ciconiidae, Threskiornithidae, Ardeidae, Scopidae, Aramidae, Eurypygidae, Phaethontidae, Procellariidae, Phalacrocoracidae, Balaenicipitidae, Accipitridae, Strigiformes, Falconinae and Psittaciformes, as well as the extinct total-clade anseriforms Presbyornithidae, the extinct total-clade palaeognaths Lithornithidae, and the extinct coliiform *Sandcoleus* (*Houde, 1988*; *Houde & Olson, 1992*; *Ericson, 1997*; *Mayr & Clarke, 2003*; *Nesbitt & Clarke, 2016*). Amongst Mesozoic
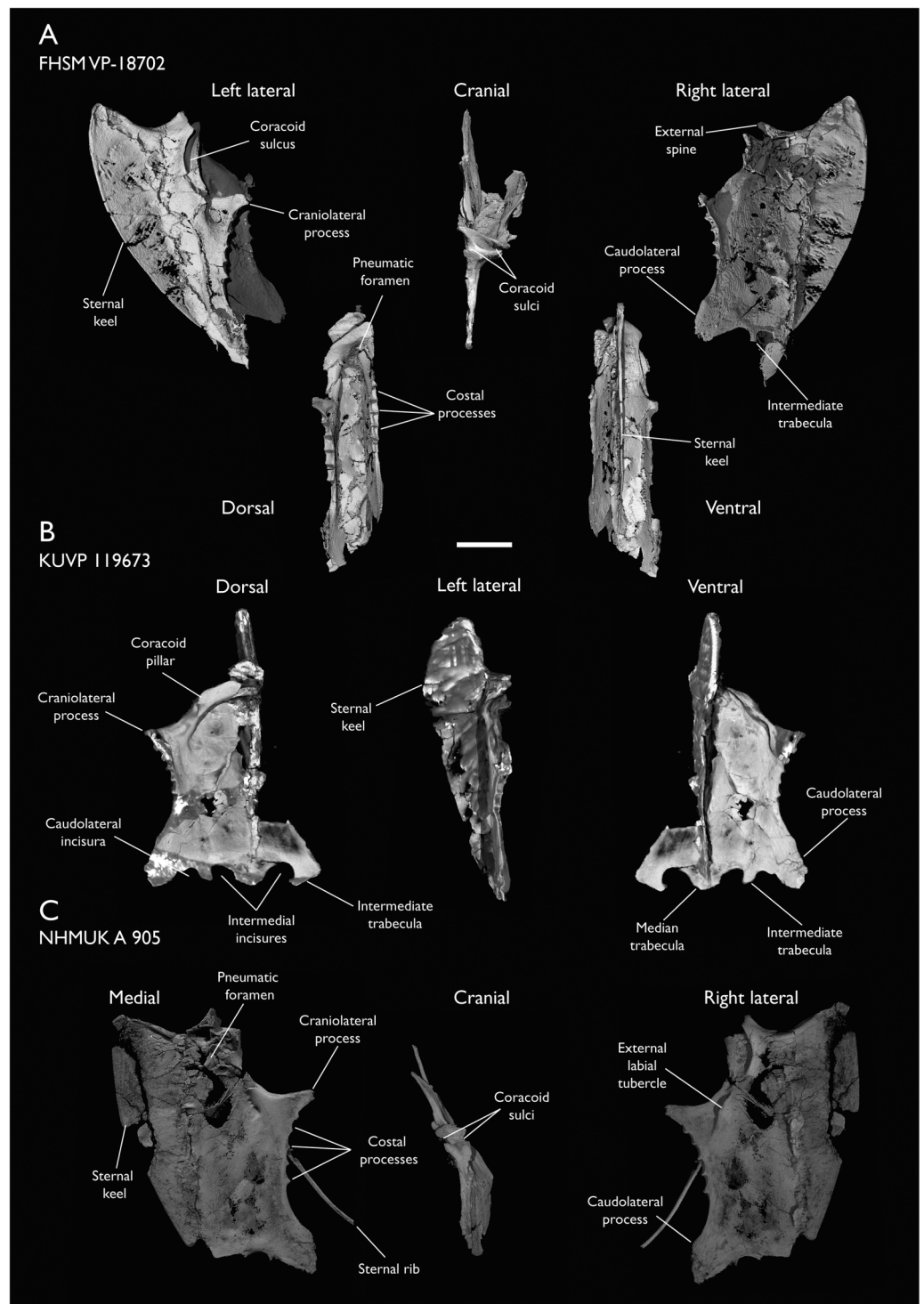
Figure 10 Sterna of *Ichthyornis*. (A) FHSM VP-18702 in left lateral, dorsal, cranial, ventral and right lateral views; (B) KUVP 119673 in dorsal, left lateral and ventral views and (C) NHMUK A 905 in medial, cranial and right lateral views. Scale bar equals 1 cm.
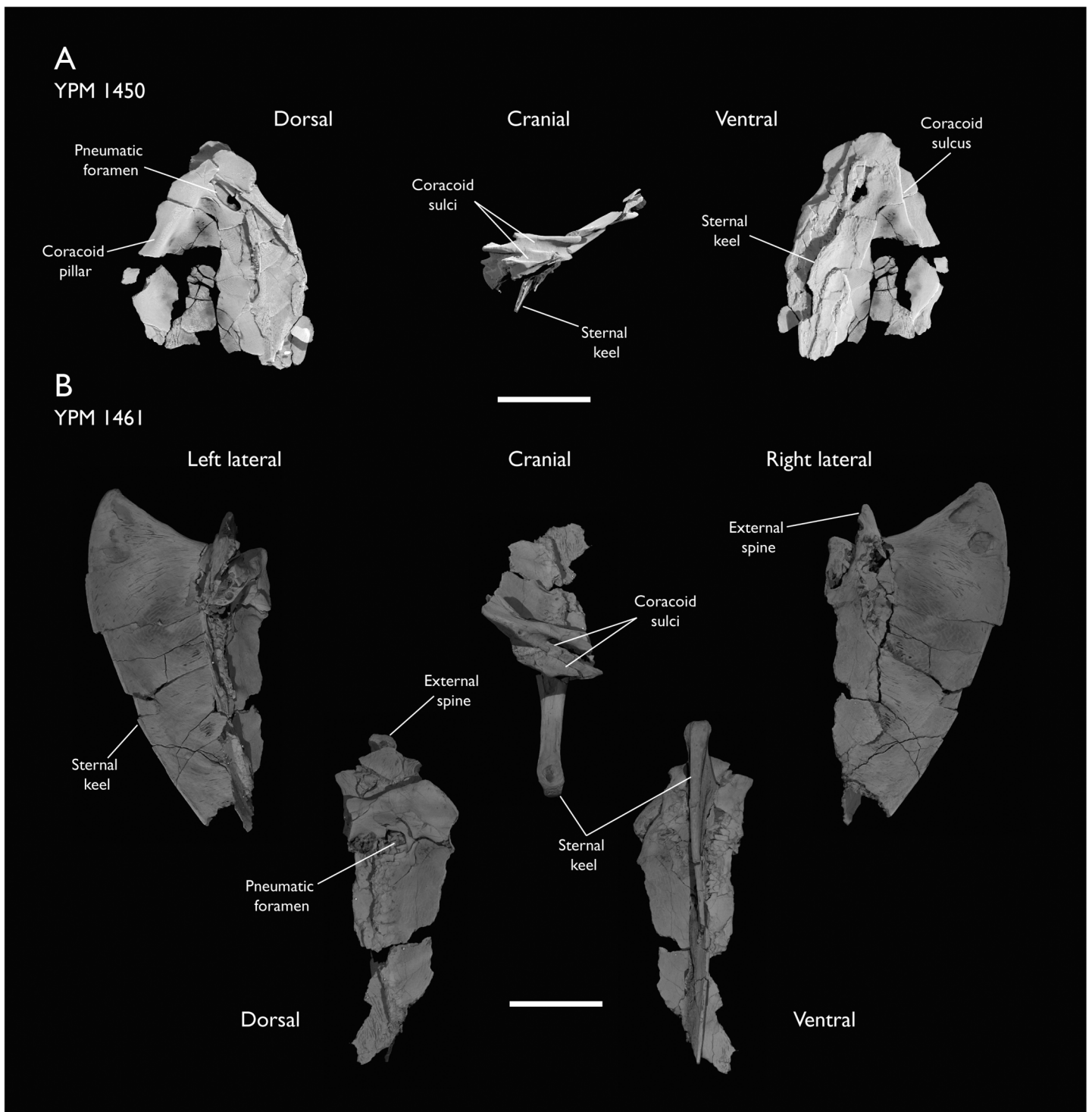
Figure 11 Sterna of *Ichthyornis*. (A) YPM 1450 in dorsal, cranial and ventral views and (B) YPM 1461 in left lateral, dorsal, cranial, ventral and right lateral views. Scale bar equals 1 cm.

Table 3 Measurements of the sternum of *Ichthyornis* specimens. Total length measurements correspond to the maximum craniocaudal length of the sternum measured from the external spine to the caudal end of the median trabecula. Rostral width, craniolateral process width and caudal width are measured for one sternal side only (from the maximum extension of these structures to the sternal midline) since no specimen preserves both complete and undistorted sides of the sternum. Rostral width corresponds to the mediolateral extension of the sternal rostrum, measured from the maximum lateral extension of the coracoid pillar. Craniolateral process width corresponds to the maximum lateral extension of the craniolateral process. Caudal width is measured from the maximum lateral extension of the external trabeculae. Maximum keel depth is measured from the cranioproximal edge of the sternal keel to its maximum ventral extension. Asterisks (*) denote measurements that might be unreliable due to breakage or distortion, but are included for completeness. All measurements are in mm. – = not measurable.

Specimen	Total length	Rostral width	Craniolat. processes width	Caudal width	Max. keel depth
FHSM VP-18702	45.38	–	–	–	13.90
KUVP 119673	39.09*	11.11	20.91	19.60	12.10*
NHMUK A 905	45.87*	–	23.31	22.23	13.68
YPM 1461	–	–	–	–	13.85

euornitheans, this condition is also present in *Iaceornis* (*Clarke, 2004*), and has been suggested to be present in *Yixianornis* (*Clarke, Zhou & Zhang, 2006*), *Gansus*, and *Ambiortus*, though the condition is difficult to confirm in these taxa due to preservational issues (*O'Connor & Zelenkov, 2013*). This morphology constitutes an unusual example of midline asymmetry in a tetrapod, and the significance of this morphology and its functional implications are poorly understood. However, its wide phylogenetic distribution across crown birds as well as Mesozoic euornitheans suggests that the sternum of the last common ancestor of crown birds may have exhibited crossed coracoid sulci.

The coracoid sulci are deep and wide at their midlines, narrowing progressively towards both their medial and lateral margins, though they exhibit a limited dorsoventral flare on their caudal end in lateral view (Fig. 10A; Fig. 11A). The sulci extend caudolaterally from the midline in ventral view, turning parallel to the midline close to the base of the craniolateral processes. The dorsal edges of the coracoid sulci are flat along their cranial surfaces, and no internal spine of the sternum is present. A short but robust cranially-pointed external spine (spina externa; *Baumel & Witmer, 1993*) extends from the midline of the ventral edge of the sulci, which then extend laterally into two short processes pointing laterally and protruding cranially well beyond the dorsal edges of the sulci, giving this region a rhomboidal shape in ventral view (Fig. 10A). This observation departs from the morphological description of *Clarke (2004)*, in which the cranial extent of these processes was assumed to be short. These processes, extending from the ventral lips of the coracoid sulci, coincide with the medial ends of both coracoid facets. Similar lateral processes of the ventral edges of the coracoid sulci are found in *Eurypyga helias*, which also shows crossed coracoid sulci, though the processes are more rounded and less marked than the condition in *Ichthyornis*. The ventral edges of the sulci turn caudolaterally just caudal to these processes, and then become completely caudally directed close to the base of the craniolateral processes, where they form a conspicuous and rounded external labial tubercle (tuberculum labri ext.; *Baumel & Witmer, 1993*). A low ridge extends ventrally from the external spine along the cranial surface of the sternal keel, which is wide and flattened (Figs. 10A and 10C).

Robust and wide coracoid pillars (pila coracoidea; *Baumel & Witmer, 1993*) extend caudolaterally from the dorsal region of the coracoid sulci as seen in KUVP 119673, forming an angle of roughly 100° between them, and delimiting a rounded internal depression (Fig. 10B). The dorsal region of the sternum (pars cardiaca; *Baumel & Witmer, 1993*) is well preserved in KUVP 119673, forming a broad and flat surface. The craniolateral processes (proc. craniolateralis; *Baumel & Witmer, 1993*) extend caudally from the coracoid pillars, pointing dorsolaterally and forming an angle of ~120° with the cranial edge of the sternum (Figs. 10A and 10C). The craniolateral processes are subtriangular in shape, elongate, and gracile, exhibiting a shallow lateral depression extending from the coracoid sulci. Two rounded shallow depressions are visible along the length of the medial surface of the craniolateral processes.

A large pneumatic foramen is present on the dorsal region of the sternum, just caudal to the coracoid pillars. This foramen was previously reported by *Clarke (2004)* in YPM 1450 and YPM 1461, but our CT-scans reveal its complete morphology for the first time (Figs. 11A and 11B). The foramen is subquadrangular, longer mediolaterally than craniocaudally and clearly delimited by thickened edges, which form almost straight angles on the vertices of the foramen (Fig. 11B). Both YPM 1450 and YPM 1461 are flattened, obscuring the internal structure of this pneumatic foramen. In contrast, in FHSM VP-18702 the external opening of the foramen is obscured by the flattening of the right side of the sternum (Fig. 10A), but it is observable in cross-section, where it opens into a large internal cavity. The right caudolateral edge of the foramen is preserved in NHMUK A 905, and the breakage of the rostral portion of the sternum allows the observation of the internal pneumatic cavity (Fig. 10C). KUVP 119673 preserves this region, but radiopaque inclusions prevent confirmation of the presence of the pneumatic foramen. A pneumatic foramen situated in the dorsal portion of the sternum is widespread and present in most major crown bird groups (*Musser & Clarke, 2020*), although it is absent in certain taxa, particularly those with reduced postcranial pneumatization, such as *Phalacrocorax carbo* or *Alca torda*. This foramen, when present, is generally large and circular, as in *Anas platyrhynchos* and *Gallus gallus*, ovoid as in *Ardea alba* or *Rynchops flavirostris*, or tear-shaped like in *Chroicocephalus novaehollandiae*, although certain taxa exhibit a condition where the foramen is divided by a medial septum, as in *Phaethon lepturus*. In certain taxa no single foramen is present, but this region of the sternum is instead perforated by a large number of smaller foramina, as in *Fregata minor*, *Puffinus lherminieri*, and, to a more extreme degree, *Chauna chavaria*. A foramen exhibiting a quadrangular shape similar to that of *Ichthyornis* was only observed in certain strisoreans, such as *Caprimulgus macrurus* and *Podargus strigoides* amongst the surveyed crown-group birds. This pneumatic foramen is absent in Hesperornithes, which are highly osteosclerotic and exhibit reduced skeletal pneumaticity (*Bell & Chiappe, 2016*, *2020*), and has not been previously reported in euornitheans stemward of *Ichthyornis*.

Five costal processes are found caudal to the caudal edges of the craniolateral processes (Figs. 10A–10C). *Clarke (2004)* describes the cranial- and caudalmost costal processes as only indicated by a narrowing in the edge of the sternum, but this does not seem to be the case in the new specimens described here, in which only the cranialmost process lacks a

clear cranial edge. Minute foramina are visible in cross-section between the costal processes, found on the caudal edge of each process, just under the dorsal ridge at the apex of each process, in a position similar to the costal pneumatic foramina of some extant birds such as *Anser albifrons* (Anatidae) and *Fregata aquila* (Fregatidae). These foramina are present in FHSM VP-18702 and NHMUK A 905, and connect to an infilled internal cavity, though they are obscured by radiopaque inclusions in KUVP 119673. The presence of pneumatic foramina between the costal processes has previously been considered a synapomorphy of the avian crown group (*Clarke, 2004*). The foramina documented here are smaller than the pneumatic foramina observed in most extant birds, so their pneumatic nature remains to be confirmed, since small pneumatic foramina have been previously described as externally indistinguishable from nutrient and neurovascular foramina (*O'Connor, 2006*).

No lateral or ziphoid processes are developed caudal to the costal processes, contrasting with the condition in *Archaeorhynchus* (*Zhou, Zhou & O'Connor, 2013*), *Yixianornis*, and *Gansus. Clarke (2004)* reported that no lateral trabeculae or caudolateral processes (proc. caudolateralis; *Baumel & Witmer, 1993*) were present in *Ichthyornis*, but the bases of these structures seem apparent in NHMUK A 905, which was described in that publication (Fig. 10C). Caudolateral trabeculae are well preserved in both FHSM VP-18702 and KUVP 119673 as well (Figs. 10A and 10B). The caudolateral processes are robust and craniocaudally wide, being twice as long as the craniolateral processes. The dorsocranial edge of each caudolateral process exhibits a very shallow, rounded, cranially-directed extension halfway along the length of the process, but no distal flare is present, unlike in *Yanornis* (*Zhou & Zhang, 2001*; *Wang & Zhou, 2020*) or *Yixianornis* (*Clarke, Zhou & Zhang, 2006*). The caudal end of the process is rounded and wide, showing an unfinished bone texture both in FHSM VP-18702 and NHMUK A 905 (Figs. 10A and 10C).

The caudal end of the sternum of *Ichthyornis* has only been briefly reported in AMNH FARB 32773 (*Torres, Norell & Clarke, 2021*), in which it is poorly preserved. Among the specimens described here, it is well preserved in FHSM VP-18702 and KUVP 119673, and we therefore describe this portion of the sternum in detail for the first time. This region clearly shows open lateral and medial sternal incisures medial to the caudolateral processes (Fig. 10B). These incisures are wide and rounded, and they do not penetrate deeply into the edge of the bone. *Torres, Norell & Clarke (2021)* reported the presence of medial incisures and possible lateral incisures, although they could not verify whether the lateral incisure was a taphonomic artifact. The lateral incisure present in FHSM VP-18702 and KUVP 119673, congruent with the condition in AMNH FARB 32773, has a flat lateral margin and slightly concave medial margin, while the medial incisure shows a concave lateral margin and a slightly convex medial margin (Figs. 10A and 10B). The medial incisure extends further cranially than the lateral incisure, in a manner similar to that in the tern *Sterna hirundo* and the gull *Chroicocephalus novaehollandiae*. This morphology lacks clear analogues amongst other Mesozoic euornitheans, in which the lateral incisure tends to extend more cranially and the medial incisure is usually enclosed, forming a fenestra (*O'Connor & Zelenkov, 2013*; *Wang et al., 2013b*, *2016*; *Zhou, O'Connor & Wang, 2014*).
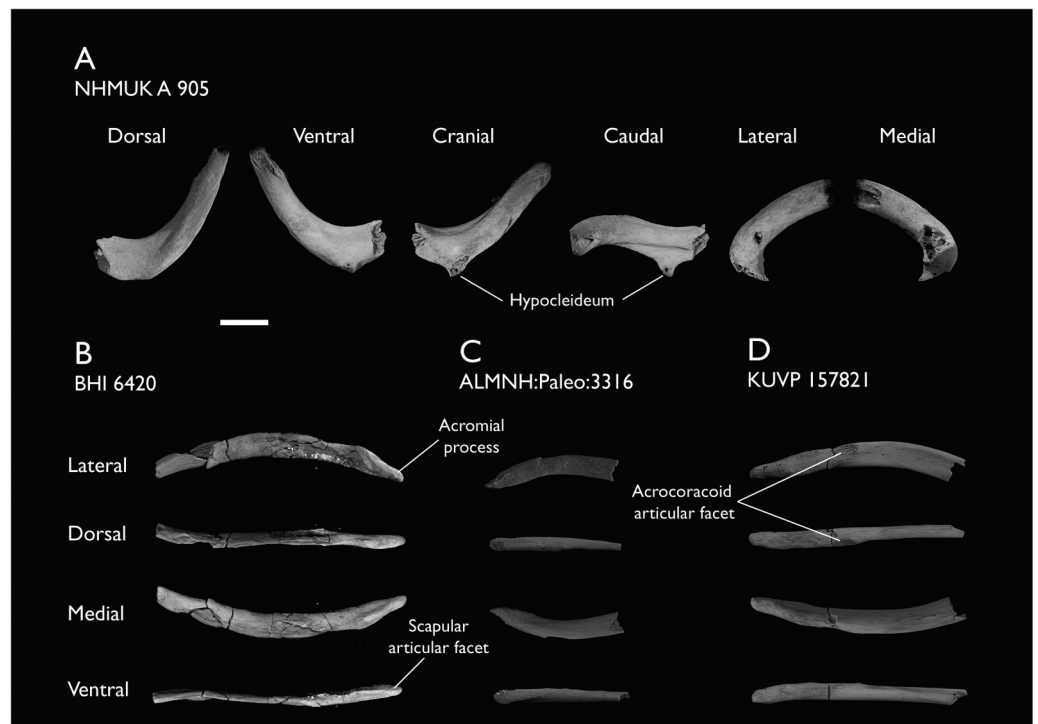
Figure 12 Furculae of *Ichthyornis*. (A) NHMUK A 905 medial furcula fragment in dorsal, ventral, cranial, caudal, lateral and medial views; (B) BHI 6420 left omal furcula fragment, (C) ALMNH: Paleo:3316 right omal furcula fragment and (D) KUVP 157821 right omal furcula fragment, in lateral, dorsal, medial, and ventral views. Scale bar equals 5 mm.

Both rounded incisures delimit a short, robust and flat intermediate trabecula (trabecula intermedia; *Baumel & Witmer, 1993*), preserved in all three studied specimens. The trabecula extends slightly less far caudally than the caudolateral processes, and it is straight and quadrangular in FHSM VP-18702, pointing caudally and widening slightly on its caudal end before ending abruptly, which might indicate breakage (Fig. 10A). The shape of the trabeculae differs in KUVP 119673, where they are short, rounded and caudomedially directed, with the medial edge extending further caudally than the lateral edge. This difference might be taphonomic since the morphology varies somewhat between the two sides of KUVP 119673 (Fig. 10B). The median trabecula is short, wide, and rounded, extending as far caudally as the intermediate trabeculae.

The sternal keel originates from a broad and flat ridge extending ventrally from the external spine, and the ventral apex (apex carinae; *Baumel & Witmer, 1993*) extends cranially slightly beyond the tip of the external spine (Figs. 10A and 11B). The keel is deep and well developed, extending for the entire craniocaudal length of the sternum. The preservation of the bone surface on the sternal keel is patchy in FHSM VP-18702 and NHMUK A 905, and no muscular attachment lines are clearly discernible. The cranial surface of the keel is flat and wide, becoming progressively narrower ventrally but widening slightly at the ventral apex. The ventral margin of the keel is thick and wide, forming a ridge which progressively narrows towards the caudal region of the keel.

Furcula

Four specimens described here include fragments of the furcula: BHI 6420, ALMNH: Paleo:3316 and KUVP 157821 preserve the omal end, while NHMUK A9 905 preserves the clavicular symphysis (Fig. 12A). Previously, only two incomplete furcula fragments had been reported for *Ichthyornis*: YPM 1755, corresponding to the fused region between both clavicles, and MSC 2503, a fragment including the right omal tip (*Clarke, 2004*). The morphology of the newly described furcular fragments differs significantly from that of the previously referred specimens, which, given the scarcity of furcular material, may be attributable to taphonomic distortion of the previously described material.

The clavicular symphyseal region is preserved in NHMUK A 905 together with part of the left clavicular ramus (Fig. 12A). The furcula is roughly U-shaped, and while the broken clavicular rami prevent a precise measurement of the interclavicular angle, the morphology appears very similar to that of *Yixianornis* (*Clarke, Zhou & Zhang, 2006*) and *Iteravis* (*Zhou, O'Connor & Wang, 2014*), in which the clavicles meet at an angle of approximately 60°. Both clavicles are completely fused at the midline, and no suture is visible. *Contra Clarke (2004)*, a clear hypocleideum (apophysis furculae; *Baumel & Witmer, 1993*) is preserved extending from the ventral surface of the symphysis, but only the base of the hypocleideum is preserved (Fig. 12A). A hypocleideum is not present in any other crownward euornitheans (*O'Connor & Zelenkov, 2013*; *Zhou, O'Connor & Wang, 2014*; *Wang et al., 2016*) but it is widespread amongst Enantiornithes and extant crown birds (*Nesbitt et al., 2009*; *Mayr, 2017a*). The hypocleideum is elongate and subtriangular in ventral view, and its caudal end extends caudally and ventrally to the clavicles. Despite being incomplete, the shape of the preserved hypocleideum points towards an elongated and enlarged lamina, similar to the condition in Laridae (*e.g.*, *Sterna hirundo*), and Galliformes (*e.g.*, *Gallus gallus*), instead of a reduced tubercle as in Procellariiformes like *Puffinus lherminieri* and Anseriformes like *Anas platyrhynchos*. It is unclear whether the hypocleideum contacted the apex of the sternal keel, as in some marine birds such as *Phaethon lepturus*, *Fregata minor*, *Morus bassanus*, and *Phalacrocorax carbo*.

Ridges extend on both craniolateral ends of the hypocleideum along the entire preserved cranial surface of the left clavicular ramus (Fig. 12A). These ridges delimit a subtriangular flat-to-convex surface on the cranial side of the symphyseal region. Similar ridges extend from the caudolateral edges of the hypocleideum onto the caudal or sternal surface of the clavicle, delimiting a concave depression on the sternal surface of the symphyseal region. The preserved left clavicle is subcircular in cross-section close to the symphyseal region, but becomes progressively mediolaterally compressed caudally, as the ridges extending from both the cranial and caudal ends of the hypocleideum become more marked.

The omal end of the furcula is preserved in BHI 6420 (left clavicle), KUVP 157821 (right clavicle) and ALMNH:Paleo:3316 (right clavicle; Figs. 12B–12D). The omal tip of the furcular ramus is tapered and very elongate, terminating in a pointed end instead of a blunt end as previously described (*Clarke, 2004*). Although most of the clavicular ramus is not preserved in either specimen, the cranial end of KUVP 157821 is slightly bowed ventrally
and shows a shallow lateral excavation, bounded by marked ridges on both the dorsal and ventral edges of the lateral surface (Fig. 12D).

The articular facet for the acrocoracoid process sits on the lateral side of the clavicular ramus and is very poorly developed. It does not extend laterally from the main body of the clavicle (Fig. 12D). The facet is delimited cranially by a short ridge or tubercle, and forms a shallow circular concavity. The morphology of this facet is sparsely described in existing Cretaceous euornithean literature; it does not seem to extend beyond the ramus of the clavicle in any crownward euornithean taxa (*Zhou, O'Connor & Wang, 2014*; *Wang et al., 2016*). Among Neornithes, the poorly developed acrocoracoid facet is seen in many taxa, including the shearwater *Puffinus lherminieri* and the plover *Charadrius rubricollis*. Just omal to the acrocoracoid facet there is a shallow, elongate facet that seems to correspond with the elongate and flattened medial surface of the procoracoid process. The omal end of the clavicle extends into an elongate and pointed acromial process (Fig. 12B), though it is not as well developed or pointed as it is in *Iaceornis* (*Clarke, 2004*). The process is robust, and it is not mediolaterally compressed as in the extant *P. lherminieri* or *C. rubricollis*, instead remaining subcircular in cross-section for the whole of its length. The acromial process bears a short and flattened facet on the ventral surface of its omal tip. The dorsal portion of this facet seems to contact the shortened acromion process of the scapula near its base.

Coracoid

Nine of the newly described specimens preserve coracoids: BHI 6420 (both), FHSM VP-18702 (both), NHMUK A 905 (both), ALMNH:Paleo:3316 (right side), KUVP 119673 (right side), KUVP 2281 (left side), KUVP 2284 (right side), and MSC 7841 (right side). Although coracoids are among the most commonly preserved elements from *Ichthyornis*, with 24 coracoids in the YPM collections (*Clarke, 2004*), the coracoids of several of the newly described specimens (BHI 6420, FHSM VP-18702, KUVP 119673 and KUVP 2281), are among the best-preserved coracoids known for *Ichthyornis* and together reveal new information about the element's morphology (Fig. 13). Measurement of the coracoid of *Ichthyornis* specimens are provided in Table 4.

The studied specimens exhibit a broad size distribution (Table 4), with the largest specimen, KUVP 2281 (4.00 cm in length), being 38% longer than the smallest complete coracoid, KUVP 2284 (2.91 cm in length). Several features of the coracoid, such as its total length, shaft width, and particularly the maximum diameter of its glenoid facet, show strong correlations with body mass in extant volant birds (*Field et al., 2013*), revealing a wide size distribution for *Ichthyornis* (see Body size estimates below). Despite these differences in size, the proportions of the omal and sternal regions of the studied coracoids remain essentially constant, though the effects of allometry are evident in the proportional length of the shaft, which is longer in the largest specimens (Table 4). For example, the sternal edge of the coracoid is 78% as long as the shaft in KUVP 2284, 65% in FHSM VP-18702 (total length 3.723 cm) and KUVP 119673 (total length 3.577 cm), and only 59% in KUVP 2281. Although generally similar in their overall morphology, the coracoids included in this study show some minor variation. While impossible to definitively resolve,
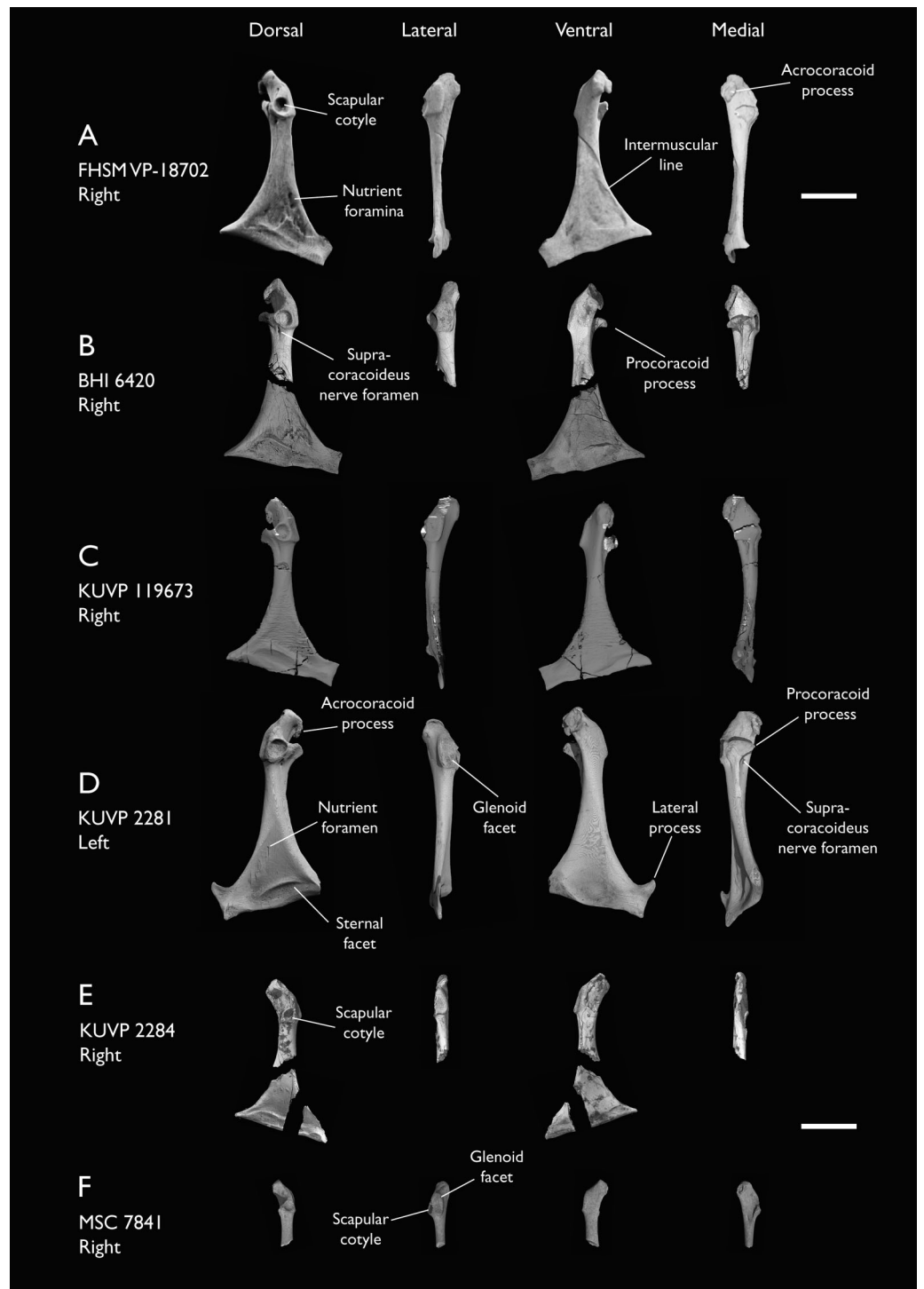
Figure 13 Coracoids of *Ichthyornis*. (A) FHSM VP-18702 right coracoid, (B) BHI 6420 right coracoid omal and sternal fragments, (C) KUVP 119673 right coracoid, (D) KUVP 2281 left coracoid, (E) KUVP 2284 right coracoid and (F) MSC 7841 right coracoid, in dorsal, lateral, ventral and medial views. Scale bar equals 1 cm.

Table 4 **Measurements of the coracoid of *Ichthyornis* specimens.** Standard coracoid measurements are taken from *Field et al. (2013)*. Total length corresponds to the maximum coracoid length measured from its omal to sternal end. Sternal facet length corresponds to the maximum mediolateral expansion of the coracoid sternal facet. Least coracoid width corresponds to the minimum mediolateral width of the coracoid shaft. Glenoid facet diameter corresponds to the maximum diameter of the glenoid or humeral articular facet. Asterisks (*) denote measurements that might be unreliable due to breakage or distortion, but are included for completeness. All measurements are in mm. – = not measurable.

Specimen	Total length	Sternal facet length	Least Cor. width	Glenoid facet diameter	Scapular cotyla max diameter	Lat. process max height
ALMNH:Paleo:3316	31.77	–	3.27	4.47	2.95	–
BHI 6420 right	–	20.98	3.49	4.59	3.21	–
BHI 6420 left	35.78	15.55*	3.23	4.36	3.10	–
FHSM VP-18702 right	33.09	20.07	3.72	4.73	3.34	–
FHSM VP-18702 left	–	–	3.64	4.71	3.20	–
KUVP 2281	35.97	17.66*	3.94	5.15	3.79	7.35
KUVP 2284	–	17.44*	2.91	3.94	2.16	–
KUVP 119673	31.65	19.69	3.19	4.60	2.78	4.32
MSC 5937	–	–	–	5.18	3.12	–
MSC 7841	–	–	2.16	3.23	1.99	–
MSC 34427	–	–	–	4.34	2.53	–
NHMUK A 905 right	35.29	–	4.04	5.43	3.63	–
NHMUK A 905 left	–	–	–	5.29	4.03*	–
YPM 1733	29.96	–	3.31	4.50	3.07	–

we suspect these differences correspond to intraspecific variation, though some previous research has asserted that coracoid morphology may be relatively strongly conserved within bird species (*Longrich, 2009*; *Longrich, Tokaryk & Field, 2011*).

The morphology of the omal region is very similar to that of previously referred *Ichthyornis* specimens (*Clarke, 2004*). The shape of the scapular cotyle is subcircular and very deeply excavated in all specimens, though the shape of the surrounding rim varies somewhat, ranging from essentially circular (KUVP 2284; Fig. 13E) to ovoid (KUVP 119673, 2281; Fig. 13D) to subtriangular (BHI 6420, ALMNH:Paleo:3316; Fig. 13B). The dorsocaudal opening of the supracoracoideus nerve foramen is positioned just caudal to the scapular cotyle. The opening lies in a short groove extending from the edge of the scapular cotyle on most specimens, such as in BHI 6420 (Fig. 13B), as described by *Clarke (2004)*, but this structure is not visible in either of the FHSM VP-18702 coracoids (Fig. 13A), similar to YPM 1446, which also lacks this groove (*Clarke, 2004*).

The glenoid facet is large and slightly concave, with very marked ventral and caudal margins forming a labrum, which separates the facet from the shaft. It is situated just lateral to the scapular cotyle, extending from its caudal end to the base of the acrocoracoid ligament scar (impressio lig. acrocoracohum.; *Baumel & Witmer, 1993*) in most specimens (Figs. 13A–13D). In KUVP 2284 the glenoid originates more cranially, with its caudal margin situated in a position roughly equivalent to the centre of the scapular cotyle, instead of its caudal edge (Fig. 12E). The shape of the glenoid facet in lateral view is ovoid in most specimens but becomes almost quadrangular in KUVP 2281 and MSC 7841 (Figs. 13D and 13F). The position and shape of the glenoid contrasts with that of other

Cretaceous ornithurines such as *Iaceornis* or *Cimolopteryx*-like taxa known mostly from coracoids (*Hope, Chiappe & Witmer, 2002*; *Agnolin, 2010*; *Longrich, Tokaryk & Field, 2011*; *Mohr et al., 2021*), in which the glenoid is situated cranial to the scapular cotyle, a condition shared with most crown-group birds.

Although *Clarke (2004*, pg. 111) described the acrocoracoid process of *Ichthyornis* as "slightly hooked in posterior view" this structure is considerably more recurved and hook-shaped in BHI 6420, FHSM VP-18702, KUVP 119673, and KUVP 2281 than it is in any of the described and figured YPM specimens (Figs. 13A–13D). In these specimens, the acrocoracoid extends dorsocaudally for roughly 25% of the surface of the triosseal canal, curving slightly along its length. It does not taper, and exhibits a large and quadrangular furcular articular surface (Figs. 13A and 13B). The lack of this very recurved acrocoracoid morphology in NHMUK A 905, ALMNH:Paleo:3316, and KUVP 2284 (Fig. 13E) is apparently due to preservational factors, in that this process appears to have been broken or eroded, which is probably true for the numerous coracoids in the YPM collections as well. The cranial surface of the acrocoracoid process is flat to slightly concave, extending parallel to the cranial end of the triosseal canal, except in KUVP 2284, in which it is situated more perpendicularly—though this may be the result of taphonomic distortion. The acrocoracoid ligament scar is shallow and dorsally elongated, and it is clearly delimited by the caudal rim of the acrocoracoid and the cranial edge of the glenoid.

Similar to the acrocoracoid, the procoracoid process in several studied specimens is much more developed than previously reported; in the specimens lacking a well-developed procoracoid, a clear breakage surface is visible just medial to the scapular cotyle. The procoracoid extends as a narrow subtriangular flange pointing ventromedially, reaching the ventral edge of the supracoracoideus sulcus, which gives the medial surface of the triosseal canal a claw-like shape (Figs. 13B–13D).

The morphology of the triosseal canal region of the coracoid in *Ichthyornis* is similar to the condition in *Gansus*, *Yixianornis* and *Ambiortus*, which also possess elongated acrocoracoid and procoracoid processes (*Clarke, Zhou & Zhang, 2006*; *O'Connor & Zelenkov, 2013*; *Wang et al., 2016*). However, the procoracoid in *Ichthyornis* is substantially more tapered than in the aforementioned taxa, in which it shows a more quadrangular shape with a blunt end. The proportions and shape of the acrocoracoid process of *Ichthyornis* show similarities with those of Lithornithidae (*Houde, 1988*), and Procellariiformes like the shearwater *Puffinus lherminieri*.

The shaft of the coracoid is long and robust, lateromedially broad, and becomes progressively dorsoventrally compressed sternally, particularly on its dorsal surface. The shaft is slightly more cylindrical and less mediolaterally expanded in KUVP 119673 and MSC 7841 (Figs. 13C and 13F), which does not seem to be attributable to preservational factors since KUVP 2281 is exceptionally well-preserved and shows a more dorsoventrally compressed and mediolaterally expanded shaft that does not seem to be taphonomically flattened (Fig. 13D). The more cylindrical shaft is reminiscent of several isolated ornithurine coracoids from the Late Cretaceous of North America which have been suggested to represent *Ichthyornis*-like forms, such as 'Ornithurine A' from *Longrich (2009)* and 'Ornithurine D' from *Longrich, Tokaryk & Field (2011)*, though these differ in

other morphological features. Both lateral and medial surfaces of the shaft are strongly concave. A marked ridge extends from the caudal end of the procoracoid process along the medial surface of the bone, reaching the sternal end of the coracoid. The angle formed between the sternal margin of the coracoid and the main axis of the shaft varies among the studied specimens and does not seem to correlate with size, varying from 68° in KUVP 2281, to 72°–74° in KUVP 2284, FHSM VP-18702, and BHI 6420, to 81° in KUVP 119673. The medial end of the sternal facet (angulus medialis coracoideum; *Baumel & Witmer, 1993*) is pointed, with a flattened medial surface. The lateral margin of the coracoid extends into a lateral process, which is broad and quadrangular. This process has only been previously reported in the specimen AMNH FARB 32773, in which it is badly crushed (*Torres, Norell & Clarke, 2021*), and it is only completely preserved in KUVP 2281 (Fig. 13D), which shows a markedly tapered, subtriangular projection that is omally-directed, similar in shape and size to that of *Gansus* and some extant taxa such as *Puffinus lherminieri*.

As in other previously described *Ichthyornis* specimens, the ventral surface of the coracoid shows a shallow depression towards the sternal facet, probably for the implantation of m. supracoracoideus. This depression is variably excavated and delimited in the newly described specimens, showing a clear medial edge and a marked intermuscular line on its lateral edge running from the omal to the sternal end of the shaft in most specimens. Only KUVP 2281 shows a well-marked ridge on its sternal edge (Fig. 13D), as in YPM 1450. The sternal facet is marked and continuous between the dorsal and ventral surfaces of the coracoid, and, as described by *Clarke (2004)*, it shows a clear projecting ridge delimiting the cranial edge of the facet on its dorsal surface. However, unlike the morphology described by *Clarke (2004)*, it does not show a "vaguely sigmoidal" shape, and is instead somewhat quadrangular, with its proximal edge running parallel to the sternal edge of the coracoid (Fig. 13D).

The dorsal surface of the coracoid is described by *Clarke (2004)* as preserving a clearly marked foramen in the impression of m. sternocoracoidei in all YPM specimens. The newly described specimens show the presence of either one (BHI 6420, KUVP 2281; Figs. 13B and 13D) or two foramina (FHSM VP-18702; Fig. 13A) in this region.

Scapula

Five of the studied specimens preserve scapulae: BHI 6420 (both), FHSM VP-18702 (left side), KUVP 2281 (left side), KUVP 119673 (right side), and NHMUK A 905 (both). The preservation of this element in the new specimens is generally excellent, and these specimens all show complete or nearly complete scapulae, at worst missing only the acromion or the caudal terminus of the bone. The scapulae of FHSM VP-18702 and NHMUK A 905 may represent the best-preserved scapulae known for *Ichthyornis* (Figs. 14A and 14C). Measurements of the scapulae of the studied specimens are provided in Table 5.

The omal end of the scapula is short, robust, and quadrangular in shape. The dorsal surface of the omal region is straight in all specimens with the exception of KUVP 2281, in which the region just distal to the acromion is raised (Fig. 14B), similar to the condition in
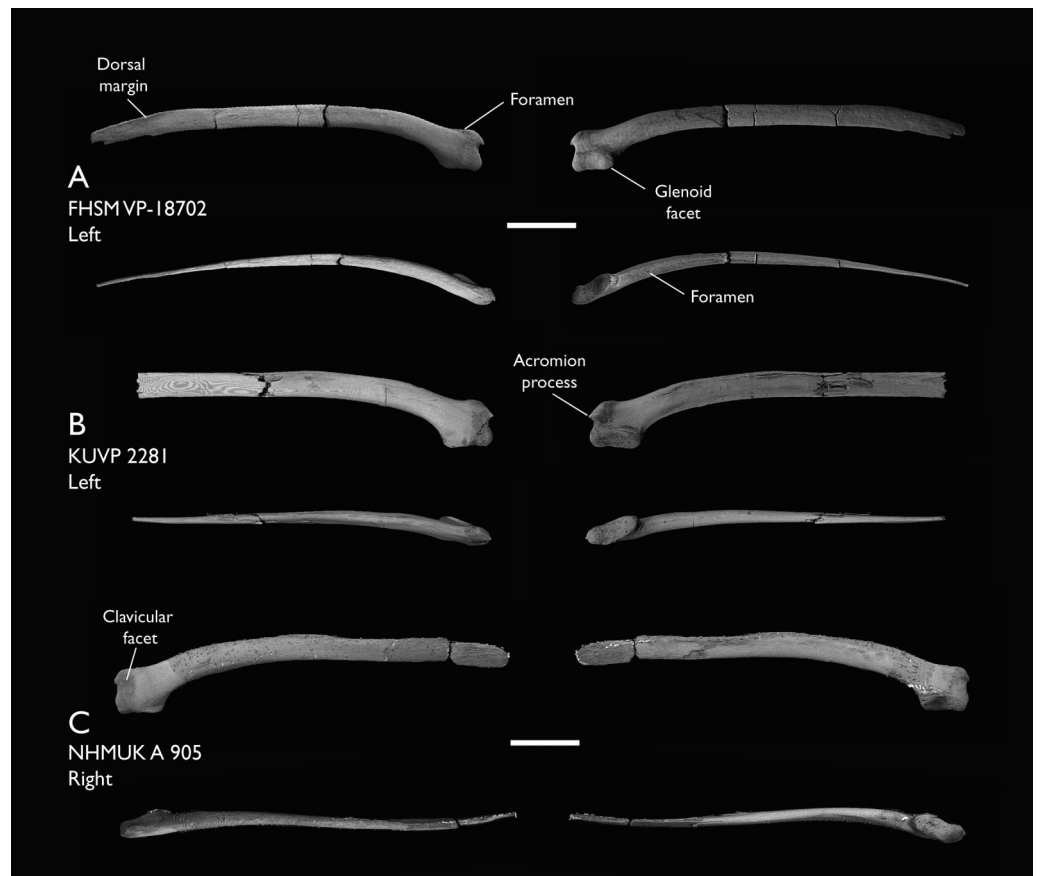
Figure 14 Scapulae of *Ichthyornis*. Views for each in clockwise order: medial, lateral, ventral, dorsal. (A) FHSM VP-18702 left scapula, (B) KUVP 2281 left scapula, and (C) NHMUK A 905 right scapula. Scale bar equals 1 cm.

Table 5 Measurements of the scapula of *Ichthyornis* specimens. Total length corresponds to the maximum scapular craniocaudal length. Glenoid facet length corresponds to the maximum craniocaudal extension of the glenoid or humeral articular facet. Omal height corresponds to the maximum dorsoventral extension of the omal end of the scapula, measured from the dorsalmost point of the omal end to the ventralmost point of the glenoid facet. Asterisks (*) denote measurements that might be unreliable due to breakage or distortion, but are included for completeness. All measurements are in mm.

Specimen	Total length	Glenoid facet length	Omal height
BHI 6420 right	53.68	6.33	–
BHI 6420 left	44.26*	6.45	6.12
FHSM VP-18702	58.27	6.52	6.26
KUVP 2281	52.46*	7.19	6.95
KUVP 119673	56.83	5.84	4.97*
NHMUK A 905 right	52.76*	6.27	7.17
NHMUK A 905 left	57.54	6.39	6.57

YPM 1718. The base of the acromion is robust and inflated, with a marked depression on its ventral end that seems to accommodate the elongated terminus of the acromial process of the furcula.

The acromion is missing or distorted in most specimens, but it is well preserved in FHSM VP-18702 and KUVP 2281 (Figs. 14A and 14B). In both specimens the acromion process extends slightly beyond the coracoid tubercle (tuberculum coracoideum; *Baumel & Witmer, 1993*), a condition differing from that seen in the YPM *Ichthyornis* scapulae, and in the recently reported AMNH FARB 32773, in which this process was described as being markedly shorter (*Clarke, 2004*; *Torres, Norell & Clarke, 2021*). The shape of the acromion process differs among the new specimens. In FHSM VP-18702 the acromion is hook-shaped, curving slightly ventromedially towards the coracoid tubercle (Fig. 14A). The tip of the acromion is missing in BHI 6420, but the shape of the preserved base suggests a similar condition to that of FHSM VP-18702. The base of the acromion is similarly shaped in NHMUK A 905 as well, but in this case the acromion is short, relatively undeveloped, and ends in a rounded, unbroken tip (Fig. 14C). By contrast, the acromion in KUVP 2281 is conical and points cranially (Fig. 14B), similar to the shape seen in YPM 1452, the holotype of *Ichthyornis victor* (*Marsh, 1880*; *Clarke, 2004*).

This variation in morphology is particularly notable, as an extremely diminutive acromion has been considered one of the autapomorphies of *Ichthyornis dispar* (*Clarke, 2004*), but no variation in the shape of the acromion or its orientation has been previously reported. It should be noted that, despite the presence of several scapulae among the YPM specimens, only a few of them preserve the proximal portion of the scapula or the acromion process, and only four specimens preserving this morphology have previously been mentioned or figured (YPM 1452, 1718, 1763; *Clarke, 2004*; and AMNH FARB 32773, *Torres, Norell & Clarke, 2021*). The disparity in the shape and length of the acromion noted here suggests either intraspecific or interspecific variation, which may have previously gone unappreciated due to the relative ease with which this element may break or erode, given its absence from many otherwise well-preserved specimens.

Despite this variation in shape, when preserved the acromion is very short in all *Ichthyornis* scapulae, which contrasts with the greatly elongated condition seen in other Late Cretaceous euornithean taxa like *Gansus*, *Apsaravis*, and *Iaceornis* (*Clarke, 2004*; *Clarke & Norell, 2002*; *Wang et al., 2016*). The proportions and general shape of the acromion in *Ichthyornis* are most similar to those of *Yixianornis* (*Clarke, Zhou & Zhang, 2006*) and *Hongshanornis* (*Chiappe et al., 2014*), in which it is short, pointed, and sharply tapered, though still more elongate than in any *Ichthyornis* specimens. Amongst extant taxa, the acromion is greatly reduced in Gaviidae (*e.g.*, *Gavia arctica*) and Anhimidae (*e.g.*, *Chauna torquata*), but neither show the pointed or recurved morphology seen in *Ichthyornis*.

The coracoid tubercle is large and ball-shaped in all of the new specimens described here, but it is slightly more proximally extended in FHSM VP-18702 (Fig. 14A). The glenoid facet is large, ovoid and mostly flat, though its distal end is medially extended. It shows very little variation among the different specimens (Figs. 14A–14C), with a morphology congruent with that described by *Clarke (2004)* for the YPM specimens.

No obvious pneumatic foramina are present, but FHSM VP-18702 preserves a very clear, small foramen situated on its medial surface, just caudal to the base of the acromion, which connects with a large internal hollow chamber in this region (Fig. 14A). Such a

hollow chamber is also present in all of the other specimens investigated here, though the foramen is not. It is difficult to establish whether this represents a genuine pneumatic structure, as such foramina are rarely unambiguously pneumatic in fossil and extant taxa, though the hollow internal cavity and thin bone walls of the element would be consistent with it being pneumatized (*O'Connor, 2006*). The presence of a pneumatic foramen on the lateral surface of the proximal end of the scapula is widespread amongst Neornithes, but it remains to be seen whether it constitutes a true synapomorphy of the group (*Clarke, 2004*).

The scapular blade is preserved in its entirety in BHI 6420, FHSM VP-18702, NHMUK A 905 and KUVP 119673 (Figs. 14A and 14C). The blade is elongate and slightly curved at its proximal- and distalmost ends, but is essentially straight for most of its length. Both BHI 6420 scapulae show greater curvature along the length of the blade with no straight central region—similar to the condition in YPM 1773 (*Clarke, 2004*). This elongated morphology is widespread amongst crownward euornitheans, such as *Yixianornis, Gansus* and *Apsaravis* (*Wang et al., 2016*; *Clarke & Norell, 2002*; *Clarke, Zhou & Zhang, 2006*). The scapular blade is thick and ovoid in cross-section just distal to the omal region, but becomes more mediolaterally compressed along its length, thinning significantly at its distal end. The blade is dorsoventrally broad, and it maintains a similar width for most of its length in all specimens, tapering progressively towards its distal end. A small, thin flange is developed distally along the dorsal edge of the blade (margo dorsalis; *Baumel & Witmer, 1993*; Fig. 14A). The surface of the blade is mostly smooth across both the lateral and medial surfaces of the bone, but a shallow groove is present on the distal lateral surface, just ventral to the dorsal flange. This groove has also been described in *Gansus*, *Hongshanornis* and *Ambiortus* (*O'Connor & Zelenkov, 2013*; *Chiappe et al., 2014*; *Wang et al., 2016*), but is absent in *Yixianornis* (*Clarke, Zhou & Zhang, 2006*).

A shallow ridge, starting just distal to the glenoid facet, extends along the cranial region of the blade in all studied specimens. *Clarke (2004)* describes this ridge as beginning just distal to a small foramen, but it appears to originate well cranial to the foramen in all of the new specimens investigated here. This foramen is situated just next to the medial side of the ridge (Figs. 14A–14C). The shallow scar suggested to be situated just dorsal to the cranial end of the ridge by *Clarke (2004)* is only visible in the NHMUK A 905 scapulae (Fig. 14C). Both the ridge and the scar were interpreted as being related to the implantation of m. scapulohumeralis cranialis and caudalis by *Clarke (2004)*.

Humerus

Complete and partial humeri are preserved in 16 of the studied specimens (Fig. 15): BHI 6420 (both, fragmentary), BHI 6421 (right, distal), FHSM VP-18702 (right proximal and left distal), KUVP 119673 (both, complete), KUVP 2300 (left, complete), KUVP 2284 (right, fragmentary), KUVP 25469 (right, distal portion), KUVP 25471 (left, complete), NHMUK A 905 (two left humeri), ALMNH:Paleo:1043 (left proximal), ALMNH: Paleo:1786 (left proximal), MSC 5794 (left proximal), MSC 5985 (left distal), MSC 7841 (both, fragmentary), MSC 7842 (right proximal, midshaft and distal fragments) and MSC 7844 (right distal). Among these, KUVP 119673 and KUVP 2300 include the best-preserved humeri for *Ichthyornis* known to date, preserving the entire element and its
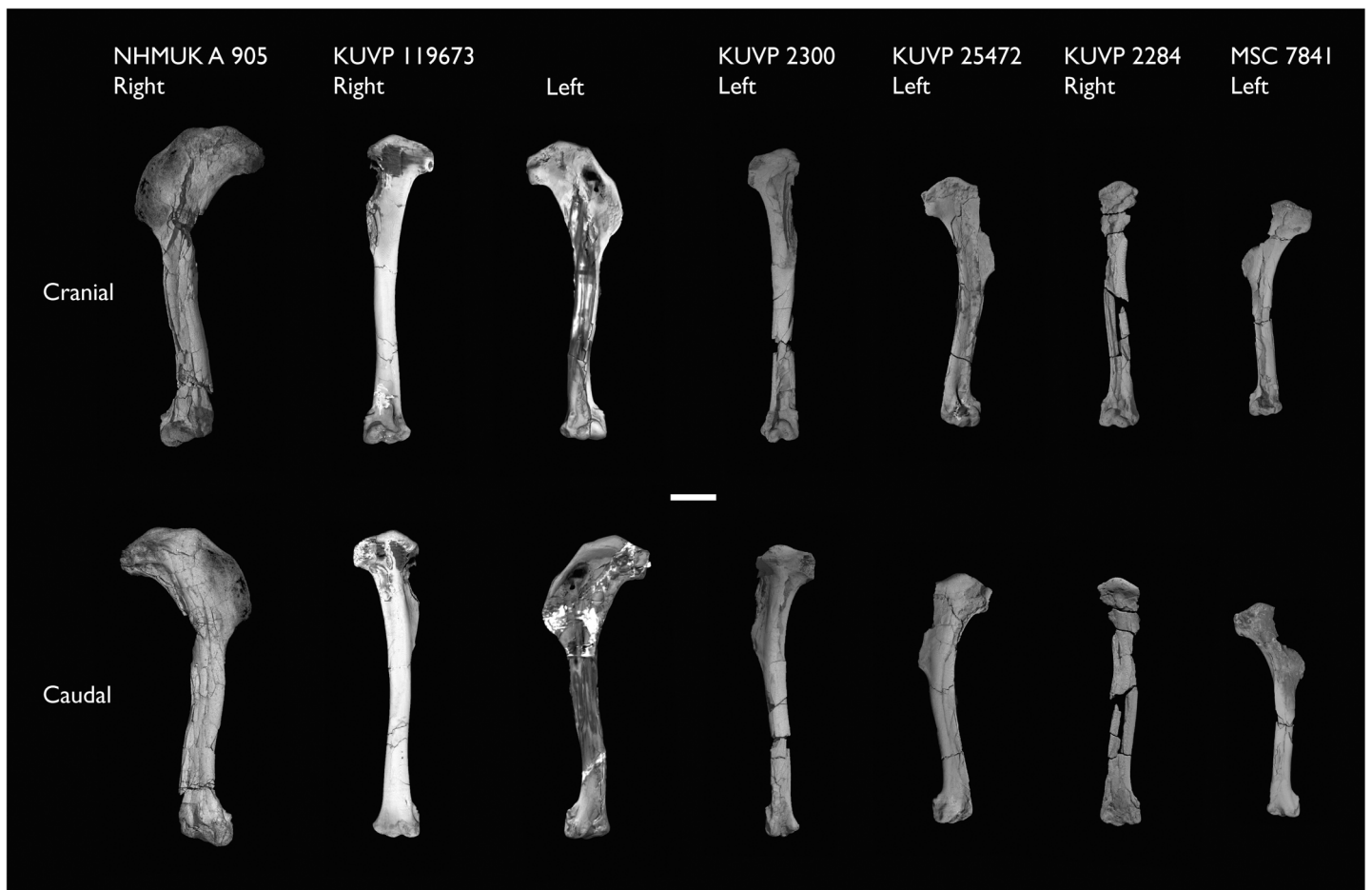
Figure 15 Size distribution of *Ichthyornis* humeri. Largely complete humeri included in this study in cranial and caudal views. Scale bar equals 1 cm.

three-dimensional morphology (Fig. 16). KUVP 119673 is particularly remarkable in this regard, as both humeri are preserved (Figs. 16A and 16B), with the left element taphonomically flattened, allowing the effects of taphonomy on humeral morphology to be assessed. Measurements of the humeri of the most complete specimens included in this study are provided in Table 6.

The proximal end of the humerus is best preserved in ALMNH:Paleo:1786, which, despite lacking a deltopectoral crest and being broken distally, preserves the entire proximal end undistorted and in three dimensions (Fig. 17A). The humeral head (caput humeri; *Baumel & Witmer, 1993*) is large, globose, and proximally convex in caudal view. It arches over the caudal surface of the humerus, exhibiting a subtle, hook-shaped apex curving medially at its dorsal end. The proximal development of the humeral head varies among the studied specimens: it is particularly well developed in ALMNH:Paleo:1786 (Fig. 17A) and BHI 6420, but is much less so in KUVP 119673 (Figs. 16A and 16B). A marked and distinct straight ridge extends dorsoventrally from the dorsal tubercle, ending just dorsal to the capital incisure (Fig. 17A). This ridge crosses over the caudalmost extension of the humeral head and delimits its distal edge.
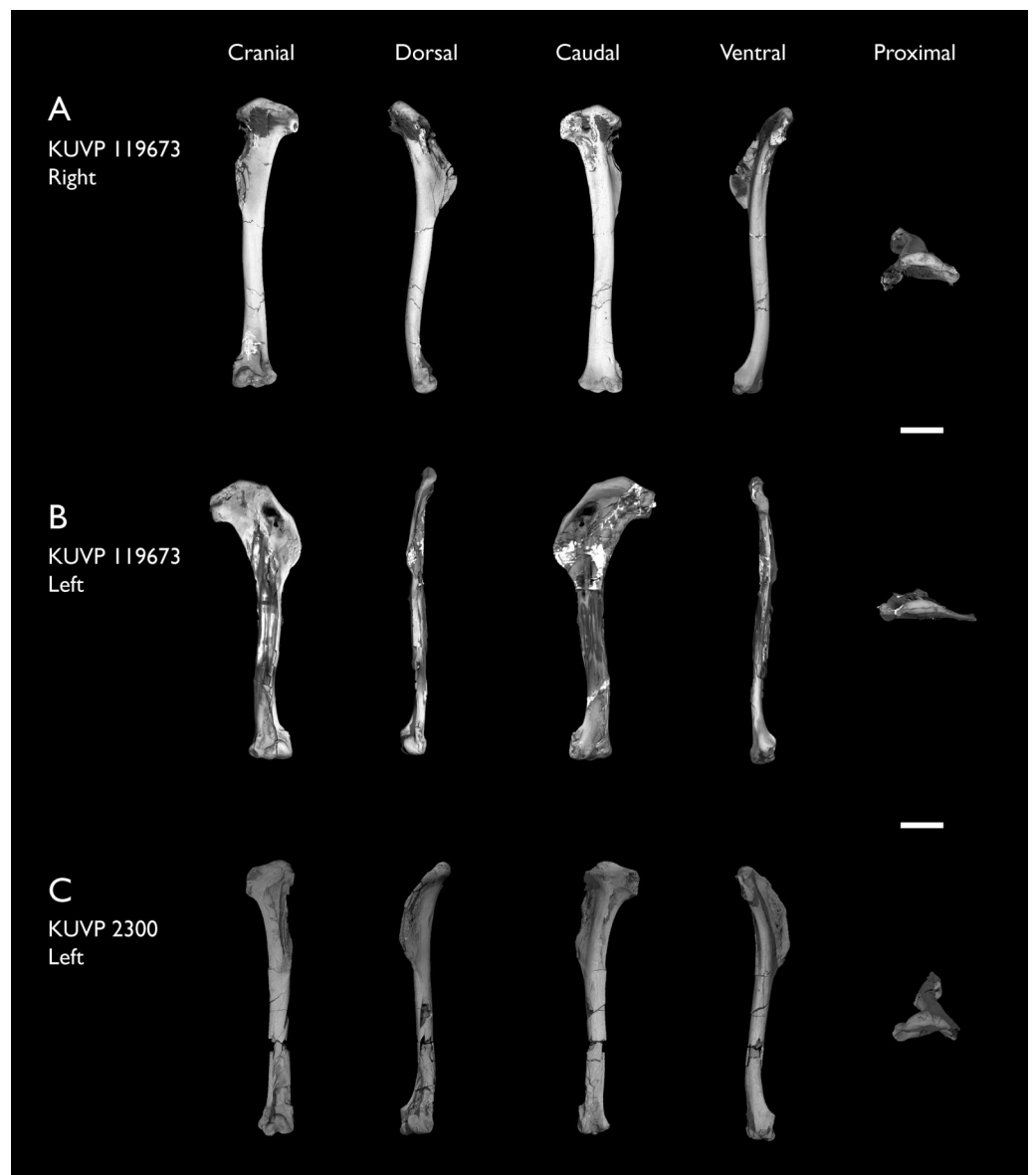
Figure 16 Three-dimensional morphology of *Ichthyornis humeri*. Showing the three-dimensionally preserved humerus of KUVP 119673 (A) and KUVP 2300 (C) in comparison with the flattened left humerus of KUVP 119673 (B), in cranial, dorsal, caudal, ventral and proximal views. Scale bar equals 1 cm.

The ventral tubercle is well developed and distinct where preserved, but its shape varies among the different specimens. The shape is subcircular to ovoid in KUVP 25471 and FHSM VP 18702, but it is subquadrangular in ALMNH:Paleo:1786 and KUVP 119673 (Figs. 16A and 16B; Fig. 17A), and practically square in BHI 6420. This shape variation does not seem to be taphonomic in origin, since most of the specimens preserving the ventral tubercle are extremely well-preserved and do not show evidence of significant deformation.
Table 6 Measurements of the humerus of *Ichthyornis* specimens. Total length corresponds to the maximum proximodistal length of the humerus. Least circumference and least diameter correspond to the minimum circumference and diameter of the humeral shaft; midshaft width is provided for those specimens in which the preservational state precluded measuring these. Proximal craniocaudal width is measured as the maximum craniocaudal extension of the humeral head. Proximal dorsoventral width is measured as the maximum extension from the dorsal to the ventral humeral tubercles, including them. Midshaft width corresponds to the craniocaudal width of the humeral shaft halfway along its length. Asterisks (*) denote measurements that might be unreliable due to breakage or distortion, but are included for completeness. All measurements are in mm. – = not measurable.

Specimen	Total length	Least circum.	Least diameter	Prox. Craniocaudal width	Prox. Dorsoventral width	Dist. Craniocaudal width	Dist. Dorsoventral width	Midshaft width
ALMNH:Paleo:1043	–	–	–	3.46	–	–	–	–
ALMNH:Paleo:1786	–	–	–	3.62	14.02	–	–	–
BHI 6420 right	–	–	–	3.49	15.83	6.94	9.70	–
BHI 6420 left	72.33*	–	–	3.49	16.53	6.81	9.74	6.86*
BHI 6421	–	–	–	–	–	–	11.98	5.32
FHSM VP-18702 right	–	–	–	4.44	17.04	–	–	–
FHSM VP-18702 left	–	–	–	–	–	12.11	5.53	6.03
KUVP 2284	55.00	–	–	3.05*	8.82*	4.20*	8.93	–
KUVP 2300	65.23	–	–	3.68	12.08	6.32	7.82	4.50
KUVP 25469	–	–	–	–	–	6.94	11.27	–
KUVP 25471	55.11	–	–	3.06	15.50	3.72*	8.41*	5.17*
KUVP 119673 right	68.96	13.11	4.01	3.66	13.73	5.27	10.80	–
KUVP 119673 left	67.70	–	–	3.55	14.16	5.72	10.32	5.54*
MSC 5794	–	–	–	3.35	–	–	–	–
MSC 5985	–	–	–	–	–	6.06	10.80	–
MSC 7841 right	47.08	–	–	2.37	–	4.48	7.27	3.70
MSC 7841 left	–	–	–	–	–	4.57	7.59	–
MSC 7842	–	–	–	3.42	9.58*	5.27	10.11	4.56
MSC 7844	–	–	–	–	–	3.55*	5.48*	–
NHMUK A 905 right	70.61	–	–	4.08	16.76	5.60	11.37	6.87
NHMUK A 905 left	–	–	–	3.86	16.61	–	–	–

The tricipital fossa (fossa tricipitalis; *Baumel & Witmer, 1993*) is extremely shallow and moderately excavated (Fig. 17A), and is bound dorsally by a broad and marked dorsal ramus (crus dorsalis; *Baumel & Witmer, 1993*) extending distally from the ventral tubercle and ventrally by a thin and narrow ventral ramus (crus ventralis; *Baumel & Witmer, 1993*). This shallow tricipital fossa is moderately visible in ALMNH:Paleo:1786 (Fig. 17A), but it is significantly more marked in flattened specimens such as BHI 6420 and the left humerus of KUVP 119673 (Fig. 16B), since both the dorsal and ventral rami become more apparent after deformation. A large and deep depression found just dorsal to the ventral process and ventrodistal to the humeral head might correspond to the secondary opening of the tricipital fossa as seen in certain extant birds such as *Chroicocephalus novaehollandiae*. This larger depression is bounded proximally by the proximal edge of the humerus, and it is clearly observable in all specimens preserving this region (Fig. 16; Figs. 17A–17C). Neither of the two tricipital fossa depressions show evidence of being associated with
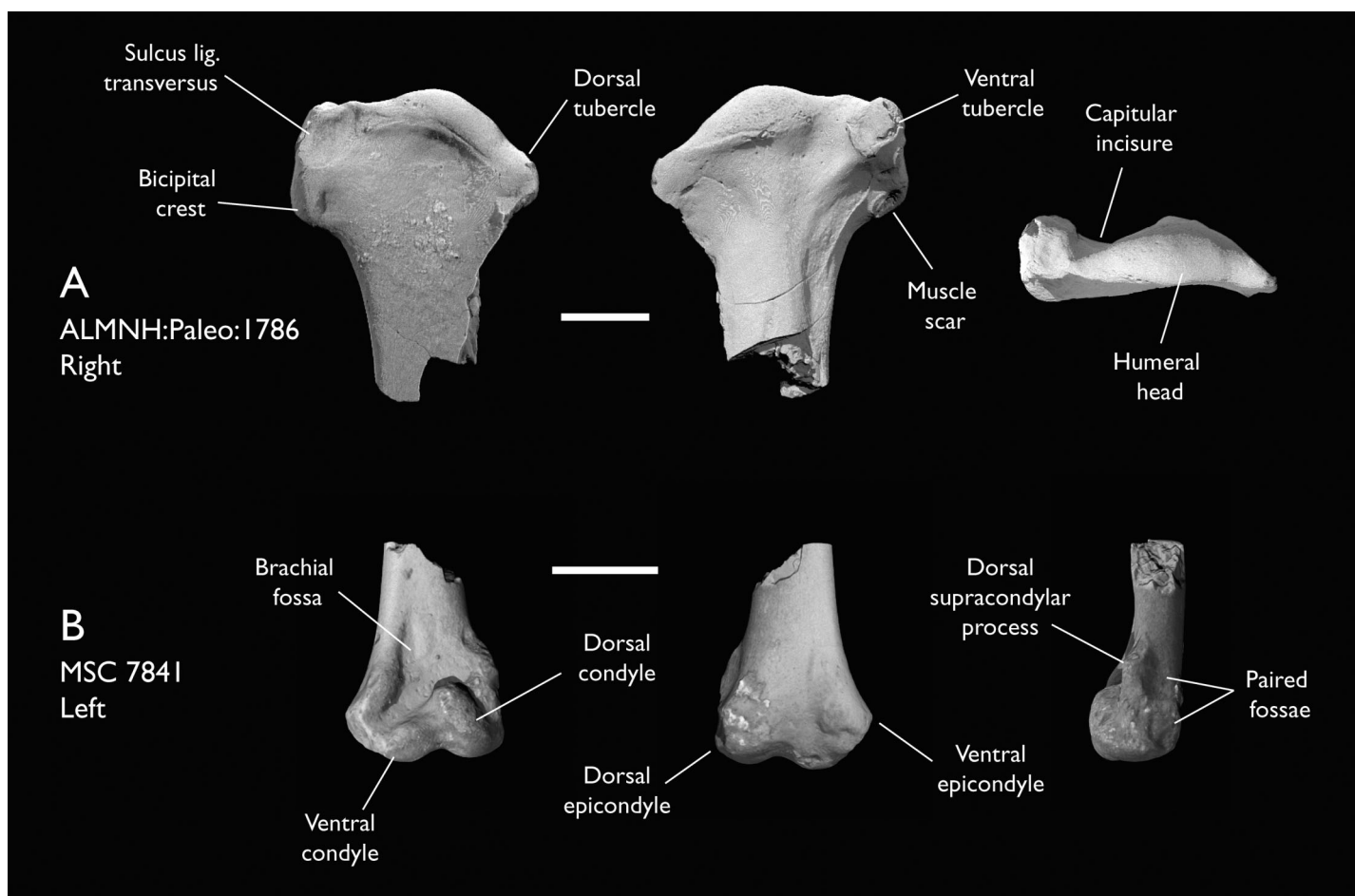
Figure 17 Detailed proximal and distal morphology of *Ichthyornis* humeri. (A) ALMNH:Paleo:1786 right proximal humerus in cranial, caudal and proximal views; and (B) MSC 7841 right distal humerus in cranial, caudal and lateral views. Scale bar equals 5 mm.

pneumatic foramina; for example, the opening evident in the right humerus of KUVP 119673 appears to be the result of breakage (Fig. 16A).

The bicipital crest is well developed in *Ichthyornis*, extending distally from the ventral tubercle, and is quadrangular in caudal view and vaguely rhomboidal in ventral view. Although the preservation of this structure in most of the studied specimens is too poor to allow clear observations, ALMNH:Paleo:1786 preserves the undistorted bicipital crest in its entirety (Fig. 17A). The cranial surface of the bicipital crest is rounded and convex, but its caudal surface is flat or slightly concave. A large rounded and shallow depression is found on the proximal portion of the ventral surface of the crest, probably corresponding to the attachment point of m. bicipitalis (*Watanabe, Field & Matsuoka, 2021*). A minute but deep rounded pit is present on the caudal surface of the crest halfway along its length, and despite its small size, is clearly visible in ALMNH:Paleo:1786 and in more flattened specimens such as the BHI 6420 and NHMUK A 905 humeri (Fig. 15A). This pit does not

seem to connect to the internal, hollow cavity of the proximal humerus, and thus probably constitutes a nutrient foramen. An ovoid and deep pit is situated on the distal surface of the bicipital crest and is visible in all the specimens preserving this region of the humerus (Fig. 15; Fig. 16; Fig. 17A). *Clarke (2004)* interpreted this depression as the attachment point for m. scapulohumeralis caudalis (*Baumel & Raikow, 1993*), and considered it as one of the autapomorphies of *Ichthyornis*.

The deltopectoral crest is well preserved on the left BHI 6420 humerus, both NHMUK A 905 humeri, KUVP 2300, and both KUVP 119673 humeri. The crest is large and has an ovoid or semiquadrangular shape (Fig. 15; Fig. 16B). The crest is extremely thin, and it becomes progressively thinner towards its edge, where it is bounded by a narrow ridge extending from the proximal dorsal tubercle. The deltopectoral crest is flattened in most of the specimens, complicating the interpretation of any muscle scars—only a subtle concave depression across most of its caudal surface is apparent. Notably, two of the specimens preserve three-dimensional deltopectoral crests: KUVP 2300 and the right humerus of KUVP 119673 (Figs. 16A and 16C). Although the deltopectoral crests in these specimens still exhibit moderate breakages and distortion, the shape and original orientation of the crest seems to be preserved, revealing that, in life, the crest would have been cranially or dorsocranially directed, similar to the condition in most crown birds (*Serrano et al., 2020*). KUVP 119673 is particularly remarkable in this regard, since it preserves both humeri, with the right element preserved in three dimensions and the left element flattened (Figs. 16A and 16B). In the flattened humeri, such as the left humerus of KUVP 119673, BHI 6420 and NHMUK A 905 (Fig. 15), the deltopectoral crest appears to be dorsally directed, but the preservation of the right humerus of KUVP 119673 (Fig. 16B) reveals that this is the product of taphonomic deformation. The deltopectoral crests of several flattened but otherwise exceptionally preserved fossil avialans, such as *Hongshanornis, Gansus*, and *Yanornis* (*Zhou & Zhang, 2001*; *Chiappe et al., 2014*; *Wang et al., 2016*), as well as previously described specimens of *Ichthyornis* (*Clarke, 2004*), have traditionally been interpreted as being dorsally directed, which has led to the hypothesis that a cranially deflected morphology constitutes a synapomorphy of crown group birds (*Clarke, 2004*; *Chiappe et al., 2014*). Only the proposed Ornithurine *Tingmiatornis* has been described as possessing a slightly cranially deflected deltopectoral crest, but this taxon has never been included in a phylogenetic analysis, and its affinities remain uncertain (*Bono et al., 2016*). The new, exceptionally preserved humeri described here underscore the considerable impact of taphonomic distortion on the preservation of the deltopectoral crest, illustrating that at last a partially cranially-directed deltopectoral crest was already present in crownward non-neornithine avialans, and that caution is needed when interpreting the presence or absence of this morphology from flattened fossil remains.

On the cranial surface of the distal end of the humerus there are two well-developed dorsal and ventral condyles of similar length (Fig. 17B). The intercondylar incisure, running ventrodistally between both condyles, is shallow, and the distinction between the condyles is not clear (Fig. 17B). The dorsal condyle is more globose and is better developed than the ventral condyle, and it curves over the concave brachial depression (fossa m. brachialis; *Baumel & Witmer, 1993*). A conspicuous nutrient foramen is positioned near
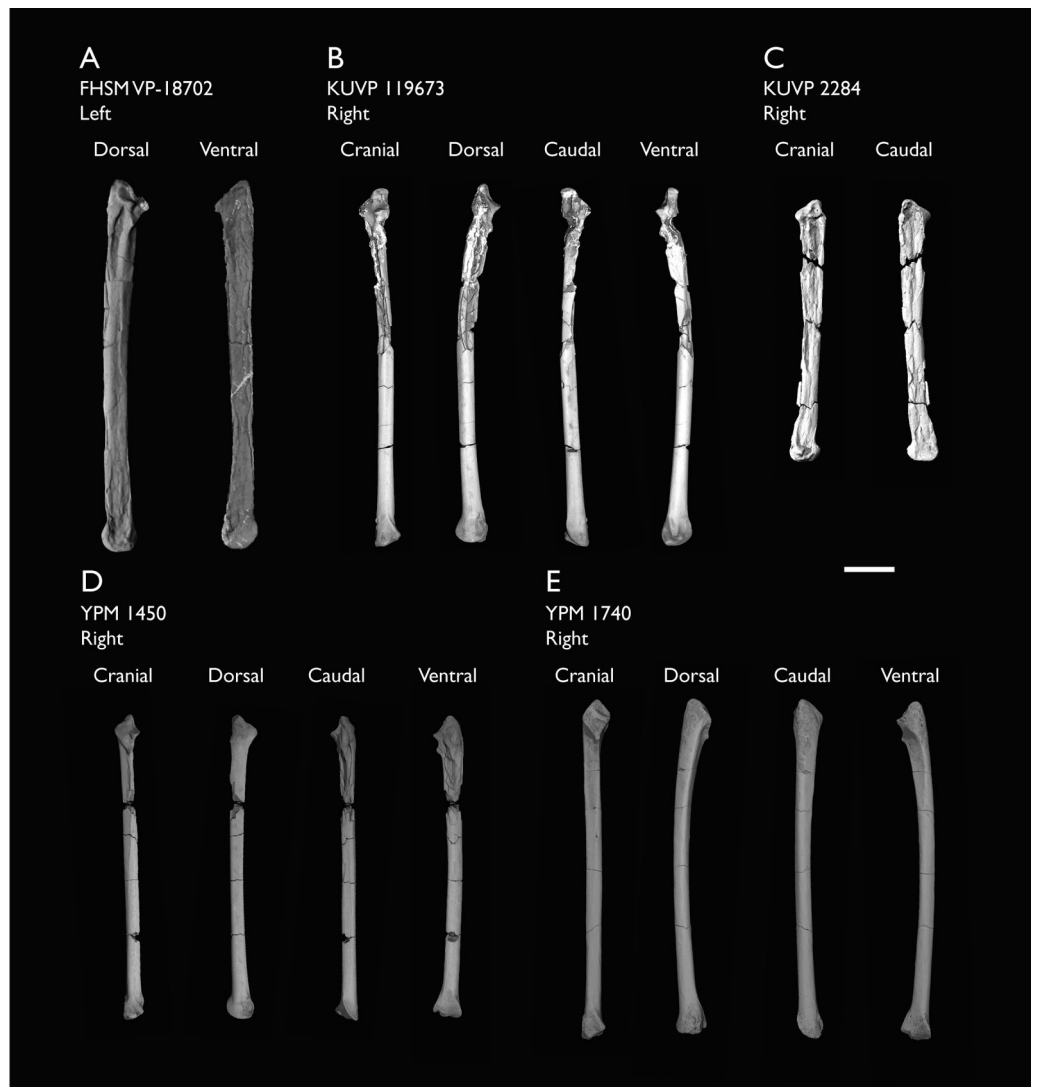
Figure 18 Ulnae of *Ichthyornis*. (A) FHSM VP-18702 in dorsal and ventral views, (B) KUVP 119673 in cranial, dorsal, caudal and ventral views, (C) KUVP 2284 in cranial and caudal views, (D) YPM 1450 and (E) YPM 1740 in cranial, dorsal, caudal and ventral views. Scale bar equals 1 cm.

the centre of the brachial depression, just proximal to the dorsal condyle. This foramen is present on some, but not all, of the YPM humeri, sometimes being present only in one of the two humeri of an individual, as in the case of the holotype (*Clarke, 2004*). The dorsal condyle projects proximally, forming a low angle with the ventral condyle, which is almost parallel to the distal edge of the humerus. The ventral epicondyle shows two complex depressions on its ventrodistal end, and another shallow depression on the cranial surface between the ventral epicondyle and the ventral supracondylar tubercle. The morphology of this region is congruent with that described by *Clarke (2004)*.

The dorsal supracondylar process is well developed and clearly preserved, extending further craniodorsally than in previously described specimens (Fig. 17B). The ventral
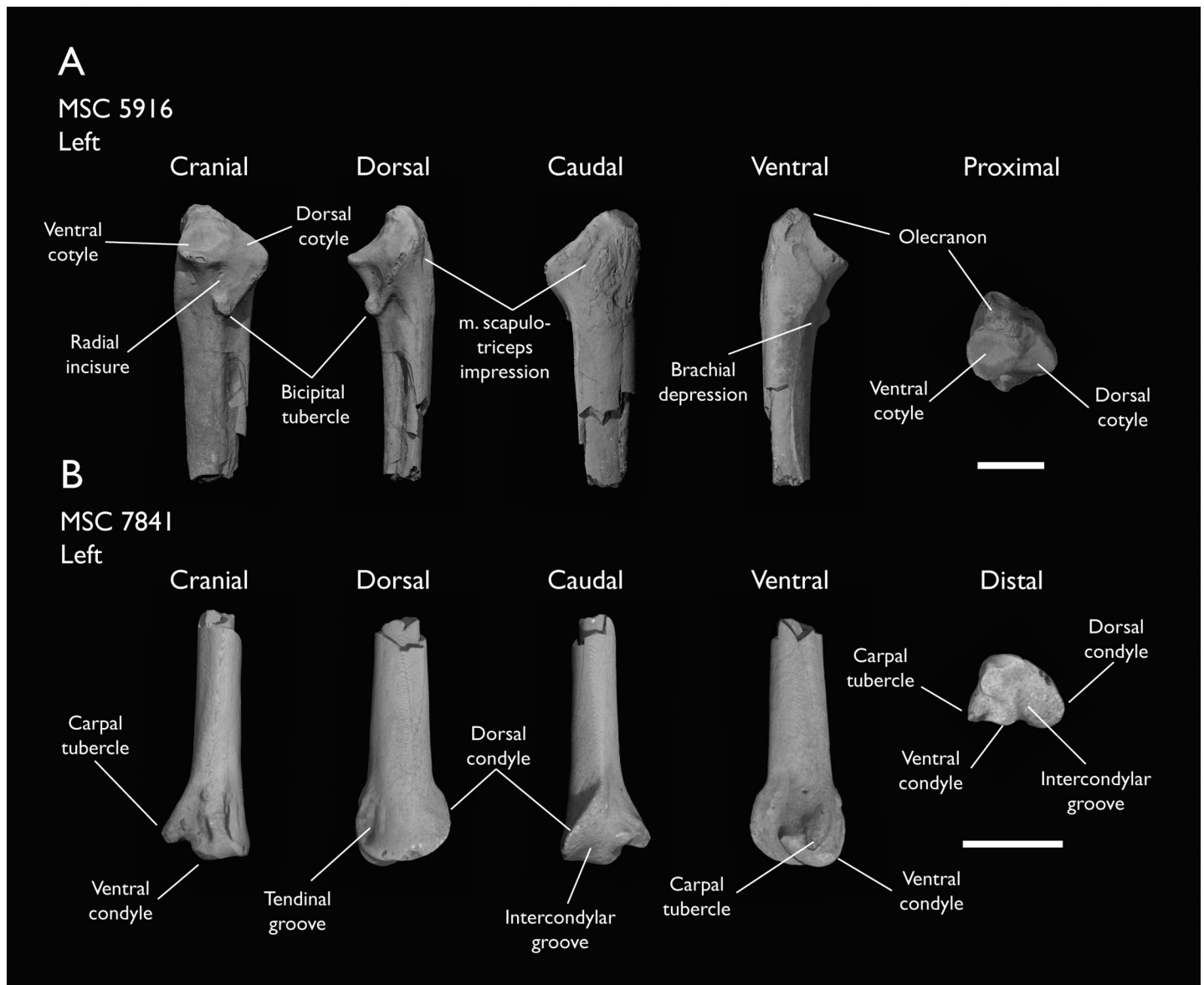
Figure 19 Detailed proximal and distal morphology of *Ichthyornis* ulnae. (A) MSC 5916 left proximal ulna and (B) MSC 7841 left distal ulna in cranial, dorsal, caudal, ventral and proximal views. Scale bar equals 5 mm.

supracondylar tubercle projects cranially but is subtler and much less developed than the dorsal supracondylar process. A shallow fossa is found just distal to the ventral supracondylar tubercle, which *Clarke (2004)* associated with the attachment point of the m. pronator superficialis. The proximal surface of the dorsal supracondylar process shows complex sculpturing, interpreted by *Clarke (2004)* as the attachment point for three different muscles.

Ulna

The ulna is preserved in eleven of the new specimens, although only FHSM VP-18702, KUVP 119673 and KUVP 2284 preserve the complete element (Figs. 18A–18C). Of these,

Table 7 **Measurements of the ulna of *Ichthyornis* specimens.** Asterisks (*) denote measurements that might be unreliable due to breakage or distortion, but are included for completeness. All measurements are in mm. – = not measurable.

Specimen	Total length	Prox. Craniocaudal width	Prox. Dorsoventral width	Dist. Craniocaudal width	Dist. Dorsoventral width	Midshaft width
BHI 6420	–	5.70*	8.47	–	–	–
BHI 6421	–	–	–	6.88	–	–
FHSM VP-18702	77.10	–	9.25*	–	7.85*	4.50*
KUVP 2284	52.49	–	6.23*	–	6.29	3.79
KUVP 119673 right	71.90	4.94	7.31*	4.97	6.90	3.20
KUVP 119673 left	–	–	–	–	7.24*	4.54*
KUVP 123459	–	–	–	5.12	6.01	–
MSC 5916	–	6.25	6.67	–	–	–
MSC 7841	–	–	–	4.54	4.84	2.23
MSC 34427	–	–	–	5.44	5.56	–
YPM 1450	61.51	5.05	5.75	4.24	5.71	2.84
YPM 1740	68.45	5.33	5.74	5.56	6.10	3.08

most are flattened or heavily distorted, and only KUVP 119673 (Fig. 18B), MSC 5916 (Fig. 19A) and MSC 7841 (Fig. 19B) are three-dimensional and generally undistorted. The two complete ulnae described by *Clarke (2004)*, YPM 1450 and YPM 1740 (Figs. 18C and 18D) remain the best preserved ulnae known for *Ichthyornis*, and the new specimens do not provide substantial new morphological information beyond that known from the YPM specimens. Measurements of the ulnae of the specimens included in this study are provided in Table 7.

The shaft of the ulna in *Ichthyornis* shows a minor degree of variation in its curvature, with some specimens showing slightly curved shafts, such as KUVP 119673 and YPM 1740 (Figs. 18B and 18E), while others such as FHSM VP-18702, KUVP 2284 and YPM 1450 show a slightly straighter shaft (Figs. 18A, 18C and 18D). Although the curvature of the shaft may be influenced by taphonomic factors, the different degree of curvature in the exceptionally preserved YPM specimens might be indicative of true intraspecific variation. As noted by *Clarke (2004)*, the bicipital tubercle is very large and extremely pointed, extending noticeably cranially, and it is most developed and evident in MSC 5916 (Fig. 19A). The brachial depression is a clear and distinct triangular depression adjacent to the bicipital tubercle; this depression is relatively shallow in YPM 1740, but is deeper and more distinct in MSC 5916 (Fig. 18A).

The olecranon process is relatively well developed, with a slightly pointed proximal end. The subround ventral cotyle extends from its cranial side (Fig. 19A). *Clarke (2004)* describes a scar present on the ventral surface of the tip of the olecranon process which is clearly preserved in MSC 5916 (Fig. 19A), but this scar is not clear in FHSM VP-18702 and KUVP 119673 (Figs. 18A and 18B), despite preservation of this region. The dorsal cotylar process (proc. cotylaris dorsalis; *Baumel & Witmer, 1993*) is subtriangular and extends dorsally well beyond the body of the ulna (Fig. 19A). Both dorsal and ventral cotyles are

well developed and of similar size, and although they are distinct, there is no clear ridge separating them (Fig. 19A).

From the bicipital process, a well-marked intermuscular line (linea intermusc.; *Baumel & Witmer, 1993*) extends along at least half the length of the shaft (Fig. 19A), but it becomes less evident after one third of its length (Figs. 18D and 18E). A small nutrient foramen is found in line with this intramuscular line in FHSM VP-18702, KUVP 119673 and the YPM specimens, in the same region where the line starts becoming less conspicuous. This foramen appears to be absent in KUVP 2284, but whether this is due to its preservational state (similar to that of FHSM VP-18702) or related to its possible early ontogenetic stage (see discussion) is unclear.

The distal portion of the ulna is well-preserved in ALMNH:Paleo:3316, KUVP 119673, KUVP 123459, MSC 6200 and MSC 7841 amongst the new specimens. In all these specimens, the length of the trochlear surface along the caudal surface of the distal ulna is approximately equal to the width of the trochlear surface, which constitutes one of the diagnostic features of *Ichthyornis* identified by *Clarke (2004)*. The distal ulna exhibits a mostly round dorsal condyle with a thin and pronounced distal edge (Fig. 19B), with a marked and deep tendinal groove on its cranial side. The ventral condyle extends distally slightly beyond the dorsal condyle, and shows a rounded distal edge. The intercondylar groove is extremely shallow in most specimens (Fig. 19B), essentially becoming a flat surface in ALMNH:Paleo:3316, but it is deeper and more marked in MSC 6200. The carpal tubercle is well-developed and projects far from the ventral surface of the ulna, although its shape and ventral extension vary among the studied specimens. This tubercle is relatively short and moderately pointed in YPM 1740 (Fig. 18E), KUVP 13459 and MSC 6200, with a shallowly excavated distal surface; it is more pointed and better developed in ALMNH: Paleo:3316 and KUVP 119673 (Fig. 19B), with a concave ventral surface, and is very well developed in YPM 1450 and MSC 7841, with an excavated ventral surface and a moderate inflation at its tip (Fig. 18D; Fig. 19B), which gives it a hooked appearance in cranial and caudal views.

Radius

The radius is preserved in ten of the new specimens included in this study. Of these, only the right radius of KUVP 119673 (divided into two fragments) and YPM 1741, and the left radius of FHSM VP-18702 and KUVP 25472 are complete (Figs. 20A–20C). Of all the other fragmentary radii, the left proximal radius of KUVP 119673 and MSC 6200 (Figs. 20B and 20D) and right distal radius of BHI 6420 and KUVP 157821 (Fig. 20E) are the best preserved. Measurements of the radii of the specimens included in this study are provided in Table 8.

As described by *Clarke (2004)*, the proximal end of the radius shows an ovoid humeral cotyle. Though Clarke describes this cotyle as slightly concave, it is essentially flat in all the studied specimens save for YPM 1741. The ulnar facet is shallow and fairly indistinct, and a moderately developed and robust tubercle extends cranially opposite of the ulnar facet (Fig. 20D). A slight ridge extends distally from the tubercle, delimiting an ovoid fossa. This fossa was described by *Clarke (2004)* as equivalent to the very marked bicipital process of
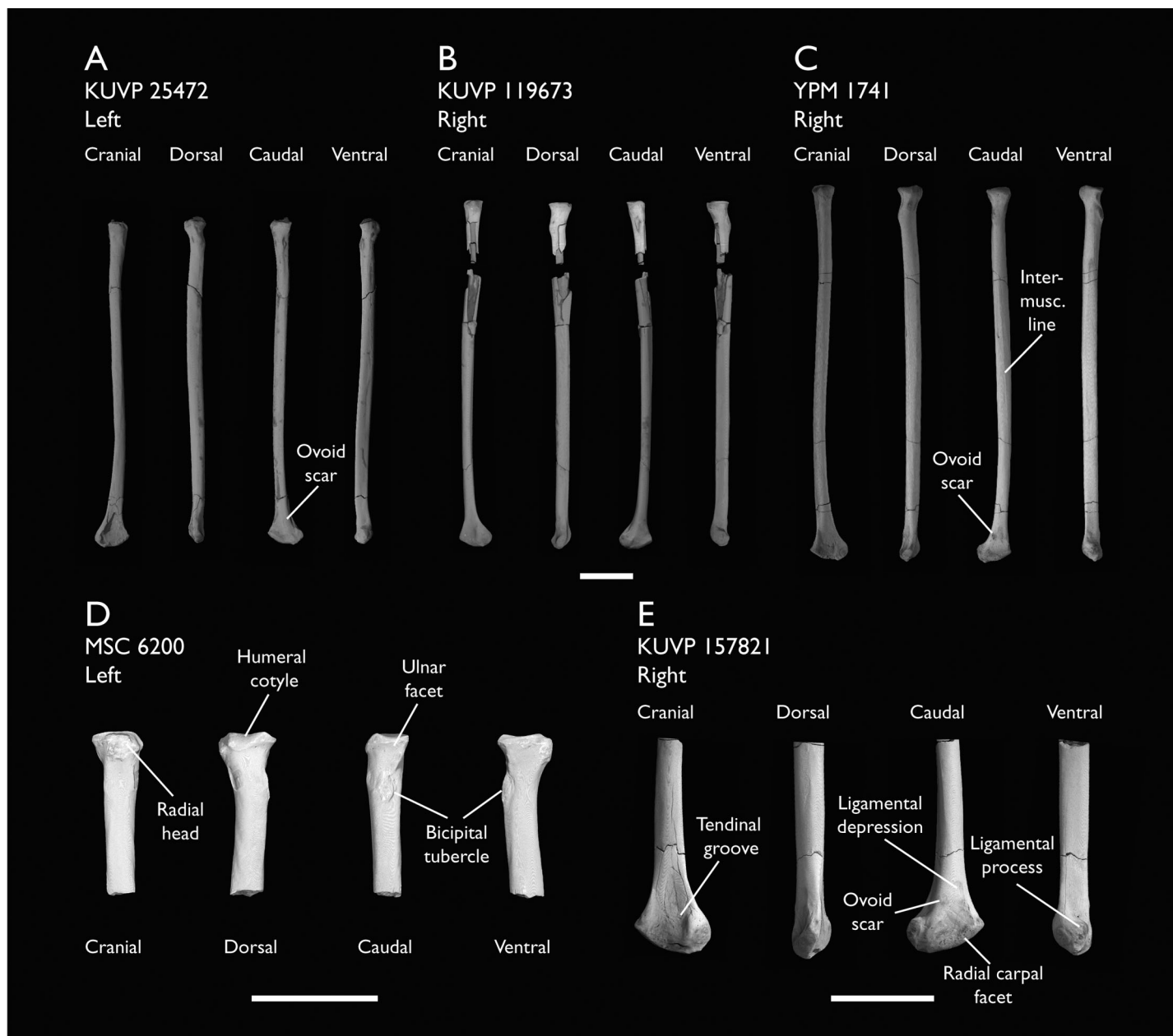
Figure 20 Radii of *Ichthyornis*. (A) KUVP 25472, (B) KUVP 119673 and (C) YPM 1471 in cranial, dorsal, caudal and ventral views, (D) proximal radius of MSC 6200 and (E) distal radius of KUVP 157821 in cranial, dorsal, caudal and ventral views. Scale bars equals 1 cm.

the ulna. Clarke noted a second conspicuous scar extending proximodistally from the tubercle; this is not visible in any of the studied specimens. Minor breakage in the shaft distal to the tubercle might have obscured this region. The ovoid bicipital tubercle is found on the caudal surface of the proximal radius; it is only moderately developed and shows a rugose texture (Fig. 20D).

The radial shaft is essentially straight in the complete new specimens (Figs. 20A and 20B), showing less curvature in cranial or caudal views than the YPM specimens

Table 8 **Measurements of the radius of *Ichthyornis* specimens.** Asterisks (*) denote measurements that might be unreliable due to breakage or distortion, but are included for completeness. All measurements are in mm. – = not measurable.

Specimen	Total length	Prox. Craniocaudal width	Prox. Dorsoventral width	Dist. Craniocaudal width	Dist. Dorsoventral width	Midshaft width
BHI 6420	–	–	–	3.19	6.63	–
FHSM VP-18702 right	–	–	–	–	6.318*	–
FHSM VP-18702 left	72.20	3.14	4.52	4.578*	6.92	3.403*
KUVP 2284	–	–	–	–	–	–
KUVP 25472	62.29		3.96	–	6.77	2.19
KUVP 119673 right	61.51	3.48	4.51	–	6.23	2.02
KUVP 119673 left	–	–	4.699*	–	–	–
KUVP 157821	–	–	–	3.87	7.56	3.12
MSC 5895	–	3.17*	4.23	–	–	–
MSC 6200	–	4.11	4.51	–	–	–
YPM 1741	71.45	4.68	4.70	4.26	7.30	2.59

(Fig. 20C). A clear and marked intermuscular line or ridge extends along most of the ventral surface of the radial shaft to the distal end of the bone (Figs. 20A–20C). *Clarke (2004)* identified this structure and extensively discussed the possible muscular attachment points in this region.

Craniodorsally, the distal end of the radius shows a very conspicuous and marked tendinal groove (sulcus tendineus; *Baumel & Witmer, 1993*). The edge of the groove forms a ridge that runs across the ventral margin of the distal end of the radius towards the shaft. *Clarke (2004)* described a very marked and prominent ovoid scar found on the caudal surface of the distal radius, in the middle of the ligamentous depression (depression ligamentosa; *Baumel & Witmer, 1993*). This scar is present in all of the studied specimens preserving the distal portion of the bone, with the exception of KUVP 15782 and BHI 6420, in which it is very faint and barely observable (Fig. 20E), and KUVP 119673, in which it is not visible (Fig. 20A). This scar constitutes one of the autapomorphies of *Ichthyornis dispar*, although its absence in KUVP 119673 together with variation in its distinctness among the rest of the specimens may cast doubt on the extent to which it is truly diagnostic for *Ichthyornis*. A second, less-marked ovoid scar is found ventral to the first scar, at the base of a slightly developed caudal process, identified by *Clarke (2004)* as the ligamental process (tuberculum aponeurosis ventralis; *Baumel & Witmer, 1993*). The articular surface for the radial carpal is found dorsal to this process.

Ulnar carpal

Three specimens included in this study contain the ulnar carpal bone: FHSM VP-18702 preserves the right ulnar carpal, ALMNH:Paleo:3316 preserves both the left and right ulnar carpals (Fig. 21A), and KUVP 2284 preserves the left ulnar carpal (Fig. 21B). Only the ulnar carpal of SMM 2503 was previously known for *Ichthyornis*, though it was missing a portion of its dorsal ramus (crus breve; *Baumel & Witmer, 1993*) (*Clarke, 2004*).
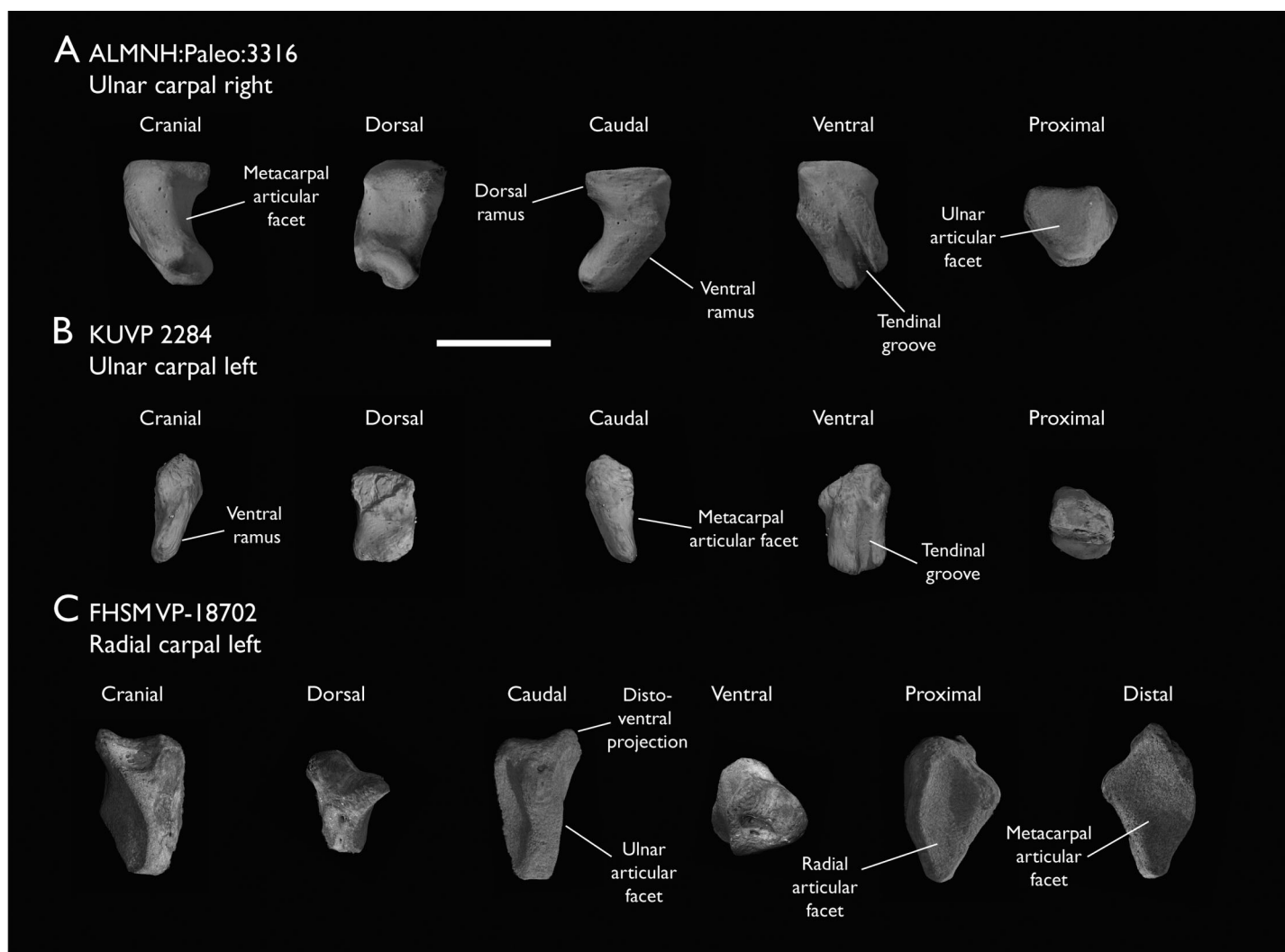
Figure 21 Free carpal bones of *Ichthyornis*. (A) ALMNH:Paleo:3316 right ulnar carpal and (B) KUVP 2284 left ulnar carpal in cranial, dorsal, caudal, ventral and proximal views; (C) FHSM VP-18702 left radial carpal, in cranial, dorsal, caudal, ventral, proximal and distal views. Scale bar equals 5 mm.

The condition of the ulnar carpal bones of both FHSM VP-18702 and ALMNH:Paleo:3316 is exceptional, whereas the ulnar carpal of KUVP 2284 is missing its entire dorsal ramus. The morphology of the ulnar carpal bone in the new specimens is essentially identical to that described by *Clarke (2004)*, with the exception of KUVP 2284.

The ulnar carpal is somewhat claw shaped in cranial view (Fig. 21A), with a short, flattened dorsal ramus and a longer, more robust ventral ramus. The metacarpal incisure (incisura metacarpalis; *Baumel & Witmer, 1993*) is shallow and rounded. The articulation facet for the ulna is flat and subtriangular in dorsal view. *Clarke (2004)* described the tip of the dorsal ramus of SMM 2503 as missing, but the morphology of this structure seems to be essentially identical in both FHSM VP-18702 and ALMNH:Paleo:3316, in which the region is slightly eroded, but without obvious signs of breakage (Fig. 21A).

The ventral ramus (crus longum; *Baumel & Witmer, 1993*) is elongate and recurved in FHSM VP-18702 and ALMNH:Paleo:3316, with a markedly concave cranial surface and a moderately convex caudal surface, and becomes slightly wider at its ventral end (Fig. 21A). In contrast, the ventral ramus seems to be essentially straight in KUVP 2284, with both its dorsal and ventral ends on the same axis (Fig. 21B). This specimen exhibits flat cranial and caudal surfaces and lacks the ventral expansion present in the other specimens, instead slightly tapering ventrally. The ventral ramus of all three specimens preserves a deep and marked tendinal groove running across most of its flat caudal surface (Figs. 21A and 21B). This tendinal groove originates at the base of the dorsal ramus of the ulnar carpal and extends to the midpoint of the ventral surface of the bone, at the articulation facet for the carpometacarpus. The groove is moderately proximodistally curved in FHSM VP-18702 and ALMNH:Paleo:3316 (Fig. 21A), but is completely straight in KUVP 2284 (Fig. 21B). A round shallow pit is found on the cranial surface of the distalmost portion of the ventral ramus in both ALMNH:Paleo:3316 radial carpals, but it seems to be absent in FHSM VP-18702 and KUVP 2284. The articular facet for the carpometacarpus, found on the cranial surface of the ventral ramus, is rounded with a moderately marked cranioventral depression in the two complete specimens; this depression is missing in KUVP 2284, in which this region is essentially flat (Fig. 21B).

The morphology of the ulnar carpal is poorly preserved in most Mesozoic avialans, preventing detailed comparisons, although it is very similar in *Iaceornis*. However, the dorsal ramus in *Iaceornis* is slightly reduced and its ventral ramus is moderately straighter than in *Ichthyornis*.

Radial carpal

Following *Clarke (2004)*, no radial carpal bones have been attributed to *Ichthyornis*, as YPM 1734, which bears a radial carpal, was reassigned as the holotype of *Iaceornis marshi* (*Clarke, 2004*). Two of the specimens studied here include exceptionally preserved radial carpals; BHI 6420 preserves the right radial carpal and FHSM VP-18702 preserves both the right and left elements (Fig. 21C). The morphology of the radial carpal is congruent in both specimens, and fills a gap in our knowledge of carpal anatomy among crownward stem birds, in which the radial carpal is rarely well-preserved or described.

All of the preserved radial carpals exhibit a dorsoventrally elongate shape, and are relatively compressed proximodistally (Fig. 21C). Their ventral surfaces are flat and concave, with a moderately developed distoventral projection. The elongated dorsal region of the radial carpal ends in a narrow tip. The flattened distal surface of the bone is rhomboidal in shape and slightly concave (Fig. 21C), forming the articular surface for the carpometacarpus (facies articularis metacarpalis; *Baumel & Witmer, 1993*). This articular surface is delimited on its cranial side by a marked ridge running dorsoventrally from the dorsal end of the radial carpal to the tip of the distoventral projection. The proximal surface of the bone is a shallow ovoid depression (Fig. 21C), forming the articular surface for the radius (facies articularis radialis; *Baumel & Witmer, 1993*).

In caudal view, the radial carpal exhibits a wide and mostly flat ridge running dorsoventrally, delimiting on one side the proximal articular surface for the radius and the

articular surface for the carpometacarpus on the distal side (Fig. 21C). This ridge continues into a process around the midpoint of its length, with two well marked foramina on the ventral side of this process. The ridge becomes flat and slightly concave dorsal to the process, corresponding to the articular surface for the ulna (facies articularis ulnaris; *Baumel & Witmer, 1993*).

A relatively wide and shallow sulcus for the tendon of m. ulnometacarpalis ventralis is found at the centre of the ventral surface of the radial carpal (Fig. 21C). The cranial end of this sulcus forms a subtle ridge running proximodistally from the base of the distoventral process to the proximal end of the sulcus. This ridge delimits a subtriangular depression with a considerable number of foramina in its cranial side. The more proximal region of the cranial side of the radial carpal preserves a flat, elevated and moderately concave surface, which roughly corresponds to the sulcus for the tendon of m. extensor carpi radialis (*Mayr, 2014*). This sulcus runs dorsoventrally and maintains the same width for most of its length, enlarging slightly at its proximoventral end.

The morphology of the radial carpal has not been thoroughly described for most comparable fossil taxa, which makes comparisons with *Ichthyornis* difficult, but the overall proportions and morphology seen in *Ichthyornis* are quite similar to those of *Iaceornis* (*Clarke, 2004*) and *Presbyornis* (J. Benito, 2021, personal observations), suggesting that a comparable shape may have characterized the radial carpal of the ancestral neornithine. The radial carpal morphology varies greatly amongst extant crown birds (*Mayr, 2014*), but the morphology in *Ichthyornis* resembles most closely that of Anatidae and Pandionidae: these taxa exhibit a generally comparable elongate shape, together with the presence of a short but distinct distoventral projection and a rounded, concave, and porous cranial surface.

Carpometacarpus

Nine of the newly studied specimens preserve carpometacarpi, but the complete element is only represented in BHI 6420 (Fig. 22C). FHSM VP-18702, KUVP 123459, KUVP 157821 and ALMNH:Paleo:3316 preserve both the proximal and distal ends of the carpometacarpus but are missing part or most of the metacarpal shafts (Figs. 22B, 22D and 22E). MSC 3394 and 34426 preserve only the distal portion of the element. The carpometacarpus of YPM 1724, already described by *Clarke (2004)* and included in this study, remains the most complete and best preserved carpometacarpus known for *Ichthyornis* (Fig. 22A). Measurements of the carpometacarpus of the specimens included in this study are provided in Table 9.

The carpometacarpus in *Ichthyornis* is a proportionally long element, extending for about half of the length of the humerus or the ulna. Out of all the carpometacarpi studied, FHSM VP-18702 stands out as being shorter than other similarly proportioned specimens such as BHI 6420 and YPM 1724, representing only 87% of their maximum length (Figs. 22A–22C). The FHSM VP-18702 carpometacarpus is divided into two proximal and distal fragments that seem to match perfectly, thus it seems that no part of its length is missing (Fig. 22B). *Clarke (2004)* reported certain carpometacarpi of differing lengths despite overall similar proportions, such as the relatively short carpometacarpus of YPM 1755
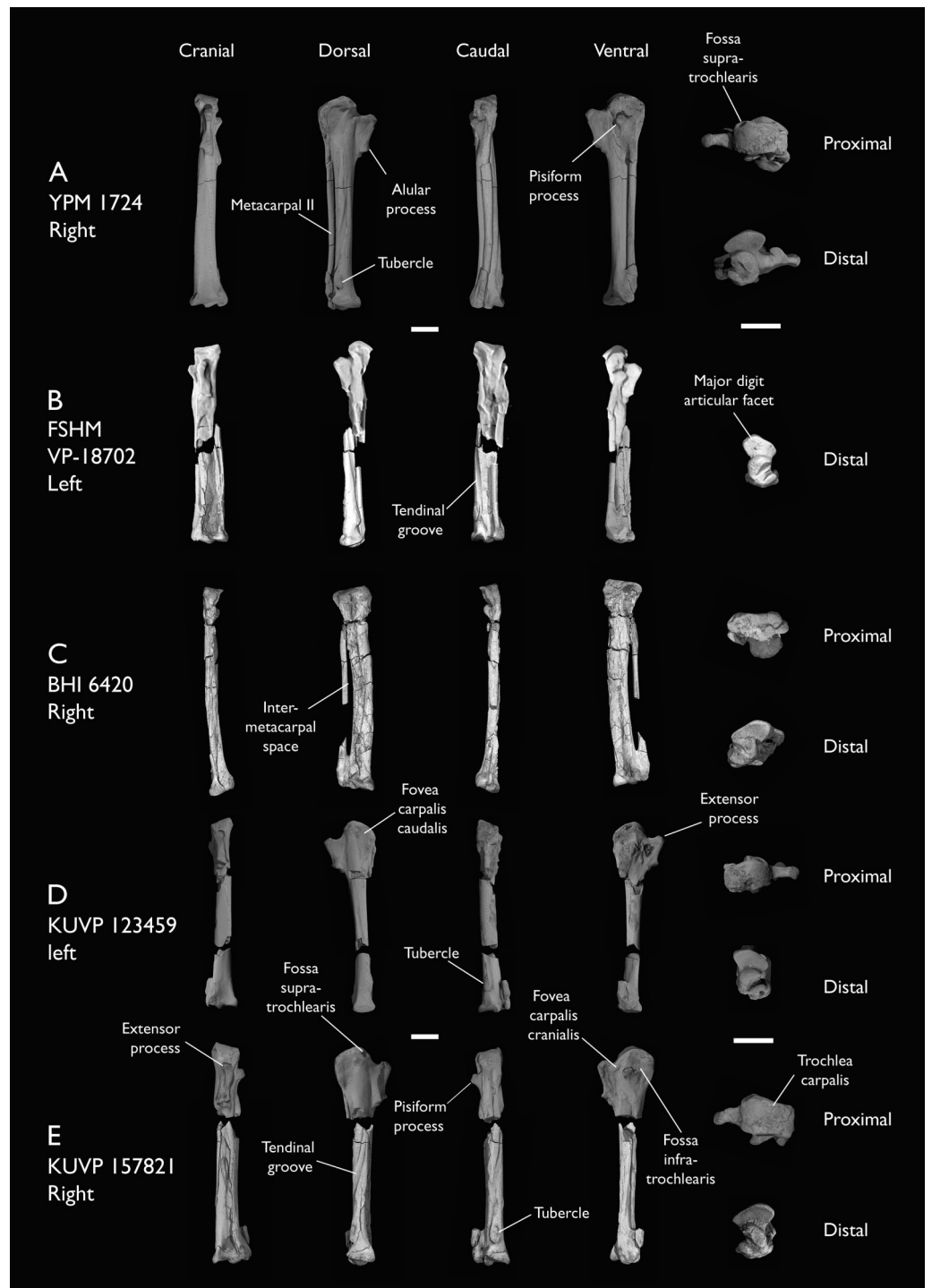
Figure 22 Carpometacarpi of *Ichthyornis*. (A) YPM 1724, (B) FHSM VP-18702, (C) BHI 6420, (D) KUVP 123459 and (E) KUVP 157821, in cranial, dorsal, caudal, ventral, proximal and distal views. Scale bar equals 5 mm.

Table 9 Measurements of the carpometacarpus of *Ichthyornis* specimens. Proximal craniocaudal width is measured as the maximum craniocaudal extension of the proximal carpometacarpus, including the extensor process of metacarpal I. Proximal dorsoventral width corresponds to the maximum dorsoventral extension of the proximal carpometacarpus, including the pisiform process. Asterisks (*) denote measurements that might be unreliable due to breakage or distortion, but are included for completeness purposes. All measurements are in mm. − = not measurable.

Specimen	Total length	Prox. Craniocaudal width	Prox. Dorsoventral width	Dist. Craniocaudal width	Dist. Dorsoventral width
ALMNH:Paleo:3316	−	−	−	6.41	4.95
BHI 6420	38.54	7.88	4.47*	6.51	4.73
FHSM VP-18702	36.03	7.24	6.29*	6.55	4.42
KUVP 123459	−	9.63	−	6.05	4.74
KUVP 157821	39.04*	10.25	6.25	7.22	5.44
MSC 2841	−	−	−	5.53	4.38
MSC 3394	−	−	−	4.56	3.10*
MSC 6202	28.21*	9.98	6.94	6.87	4.74
MSC 34426	−	−	−	6.60	4.39
YPM 1742	39.58	10.99	5.18	6.56	5.24

Table 10 Measurements of the manual phalanx II:1 of *Ichthyornis* specimens. Total length and distal craniocaudal width measurements include the internal index process, when preserved. Asterisks (*) denote measurements that might be unreliable due to breakage or distortion, but are included for completeness. All measurements are in mm.

Specimen	Total length	Prox. Craniocaudal width	Prox. Dorsoventral width	Dist. Craniocaudal width	Dist. Dorsoventral width	Max. Craniocaudal width
ALMNH:Paleo:3316	22.03	5.96	4.80	5.60	3.37	7.32
BHI 6420	23.81	4.99	2.98*	6.41	3.09	8.11
BHI 6421	20.93	3.96	4.91	5.80	3.95	6.90
FHSM VP-18702	23.44*	5.45*	5.08	5.17*	3.42*	6.97
KUVP 2284	15.63	3.33	2.74	3.39	2.36	4.91
MSC 5895	20.70	4.32	4.33	5.82	4.18	6.58*
MSC 6201	19.97*	4.36	4.36	4.97*	3.74	7.08

compared with the similarly proportioned but longer one of YPM 1773. However, none of the other YPM specimens preserved enough material for further comparison. Comparison of BHI 6420 and FHSM VP-18702 reveals virtually equal lengths for several of their skeletal elements, such as the coracoid, the scapula, and the major manual digit phalanx (Tables 4, 5 and 10), and both specimens are otherwise comparable in their morphology and estimated mass (see body mass estimates below), seemingly confirming substantial variation in carpometacarpus length within *Ichthyornis*. Future work might clarify whether this disparity corresponds to intraspecific or interspecific variation.

As described by *Clarke (2004)*, both the proximal and distal articular surfaces of the carpometacarpus bear a large number of small foramina, which can be observed in all the studied specimens except for FHSM VP-18702, although their absence in this specimen might be preservational. The carpal trochlea (trochlea carpalis; *Baumel & Witmer, 1993*) is large and well developed, and is flat in proximal view in all specimens. No groove is present between the lateral and medial condyles (Fig. 22A). Both condyles share a similar caudal

extension and extend parallel to each other, contrary to the condition widespread among crown birds in which the medial condyle extends further caudally (*Livezey & Zusi, 2006*). Therefore, no distinct ulnocarpal articular facet is developed on the dorsal surface of the medial condyle, a condition roughly comparable to that of *Chauna*. The cranial surface of the proximal carpometacarpus is mostly flat, and the supratrochlear fossa (fossa supratrochlearis; *Baumel & Witmer, 1993*) is shallow and only moderately developed (Fig. 22A). The attachment point for the ligament ulnocarpo-metacarpale dorsale (*Baumel & Raikow, 1993*; *Watanabe, Field & Matsuoka, 2021*) is present just cranial to the supratrochlear fossa, visible as a shallow, rounded and faint depression in YPM 1724 and KUVP 25472 (Fig. 22A), and much more deeply excavated and distinct in KUVP 157821 (Fig. 22E). A rounded, pit-like scar is situated on the cranial edge of the lateral condyle just proximal to this depression in all the studied specimens, congruent with the attachment point for the m. ulnocarpalis dorsalis (*Watanabe, Field & Matsuoka, 2021*).

The pisiform process is situated at approximately the same level as the proximal end of the extensor process, whereas it is usually more distally situated in crown group birds (*Clarke, 2004*). It is short and robust, projecting slightly cranioventrally and overhanging slightly over the cranial carpal fovea, but not as far as in the surveyed charadriiforms. The pisiform appears to be proportionally larger in FHSM VP-18702 (Fig. 22B), although the surrounding region is heavily distorted, which complicates an accurate comparison. The caudoproximal surface of the pisiform process is flat in all the studied specimens except FHSM VP-18702 and KUVP 157821, in which a minute and shallow fovea for the aponeurosis ventralis (*Baumel & Raikow, 1993*) is developed (Figs. 22B and 22E). A faint ridge extending distally from the pisiform process and reaching metacarpal III is visible in YPM 1724 and especially in KUVP 157821 (Figs. 22A and 22E), but is not preserved in the rest of the specimens. A shallow oval scar is situated caudal to this ridge only in KUVP 157821 (Fig. 22E), congruent with the attachment point for the ligament ulnocarpo-metacarpale ventrale (*Watanabe, Field & Matsuoka, 2021*). The infratrochlear fossa (fossa infratrochlearis; *Baumel & Witmer, 1993*) is shallow and poorly defined, as is the cranial carpal fovea.

Metacarpal I extends distally up to the distal extension of the proximal metacarpal symphysis as described by *Clarke (2004)* in YPM 1724, FHSM VP-18702, and KUVP 157821 (Figs. 22A, 22B and 22E), although it seems to end slightly more proximally in KUVP 25472 and ALMNH:Paleo:3316. The extensor process is subtriangular, and the cranial edge of metacarpal I is straight, running proximodistally between the cranialmost extension of the extensor process and the alular facet, subparallel to the main axis of the carpometacarpus (Fig. 22A). This is in contrast to most surveyed crown birds, in which the extensor process is significantly more cranially projected than the alular facet and the cranial edge of metacarpal I is positioned diagonal to the main axis of the carpometacarpus, as in *Puffinus lherminieri* or *Sterna hirundo*. The cranial edge of the process is thickened and the ventral surface is slightly concave, although it does not develop into a large concavity continuous with the cranial carpal fovea (fovea carpalis cranialis; *Baumel & Witmer, 1993*) as in Galliformes. In KUVP 157821 the ventral surface of the extensor process shows a large, round and deep depression (Fig. 22E); it is unclear if

this is taphonomic in origin, although the surrounding proximal carpometacarpus is well-preserved. A similar rounded depression is present in this region in *Iaceornis*. The articular surface for the alular digit is flat and shelf-like, and is moderately dorsoventrally expanded, as in *Sterna hirundo*.

Metacarpal II is long, robust, and circular in cross-section. A flat scar is present on its proximal dorsocaudal surface in both YPM 1724 and KUVP 157821, starting in a position equivalent to the alular articular surface on the cranial surface (Figs. 22A and 22E). This scar was interpreted by *Clarke (2004)* as equivalent to the intermetacarpal process where developed, serving as an insertion point for the m. extensor metacarpi ulnaris. This scar runs parallel to the tendinal groove (sulcus tendineus; *Baumel & Witmer, 1993*) until the midpoint of metacarpal II. The scar appears to be entirely absent in all other studied specimens. The tendinal groove is wide and marked; it runs proximodistally across the cranial surface of metacarpal II until its midpoint, after which it is deflected caudally, wrapping around metacarpal II, in a similar manner to that of *Sterna hirundo*.

Metacarpal III is significantly reduced in both craniocaudal and dorsoventral diameter compared with metacarpal II, and it is mostly straight and parallel to it, defining an extremely narrow intermetacarpal space (Figs. 22A, 22C and 22E). Although most crownward Mesozoic euornitheans share an extremely reduced intermetacarpal space, the condition in *Ichthyornis* is narrower than in comparable taxa such as *Gansus* (*Wang et al., 2016*) and *Iaceornis* (*Clarke, 2004*). Several crown bird groups with an elongated carpometacarpus also exhibit a straight metacarpal III, such as *Puffinus lherminieri*, *Sterna hirundo*, and *Presbyornis pervetus*, but such a reduced intermetacarpal space is uncommon, restricted mostly to ecologically specialized taxa such as Sphenisciformes and Gaviiformes. Metacarpal III is slightly craniocaudally compressed in its proximal region, but becomes progressively more circular in cross-section along its length. A tear-shaped and moderately ventrally developed tuberosity is visible on the ventral surface of metacarpal III, just proximal to the distal end of the proximal metacarpal symphysis, observable in YPM 1724 and KUVP 157821 and only faintly visible in FHSM VP-18702 (Figs. 22A, 22B and 22E). A similar tuberosity appears to be present in *Iaceornis*, and is variably present among crown bird lineages, including *Crypturellus variegatus* and, combined with a shallow scar, *Sterna hirundo* and *Scolopax rusticola*, in which it is associated with a second attachment point for the ligament ulnocarpo-metacarpale ventrale (*Watanabe, Field & Matsuoka, 2021*).

Metacarpals II and III are almost equal in their distal extent, and the intermetacarpal symphysis is flat to moderately concave in cranial view. The dorsodistal terminus of metacarpal II defines a large and oval-shaped flat distal surface for the articulation of the major manual digit. This region bears a large and rounded dorsal process.

Phalanx II-1

Six of the studied specimens preserve the first phalanx from the second digit, most of them in excellent condition: FHSM VP-18702 (left), BHI 6420 (left and right), BHI 6421 (right), ALMNH:Paleo:3316 (right), KUVP 2284 (right) and MSC 6201 (right) (Figs. 23A–23E). These show a clear size distribution, with KUVP 2284, the smallest specimen (Fig. 23B),
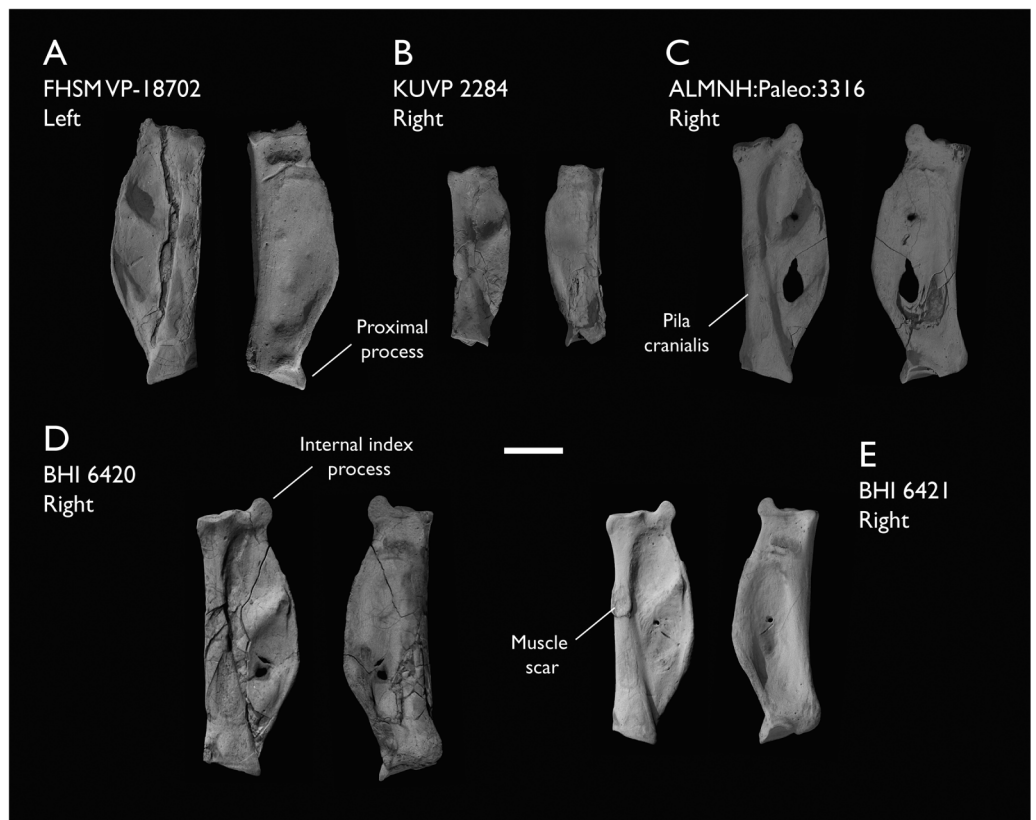
Figure 23 Manual phalanx II-1 of *Ichthyornis*. (A) FHSM VP-18702 left phalanx, (B) KUVP 2284 right phalanx, (C) ALMNH:Paleo:3316 right phalanx, (D) BHI 6420 right phalanx and (E) BHI 6421 right phalanx, in dorsal (left) and ventral (right) views. Scale bar equals 5 mm.

being only ~66% of the length of the largest specimens, BHI 6420 and FHSM VP-18702 (Figs. 23A and 23D; Table 10).

The phalanx is elongate, and around 60% of the length of the carpometacarpus (Table 9). The element is dorsoventrally flattened and caudally expanded. The proximal articular surface is roughly quadrangular in proximal view, with a large, marked concave depression on its caudoventral margin for the major digit articular facet of the carpometacarpus. A robust and well-developed caudoproximally-directed process bounds this depression cranially. The development of this process varies among the studied specimens and apparently exhibits negative allometry: it is very short in FHSM VP-18702 and BHI 6421 and proportionally longer in ALMNH:Paleo:3316 and MSC 6201 (Figs. 23A, 23C and 23E). *Clarke (2004)* hypothesized that this process could represent a synapomorphy of *Ichthyornis dispar* + Neornithes, but this feature seems to be obscured in most comparable Mesozoic euornitheans, so this hypothesis cannot be properly assessed at present. A process comparable to that of *Ichthyornis* is widespread among extant birds, with a similar extension observable in, for example, *Gallus gallus* and *Stercorarius antarctica*.

A large tubercle is present just distal to the proximal articular surface on the cranioventral surface of the phalanx, likely for the distal implantation of the m. abductor digiti majoris (*Baumel & Raikow, 1993*). This tubercle extends into a marked ridge that delimits the ventral side of the cranial pillar (pila cranialis; *Baumel & Witmer, 1993*). The cranial pillar is robust and dorsoventrally wide, with a mostly flat cranial surface and a rounded dorsal surface. A very large oval muscle scar is present on the dorsal surface of the pila between 50% (ALMNH:Paleo:3316) and 55% (BHI 6421) of its distal extent in all specimens (Figs. 23A, 23C, 23D and 23E) except for KUVP 2284, in which a very shallow impression is only faintly observable (Fig. 23B). The craniocaudal width of the scar is approximately equal to the width of the dorsal surface of the cranial pillar in all specimens except BHI 6421, in which it is wider than the pillar (Fig. 23E). The proximal and cranial margins of the scar are raised, and its dorsal surface is flat. A similar scar has apparently only been described in *Yixianornis* (*Clarke, Zhou & Zhang, 2006*) among Mesozoic euornitheans, and no equivalent scar is present in this region for any surveyed crown bird.

The dorsal surface of the phalanx caudal to the cranial pillar shows two large rounded depressions, with the proximal depression larger than the distal one. These depressions, present in most extant birds examined, are not perforated, though the bone becomes very thin at their centre and both BHI 6420 and ALMNH:Paleo:3316 show breakage in this region (Figs. 23C and 23D). The proximal depression shows a large foramen on its distal edge in several specimens, which penetrates the bone only in BHI 6421. Both depressions are separated by a wide caudodistally directed ridge (pila obliqua fossae; *Livezey & Zusi, 2006*) extending from a position roughly equivalent to the aforementioned scar, although this varies among the different specimens, and is situated distinctly proximal to the scar in BHI 6421. The caudal termination of this ridge is dorsally raised, with a marked groove on its caudal surface, likely for the passage of the m. interosseus ventralis tendon (*Baumel & Raikow, 1993*; *Vazquez, 1995*). The ventral surface of the phalanx is mostly flat, showing a shallow and large depression extending proximodistally along most of its surface. A shallow and narrow groove is found on the distal portion of the ventral surface, running craniocaudally and reaching the caudal margin of the phalanx. This groove is mostly straight and horizontal in most specimens, but shows pronounced cranial curvature in ALMNH:Paleo:3316 and distal curvature at its midpoint in FHSM VP-18702 (Figs. 23A and 23C). The caudal edge of the phalanx forms a wide curve between the proximal and the distal articular surfaces, but in KUVP 2284 and, to a lesser degree, in FHSM VP-18702, this curve ends abruptly at around 90% of the phalanx length (Figs. 23A and 23B), distal to which the caudal edge becomes straight, similar to the condition in *Iaceornis marshi* (*Clarke, 2004*). In both specimens, this point is equivalent to the point where the ventral craniocaudal groove reaches the caudal edge of the phalanx. The caudal edge of the phalanx is slightly widened craniocaudally and dorsally recurved, forming a narrow ridge that expands around the midpoint of the caudal surface, where it meets the caudal end of the pila obliqua fossae.

The distal articular surface is dorsoventrally expanded with respect to the cranial pillar, and mostly flat, with a moderately developed condyle for phalanx II-2 in its centre. A short tubercle is present just proximal to the craniodorsal edge of the articular surface. A smaller
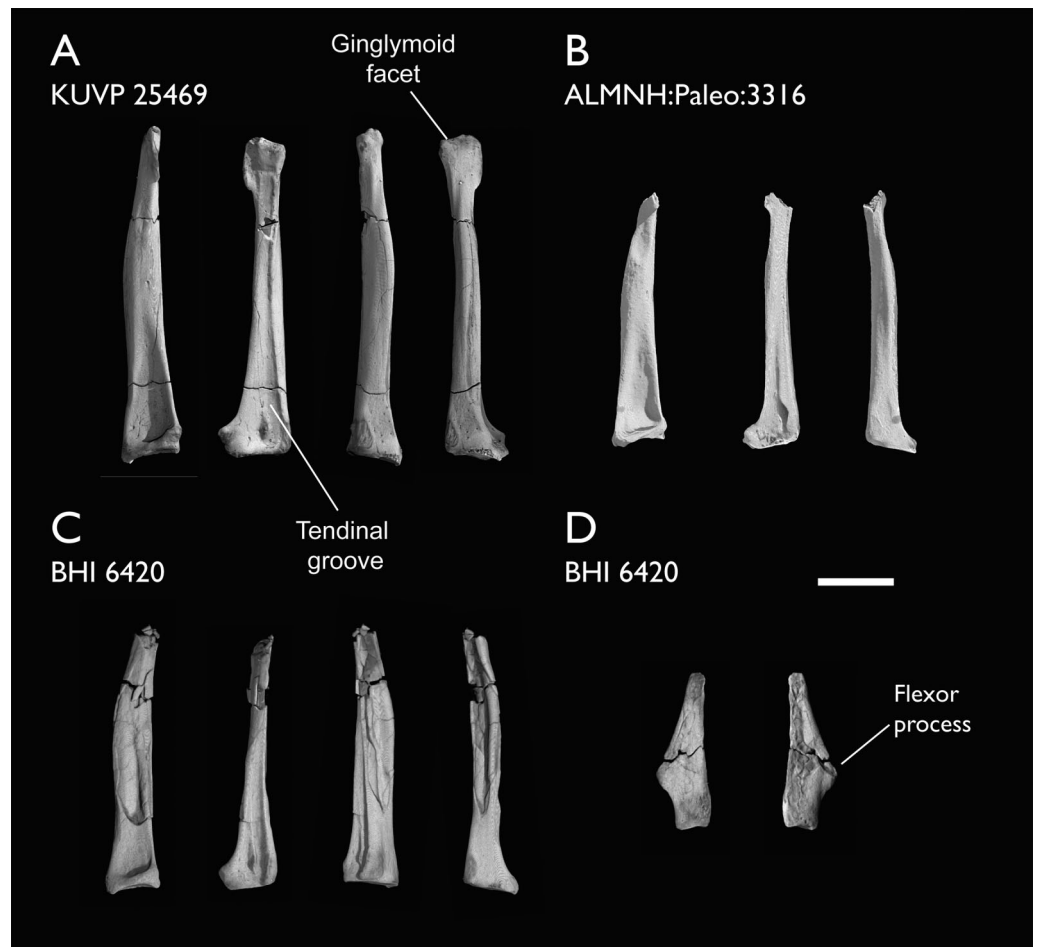
Figure 24 Manual phalanges II-2 and III-1 of *Ichthyornis*. (A) KUVP 25469 right II-2 phalanx, (B) ALMNH:Paleo:3316 right II-2 phalanx and (C) BHI 6420 right II-2 phalanx in caudal, ventral, dorsal and cranial views; and (D) III-1 phalanx in dorsal and ventral views. Scale bar equals 5 mm.

but better-defined tubercle is present on the cranioventral edge of the articular surface in FHSM VP-18702 and BHI 6421 (Figs. 23A and 23E), though it is broken in all other specimens. This tubercle seems to serve as an attachment point for the m. flexor digitorum superficialis where present, as in *Stercorarius antarctica* (*Watanabe, Field & Matsuoka, 2021*). A large distal internal index process can be observed on the caudal edge of the bone in all specimens except KUVP 2284 (Fig. 23B), though only the base of the process is preserved in most of them. The process is rounded and convex on its caudal side and slightly concave on its cranial margin, reaching its maximum distal projection close to the cranial margin. It varies in size among specimens, and is proportionally largest in ALMNH:Paleo:3316 (Fig. 23C), extending further distally than in the other specimens. In KUVP 2284, which preserves the smallest phalanx II-1, the process is not developed, and only a limited distal tubercle is present in its place, in a similar manner to the condition in *Iaceornis* or *Yixianornis*. The presence of an internal index process has been considered one of the autapomorphies of *Ichthyornis dispar* (*Clarke, 2004*). Its absence in

Table 11 Measurements of the manual phalanx II:2 of *Ichthyornis* specimens. Asterisks (*) denote measurements that might be unreliable due to breakage or distortion, but are included for completeness purposes. All measurements are in mm. – = not measurable.

Specimen	Total length	Prox. Craniocaudal width	Prox. Dorsoventral width	Dist. Craniocaudal width
ALMNH:Paleo:3316	17.91*	3.43	3.87	–
BHI 6420	17.46*	3.91	3.49	–
KUVP 25469	22.39	4.90	3.98	2.56

KUVP 2284 could be due to ontogenetic factors (*e.g.*, if this specimen—the second smallest of those surveyed—is ontogenetically immature, perhaps the process had yet to develop). Although the ontogenetic development of the internal index process has not been previously investigated, we verified that it is absent in a *Macronectes giganteus* chick, but present and well developed in adults, lending further support to the identification of KUVP 2284 as a possible juvenile individual.

Alternatively, the lack of an internal index process in KUVP 2284 may indicate that this specimen represents a previously unrecognized taxon of small ornithurine from the Niobrara Formation. An internal index process is unique to *Ichthyornis* among known Mesozoic avialans, but its distribution is widespread within Neoaves, being present at least in Strisores, Columbiformes, Pterocliformes, Otididae, Gruidae, Charadriiformes, Procellariiformes, Suliformes, Pelecanidae, and Psittaciformes (*Stegmann, 1963*, *1978*). This raises the question of whether the process may represent a crown bird symplesiomorphy, or whether its presence among some extant neoavians represents the convergent acquisition of an *Ichthyornis*-like morphology in this extant clade. The large and rounded process in *Ichthyornis* is particularly reminiscent of the morphology exhibited by certain extant representatives of Charadriiformes, such as *Glareola pratincola* and *Sterna hirundo*, as well as certain Procellariiformes like *Puffinus lherminieri*.

Phalanx II-2

The second phalanx of the major digit is preserved in three of the studied specimens, BHI 6420, KUVP 25469 and ALMNH:Paleo:3316, all from the right manus (Figs. 24A–24C). All three specimens are in exceptionally good condition, preserving clear muscle attachments not previously described for Mesozoic euornitheans, but only KUVP 25469 preserves the distalmost portion of the element (Fig. 24A). The phalanx is an elongate, narrow, and straight element with strongly craniocaudally expanded proximal and distal articular surfaces. The length of this phalanx is approximately equal to that of the proximal phalanx (Table 11). Both the cranial and the ventral surfaces of the shaft are deeply excavated.

The proximal articular surface is mostly flat and shelf-like, with a shallow depression on its cranial side that matches the tuberosity developed on the distal articular surface of the proximal phalanx. A moderately developed tubercle is present just distal to the articular surface on the cranial surface of the phalanx, extending distally into a shallow ridge that delimits the ventral edge of the cranial surface of the phalanx, but does not reach the distal articular surface (Fig. 24A). This tubercle has a flat proximal surface and preserves a rough

cranial texture in all studied specimens, and it most likely corresponds to the implantation scar for the m. extensor longus digiti majoris (*Baumel & Raikow, 1993*). A similar but considerably better developed tubercle is present at a comparable position on the caudal surface of the bone, just distal to the proximal articular surface. This tubercle extends into a thin and caudally expanded ridge that delimits the caudal surface of the phalanx, reaching the distal region of the phalanx but becoming progressively shallower, and it articulates exactly with the internal index process of the proximal phalanx.

The dorsal surface of the phalanx shows a large and deep excavation on its proximal end for the attachment of the leading primary feather (*Hieronymus, 2016*). This excavation decreases in depth distally, becoming flat and indistinct on the distal third of the phalanx (Figs. 24A and 24C), contrary to the condition in most crown-group birds, in which this concavity extends along the whole length of the phalanx (*Hudson et al., 1969*; *Hudson, Shreiweis & Wang, 1972*; *Vazquez, 1995*; *Hieronymus, 2015*). The ventral surface of the phalanx shows a shallow depression on its proximal portion but becomes essentially flat distally, with the exception of a deeply excavated groove, which extends along the whole length of the ventral surface. The cranial edge of the groove is delimited by the ridge extending distally from the m. extensor longus digiti majoris tubercle, and caudally by a shallow ridge (Fig. 24A). On the proximal end of the groove, this caudal ridge extends into a thin and delicate tubercle or flange present on all three specimens (Figs. 24A–24C). A large and round tubercle is present in this region in Alcidae for the distal implantation of the m. flexor digitorum superficialis and profundis (*Watanabe, Field & Matsuoka, 2021*), and the presence of the ventral groove in *Ichthyornis* indicates that the tendons of at least some of these muscles extended along the whole ventral margin of the phalanx. If that was the case, the flange at the proximal end of the groove may represent the base of a retinaculum covering both tendons in *Ichthyornis*. While in most crown birds both tendons attach only on the proximal region of phalanx II-2, the m. flexor digitorum superficialis extends to the distal end of the phalanx in Tinamidae and Galliformes (*Hudson & Lanzillotti, 1964*; *Hudson, Shreiweis & Wang, 1972*) and into the proximal region of phalanx II-3 in extant birds that retain it, such as Anseriformes (*Zusi & Bentz, 1978*) and juvenile *Opisthocomus* (*Hudson & Lanzillotti, 1964*). The tendinal groove is much more developed and deeply excavated in *Ichthyornis* than in either group, and it is open distally, indicating the probable presence of a large and functional ungual phalanx.

The distal region of the phalanx is dorsoventrally compressed and craniocaudally expanded (Fig. 24A). A large flange-like projection is present along the caudal edge of the distal end, with a slightly concave ventral surface, which likely housed the distal implantation of the m. interosseous ventralis (*Baumel & Raikow, 1993*). The distal articular surface is only weakly ginglymoid (*contra Clarke, 2004*, in which it is described as well developed), but evidences the presence of a third phalanx on digit II forming an ungual, which is not preserved in the studied specimens (Fig. 24A). A third manual ungual phalanx is well developed in several volant Mesozoic euornitheans such as *Yixianornis, Iteravis*, and *Gansus* (*Clarke, Zhou & Zhang, 2006*; *Liu et al., 2014*; *Zhou, O'Connor & Wang, 2014*; *Wang et al., 2016*), which show similar distal expansions on phalanx II-2. A greatly reduced third phalanx is present in Lithornithidae (*Houde, 1988*; *Nesbitt & Clarke, 2016*)
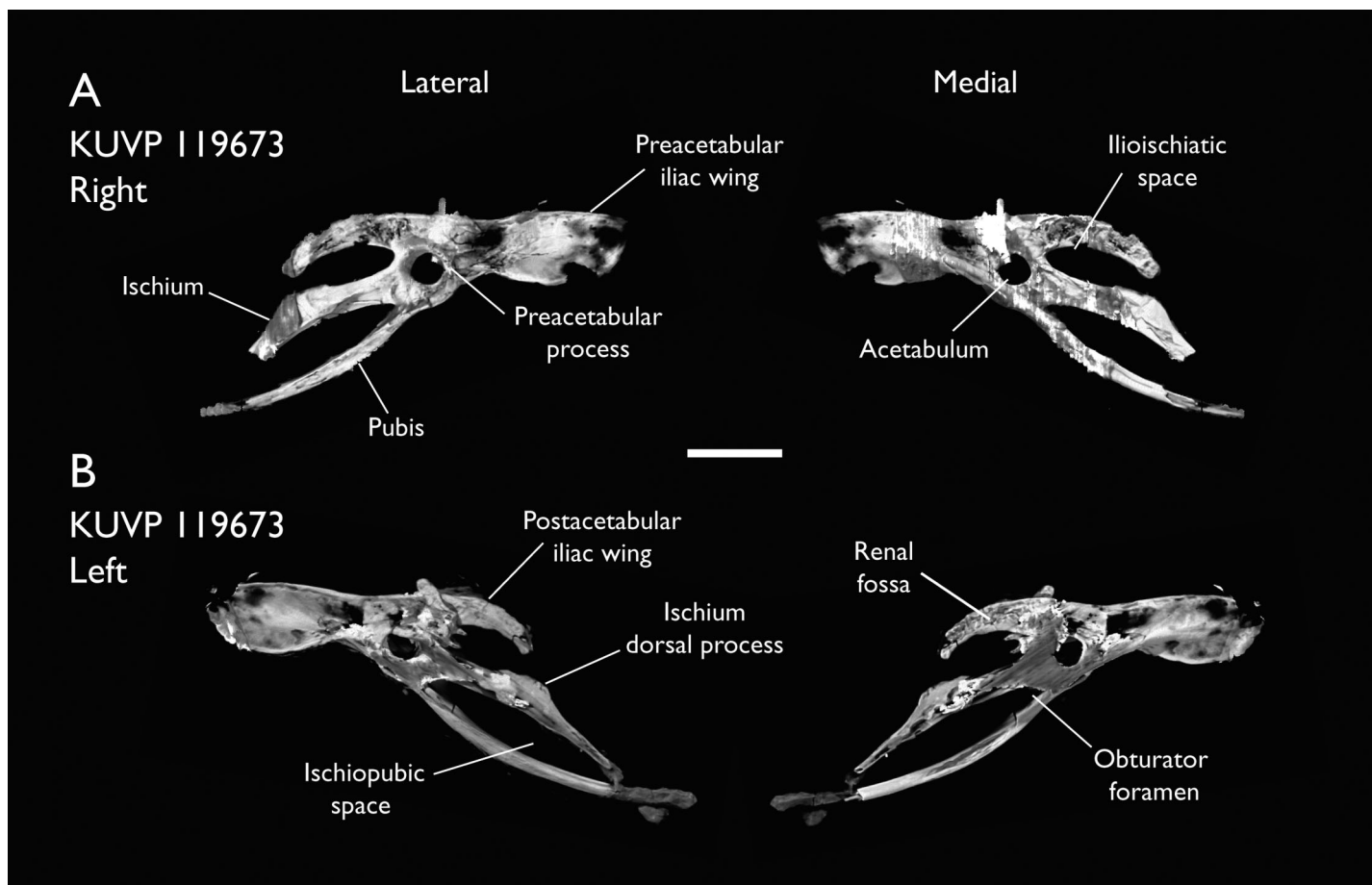
Figure 25 **Pelves of *Ichthyornis* specimen KUVP 119673.** (A) Right pelvis and (B) left pelvis, in lateral and medial views. Scale bar equals 1 cm.

and certain extant bird lineages, as previously mentioned. Two shallow projections are present on both sides of the groove for either M. flexor digitorum superficialis or profundis. Both projections preserve deep pits on their distal surfaces, likely for the collateral ligaments of the third phalanx.

Phalanx III-1

The single phalanx of the minor digit is preserved only in BHI 6420 (Fig. 24D). This element was previously only known for YPM 1775, in which both preserved phalanges lacked their distal portions (*Clarke, 2004*). In contrast, the distal portion is mostly preserved in BHI 6420.

The phalanx is a robust and elongate element, approximately half the length of phalanx II-1, and is dorsoventrally compressed (Fig. 24D). The proximal surface of the phalanx is wide and wedge-like, with a moderately developed tuberosity on its cranioventral surface, similar to the morphology described for *Iteravis* (*Zhou, O'Connor & Wang, 2014*). This tuberosity likely articulated both with the minor metacarpal and the proximal phalanx of the major digit. The cranial margin of the phalanx is mostly straight, but the caudal margin

Table 12 Measurements of the pelvic elements of *Ichthyornis* specimens. Maximum length corresponds to the total craniocaudal length of the fused pelvic element. Ilium maximum height is measured as the maximum dorsoventral extension of the preacetabular iliac wing. Asterisks (*) denote measurements that might be unreliable due to breakage or distortion, but are included for completeness. All measurements are in mm.

Specimen	Max length	Illium length	Illium max height	Ischium length	Pubis length
KUVP 119673 right	56.27	35.04	7.63	25.03	34.40
KUVP 119673 left	48.51*	36.83	7.81	18.93*	28.48*

shows a large and well-developed flange-like flexor process halfway along the length of the phalanx, giving the phalanx a roughly triangular shape. The flexor process shows a marked pit on its dorsal surface for the implantation of the m. flexor digiti minoris (*Baumel & Raikow, 1993*). The dorsal surface of the phalanx is mostly flat, while the ventral surface is moderately concave. The distal end of the phalanx is tapered, though the distalmost portion appears to be broken (Fig. 24D).

The morphology of phalanx III-1 in *Ichthyornis* is similar to that of certain other crownward ornithurines such as *Gansus* and *Iteravis* (*Liu et al., 2014*; *Zhou, O'Connor & Wang, 2014*; *Wang et al., 2016*), but more elongate and with a more strongly projected flexor process than in *Yixianornis* (*Clarke, Zhou & Zhang, 2006*). The morphology of the YPM 1775 III-1 phalanx was compared to that of Tinamidae by *Clarke (2004)*, but despite the presence of a comparable flexor process, the phalanx is much more elongate in *Ichthyornis*, which could not be appreciated from the partially preserved phalanges in YPM 1775. While similar morphologies are developed across multiple crown-bird lineages such as Tinamidae or Anseriformes, the condition in *Ichthyornis* appears most similar to that of certain Lithornithidae such as *Calciavis grandei* (*Nesbitt & Clarke, 2016*) or some extant taxa like *Columba livia* (Columbiformes) or *Rynchops flavirostris* (Charadriiformes).

Pelvic girdle

The complete pelvic girdle is preserved in KUVP 119673, which preserves the fused ilia, ischia and pubes from both the left and right sides, disarticulated from the synsacrum (Figs. 25A and 25B). KUVP 157821 preserves portions of the preacetabular ilium in association with the synsacrum, but these are extremely fragmentary. Amongst the YPM material, only one specimen preserves a semi-complete pelvic girdle, YPM 1732, in articulation with the synsacrum. Despite the large number of complete and partial synsacra found amongst the studied specimens (see above), no other specimen beyond KUVP 157821 preserves any pelvic remains, evidencing the weak fusion between the pelvic girdle and the sacral vertebrae in all but the largest specimens. Both sides of the KUVP 119673 pelvis are mediolaterally flattened and include radiopaque inclusions, which hampers the identification of some minor features such as muscle attachment impressions. Despite this, both sides preserve the entire surfaces of all the elements, except for the distal right ischium (Fig. 25A). Measurements of KUVP 119673 pelvic elements are provided in Table 12.

The ilium in YPM 1732 is missing most of its preacetabular and postacetabular portions, but the outline of these regions was illustrated by *Marsh (1880)*. It is not clear whether this illustration was based on portions of the bones that have since been lost, or if the illustrations reflect hypothetical reconstructions (*Clarke, 2004*). Supporting the latter alternative, the iliac morphology preserved in KUVP 119673 differs considerably from that illustrated in *Marsh (1880)*, particularly with regard to the shape of the postacetabular region. The preacetabular wing of the ilium is elongate, reaching toward the caudal end of the first sacral vertebra. The ilium shows rounded cranial and ventral margins and a mostly straight dorsomedial margin; it reaches its maximum dorsoventral height at around 40% of its preacetabular length measured from its rostral tip (Table 12), narrowing drastically just cranial to the acetabulum (Figs. 25A and 25B). No ossified tendons like those preserved in YPM 1732 are present on either side of the KUVP 119673 pelvis. The preacetabular lateral surface is strongly concave, with a shallow groove running craniocaudally through the centre of most of the lateral surface, defining a large attachment surface for the m. iliotrochantericus caudalis and cranialis, but no clear demarcation is visible between the attachment surfaces of both muscles. Both the dorsal and ventral margins of the preacetabular wing are thickened and slightly laterally recurved. The medial surface of the preacetabular wing is strongly convex, with a marked ridge, equivalent to the aforementioned lateral groove, running along most of its length. This ridge shows a moderate ventral curvature and forms the ventral side of the acetabulum where it meets the pubis, which seems continuous with this ridge medially. The acetabulum is large and circular, with its dorsal margin strongly thickened, extending into a moderately developed antitrochanteric process that does not show a clear lateral tip (Fig. 25A).

The postacetabular ilium, which does not fuse with the ischium, is oriented dorsoventrally, *contra Clarke (2004)*. *Marsh (1880)* illustrated a reconstructed laterally oriented and mediolaterally wide postacetabular ilium, but the illustration was noted by *Clarke (2004)* as differing from the preserved material. The postacetabular iliac wing in KUVP 119673 is short, reaching distally as far as the dorsal process of the ischium and being 70% of the length of the preacetabular wing (Figs. 25A and 25B). The postacetabular illium is dorsoventrally narrow, gently curving ventrally along its length, approaching but not fusing with the ischium, and defining an ovoid ilioischiatic space (Fig. 25A; foramen ilioischiadicum; *Baumel & Witmer, 1993*). The lateral surface of the postacetabular ilium is strongly convex, with a marked ridge running along its entire length, parallel to both the dorsal and ventral margins of the element. Conversely, the medial surface of the bone is strongly concave, defining a deeply excavated and elongated renal fossa (Fig. 25B; *Livezey & Zusi, 2006*). Given the reduced postacetabular iliac morphology, it is not clear whether the ilium contacted the caudal transverse processes of the synsacrum. In most other Mesozoic euornitheans, such as *Yixianornis* or *Yanornis* (*Zhou & Zhang, 2001*; *Clarke, Zhou & Zhang, 2006*), the postacetabular iliac wing is similarly dorsoventrally narrow, but in contrast to *Ichthyornis*, it does not show any significant dorsoventral curvature and it does not approach the dorsal process of the ischium. The morphology of the *Ichthyornis* ilium differs from that of *Yixianornis, Gansus* and *Iteravis* (*Clarke, Zhou & Zhang, 2006*; *Liu et al., 2014*; *Zhou, O'Connor & Wang, 2014*; *Wang et al., 2016*), in which both pre- and

postacetabular wings are of similar length, the preacetabular wing does not show significant variation in its dorsoventral width along its length, and the postacetabular wing is not markedly dorsoventrally recurved. The morphology in *Ichthyornis also* differs from that of Hesperornithes, in which the ilium has an extremely elongate and enlarged postacetabular wing (*Bell & Chiappe, 2016*, *2020*). Conversely, the ilium of *Ichthyornis* is very similar to that of more stemward euornitheans like *Schizooura* (*Zhou, Zhou & O'Connor, 2012*) and *Eogranivora* (*Zheng et al., 2018*), in which the postacetabular ilium is shortened (although more so in these taxa than in *Ichthyornis*, in which it extends for 50% of the length of the preacetabular wing), and the preacetabular wing is dorsoventrally constricted close to the acetabulum.

The ischium in *Ichthyornis* is extremely elongate, extending into a strap-like structure almost reaching the caudal end of the pubis (Fig. 25B). The ischium shows a convex dorsal margin with a moderately developed and wide dorsal process near its midpoint. The dorsal process on both sides of KUVP 119673 is significantly shorter than the triangular and elongate flange-like extension visible in YPM 1732, but there are no signs of breakage (Figs. 25A and 25B). Its ventral margin is weakly concave, and no projection demarcating the obturator foramen area is visible, contrary to the condition described for YPM 1732 (*Clarke, 2004*). The caudal extension of the ischium is ventrally deflected and is strongly tapered, with its caudalmost extent, preserved only on the left side, almost reaching the pubis, but not completely closing the ischiopubic space. The lateral surface of the ischium is mostly flat, with a marked ridge extending from the antitrochanteric process and running across the whole length of the ischium. The ridge runs through the centre of the lateral surface proximally but becomes continuous with the ventral surface distally. An equivalent groove is developed on the medial surface (Fig. 25A), with a similar shape and extension to the lateral ridge. The ischium in *Ichthyornis* is essentially identical to that of *Gansus* and *Yixianornis* in its length and shape, with a similar extension of the dorsal process, which is shorter in *Iteravis*. The lateral ridge is present as well in most other crownward euornitheans, similarly extending along the whole length of the ischium in *Yixianornis* and *Iteravis*, but only reaching the midpoint of the ischium in *Gansus*.

The pubis is a robust and elongate rod-like element, and is longer than the entire craniocaudal length of the ilium (Fig. 25B). The pubis is strongly curved dorsoventrally, with its caudal tip pointing dorsally, and delimiting an almond-shaped ischiopubic space, with a very reduced caudal opening obscured by radiopaque inclusions on the left pelvis (Fig. 25B). This morphology of the ischiopubic space is similar to that of *Gansus* but contrasts with the condition in *Apsaravis*, in which the ischium and the pubis run parallel to each other and the space between both is greatly reduced. The pubis does not seem to taper along its length, although its caudalmost extent is not well preserved and it is unclear whether a moderate distal expansion existed as in *Iteravis* and *Gansus*. Since both pubes are separated and mediolaterally flattened, whether they exhibit any mediolateral curvature and contacted medially, as in *Yanornis*, *Yixianornis*, *Gansus* and *Iteravis*, cannot be directly observed. The pubes of YPM 1732 were illustrated by *Marsh (1880)* as not contacting medially, although since the only observable pubis of this specimen is missing most of its length this cannot be verified at present. As mentioned above, *Marsh (1880)*
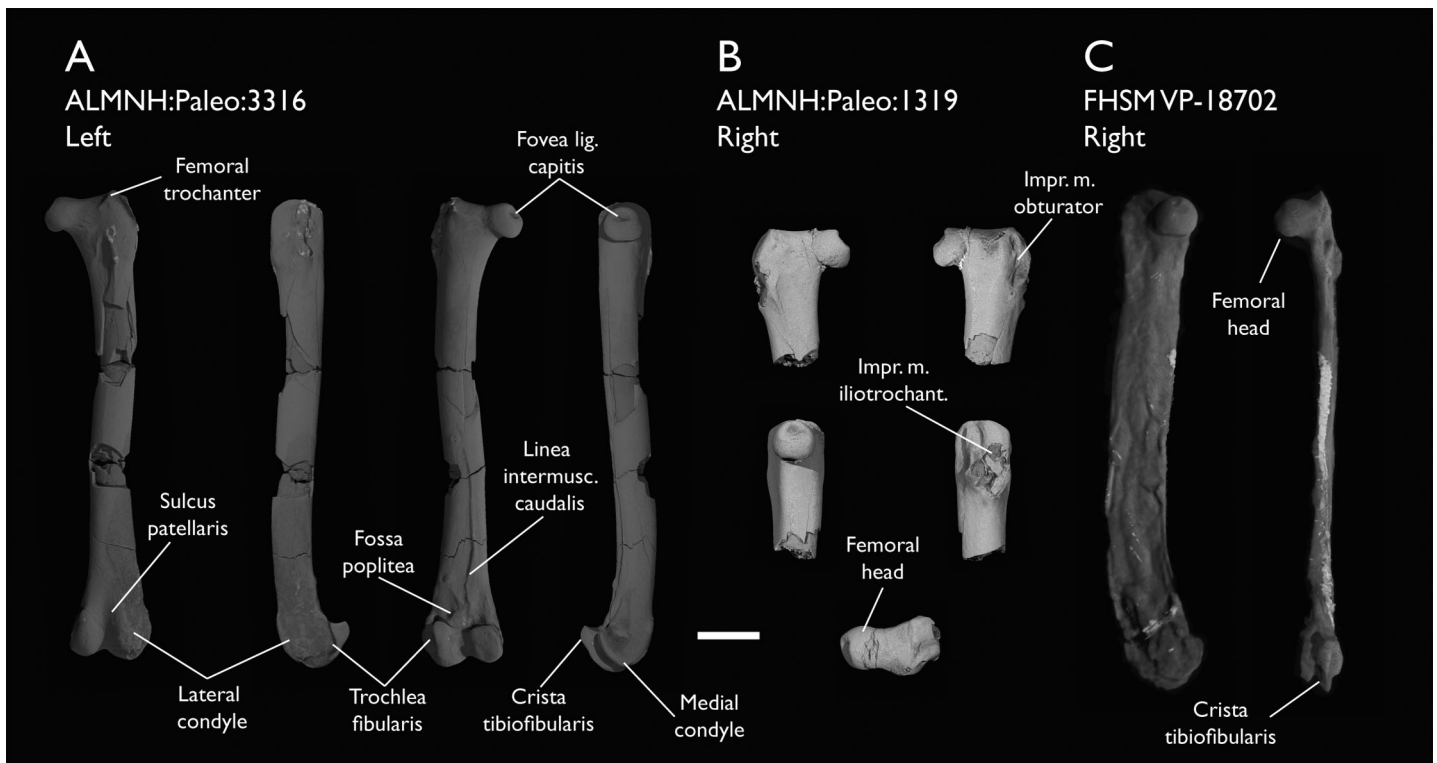
Figure 26 Femora of *Ichthyornis*. (A) ALMNH:Paleo:3316 left femur in cranial, lateral, caudal and medial views; (B) proximal right femur of ALMNH:Paleo:1319 in (clockwise order from upper left) cranial, caudal, lateral, dorsal and medial views and (C) right femur of FHSM VP-18702 in medial (left) and caudal (right) views. Scale bar equals 5 mm.

Table 13 Measurements of the femur of *Ichthyornis* specimens. Least circumference and least diameter correspond to the minimum circumference and diameter of the humeral shaft; midshaft width is provided for those specimens in which the preservational state precluded measuring these. Proximal mediolateral width is measured as the maximum mediolateral extension of the femur, including the femoral head and the femoral trochanter. Midshaft width corresponds to the mediolateral width of the femoral shaft halfway along its length. All measurements are in mm. – = not measurable.

Specimen	Total length	Least circum.	Least diameter	Prox. Mediolateral width	Dist. Mediolateral width	Dist. Craniocaudal width
ALMNH:Paleo:1314	–	–	–	–	6.53	5.75
ALMNH:Paleo:1319	–	–	–	8.02	–	–
ALMNH:Paleo:3316	38.27	10.38	3.10	7.69	6.49	5.64
FHSM VP-18702	41.57	–	–	–	–	5.83
KUVP 119673	–	–	–	–	6.09	–

illustration was noted by *Clarke (2004)* to differ from the preserved material, and the morphology of the ilium illustrated by Marsh is strikingly different from that described in this study, casting additional doubt on Marsh's interpretations of the pelvis. The lack of completely preserved pubic bones precludes inferences of the precise phylogenetic origins of the unfused pubic symphysis characteristic of crown birds, and, by extension, strong inferences regarding the maximum diameter of *Ichthyornis* eggs, despite earlier studies positing that *Ichthyornis* provides the earliest evidence of a fully open pubic symphysis

homologous with that of crown birds (*Mayr, 2017b*). No preacetabular tubercle or pectineal process is developed on the cranial surface of the pubis, as noted by *Clarke (2004)*, contrasting with the condition in Hesperornithes, in which this process is extremely well developed (*Bell & Chiappe, 2016*, *2020*).

Femur

Five of the new specimens preserve femoral remains. FHSM VP-18702 preserves a complete but severely distorted and laterally flattened right femur, and beyond the three-dimensionally-preserved femoral head, no other features are discernible (Fig. 26C). KUVP 119673 preserves a craniocaudally flattened partial right femur, and few recognizable features apart from the general shape of the two distal condyles are observable. ALMNH: Paleo:3316 preserves a complete and undistorted left femur exhibiting only minimal breakage, representing the best-preserved *Ichthyornis* femur known to date (Fig. 26A). ALMNH:Paleo:1314 preserves the distal portion of the femur in three dimensions, although the surface of the bone is eroded, obscuring most features. ALMNH:Paleo:1319 preserves only the proximal portion of the right femur, albeit in excellent condition (Fig. 26B). The morphology of the femur in the studied specimens is generally congruent with that described by *Clarke (2004)*, although the exceptional quality of the new specimens allows for a more detailed description. Measurements of the femora of the specimens included in this study are provided in Table 13.

The femoral head is large and globose, with a slightly flattened articular facet for the acetabulum (facies artic. acetabularis; *Baumel & Witmer, 1993*), and a deeply excavated depression found on the ventral surface of the femoral neck (coll. fem.; *Livezey & Zusi, 2006*), where it meets the femoral shaft and the antitrochanteric articular facet (Fig. 26B). A round and deep capital ligament fossa is found in all three specimens, even in the extremely distorted femur of FHSM VP-18702. This fossa is present in many crownward euornitheans, such as *Gansus* (*Wang et al., 2016*) and *Apsaravis* (*Clarke & Norell, 2002*), although it is absent in more stemward euornitheans such as *Similiyanornis* and *Abitusavis* (*Wang & Zhou, 2020*). The femoral trochanter is poorly developed proximally, and it does not extend further dorsally than the femoral head, hence no notable trochanteric fossa is developed (Figs. 26A and 26B). Although the development of the femoral trochanter is poorly characterized among stem euornitheans, the minimal dorsal extent of the trochanter in *Ichthyornis* is similar to the condition in *Patagopteryx* (*Chiappe, 2002*), *Gansus* (*Wang et al., 2016*) and *Abitusavis* (*Wang et al., 2020c*), but distinct from *Vorona* (*Forster et al., 2002*), *Apsaravis* (*Clarke & Norell, 2002*) *Iteravis* (*Zhou, O'Connor & Wang, 2014*) and Hesperornithes (*Zinoviev, 2011*; *Bell & Chiappe, 2016*, *2020*; *Bell, Wu & Chiappe, 2019*), in which it extends beyond the femoral head. The dorsal extension of the femoral trochanter has been suggested to have a strong correlation with the swimming capabilities of water-dwelling birds, and in particular, a short femoral trochanter at the same level as the femoral head appears to be associated with foot-propelled swimming (*Raikow, 1970*, *1985*; *Zinoviev, 2011*; *Clifton, Carr & Biewener, 2018*; *Bell, Wu & Chiappe, 2019*). The condition in *Ichthyornis* is comparable to that of several crown birds exhibiting foot-propelled swimming, such as *Anas platyrhynchos* and *Anser albifrons* (Anseriformes),

Puffinus lherminieri, Hydrobates leucorhous and *Diomedea cauta* (Procellariiformes), *Morus bassanus* and *Phalacrocorax carbo* (Suliformes) and *Phaethon lepturus* (Phaethontiformes), while it is slightly more developed in specialized foot-propelled diving taxa such as *Podiceps auritus* (Podicipediformes) and *Gavia arctica* (Gaviiformes; *Bell, Wu & Chiappe, 2019*). In contrast, the femoral trochanter is usually much more developed in taxa that are associated with aquatic habitats but which are less natatorial, such as *Chauna chavaria* (Anseriformes), *Rallus striatus* (Gruiformes), *Sterna hirundo* and *Rynchops flavirostris* (Laridae), and *Charadrius rubricollis* (Charadriidae), and in most land-dwelling birds, such as *Crypturellus variegatus* (Tinamidae) or *Gallus gallus* (Phasianidae). The trochanteric crest is short and does not extend cranially beyond the main body of the femur, contrary to most surveyed extant birds, with the exception of *Puffinus lherminieri*. The barely developed crest is visible in ALMNH:Paleo:3316, extending from the dorsal onto the cranial surfaces of the femoral trochanter, but it is even less developed in ALMNH:Paleo:1319 (Figs. 26A and 26B). The cranial surface of the proximal femur is moderately concave and delimited laterally by the trochanteric crest, and its surface is pierced by numerous foramina in both ALMNH:Paleo:1043 and ALMNH:Paleo:1319. (Fig. 26B) A large ovoid muscle attachment scar extends from this region into the femoral shaft, probably for the m. femorotibialis intermedius, delimiting on its lateral edge a shallow cranial intermuscular line, which extends from the distal end of the trochanteric crest but quickly becomes indistinct, contrary to the condition in *Gansus* (*Wang et al., 2016*).

The lateral surface of the proximal femur preserves several deep and well-developed pits and grooves, which allow for a precise reconstruction of the muscular attachment points of the femoral trochanter (Figs. 26A and 26B). Three small scars are found on the trochanteric caudolateral surface; of these, the dorsalmost pit-like scar is the deepest, probably corresponding to the attachment point for the m. obturator (impr. m. obtur; *Livezey & Zusi, 2006*). Distal to this pit, there is a short longitudinal groove extending proximodistally, and just distal to that, there is a slightly shallower comma-shaped scar; these probably correspond to the attachments for the m. iliofemoralis externus and m. ischiofemoralis. A well-developed crest (apparently corresponding to the "trochanter minor" of *Ghetie, 1976*) is situated just craniolateral to these scars; this crest is vaguely sigmoidal in shape, curving caudally on its distal end, and extending distally for about 11% of the total femoral length. Two deeply excavated consecutive grooves run proximodistally just parallel to the craniolateral surface of this crest (Fig. 26B); the proximal and more elongated one corresponds to the attachment for m. iliotrochantericus caudalis, while the shorter and more curved distal groove serves as the attachment for m. iliotrochantericus cranialis or medius (*Baumel & Raikow, 1993*).

The femoral shaft is only well preserved in ALMNH:Paleo:3316, although multiple breakages along its length obscure the muscular scars on its surface. The shaft is mostly straight along its length, narrowing distally. It is only moderately curved caudally on its distal portion, where the shaft becomes significantly broader in cross-section (Fig. 26A). The caudal intermuscular line is visible and very marked along the distal half of the shaft, separating the attachment regions for the m. femorotibialis lateralis and medialis.

Although it is possible that the intermuscular line extended further proximally, the breakages in the region make this difficult to assess. Contrary to the condition in all surveyed extant birds, the caudal intermuscular line in *Ichthyornis* does not divide into two distinct branches until very close to the distal femoral condyles, not delimiting a large popliteal plane. A large and very well marked foramen is present approximately at the midpoint along the shaft length, just lateral to the apparent proximal origin of the caudal intermuscular line (Fig. 26A); a similar foramen is variably present in several crown bird lineages, including anseriforms such as *Anas platyrhynchos*, and suliforms like *Morus bassanus* and *Phalacrocorax carbo*.

The distal femur is only well preserved in ALMNH:Paleo:3316, since although ALMNH:Paleo:1314 preserves this region, its bone surface is mostly eroded. The cranial surface of the distal femur shows a wide but shallow and poorly defined patellar groove, which continues into a deep intercondylar groove distally (Fig. 26A). The distribution of the patellar groove amongst non-neornithine euornitheans is poorly known due to preservation, although it is inferred to be absent in *Yixianornis* (*Clarke, Zhou & Zhang, 2006*), but present in *Apsaravis* (*Clarke, Zhou & Zhang, 2006*) and Hesperornithes such as *Parahesperornis* (*Bell & Chiappe, 2020*). The presence of a patellar groove is widespread among crown birds, but the wide and poorly defined groove in *Ichthyornis* is most similar to the condition in Procellariiformes like *Ardenna tenuirostris* and Suliformes such as *Morus bassanus*. Both distal condyles are well developed, with the lateral condyle being larger and extending further distally than the medial condyle. The cranial surface of both tubercles is rounded and poorly defined, and no clear cranial ridges delimiting the patellar groove are developed on either condyle. The proximocranial termination of the medial condyle develops into a moderately developed tubercle, while the lateral condyle extends gradually from the cranial surface of the shaft. Two deep and pit-like adjacent impressions of similar size are present along the craniodistal edge of the lateral condyle (Fig. 26A). The one situated more cranially corresponds to the depression of the m. tibialis cranialis tendon, while the one situated more laterally corresponds to the impression of the lig. collaterale laterale (*Baumel & Witmer, 1993*).

The lateral surface of the lateral condyle is mostly eroded, but the fibular trochlea is well marked and developed, extending laterally from the lateral surface of the condyle along almost 1/5th of the total distal width of the femur (Fig. 26A). The lateral extension of the fibular trochlea is not known in most non-neornithine euornitheans, but the condition in *Ichthyornis* is much less prominently developed than the condition in Hesperornithes or in extant diving birds, such as *Phalacrocorax carbo*. A small and poorly developed tubercle for the attachment of m. gastrocnemialis lateralis is present on the proximal end of the fibular trochlea, and just distal to it, a wide but shallow and poorly defined impression for the ansae m. iliofibularis is visible (*Baumel & Witmer, 1993*). The tibiofibular crest is large, subtriangular in lateral and medial views (Fig. 26A), and its caudal tip is slightly proximally curved, exhibiting a morphology particularly reminiscent of the condition in the hesperornithean *Fumicollis* (*Bell & Chiappe, 2015*, *2020*), but distinct from that of other Hesperornithes, in which the crest is much more rounded. Among extant birds, the general shape of the tibiofibular crest is remarkably similar to that of the tinamou *Crypturellus*

variegatus and the suliform *Phalacrocorax carbo*, while the morphology is much more rounded and less caudally extensive in most other surveyed crown birds. A shallow, rounded, and poorly marked depression is found just proximal to the tibiofibular crest, probably corresponding to the impression for the lig. cruciati caudalis (*Baumel & Witmer, 1993*). Immediately proximal to this depression, a short unidentified ridge extends laterodistally, and a small but marked tubercle is found just proximal to it.

The medial condyle lacks a distinct medial epicondyle, but a large shallow and rounded depression is present on its medial surface for the attachment of the medial collateral ligament. The medial condyle is mediolaterally wide and extends medially past the medial surface of the distal femur. Its distal surface is mostly flat, and the medial condyle shows a subquadrangular shape in caudal view. A moderately developed medial supracondylar crest extends from the medial condyle towards the shaft, meeting one of the distal termini of the caudal intermuscular line.

A shallow but well-defined ovoid popliteal fossa is present just proximal to the medial condyle on the caudal surface of the distal femur (Fig. 26A). The fossa is proximodistally short but lateromedially wide, and lies almost parallel to the distal surface of the femur. The presence of a popliteal fossa is uncertain in most non-neornithine euornitheans, but it is present in Hesperornithes such as *Parahesperornis* (*Bell & Chiappe, 2020*). A popliteal fossa of comparable depth and shape to that of *Ichthyornis* is variably present among crown birds, such as *Chroicocephalus novaehollandiae* (Laridae) and *Morus bassanus* (Sulidae). A large foramen is present at the deepest point of the popliteal fossa, similar to the condition in all surveyed crown birds. The caudal surface of the distal femur just proximal to the popliteal fossa is rugose and complex, with multiple ridges and depressions extending from the caudal intermuscular line, probably representing muscle or ligament attachment points, but these are unidentifiable at present. The caudodistal surface of the distal femur shows an extremely deep and distinct impression of the lig. cruciati cranialis between both distal condyles.

Tibiotarsus

Five of the studied specimens preserve partial tibiotarsi, in all cases preserving the distal end of the element (Figs. 27A–27C). Only ALMNH:Paleo:3316 preserves the proximal portion of the left tibiotarsus together with the distal end of the same bone (Fig. 27A). However, even that element is broken, and at least a small portion of the shaft appears to be missing since the fractured ends do not precisely match. As such, a precise estimate of tibiotarsus length, and therefore a definitive assessment of complete hindlimb proportions, is not presently possible. Despite the illustration of a complete tibiotarsus from the holotype of *Ichthyornis victor* in *Marsh (1880)*, no complete tibiotarsi are currently known for *Ichthyornis*, and the element illustrated by Marsh might have been lost or broken (*Clarke, 2004*). Measurements of the tibiotarsal fragments from the specimens included in this study are provided in Table 14.
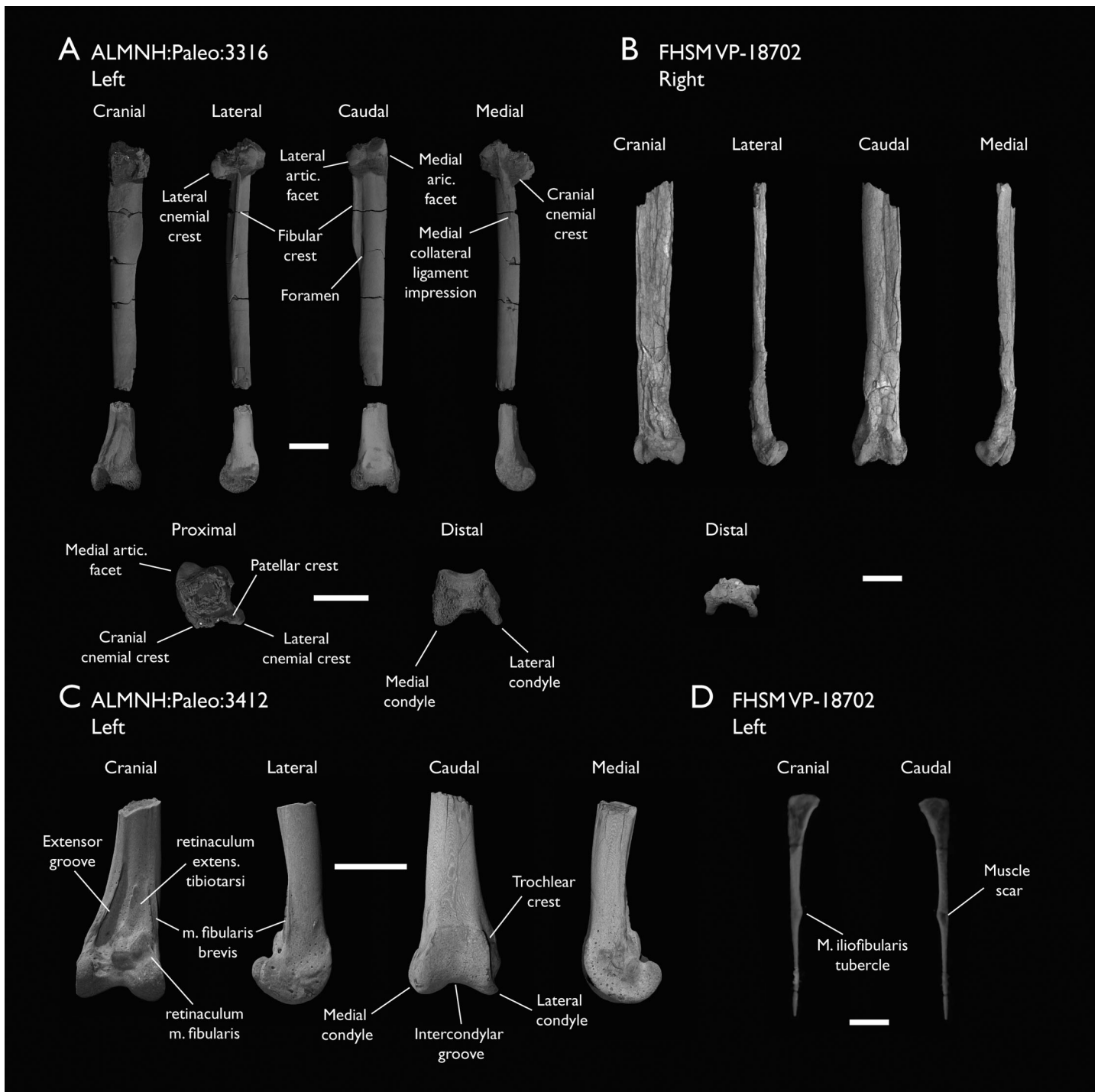
Figure 27 Tibiotarsi and fibula of *Ichthyornis*. (A) ALMNH:Paleo:3316 left tibiotarsus proximal and distal fragments, (B) FHSM VP-18702 right tibiotarsus, (C) ALMNH:Paleo:3412 left distal tibiotarsus and (D) FHSM VP-18702 right fibula. Scale bars equal 5 mm.

The proximal end of the left tibiotarsus in ALMNH:Paleo:3316 is crushed and distorted proximodistally, but preserves several features that have not been previously illustrated. The specimen may represent the best-preserved proximal tibiotarsus from *Ichthyornis*

Table 14 Measurements of the tibiotarsus of *Ichthyornis* specimens. Midshaft width corresponds to the craniocaudal or mediolateral width of the tibiotarsus shaft halfway through its length, depending on the preservation of each specimen. Asterisks (*) denote measurements that might be unreliable due to breakage or distortion, but are included for completeness. All measurements are in mm. – = not measurable.

Specimen	Total length	Prox. Craniocaudal width	Prox. Mediolateral width	Dist. Craniocaudal width	Dist. Mediolateral width	Midshaft width
ALMNH:Paleo:3316	43.88	6.24	7.77	4.92	6.43	3.04
ALMNH:Paleo:3412	–	–	–	5.46	6.21	3.01
BHI 6421	–	–	–	4.98	5.71*	2.50
FHSM VP-18702	–	–	–	4.29	7.25	4.66
KUVP 119673	–	–	–	–	–	–

known to date. The proximal surface is damaged, but the patellar crest (crista patellaris; *Baumel & Witmer, 1993*) and the lateral and medial articular surfaces are well preserved (Fig. 27A). The width of the proximal portion of the tibiotarsus seems to be significantly greater than that of the shaft, in contrast to the condition in YPM 1450, though this might be caused by distortion of this region in ALMNH:Paleo:3316. The medial articular surface is larger than the lateral articular surface (*contra Clarke, 2004*, where it is described as slightly smaller), and it extends further both proximally and caudally with respect to the lateral articular surface (Fig. 27A). The proximal surface of the medial articular surface is flat and ovoid in proximal view, and is slightly inclined proximodistally with respect to the main axis of the tibiotarsus. The lateral articular surface is more reduced in size and lacks a well-preserved proximal surface, though the preserved portion of the structure suggests a convex morphology as described by *Clarke (2004)*. Contrary to *Clarke (2004)*, a well-developed and obvious fibular crest is present, running along half of the preserved proximal portion of the tibiotarsus, and extending laterally as far as the lateral articular surface (Fig. 27A). The crest seems to be continuous with the lateral articular surface, contrary to the condition illustrated by *Marsh (1880)* in which the crest appears to be absent, but Marsh's interpretation might have been a result of distortion of the proximal end of the tibiotarsus in YPM 1450. The cranial surface of the fibular crest is flat, but its caudal surface is slightly concave, with a thickened lateral edge. The morphology of the fibular crest is fairly similar to the condition in *Gansus*, particularly with regard to its lateral projection (*Wang et al., 2016*). A large, deep foramen is present just medial to the distal terminus of the fibular crest (Fig. 27A). The foramen is found at the end of a short but deep sulcus running next to the medial end of the crest. A similar foramen is variably present in crown birds, but the condition in *Ichthyornis* is most similar to that of Anseriformes, particularly in *Anser albifrons*. A flexor fossa is not apparent, but this may be an artifact of poor preservation.

Two cnemial crests are present in ALMNH:Paleo:3316, but only the lateral crest is well-preserved (Fig. 27A). The cranial cnemial crest is missing its proximal and cranial ends, but the preserved portions indicate that it was large and robust. The cranial surface of the cnemial crest is subcircular in medial view, and its cranial extension is approximately

equal to the shaft diameter. The preserved portion of the cranial cnemial crest does not show any lateral curvature, delimiting a completely flat gastrocnemial surface (facies gastrocnemialis; *Baumel & Witmer, 1993*). The lateral cnemial crest is thick and robust, slightly longer in its lateral extension than the cranial extension of the cranial cnemial crest, but it is proximodistally shorter, with its proximal end distal to that of the cranial crest. It shows a slight caudolateral curvature, with a flat cranial surface and a moderately convex caudal surface (Fig. 27A). No patellar crest is preserved, but given the limited proximal extension of the lateral cnemial crest, it was probably not strongly developed. Although distortion of the proximal region of the tibiotarsus might obscure the true proximal extent of both cnemial crests, their visible morphology is congruent with that described for YPM 1450 (*Clarke, 2004*), and contrasts with the condition in other crownward euornitheans like *Gansus* and *Iteravis*, in which the cnemial crests are moderately cranially projected.

The shaft is not completely preserved in any of the studied specimens, but ALMNH: Paleo:3316, BHI 6421 and FHSM VP-18702 preserve large portions of it (Figs. 27A and 27B). The shaft is mostly straight but shows a moderate lateral twist close to the distal end of the bone in BHI 6421, and reaches its narrowest point distally at around 75% of its length. While no impressions are visible in ALMNH:Paleo:3316, a shallow and narrow fibular impression runs across the length of the shaft in BHI 6421, reaching the distal portion of the element.

A flat, oval-shaped impression is visible on the medial surface of the shaft, just medial to the cranial cnemial crest (Fig. 27A). This impression is congruent with that of the ligamentum collateralis medialis (*Baumel & Witmer, 1993*), and extends into a shallow ridge that runs across the medial surface of the shaft, with a similar distal extension to that of the fibular crest.

The distal portion of the tibiotarsus is well preserved in ALMNH:Paleo:3316, ALMNH: Paleo:3412, and BHI 6421, and is considerably craniocaudally flattened in FHSM VP-18702 (Figs. 27A–27C). The observable morphology is congruent in all of these specimens, and agrees well with that previously reported for *Ichthyornis* (*Clarke, 2004*), although the specimens described here are the first undistorted examples reported thus far. The extensor groove (sulcus extensorius; *Baumel & Witmer, 1993*) is deep and marked, running moderately obliquely to the main axis along the medial side of the shaft, terminating just proximal to the medial condyle (Fig. 27C). The medial edge of the groove is delimited by a thin but sharp ridge, which terminates just proximal to the lateral condyle.

No supratendinal bridge is present in any of the studied specimens. A supratendinal bridge is not preserved in any of the YPM *Ichthyornis* specimens either, but *Clarke (2004)* did not dismiss its possible presence given the poor state of preservation of the YPM specimens. The exceptionally preserved ALMNH specimens and BHI 6421 indicate that the lack of a supratendinal bridge in *Ichthyornis* is genuine (Figs. 27A and 27C). This structure therefore optimizes as a synapomorphy of the most exclusive clade composed of Neornithes and the most crownward-known stem birds based on its presence in *Iaceornis marshi* (*Gauthier, 1986*; *Martin, 1987*; *Cracraft, 1988*; *Mayr & Clarke, 2003*; *Clarke, 2004*) and crown birds.

Several tubercles, impressions and scars are visible on the cranial surface of the distal tibiotarsus in all of the studied specimens. The largest of these, a large subtriangular concave surface, is situated just lateral to the extensor groove (Fig. 27C). This surface is sharply raised on its distal end, extending cranially along at least 60% of the lateral condyle's length. This surface might correspond to the implantation for the retinaculum extensorium tibiotarsi and the passage of the m. extensor digitorum longus (*Baumel & Raikow, 1993*), as interpreted by *Clarke (2004)*. On the laterodistal end of this concave surface there is a raised ovoid tubercle which extends only slightly further cranially (Fig. 27C). It likely corresponds to the implantation region for the retinaculum m. fibularis (*Baumel & Raikow, 1993*). Lateral to both, there is a shallow groove which extends from the lateral side of the fibular groove, turning progressively medially closer to the proximal end of the extensor groove and then laterally closer to the proximal edge of the lateral condyle, with a marked foramen on its distal end (Fig. 27C). This groove is delimited by two sharp ridges along most of its length and corresponds with the impression of the m. fibularis brevis. The morphology of this region is not well described in the literature for most Mesozoic euornitheans, but the muscle impressions and tubercles in *Ichthyornis* seem to correspond broadly with the three tubercles described in *Gansus* (*Wang et al., 2016*). Despite presumed changes in muscular configuration associated with the evolutionary origin of a supratendinal bridge (*Hutchinson, 2002*), the muscle implantation arrangement is remarkably similar to the condition in extant Laridae such as *Chroicocephalus* and *Sterna*.

Both distal condyles are very similar in size, shape, and distal extent, and are approximately round in lateral and medial view (Figs. 27A and 27C). The lateral condyle is slightly wider and broader than the medial condyle, which in turn extends slightly further cranially. The intercondylar groove is wide and shallow, and the proximal ends of both condyles gradually slope towards the midline of the cranial surface. The medial surface of the medial condyle is concave and excavated, with a moderately developed medial epicondyle. The lateral surface of the lateral condyle is mostly flat, and no lateral epicondyle is present. In caudal view, raised ridges (trochlear crests) extending from the distal edges of both condyles delimit a well-developed and subquadrangular caudal tarsometatarsal articulation (trochlea cartilaginis tibialis, *Baumel & Witmer, 1993*). The proximal edge of the trochlea is almost completely horizontal. Proximal to the trochlea, a shallow groove running parallel to the edge of the trochlea is visible in ALMNH: Paleo:3412 and BHI 6421 (Fig. 27C).

Fibula

The fibula has never been previously recovered or described for *Ichthyornis*, but three fibulae are preserved between two of the new specimens described here. In FHSM VP-18702 both fibulae are preserved in disarticulation, with an almost complete right fibula and the proximal portion of the left fibula (Fig. 27D). KUVP 119673 preserves a left fibula which is disarticulated, but in association with the distal tibiotarsus. Most of this specimen's proximal morphology is taphonomically distorted.

The preservation of the fibulae in the new specimens does not allow a comprehensive description, as several features are either obscured or indistinct. The fibula is very slender and elongate (Fig. 27D). In all three preserved fibulae, the element appears rather flat and mediolaterally compressed, but it is unclear whether this is taphonomic in nature or representative of the original morphology. The lateral surface of the proximal fibula in FHSM VP-18702 appears mostly flat to slightly convex, but a shallow tubercle seems to be developed at its midpoint. The medial surface is shallowly excavated and mostly concave. A small foramen seems to be developed on the medial surface (Fig. 27D). It is unclear whether this is opening represents an artifact of preservation, although a similarly excavated foramen is present in this region in *Parahesperornis* (*Bell & Chiappe, 2020*). The proximal end of the fibula is subtriangular in lateral view, with a slightly convex articular surface for the femur and a relatively large, caudally directed crest. The mediolateral extension of the fibula at its widest point is approximately equal to the maximum width of the tibiotarsal shaft.

The fibular shaft is thick and subtriangular in cross section along its proximal half, with a slightly narrower caudal edge conferring a keeled shape (Fig. 27D). A marked and distinct tubercle for the m. iliofibularis (*Baumel & Witmer, 1993*) is developed halfway along the preserved portion of the shaft. As in other Ornithurae (including crown birds; *Chiappe, 1996*), the tubercle is caudally directed and shows a deep excavation on its lateral surface both in FHSM VP-18702 and KUVP 119673. The width of the shaft remains mostly constant proximal to the m. iliofibularis tubercle, but distal to the tubercle the shaft tapers considerably and becomes extremely thin and rod-like (Fig. 27D). None of the specimens preserve the complete length of the fibular shaft, but it would have probably extended more than halfway along the length of the tibiotarsus and into the distal region of the element, since fibular impressions are apparent on the lateral surface of the distal tibiotarsus in BHI 6421. This inferred length of the fibula seems longer than that reported for *Gansus* and *Iteravis* (*Liu et al., 2014*; *Zhou, O'Connor & Wang, 2014*; *Wang et al., 2016*), and is substantially longer than that of *Yixianornis* and *Yanornis* (*Zhou & Zhang, 2001*; *Clarke, Zhou & Zhang, 2006*; *Wang & Zhou, 2020*), which both show highly reduced fibulae. The general morphology and distal extent of the *Ichthyornis* fibulae appear remarkably similar to those of the Common Tern (*Sterna hirundo*), which also shows an expanded, convex proximal end and a very elongate fibular shaft.

Tarsometatarsus

Six of the studied specimens include at least one tarsometatarsus (Figs. 28A–28D). Of these, only FHSM VP-18702 preserves a complete element, and, although this element is highly distorted, it apparently represents the first occurrence of a complete tarsometatarsus for *Ichthyornis* (Fig. 28B). Although the remaining tarsometatarsi are broken to varying extents, four of them from the ALMNH collections are exceptionally well-preserved: ALMNH:Paleo:3316 preserves both the proximal and distal portions of the left tarsometatarsus (though a small part of the shaft is missing; Fig. 28A), ALMNH:Paleo:1677 includes only the proximal end, and ALMNH:Paleo:1310 and ALMNH:
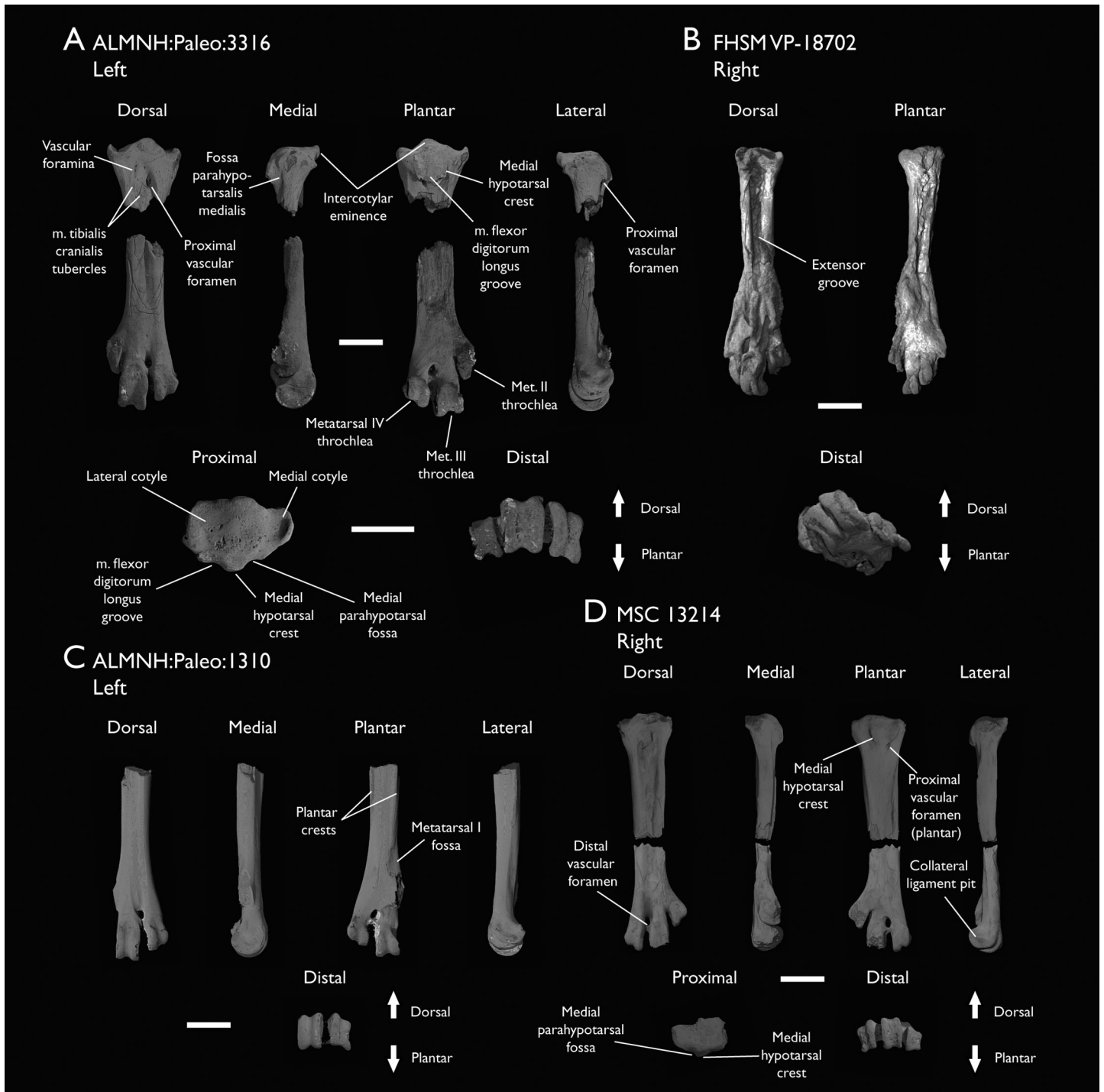
Figure 28 Tarsometatarsi of *Ichthyornis*. (A) ALMNH:Paleo:3316 left tarsometatarsus proximal and distal fragments, (B) FHSM VP-18702 right tarsometatarsus, (C) ALMNH:Paleo:1310 left distal tarsometatarsus and (D) MSC 13214 right tarsometatarsus proximal and distal fragments. Scale bar equals 5 mm.

Table 15 Measurements of the tarsometatarsus of *Ichthyornis* specimens. Total length corresponds to the maximum proximodistal extension of the tarsometatarsus, measured from the proximal intercotylar eminence to the distalmost point of metatarsal III trochlea. Proximal dorsoplantar width measurements include the hypotarsus, when preserved. Distal dorsoplantar width corresponds to the maximum dorsoplantar extension of metatarsal III trochlea. Distal mediolateral width is measured from the medialmost point of metatarsal II trochlea to the lateralmost point of metatarsal IV trochlea. Midshaft width corresponds to the mediolateral width of the tarsometatarsus shaft halfway through its length. Trochleae widths correspond to the maximum mediolateral extension of metatarsal II, III and IV trochleae. Asterisks (*) denote measurements that might be unreliable due to breakage or distortion, but are included for completeness. All measurements are in mm. – = not measurable.

Specimen	Total length	Prox. Dorsoplantar width	Prox. Mediolateral width	Dist. Dorsoplantar width	Dist. Mediolateral width	Midshaft width	Trochlea II width	Trochlea III width	Trochlea IV width
ALMNH:Paleo:1310	–	–	–	3.82	–	3.19	–	2.51	2.99
ALMNH:Paleo:1311	–	–	–	3.67	7.66	2.88	2.40	2.32	2.78
ALMNH:Paleo:1677	–	5.08	7.40	–	–	–	–	–	–
ALMNH:Paleo:3316	–	4.84	7.24	3.72	7.43	3.42	2.65*	2.54	2.74
FHSM VP-18702	29.13	4.21	5.69*	–	7.78*	3.78	–	1.93*	1.75*
MSC 13214	–	4.47	6.12*	3.73*	7.77	3.48	2.36	2.26*	2.25

Paleo:1311 are both distal tarsometatarsi (Figs. 28C and 28D). Additionally, MSC 13214 preserves the proximal and the distal portions of the element, both in exceptional condition. Measurements of the tarsometatarsi of the specimens included in this study are provided in Table 15.

The tarsometatarsus in *Ichthyornis* is completely fused, with both tarsals and metatarsals completely indistinguishable from one-another except in the distal region, where the articular surfaces for the pedal phalanges of metatarsals II–IV are distinct. The whole element is short and robust, with the tarsometatarsus of FHSM VP-18702 measuring 60% of the length of the femur (Figs. 28B; Tables 13 and 15).

The tarsometatarsus exhibits reduced mediolateral expansion at both the proximal and distal regions in relation to its shaft. The generally stout form of the *Ichthyornis* tarsometatarsus is reminiscent of the tarsometatarsi of *Yanornis* and *Yixianornis* (*Clarke, Zhou & Zhang, 2006*), and differs from the more elongate condition in the more closely related *Iteravis* and *Gansus* (*Liu et al., 2014*; *Zhou, O'Connor & Wang, 2014*; *Wang et al., 2016*). Metatarsal I is not preserved in any of the studied specimens, indicating that it probably separated easily after death.

The proximal region of the tarsometatarsus is best preserved in ALMNH:Paleo:3316, with no apparent distortion or breakage (Fig. 28A). The proximal end of metatarsal III is situated plantar to those of metatarsals II and IV. The intercotylar eminence (eminentia intercotylaris; *Baumel & Witmer, 1993*) is moderately developed, projecting only slightly proximally with respect to the lateral and medial edges of the tarsometatarsal cotyles (Fig. 28A). The dorsal edge of the eminence extends slightly dorsally beyond the rest of the proximal surface of the tarsometatarsus, and is slightly proximodistally recurved in lateral view, defining a marked and globose surface on its proximal end in dorsal view. Both cotyles are shallow and concave in proximal view, and, contrary to *Clarke (2004)*, the lateral cotyle has a larger proximal surface than the medial cotyle. The medial cotyle is

situated slightly more proximally than the lateral cotyle, is more deeply concave, and is delimited by a thickened ridge dorsally and medially, with the ridge projecting slightly less proximally than the intercotylar eminence on its medial side. A similar but less-developed ridge is present on the lateral cotyle, which ends distal to that of the medial condyle. The proximal extension of the medial cotylar edge does not seem to be evident in the YPM tarsometatarsi, as illustrated and described previously (*Clarke, 2004*), and seems to be broken in ALMNH:Paleo:1677.

Several foramina are present in the proximal depression between metatarsals, as described by *Clarke (2004)*. A large foramen penetrates the bone in the space between metatarsals III and IV, and opens plantarly just distal to the hypotarsus (Fig. 28A). Similar large, proximal vascular foramina are also found in some Mesozoic euornitheans such as *Gansus* and *Apsaravis* (*Clarke & Norell, 2002*; *Wang et al., 2016*), as well as among crown-birds such as *Sterna hirundo* and *Puffinus lherminieri*, but they differ from the condition in Hesperornithes, in which these do not perforate the tarsometatarsus (*Bell & Chiappe, 2020*). An additional, previously undescribed minute foramen is present between metatarsals III and IV, proximal to the large foramen. *Clarke (2004)* described a series of three foramina present between metatarsals II and III, but only two can be seen in this region in ALMNH:Paleo:3316. Contrary to *Clarke (2004)*, no corresponding foramen is present opposite to these on the plantar surface of the new tarsometatarsi.

The extensor groove is deeply excavated and wide, extending for most of the length of the shaft. Only FHSM VP-18702 preserves the whole length of the extensor groove, but its poor preservation distorts the morphology of this region (Fig. 28B). The proximal portion of the extensor groove is well-preserved in ALMNH:Paleo:3316, ALMNH:Paleo:1677, and MSC 13214. The two tubercles described by *Clarke (2004)* for the implantation of m. tibialis cranialis are present in all three specimens but are less distinct than in YPM 1739. The tubercle on the lateral surface of metatarsal II, situated at the same height as the large foramen, is a shallow and slightly concave scar in ALMNH:Paleo:3316 and in MSC 13214, and it is barely observable in ALMNH:Paleo:1677, instead of representing a clear tubercle. The tubercle on the dorsal surface of metatarsal III is large and clearly developed in ALMNH:Paleo:3316 and in MSC 13214, although its morphology would be better described as a raised, flat, ovoid surface rather than a tubercle. A pair of tubercles is developed in the extensor groove in *Gansus* (*Wang et al., 2016*), while a single one is present in Hesperornithes (*Bell & Chiappe, 2016*, *2020*).

The hypotarsus and the proximal plantar surface are well preserved in ALMNH:Paleo:3316 and in MSC 13214, but eroded and crushed in ALMNH:Paleo:1677 and FHSM VP-18702. Although YPM 1739 preserves part of the hypotarsus, several of the distinctive features present in the newly described specimens are not preserved in the YPM material (*Clarke, 2004*). The hypotarsus in *Ichthyornis* is a roughly quadrangular patch of bone, situated mostly behind the lateral cotyle (Fig. 28A). It shows a very limited plantar projection, with a flattened plantar surface showing only very shallow grooves and ridges. The hypotarsus extends distally for about 10% of the length of the tarsometatarsus, terminating just proximal to the plantar opening of the proximal vascular foramen in a sharp depression. A shallow groove is visible running proximodistally, interpreted here as

the sulcus for the m. flexor digitorum longus (*Hutchinson, 2002*; *Mayr, 2016*). A weakly developed ridge is present on the lateral edge of the groove; it has a flat lateral surface, congruent with the lateral hypotarsal crest as described by *Clarke (2004)*. The medial side of the groove is delimited by a wide and robust ridge, likely homologous with the medial hypotarsal crest (crista medialis flexoris digitorum longus; *Mayr, 2016*). The crest is situated just plantar to the intercotylar eminence, projecting further plantarly than the lateral ridge, and has a flattened plantar surface (Fig. 28A). The distal end of the medial crest is broken off in ALMNH:Paleo:3316, but complete in MSC 13214, where it does not extend into a medianoplantar crest (crista medianoplantarus; *Baumel & Witmer, 1993*). The medial surface of the medial crest is concave and moderately excavated, forming a proximodistally directed groove in a similar position to the medial parahypotarsal fossa (fossa parahypotarsalis medialis; *Baumel & Witmer, 1993*) that serves as an attachment point for the m. flexor hallucis brevis (*Vanden Berge & Zweers, 1993*). The morphology of the hypotarsus in *Ichthyornis* differs from the rudimentary condition in other crownward euornitheans like *Gansus, Yixianornis*, and *Changmaornis* (*Wang et al., 2013b*) as well as Hesperornithes (*Bell & Chiappe, 2016*, *2020*), in which the hypotarsus, if developed, shows no distinct ridges or grooves. In contrast, the condition in *Ichthyornis* is not dissimilar from that of Lithornithidae, in which a single shallow groove for the m. flexor digitorum longus is medially bounded by a wide, weakly projecting medial crest, which in turn delimits a concave surface on its medial side (*Houde, 1988*; *Nesbitt & Clarke, 2016*). This condition is also reminiscent of the morphology seen in the possible early euornithean *Kaririavis* (*Carvalho et al., 2021*), in which a single tendinal groove for the m. flexor digitorum longus is developed, although in this taxon the hypotarsus exhibits a subtriangular shape, and instead of exhibiting a sharp distal terminus, it extends into an elongated ridge continuing along most of the plantar surface of the tarsometatarsus. The morphology exhibited by *Kaririavis* might suggest the independent development of a hypotarsus in this taxon, especially in light of its uncertain, yet probably stemward phylogenetic position, and the complex combination of plesiomorphic and derived features it exhibits (*Carvalho et al., 2021*). Among crown birds, the hypotarsal morphology of *Ichthyornis* is most reminiscent of taxa with asulcate hypotarsi like Cathartidae and Cariamiformes (*Mayr, 2016*). In these, while the hypotarsus is significantly more plantarly projected and shows a flattened proximal surface, the medial and lateral crests are poorly developed, the sulcus for the m. flexor digitorum longus is extremely shallow, and the medial surface of the medial crest is concave and excavated. While this morphology has arisen independently among several crown bird lineages (*Mayr, 2016*), the similarity between Lithornithidae and *Ichthyornis* may indicate that this condition is plesiomorphic for crown group birds.

The shaft of the tarsometatarsus is mostly straight, with its narrowest point situated about halfway between the proximal and distal ends of the bone (Figs. 28A–28C). On the dorsal surface, the extensor groove becomes progressively shallower, but remains visible along the whole length of the shaft. The groove is bounded laterally and medially by two shallow, subparallel ridges deriving from the distal termini of the medial and lateral cotyles respectively, which extend into the articular trochleae of metatarsals III and IV (Figs. 28A

and 28C). The plantar surface of the shaft is mostly flat and featureless. Moderately extended lateral and medial plantar crests are visible in FHSM VP-18702, ALMNH:Paleo:1310, and in MSC 13214, bounding the flexor groove (sulcus flexorius; *Baumel & Witmer, 1993*). The lateral plantar crest terminates halfway along the length of the shaft, but a shallow ridge extends from its distal tip to the lateral surface of the metatarsal IV trochlea. The medial plantar crest extends further distally, terminating at the proximal edge of the metatarsal I fossa, which is only well-preserved in ALMNH:Paleo:1310 (Fig. 28C). The fossa is shallow and poorly excavated, but it is clearly divided into a proximal and a distal concave region, separated by a weakly developed horizontal ridge. A marked intermuscular line runs proximodistally across the midline of the plantar surface of the shaft, starting just distal to the distal terminus of the lateral plantar crest.
As described by *Clarke (2004)*, the intermuscular line runs parallel to the main axis of the shaft before turning laterally and meeting with the metatarsal IV trochlea (Figs. 28C and 28D).

Metatarsals III and IV delimit a very large, ovoid distal vascular foramen situated far distally, at a similar height to the metatarsal II trochlea and with its distal margin at a similar position to the proximal margin of the metatarsal III trochlea. The dorsal opening of the foramen is found at the distal end of a deep sulcus formed between both metatarsals, and is seemingly continuous with the extensor groove in ALMNH:Paleo:1310. However, the groove between the metatarsals is less marked proximally and does not contact the extensor groove in the other newly described specimens that preserve this region.
The foramen shows a single plantar opening of similar size, but rounder in shape, at the same height along the shaft (Figs. 28A, 28C and 28D). This foramen has two plantar exits in most crown birds, but the single plantar opening is found in several Mesozoic euornitheans, including *Gansus*, *Apsaravis* and the Hesperornithes (*Clarke & Norell, 2002*; *Wang et al., 2016*; *Bell & Chiappe, 2016*, *2020*). The distal vascular foramen is weakly or partially enclosed distally, as previously described by *Clarke (2004)*, with the distal bone margin being very narrow and extremely porous.

Of the fused metatarsals, metatarsal II is the shortest and most proximally situated, with its distal end at a height close to that of the proximal end of the metatarsal III trochlea (Figs. 28A and 28D). Metatarsals III and IV show a similar distal extension, with metatarsal III extending slightly further distally (Figs. 28A–28D). The metatarsal trochleae are essentially coplanar and aligned with the major dorsoplantar axis of the tarsometatarsal shaft, defining a flat and featureless plantar surface of the distal tarsometatarsus. Only the metatarsal II trochlea is slightly more plantarly positioned (Figs. 28A and 28D). This morphology differs from that found in most other Mesozoic euornitheans, including *Yanornis, Changmaornis, Gansus, Iteravis, Apsaravis,* and Hesperornithes (*Zhou & Zhang, 2001*; *Clarke & Norell, 2002*; *Wang et al., 2013b*, *2016*; *Liu et al., 2014*; *Zhou, O'Connor & Wang, 2014*; *Bell & Chiappe, 2016*, *2020*), in which metatarsal II is plantarly deflected. In *Gansus*, metatarsal IV is more plantarly situated than metatarsal III as well, defining a deeply concave plantar surface, with the cranial surface of the metatarsal II trochlea situated at the midpoint between the dorsal and plantar surfaces of metatarsal II (*Wang et al., 2016*). The relative dorsoplantar position of the distal terminus of each metatarsal is
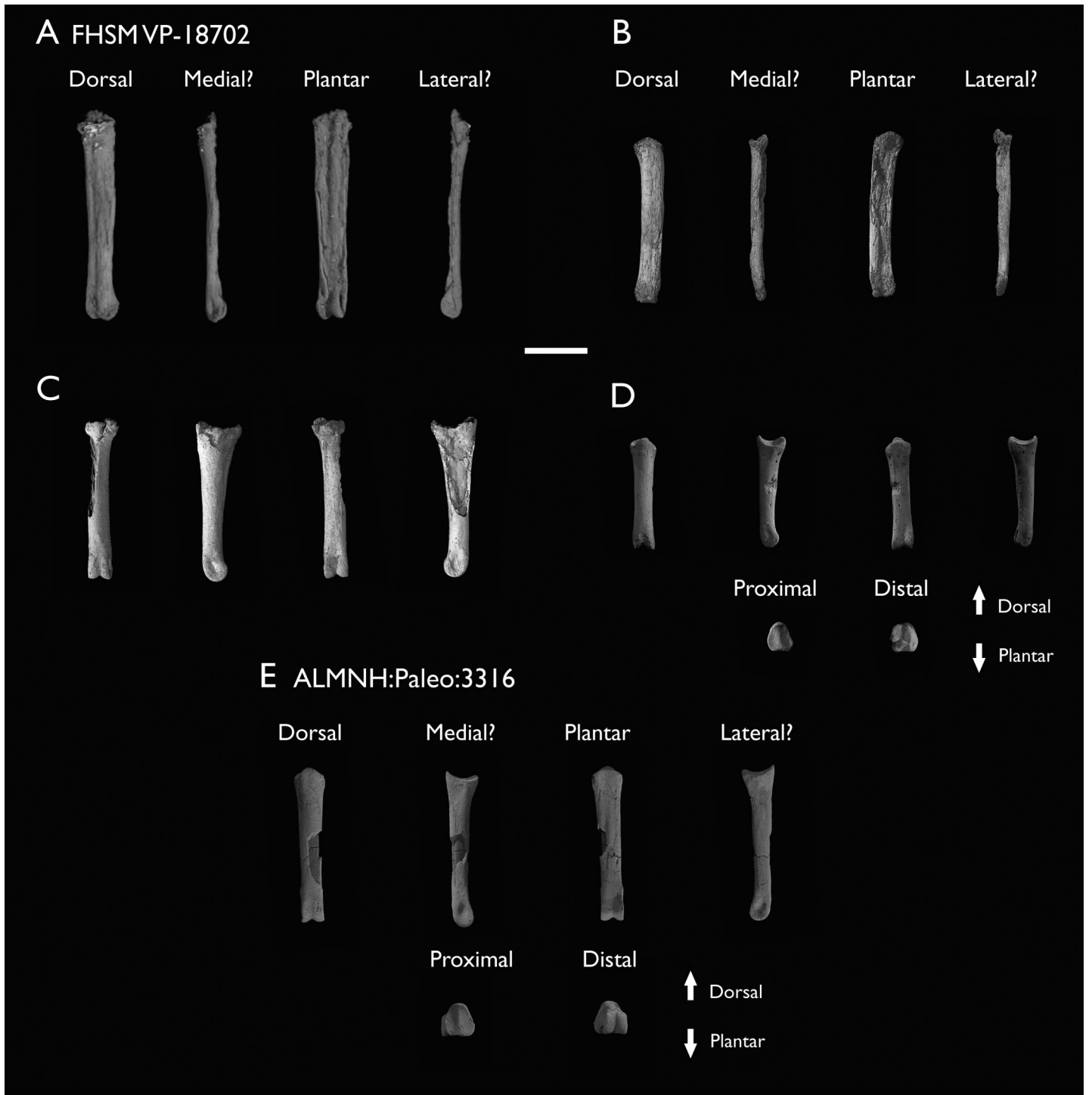
Figure 29 Pedal phalanges of *Ichthyornis*. FHSM VP-18702 (A) phalanx III:1?, (B) phalanx III:2?, (C) phalanx IV:1? (D) phalanx IV:2?; ALMNH: Paleo:3316 (E) phalanx IV:1? Scale bar equals 5 mm.

highly variable among crown-group birds, but the morphology in *Ichthyornis* is reminiscent of the condition in Procellariiformes such as *Puffinus lherminieri* and *Daption capense*, though the flat and featureless distal plantar surface is more similar to

Table 16 Measurements of the pedal phalanges of *Ichthyornis* specimens. Asterisks (*) denote measurements that might be unreliable due to breakage or distortion, but are included for completeness. All measurements are in mm.

Specimen	Total length	Proximal width	Distal width
ALMNH:Paleo:3316	12.39	2.38	1.85
FHSM VP-18702: Phalanx 1	17.19	2.76	1.81*
FHSM VP-18702: Phalanx 2	9.17	2.14	1.74
FHSM VP-18702: Phalanx 3	12.95	2.76*	1.94
FHSM VP-18702: Phalanx 4	13.52	2.33	1.82

Tinamiformes such as *Crypturellus variegatus*. The trochleae of metatarsals II–IV all show a very well-developed ginglymoid morphology, with deep collateral ligament pits on their lateral and medial surfaces (Figs. 28A, 28C and 28D). In metatarsal II (most clearly visible in ALMNH:Paleo:1311), the ginglymoid condition is slightly less developed than in metatarsal III and IV, with the sulcus between both lateral and medial ridges of the trochlea being very shallow, and the lateral ridge projecting significantly less distally than the medial ridge (Figs. 28A and 28D). The ginglymoid morphology of the metatarsal II trochlea contrasts with the condition in other euornitheans, such as *Gansus* and *Apsaravis*, in which the articular surface of metatarsal II is rounded (*Clarke & Norell, 2002*; *Wang et al., 2016*). The trochlea of metatarsal III is the widest and proximodistally longest, differing from the condition in Hesperornithes, in which the trochlea of metatarsal IV is the largest (*Bell & Chiappe, 2020*). The distal terminus of metatarsal IV is dorsolaterally oriented, and its trochlea is highly asymmetrical, with the medial trochlear ridge terminating well dorsal to the lateral trochlear ridge. The lateral surface of the trochlea extends into an elongated flange that continues further plantarly than the metatarsal II trochlea (Figs. 28A and 28D).

Pedal phalanges

No complete pes is known for *Ichthyornis*, and only a single pedal phalanx is preserved amongst the YPM material (*Clarke, 2004*). Two of the newly described specimens include pedal phalanges: FHSM VP-18702 preserves four phalanges (Figs. 29A–29D) and ALMNH:Paleo:3316 preserves a single phalanx (Fig. 29E); these are all disarticulated and none represent ungual phalanges. Unfortunately, definitively establishing which digits they belonged to, and what position they occupied within those digits, is challenging. Measurements of the pedal phalanges of the specimens included in this study are provided in Table 16.

The largest phalanx from FHSM VP-18702 is badly flattened and lacks most of its proximal articular surface (Fig. 29A). The phalanx is completely straight, with no lateromedial curvature. The distal articular surface shows a strong ginglymoid condition, with deep pits on its lateral and medial surfaces for the collateral ligaments. This phalanx is greatly elongated compared with the FHSM VP-18702 tarsometatarsus (the phalanx is 60% as long as the tarsometatarsus; Tables 15 and 16). Such elongated phalanges are not known among any other Mesozoic euornitheans, even in those with shortened
tarsometatarsi like *Yixianornis* or elongated pedal phalanges like *Gansus* (*Clarke, Zhou & Zhang, 2006*; *Wang et al., 2016*), in which the proximal digit III phalanx (the longest phalanx) represents around 40% of the total length of the tarsometatarsus. A similar proportion of around 40% is found in Hesperornithes such as *Hesperornis* and *Parahesperornis*, for which the proximal phalanx of digit IV is the longest one. Proportions comparable to *Ichthyornis* between the longest phalanx and the tarsometatarsus are found in several predominantly aquatic crown bird lineages, including Anseriformes, such as *Anas platyrhynchos* (56%), Gruiformes like *Fulica atra* (55%) or Suliformes like *Morus bassanus* (62%). The lack of a well-preserved proximal articular surface, together with the significant mediolateral compression of FHSM VP-18702 complicates the identification of the position of this phalanx. Its extremely elongate condition together with the width of its proximal end (greater than that of the metatarsal III trochlea) suggest that it most likely represents the proximal phalanx of digits II or III.

The second-longest phalanx of FHSM VP 18702 is also dorsoventrally flattened, and while its proximal articular surface is preserved, the distal trochlea is greatly distorted (Fig. 29B). The phalanx shows limited mediolateral curvature, but this appears to be a taphonomic artifact. The phalanx is elongate, and is 82% of the length of the longest phalanx (Table 16). The proximal articular surface, though distorted, appears mostly symmetrical, with two similarly sized cotyles, which suggest that it does not represent the proximal phalanx of digits II or IV. Its proximal end has a similar width to the distal trochlea of the longest phalanx, which suggests that it is most likely the second phalanx of digit III.

The third-longest phalanx is only slightly shorter than the second, and it is well preserved, mostly three-dimensionally (Fig. 29C). The dorsal surface of the phalanx is mostly flat, but the plantar surface is moderately arched. The shaft is mostly straight with no significant proximodistal reduction in width, though the proximal articular surface is significantly wider than the shaft. The proximal articular surface is mediolaterally crushed, but preserves both articular cotyles, which appear slightly asymmetrical. Despite some taphonomic compression, the width of the proximal articular surface is greater than that of the distal trochlea of the longest phalanx. However, the proximal articular surface appears to be considerably wider than the trochleae of metatarsals II and IV as well, which, despite being badly compressed, are not wider than the trochlea of metatarsal III in other specimens (Table 16). This suggests that this phalanx might represent the second phalanx of digits II or IV, for which no proximal phalanges are preserved, complicating direct comparisons. The distal articular surface of the phalanx is well-preserved and strongly ginglymoid.

The shortest phalanx of FHSM VP-18702 extends for only 52% of the length of the longest phalanx (Table 16). It is extremely well preserved, with the only noticeable blemish being the fact that its distal articular surface is slightly eroded (Fig. 29D). The shaft is mostly straight, and only narrows proximodistally to a slight degree such that the proximal surface is not significantly wider than the shaft. Its plantar surface is more strongly arched than that of the third-longest phalanx, and the ginglymoid morphology of its distal articular surface is more weakly developed. The proximal articular surface preserves two
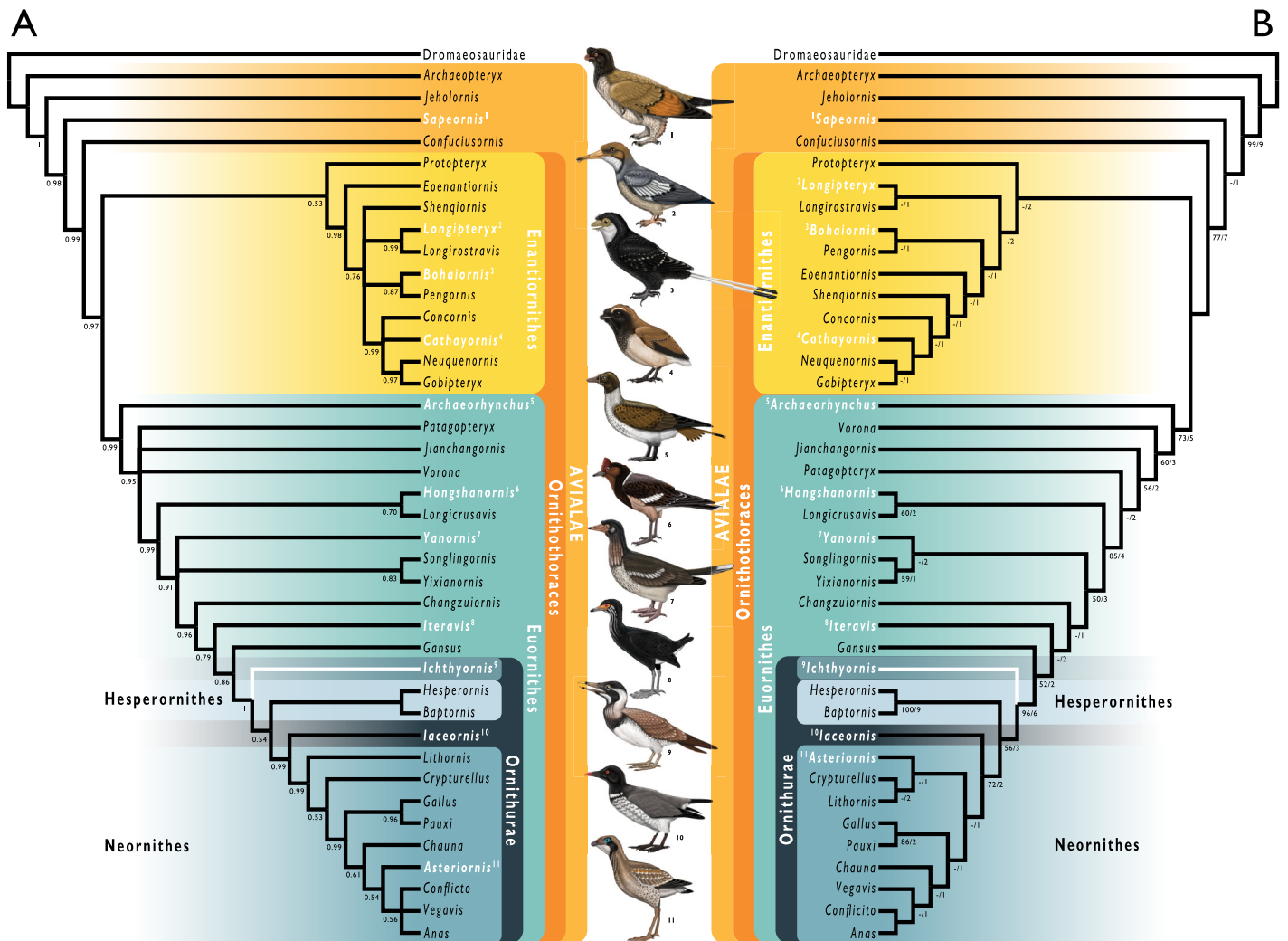
Figure 30 Phylogenetic results of analyses using a modified version of the morphological matrix from *Torres, Norell & Clarke (2021)*, **excluding** *Apsaravis ukhaana*. (A) Results from Bayesian inference; node values indicate Bayesian posterior probabilities. (B) Results of parsimony analyses: single most parsimonious tree, branch values indicate bootstrap support values (left of bar) and Bremer decay indices (right of bar). Taxonomic names in white indicate taxa illustrated in the figure, the corresponding illustration is indicated by the superscript numbers. Branches in white indicate the position of *Ichthyornis dispar*, the focal taxon of this study. Illustrations courtesy of R. Olivé, used with permission.

symmetrical and equally sized trochleae. The dorsal proximal margin does not exhibit a strong extensor tubercle, but robust flexor tubercles are found on the plantar surface. The short and stout proportions of this phalanx are congruent with its identity as the second or third phalanges of Digit IV, which exhibits a greater number of non-ungual phalanges (four) than the rest of the digits in most crown birds and in crownward avialans such as *Gansus* (*Wang et al., 2016*) and *Apsaravis* (*Clarke & Norell, 2002*).

The only pedal phalanx belonging to ALMNH:Paleo:3316 is well-preserved, missing only part of the bone surface of the shaft (Fig. 29E). The phalanx is similar in length to the third-longest phalanx of FHSM VP-18702 (Table 16). The shaft is mostly straight with subparallel lateral and medial surfaces, with no significant reduction in width towards the
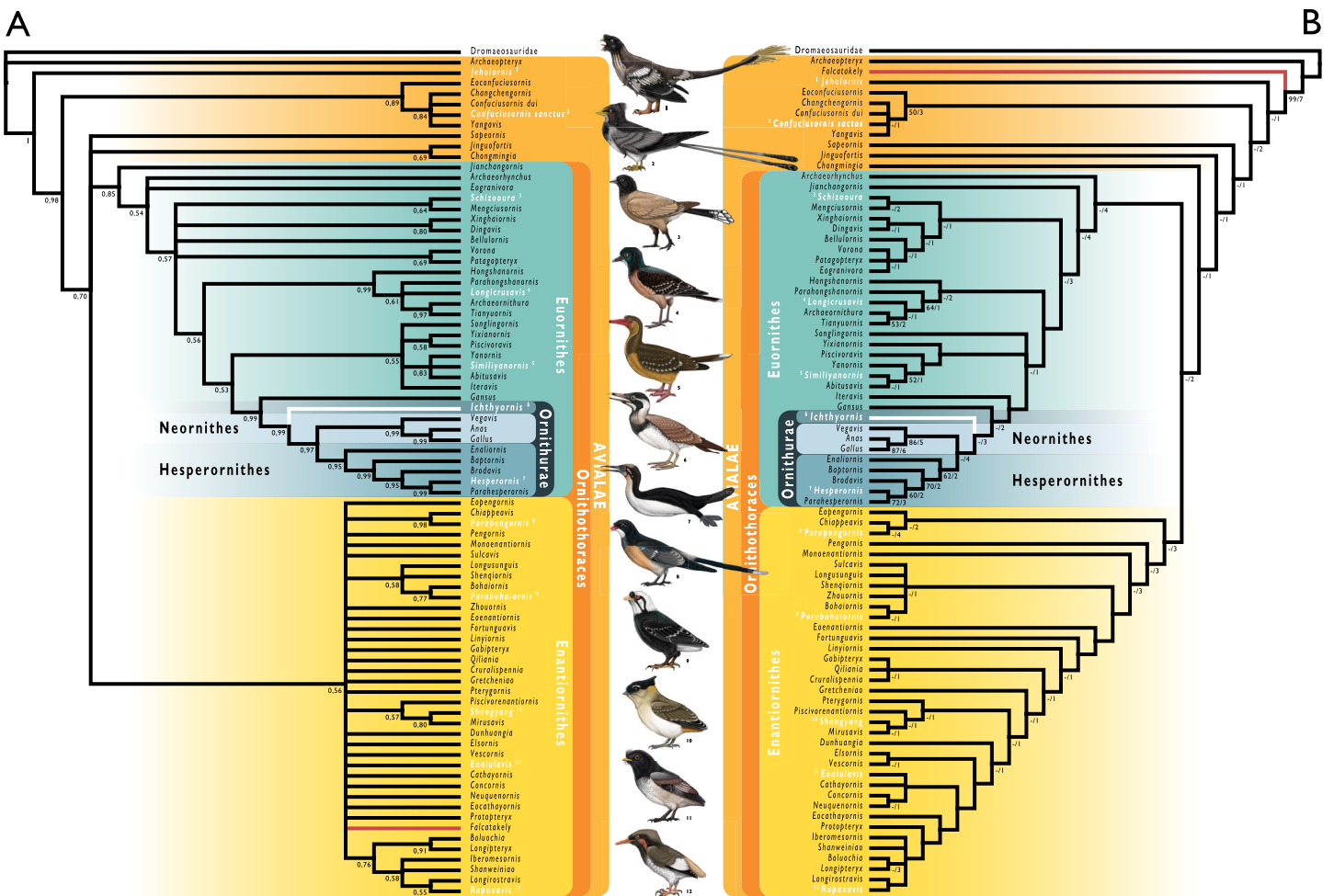
Figure 31 Phylogenetic results of analyses using a modified version of the morphological matrix from *Wang et al. (2020c)*, excluding *Apsaravis ukhaana*. (A) Results from Bayesian inference; node values indicate Bayesian posterior probabilities. (B) Results from parsimony analyses; strict consensus of ten most parsimonious trees, branch values indicate bootstrap support values (left of bar) and Bremer decay indices (right of bar). Taxonomic names in white indicate taxa illustrated in the figure. Branches in red indicate the position of *Falkatakely forsterae*, highlighting remarkable lability in its phylogenetic position recovered from analyses employing different phylogenetic optimality criteria. Branches in white indicate the position of *Ichthyornis dispar*, the focal taxon of this study. Illustrations courtesy of R. Olivé, used with permission.

distal end, and the ventral surface of the shaft is only moderately arched. The proximal articular surface, only slightly mediolaterally wider than the shaft, shows two slightly asymmetrical cotyles. The dorsal surface extends well proximally, but does not form a clear extensor tubercle. The ventral surface has only weakly-developed flexor tubercles.

The width of the proximal articular surface is similar to that of the ALMNH:Paleo:3316 metatarsal IV trochlea, which, together with its slightly asymmetrical cotyles, suggests it represents the proximal phalanx of digit IV. The distal articular surface its strongly ginglymoid, with very deep pits for the collateral ligaments.
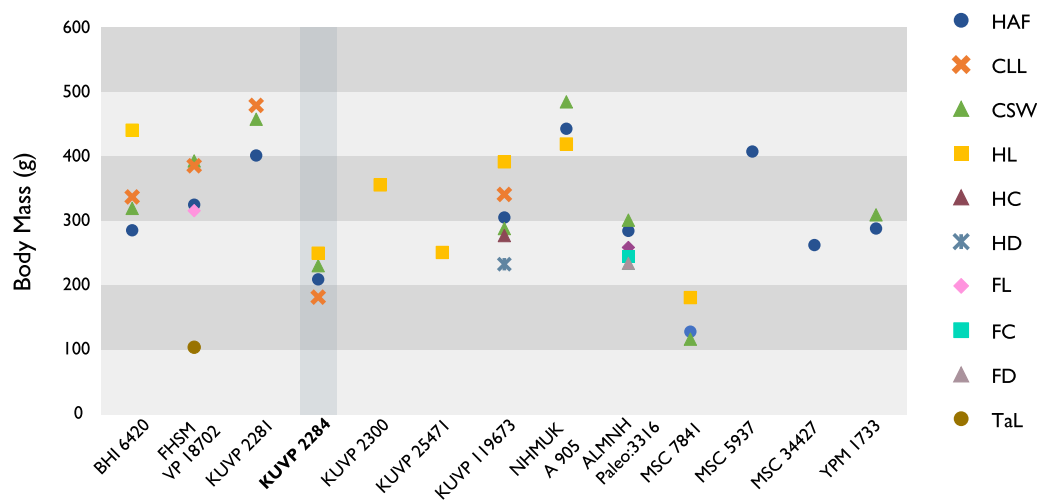
Figure 32 Body mass estimates for selected *Ichthyornis* specimens. Body mass correlates represented, in order of increasing Percent Prediction Error (after *Field et al., 2013*) are: maximum diameter of the coracoid's humeral articulation facet (HAF), maximum coracoid lateral length (CLL), least coracoid shaft width (CSW), maximum humerus length (HL), least humerus shaft circumference (HC), least humerus shaft diameter in cranial view (HD), maximum femur length (FL), least femur shaft circumference (FC), least femur shaft diameter in cranial view (FD) and maximum tarsometatarsus length (TaL). The vertical box and bold text indicate the probable immature nature of specimen KUVP 2284.

PHYLOGENETIC RESULTS

To assess the referral of the new specimens to *Ichthyornis*, all well-represented specimens were initially incorporated into phylogenetic analyses as distinct operational taxonomic units (OTUs). Despite multiple morphological differences among several of the new specimens, the parsimony analyses recovered all the new specimens in an exclusive monophyletic group with YPM 1450, the holotype of *Ichthyornis*, using both the *Torres, Norell & Clarke (2021)* dataset (Trees S1 and S2) and the *Wang et al. (2020c)* dataset (Trees S5 and S6). By contrast, Bayesian inference analyses employing both datasets recovered all *Ichthyornis* specimens in a polytomy comprising the holotype and the clade formed by Hesperornithes + crown birds (Trees S4, S7 and S8) or in a polytomy with *Apsaravis*, Hesperornithes and crown birds (Tree S3); however, forcing all the *Ichthyornis* specimens to form an exclusive monophyletic group requires only a single additional step. All subsequent analyses were performed using a single combined OTU for *Ichthyornis*.

As discussed in the Methods, *Apsaravis* was identified as a wildcard taxon, and its phylogenetic position was remarkably variable depending on the optimality criteria used. Analyses excluding *Apsaravis* recovered much more consistent results, and therefore, these will be the results discussed below. See the Supplemental Information for results including *Apsaravis*.

Parsimony analysis using the *Torres, Norell & Clarke (2021)* dataset returned a single most parsimonious tree with 579 steps (consistency index = 0.516, retention index = 0.805). The crownward portion of the strict consensus tree is well resolved, although bootstrap support values are relatively low overall (Fig. 30B). *Ichthyornis* is

recovered stemward of Hesperornithes, and *Iaceornis* is recovered crownward of both, as the sister taxon to crown birds (Neornithes). Bayesian analysis of the *Torres, Norell & Clarke (2021)* dataset recovered an identical topology of the crownward portion of the phylogeny, with high posterior probabilities supporting the positions of *Ichthyornis*, Hesperornithes and crown birds (Fig. 30A). An alternative topological arrangement in which *Ichthyornis* is crownward to Hesperornithes requires a single additional step. Topological differences between parsimony and Bayesian analyses are more pronounced among more stemward euornitheans, with both methods recovering a monophyletic Hongshanornithidae, while Songlingornithidae is recovered only by parsimony analyses.

Parsimony analysis using the *Wang et al. (2020c)* dataset returned 10 most parsimonious trees with 1395 steps (consistency index = 0.281, retention index = 0.661). Similar to the previous analyses, the crownward region of the tree is well resolved, but bootstrap values are low (Fig. 31B). *Ichthyornis* is recovered stemward to Hesperornithes, which emerge as the sister taxon to the crown group. Bayesian inference recovers an identical topology for the crownward portion of the tree, with very high posterior support values (Fig. 31A). Alternative topological arrangements in which *Ichthyornis* is crownward to Hesperornithes, or forms an exclusive clade with them, require three or five additional steps, respectively. Relationships among stemward euornitheans differ substantially between the parsimony and the Bayesian inference results, with Bayesian analyses recovering *Vorona* and *Patagopteryx* in an exclusive clade, as well as a monophyletic Songlingornithidae, despite recent iterations of this dataset recovering a monophyletic Yanornithidae instead (*Wang et al., 2020c*, *2021*). Notably, the position of *Iteravis* varies under alternative optimality criteria, emerging stemward of *Gansus* in the parsimony analysis but within Songlingornithidae under Bayesian inference.

Body mass estimates

We estimated the total body mass for several of the new *Ichthyornis* specimens following the equations from *Field et al. (2013)*. Several different measurements were taken for these estimates (Fig. 32), providing a total mass distribution for our sample between 104.43 g and 480.67 g. As reported by *Field et al. (2013)*, these measurements recover estimates with variable accuracy, and measurements of the coracoid provide particularly precise estimates of volant bird body mass. The coracoid happens to be the most commonly preserved skeletal element in our sample, and measurements of maximum diameter of the coracoid humeral articulation facet, maximum coracoid lateral length, and the coracoid shaft least width could be obtained from ten, five and nine specimens respectively (Table 4). Maximum humeral length could be taken for seven specimens, although it this proxy recovered systematically higher mass estimates than the coracoid measurements, suggesting that the humeri of *Ichthyornis* were proportionally long (Fig. 32; Table 6). In contrast, the total tarsometatarsal length, which could only be measured for FHSM VP-18702 (Table 15), recovered a mass estimate notably smaller than those derived from any other measurement. However, tarsus length is highly ecologically variable, making it a particularly poor predictor of volant bird body mass (*Field et al., 2013*); as such, we considered this estimate unreliable. Where specimens preserved both right and left skeletal

elements, recovered mass estimates were averaged (Fig. 32). In certain cases, specimens preserving both paired elements produced notably different body mass estimates, such as BHI 6420 and NHMUK A 905. Both of these specimens are flattened, and the differing estimates might be caused by taphonomic deformation, although the possibility that these specimens could represent composites of multiple individuals cannot be ruled out.

Overall, the body mass estimates provide a relatively wide mass distribution for *Ichthyornis*, with the largest specimens being between 2.5 and 4.2 times the size of the smallest, depending on the measurements taken. NHMUK A 905 (426.64 to 486.18 g) and KUVP 2281 (402.65 to 459.27 g) were recovered as the largest individuals, while KUVP 2284 (182.48 to 250.80 g) and MSC 7841 (117.15 to 181.79 g) were the smallest. As discussed above, the studied specimens exhibit probable evidence of ontogenetic variation, particularly in the case of KUVP 2284, which might represent a juvenile individual; as such, the small body size estimate for these specimens may be indicative of an early ontogenetic stage.

DISCUSSION

Novel morphological information

This work reveals the preservation of several skeletal elements previously unknown for *Ichthyornis*, as well as considerable novel morphological information for skeletal elements previously represented only by fragmentary or poorly preserved specimens. Amongst the new material, the vertebral series stands out as especially significant, as only a few isolated vertebrae have been previously described (*Marsh, 1880*; *Clarke, 2004*). Only three YPM specimens, YPM 1450, 1732 and 1733, preserve any significant vertebral material, but in all cases, the presacral and caudal vertebrae are isolated and fragmentary. As described above, three of the new specimens, KUVP 25472, KUVP 119673, and ALMNH:Paleo:3316, preserve a substantial portion of the vertebral column, revealing in unprecedented detail the vertebral morphology of *Ichthyornis*. While the incomplete nature of the specimens currently makes it impossible to establish the total number and exact position of all vertebrae, the preservation of the partial cervical series in KUVP 119673 and the almost complete thoracic series in KUVP 25472 allow for a much more precise estimate than was previously possible. These specimens illustrate that *Ichthyornis* had at least eleven cervical and ten thoracic vertebrae (Figs. 4–7), a count similar to those of closely related taxa such as *Gansus* (*Wang et al., 2016*) and *Yixianornis* (*Clarke, Zhou & Zhang, 2006*). The vertebral morphology of the new specimens is very similar to that described by *Marsh (1880)* and *Clarke (2004)*, although the new specimens provide a better characterization of the cervicothoracic transition.

The synsacrum of *Ichthyornis* was previously known from only three YPM specimens, which notably diverged in the number of fused sacral vertebrae, exhibiting either 10 or 12 ankylosed sacrals *Clarke (2004)*. Here, the synsacrum is preserved in four of the new specimens, and three of them preserve the element in its entirety (Fig. 8). As described above, the new material reveals a pattern of vertebral fusion not dissimilar to that exhibited by some extant birds, such as *Gallus gallus* and *Ardea cinerea*, during post-hatching ontogeny (*Bui & Larsson, 2021*; J. Watanabe, 2021, personal communications). The new
specimens show the presence of variably ankylosed sacral vertebrae on the anterior end of the sacrum, and the fusion of additional vertebrae to the caudal end of the element. While this variability is presumably ontogenetic, there seems to be no close correlation between the size of the specimens and the degree of fusion they exhibit, recalling similarly idiosyncratic fusion patterns across the skeleton in other Mesozoic dinosaurs (*Longrich & Field, 2012*; *Bailleul et al., 2016*; *Griffin et al., 2021*), and potentially pointing towards greater intraspecific or interspecific variation than previously recognized (see discussion of intraspecific variation below). Two of the new specimens preserve caudal vertebrae, although these do not reveal significant new morphological information, and no pygostyle is preserved among the studied material. This element remains unknown for *Ichthyornis*.

The ribs of *Ichthyornis* have not been previously described in detail. Both vertebral and sternal ribs are preserved in the new specimens, and, although well preserved in several instances, none appear to be entirely complete (Figs. 9C and 9D). Considering this abundance of costal material, the absence of any preserved uncinate processes is striking. The sternum is preserved in three of the new specimens, and although all of them are variably distorted, together they provide an unprecedented level of information on the sternal morphology of *Ichthyornis* (Fig. 10), our understanding of which was previously based on very incomplete remains (Fig. 11). The caudal portion of the sternum was previously very poorly known, and the new specimens, particularly KUVP 119673, reveal the presence of short, rounded, and open sternal incisures, dissimilar to those of other crownward euornitheans such as *Gansus* (*Wang et al., 2016*). The new specimens also provide the first detailed view on furcular morphology in *Ichthyornis*, as only fragments of this element have been previously reported. Contrary to the hypothesis presented by *Clarke (2004)*, *Ichthyornis* exhibits a clear hypocleideum extending from the clavicular symphysis (Fig. 12A), a feature not previously found in any crownward euornitheans. The omal ends of the furcula also differ from the condition described by *Clarke (2004)*, tapering omally instead of terminating in a blunt end.

Nine of the new specimens preserve one or both coracoids. In several cases, such as BHI 6420, FHSM VP-18702, KUVP 119673, and KUVP 2281, these represent the best-preserved coracoids known for *Ichthyornis*, exceeding the completeness and quality of preservation seen in any YPM specimens (Fig. 13). The new material shows that both the acrocoracoid and procoracoid processes were more strongly developed and hooked than previously recognized, together forming a claw-like shape, although these are broken in multiple specimens (*Clarke, 2004*). The scapula is preserved in five of the new specimens, which exhibit surprising variation in the morphology of the acromion process, the extremely reduced morphology of which was previously considered a diagnostic feature of *Ichthyornis* by *Clarke (2004)*. Although the acromion is always small, it is variably absent, rounded, pointed and triangular, or hooked and recurved (Fig. 14). This variability might illustrate a greater degree of intraspecific variation than has been previously recognized (see below).

The humerus is the most commonly reported skeletal element for *Ichthyornis*, although all previously described specimens are variously flattened. Despite the abundance of previously described *Ichthyornis* humeri (*Marsh, 1880*; *Harrison, 1973*; *Olson, 1975*; *Lucas*

& Sullivan, 1982; Fox, 1984; Clarke, 2004; Porras-Múzquiz, Chatterjee & Lehman, 2014; Shimada & Wilson, 2016), the twelve new specimens described here that bear humeri provide a wealth of novel morphological data (Figs. 15–17). Particularly remarkable is the three-dimensional preservation of two humeri, the left humerus of KUVP 2300 and the right humerus of KUVP 119673, which reveal a craniodorsally oriented deltopectoral crest (Fig. 16), and a curved, sigmoidal humeral shaft, previously only reported by Shimada & Wilson (2016), who attributed this novel shape to either taphonomic distortion of the specimen or interspecific variation. The preservation of both a flattened left and a three-dimensional right humerus in KUVP 119673 (Figs. 16A and 16B) reveal that these important features are genuine and easily obscured by taphonomic flattening, which emphasizes the need for caution in interpreting the morphology of flattened avialan fossils. In contrast to the exceptionally preserved humeri described here, neither the ulna nor the radius is especially well represented among the new specimens, and no previously undescribed morphological details of these elements are discernible. The free carpal elements are well represented amongst the new material, and we describe the radial carpal bone of *Ichthyornis* for the first time as well as the first complete ulnar carpals (Fig. 20). The morphology of the radial carpal is similar to that of *Iaceornis* and is reminiscent of the radial carpal of the stem-anseriform *Presbyornis* (J. Benito, 2021, personal observations).

Although several of the new specimens preserve carpometacarpi, the carpometacarpus of YPM 1714, previously described by Marsh (1880) and Clarke (2004), remains the best-preserved *Ichthyornis* carpometacarpus known to date (Fig. 22A). Here, the extremely short carpometacarpus of the large individual FHSM VP-18702 confirms a pattern of variation in carpometacarpus length among otherwise similarly sized and proportioned individuals (Fig. 22B), as initially noted by Clarke (2004). The morphology of the manual phalanges preserved amongst the new material is virtually identical to that of previously described *Ichthyornis* material (Figs. 23 and 24), with the exception of the proximal phalanx of the major digit of KUVP 2284, which lacks an internal index process (Fig. 23B; see intraspecific variation below). The exceptional level of preservation of the new specimens may facilitate a detailed investigation of the muscular and ligament attachments of the hand in future work.

Only one of the new specimens, KUVP 119673, preserves pelvic remains, but these constitute the most complete pelves known for *Ichthyornis* (Fig. 25). Although partially complete pelves in anatomic connection were previously known from YPM 1732, significant portions of the ilium and pubis were missing, and their anatomy was inferred in illustrations by Marsh (1880). The well preserved pelves of KUVP 119673 show a markedly different morphology from that reconstructed by Marsh (1880), with narrow and blade-like postacetabular ilia similar to those of other crownward euornitheans such as *Gansus* (You et al., 2006; Wang et al., 2016).

Hindlimb material for *Ichthyornis* is much scarcer than forelimb material within the YPM collections, and the same is true for the new specimens. Only one specimen, ALMNH:Paleo:3316, preserves a mostly complete, three-dimensional hindlimb, although multiple other specimens include fragmentary tibiotarsi and tarsometatarsi. The femur of ALMNH:Paleo:3316 is three-dimensionally preserved and constitutes the best-preserved
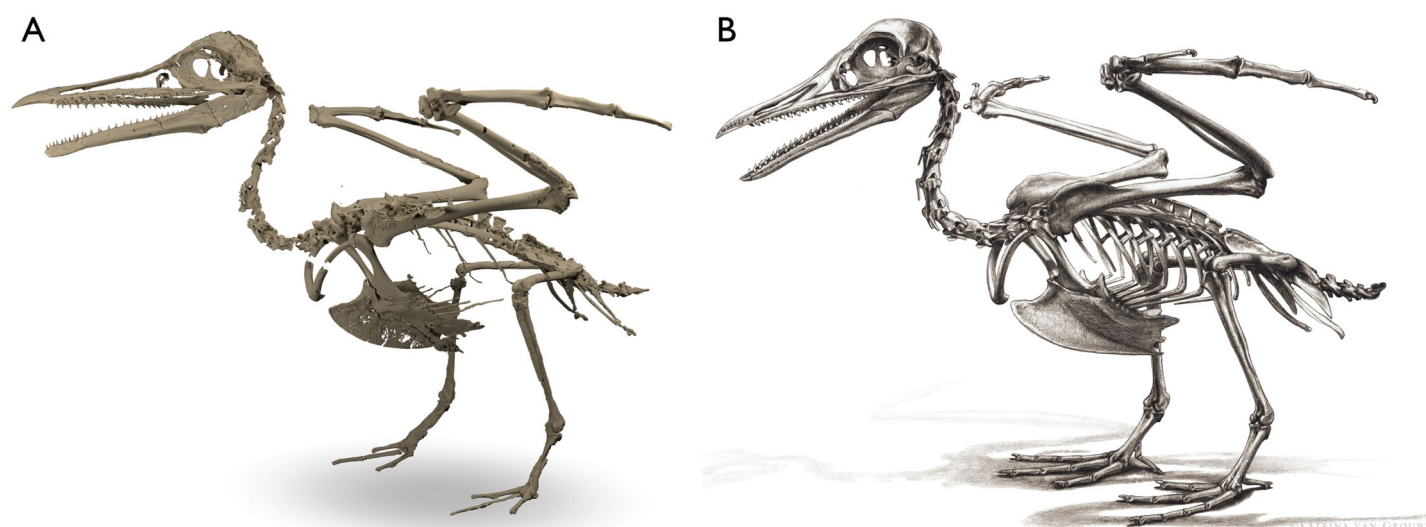
Figure 33 Skeletal reconstructions of *Ichthyornis dispar*. (A) Three-dimensional skeletal reconstruction using a composite of the specimens described in this study; (B), complete skeletal reconstruction of *Ichthyornis dispar*, including reconstructed fragmentary and missing elements. The reconstruction shown here includes unfused uncinate processes on the thoracic ribs, which we consider to be the most conservative explanation for their absence in known specimens of *Ichthyornis*; see the morphological description for discussion on the presence of uncinate processes in *Ichthyornis*. Skeletal reconstruction courtesy of K. van Grouw, used with permission.

femur of *Ichthyornis* known so far (Fig. 26A). Importantly, discrete features of its morphology do not differ substantially from those described by *Marsh (1880)* and *Clarke (2004)* based on taphonomically flattened YPM material. The proximal tibiotarsus of ALMNH:Paleo:3316, although fragmentary and somewhat distorted, preserves several features not previously observed in *Ichthyornis* (Fig. 27A). Two of the new specimens preserve fibulae, and although these are poorly preserved, they represent the first fibulae described for the taxon (Fig. 27D). Multiple specimens include well-preserved tarsometatarsi, and among them FHSM VP-18702 is particularly remarkable for exhibiting the first complete *Ichthyornis* tarsometatarsus (Fig. 28). The excellent preservation of the tarsometatarsi of ALMNH:Paleo:3316 and MSC 13214 enables for the first time the description of a rudimentary hypotarsus (Fig. 28A), which illustrates a remarkable combination of stem- and crown bird-like morphological features. The pedal phalanges of *Ichthyornis* are described in detail for the first time (Fig. 29); although it is impossible to infer their position with certainty, precluding a complete reconstruction of foot anatomy for *Ichthyornis*, the proportions of these phalanges in comparison with the rest of hindlimb elements suggest a greatly enlarged pes, presumably adapted for foot-propelled swimming.

Together, the 40 new specimens reported here provide us with the most complete view of *Ichthyornis* postcranial morphology to date, greatly updating our understanding of this taxon. This new material allows an almost complete reconstruction of the *Ichthyornis* postcranial skeleton (Fig. 33), making *Ichthyornis* one of the most complete and best-preserved Mesozoic avialans known to date (*Brocklehurst et al., 2012*; *Pittman et al., 2020b*). In addition to their completeness, many *Ichthyornis* fossil remains are notable for their exceptional three-dimensional preservation, a condition rarely seen among Mesozoic

avialans, which are usually flattened, crushed, or otherwise distorted (*Field et al., 2018b*; *Hu et al., 2020*). The unprecedented completeness and quality of these remains should allow for extensive reconstructions of soft tissue, and explorations of functional morphology and biomechanics at a level of detail previously impossible for crownward Mesozoic avialans.

Although reconstructing the ecology and lifestyle of *Ichthyornis* is not the primary aim of this work, the new material described here enables some new inferences into its biology. *Ichthyornis* shows similar wing proportions to volant extant birds, especially marine soaring taxa. The brachial index (BI, *sensu Nudds, Dyke & Rayner, 2006*), which measures the proportion between the humerus and the forearm, has been considered to provide a reasonable proxy for avian flight capabilities, correlating with specific ecologies and flight styles (*Nudds, Dyke & Rayner, 2006*; *Karoullas & Nudds, 2021*). The BI of *Ichthyornis* could only be measured for KUVP 2284 and KUVP 119673, since these are the only specimens preserving both complete humeri and ulnae. In KUVP 119673, the BI is 0.94, similar to taxa such as terns (*e.g.*, *Sterna hirundo*; 0.89), gulls (*e.g.*, *Chroicocephalus novaehollandiae*; 0.89), shearwaters (*e.g.*, *Puffinus lherminieri*; 0.99) and tropicbirds (*e.g.*, *Phaethon lepturus*; 0.92) (see Supplemental Information). In contrast, in KUVP 2284 the BI is 1.05, more similar to the proportions of non-marine taxa such as geese (*e.g.*, *Anser albifrons*; 1.04) and coots (*e.g.*, *Fulica atra*; 1.01). As discussed above, KUVP 2284 might represent a juvenile individual, and its distinct proportions, with a humerus longer than the ulna, might be related to its early developmental stage.

None of the studied three-dimensional *Ichthyornis* forelimb elements show any evidence of the flattened morphology observed in specialized wing-propelled divers (*Habib, 2010*; *Watanabe, Field & Matsuoka, 2021*). Instead, *Ichthyornis* appears to exhibit several hindlimb features related to swimming, and several anatomical features may point towards it having exhibited a paddle-swimming ecology. These include a reduced femoral trochanter, a character state associated with foot propelled-diving (*Zinoviev, 2011*; *Clifton, Carr & Biewener, 2018*; *Bell, Wu & Chiappe, 2019*) and observed in taxa such as *Anas platyrhynchos*, *Puffinus lherminieri*, *Phaethon lepturus*, *Phalacrocorax carbo* and *Morus bassanus*, but absent in non-natatorial taxa such as *Sterna hirundo* or *Charadrius rubricollis*, in land-dwelling birds such as *Gallus gallus* and wing-propelled swimmers such as *Alca torda*. While the leg proportions of *Ichthyornis* cannot be completely reconstructed due to a lack of entirely complete tibiotarsi, the extremely short tarsometatarsus and elongated pedal phalanges are similar to the proportions observed in foot-propelled swimmers like *Anas platyrhynchos* and *Phalacrocorax carbo*. Only the ecological preferences of a few crownward euornitheans have been assessed in detail, particularly those of *Gansus* (*You et al., 2006*; *Li et al., 2011*; *Nudds et al., 2013*) and the extremely specialized diving Hesperornithes (*Bell, Wu & Chiappe, 2019*). In the case of *Gansus*, which is recovered in a phylogenetic position just stemward of *Ichthyornis* in the present study, the interpretation of its ecology is complicated by a unique combination of characters, with aspects of its forelimb morphology similar to Apodiformes, but hindlimb proportions reminiscent of aquatic taxa as Podicipedidae or Phalacrocoracidae (*Nudds et al., 2013*). The extremely elongated pes of *Ichthyornis* is similar to that of *Gansus*, but the rest of the hindlimb elements are proportionally much shorter in *Ichthyornis*, particularly

the tarsometatarsus, resulting in a pes that would have been proportionally much larger. Understanding exactly how this hindlimb anatomy would have related to swimming capabilities will require a more in-depth functional investigation, but these observations minimally lend support to the interpretation of *Ichthyornis* as capable foot-propelled swimmer and marine soarer.

Morphological variation in *ichthyornis*

Although eight different species of *Ichthyornis* have been previously named, five of these were synonymized into *I. dispar* by *Clarke (2004)*, while two were split into the separate genera *Guildavis* and *Apatornis*. *Clarke (2004)* found no basis for distinguishing different species within the genus *Ichthyornis*, though recognized a considerable range of size variation and moderate morphological disparity among the YPM *Ichthyornis* specimens. The substantial degree of variation within the YPM sample and the incomplete nature of much of the material made it impossible to rule out the hypothesis of considerable intraspecific variation, thus, there was no firm basis for the separation of *Ichthyornis* into distinct species-level taxa.

Within the YPM collections, only two specimens are smaller than the holotype (YPM 1450), and most of the YPM sample (85.7%) includes specimens substantially larger than the holotype (*Clarke, 2004*). Clarke illustrated a continuous size distribution among the YPM specimens on the basis of humeral and ulnar measurements, illustrating the absence of clearly distinguishable discrete size classes (*Clarke, 2004*). Among the specimens included in the current study that preserve complete humeri, 62.5% represent specimens with a substantially greater humeral length than the *Ichthyornis* holotype (with their humeri being at least 90% or more of the total humeral length of the largest known individual), 25% are of a similar size to the holotype, and only one specimen (MSC 7841) is notably smaller than the holotype (Table 6). One of the new specimens, BHI 6420, preserves what appears to be the longest *Ichthyornis* humerus recorded so far, exceeding the length of the largest previously recorded individual, YPM 9685. Humerus length provides a reasonably, though not exceptionally, accurate proxy for body mass among extant flying birds (*Field et al., 2013*; see Body Mass Estimation section), and the humeral size distributions discussed above are matched by similar size patterns for all of the other long bones examined (see measurements in Supplemental Information).

Fossil remains identified as belonging to *Ichthyornis* have been described from a stratigraphic interval spanning over 10 million years, and *Clarke (2004)* observed size differences apparently related to stratigraphic provenance. The oldest specimens among the YPM material, from the Cenomanian (approximately 95 MYA), seem to have been amongst the largest described, but the younger specimens from the Turonian (approximately 93.9 MYA) and the Coniacian (approximately 89.8 MYA) are substantially smaller, although it is unclear whether these observations reflect an evolutionary anagenetic signal. In contrast, a broad size distribution apparent among specimens deriving from the Santonian (approximately 86.3 MYA) and the Campanian (approximately 83.5 MYA), the interval from which the holotype of *I. dispar*, the majority of the YPM material, and all of the specimens described here derive. Similarly-sized

individuals are found among the specimens deriving from the Santonian Smoky Hill Member of the Niobrara Formation and the Campanian Mooreville Formation, and both very large (BHI 6420, KUVP 2281, NHMUK A905, MSC 5932) and very small (KUVP 2284, MSC 7841) specimens are known from both localities. See the Body Mass Estimation section above for detailed information on the size distribution of the specimens described here.

As discussed above, most of the new specimens described in this work were referred to *Ichthyornis* based on the presence of nine unambiguous diagnostic features previously put forward by *Clarke (2004)*, although we observe a previously unappreciated amount of variation for a selection of these characters. In cases where diagnostic features were not preserved, our referrals were based on morphological similarity to previously published *Ichthyornis* material (Table 1). Despite some morphological variation within our sample, when several of the most complete specimens (BHI 6420, 6421, FHSM VP-18702, KUVP 2281, KUVP 2284, KUVP 157821, KUVP 25472, KUVP 119673, NHMUK A 905 and ALMNH:Paleo:3316) were included as distinct operational taxonomic units in our phylogenetic analyses, they all formed a clade with the *I. dispar* holotype, YPM 1450, supported by strong node support values across alternative optimality criteria (see Phylogenetic Analysis section). All specimens formed a polytomy within this clade, and no consistent internal relationships were recovered among the different specimens included in the analyses. On the basis of these analyses, we considered it appropriate to refer all of these specimens to *I. dispar*.

As detailed above, the morphology of the acromion process of the scapula—one of the autapomorphies of *I. dispar* suggested by *Clarke (2004)*—shows a greater degree of variation among the new specimens than had previously been observed in *Ichthyornis*, with only KUVP 2281 and KUVP 119673 exhibiting the extremely diminutive and pointed acromion supposedly diagnostic for *I. dispar*. In contrast, several specimens show differing morphologies that do not seem to be related to taphonomic distortion, such as a longer hooked process in FHSM VP-18702 (Fig. 14A), a larger and more globose acromion on BHI 6420 and the right scapula of NHMUK A 905, and an essentially absent, undeveloped acromion on the left scapula of NHMUK A 905 (Fig. 14C). The oval scar described by *Clarke (2004)* as present on the distal radius of *I. dispar* is visible in FHSM VP-18702, and KUVP 25472 (Fig. 20A), very faint in KUVP 157821 and BHI 6420 (Fig. 20E) and it is conspicuously absent in KUVP 119673 (Fig. 20B), despite the excellent preservation of this specimen. *Clarke (2004)* discussed variability in the position and development of this character that might be related to size, with the scar apparently being fainter in smaller individuals. However, this does not seem to hold true among the new specimens evaluated here, particularly for BHI 6420, which appears to be among the largest *Ichthyornis* individuals recorded. Lastly, the presence of an internal index process—another possible autapomorphy of *I. dispar*—is observable in all the specimens preserving the first phalanx of the major manual digit, even when broken (as in MSC 6201), with the clear exception of KUVP 2284, in which this process is undeveloped (Fig. 23B; discussed above). We consider it most likely that the unusual morphology of KUVP 2284 is related to its small size and probable early ontogenetic stage, as this feature is absent in early ontogenetic stages of

some extant marine birds such as *Macronectes giganteus*. Alternatively, the complete lack of an internal index process might point towards KUVP 2284 belonging to another species closely related to *I. dispar*.

Beyond this variability in the diagnostic characters of *Ichthyornis dispar*, the specimens included in this study show additional morphological variation. Excluding variability that might be attributed to preservational factors, such as the curvature of the humeral shaft or the orientation of the deltopectoral crest, two of the elements exhibiting the most striking differences among individuals are the synsacrum and the carpometacarpus. As discussed in the description, the four preserved synsacra show an apparent pattern of vertebral fusion similar to that of certain extant bird groups, which might point towards these specimens representing different ontogenetic stages. However, this does not seem to correlate well with size, with smaller specimens like ALMNH:Paleo:3316 showing a greater degree of fusion and a larger number of postacetabular sacral vertebrae than the larger KUVP 119673, and a comparable degree of fusion to that of the much larger KUVP 157821 (Figs. 8B–8D). Additionally, some individuals of similar size, such as FHSM VP-18702 and KUVP 119673, exhibit differing degrees of synsacral fusion. A comparable pattern in which larger specimens were noted to exhibit morphology consistent with a relatively early ontogenetic stage was previously noted by *Clarke (2004)*, with reference to the axis of YPM 1775, the mandible of YPM 1735, and the ulna of YPM 1740. The extent to which this mismatch between size and apparent levels of ontogenetic maturity reflects intraspecific or interspecific variation is challenging to assess at present, but recalls similar patterns observed in other groups of fossil and extant archosaurs (*Bailleul et al., 2016*; *Griffin et al., 2021*), and patchy stratigraphic sampling precludes our ability to evaluate any potential anagenetic patterns. Notable variation in adult size has been previously inferred to be ancestral to archosaurs, and documented in many stem-birds (*Sander & Klein, 2005*; *Hone, Farke & Wedel, 2016*; *Griffin & Nesbitt, 2016*; *Carr, 2020*; *Chapelle, Botha & Choiniere, 2021*). Whether *Ichthyornis* exhibited comparable variability in adult size is difficult to establish, but this interpretation provides a possible explanation for the considerable variation in size and morphology we observe, despite the near-crown position of *Ichthyornis* and its similar growth patterns to extant birds (*Chinsamy, Martin & Dobson, 1998*).

As discussed above, the basis for recognizing both *Apatornis* and *Guildavis* as distinct from *Ichthyornis* rests solely on sacral morphology, as no other skeletal remains are associated with those taxa *Clarke (2004)*. The new specimens, which despite their differing synsacral anatomy are otherwise diagnosable as *I. dispar* on the basis of additional skeletal material, raise the distinct possibility that both *Guildavis* and *Apatornis* might fall within the range of variation of *Ichthyornis*. The validity of *Apatornis* and *Guildavis* may therefore necessitate future reevaluation.

The morphology of the carpometacarpus is generally consistent among the new specimens, with the exception of that of FHSM VP-18702, which exhibits a markedly smaller carpometacarpus than that seen in similarly sized individuals such as BHI 6420 (Figs. 22B and 22C). A similar observation was reported by *Clarke (2004)* for a single

individual, YPM 1755, which exhibits a shorter carpometacarpus than other specimens of similar size.

Of all the specimens included in this study, KUVP 2284 is the most morphologically distinct, exhibiting an intriguing number of differences with respect to the other individuals. In addition to the absence of an internal index process as noted above, the glenoid facet of KUVP 2284 lies further towards the omal end of the coracoid with respect to the scapular cotyle than in any other specimen, with the position of the sternal end of the glenoid omal to that of the scapular cotyle (Fig. 13E). Although the coracoid of KUVP 2284 is small and relatively poorly preserved, this feature does not seem to be related to taphonomic distortion of the element, and is not present on the even smaller coracoid of MSC 7841 (Fig. 13F). KUVP 2284 also shows a proportionally short humerus; indeed, it is the only specimen in which the humerus is shorter than the ulna (Tables 6 and 7). The humerus tends to be particularly elongated in soaring marine birds, and although its proportional length varies during ontogeny, its longitudinal growth seems to stop by the time of fledgling (*Watanabe, 2017*, *2018*). However, a similar condition has been observed in the stemward euornithean *Archaeorhynchus*, in which at least one early-stage juvenile specimen shows an ulna that is shorter than the humerus, with it being subequal or longer in other later stage subadult and adult specimens (*Foth et al., 2021*). The radial carpal of KUVP 2284 is poorly preserved, but its morphology differs from that of other specimens as well, with a practically straight ventral ramus showing very little curvature (Fig. 21B). The intriguing suite of morphological differences exhibited by KUVP 2284, which is otherwise similar to other *Ichthyornis* specimens, might be related to its relatively small size (it is the second-smallest of the new specimens). However, at present it is unclear whether these differences might be related to a relatively early ontogenetic stage (with KUVP 2284 representing a rare juvenile individual), or whether they might be related to further intraspecific or interspecific variation. Unfortunately, with the exception of the coracoid of MSC 7841, other specimens of comparably small size are too fragmentary to evaluate whether they show a similar morphology to that of KUVP 2284.

The level of morphological variability within the *Ichthyornis* specimens described here is moderate overall, and most individuals exhibit congruent morphologies. For all of the features noted to exhibit some degree of variation, such variation was only observed in single specimens, complicating the study of broader patterns of variation within *Ichthyornis*. Neither the variable features noted here nor those identified by *Clarke (2004)* appear to exhibit any correlation with temporal or geographic provenance, and size differences appear to be the major factor influencing morphological variability in most cases, other than in the synsacrum. As a consequence, it is not currently possible to establish whether any of these morphological differences reflect interspecific variation, and we follow *Clarke (2004)* in considering that there is no basis for the establishment of distinct *Ichthyornis* species at present. The use of quantitative techniques such as geometric morphometrics has previously been used to evaluate the degree of intraspecific variation in fossil species, and to discern between the variability caused by taphonomic factors and that related to plausible intra- and interspecific biological variability (*Hedrick et al., 2019*;

Lefebvre et al., 2020). Such an approach might be applicable in future studies in order to evaluate potential patterns of interspecific and intraspecific variation in *Ichthyornis*.

Phylogenetic position

As discussed above, despite the presence of several morphological differences among the new *Ichthyornis* specimens, all of them were recovered very close to the *Ichthyornis* holotype YPM 1450 in phylogenetic analyses that treated the new specimens as distinct operational taxonomic units. In these analyses, the synapomorphies supporting an *Ichthyornis* clade corresponded to the features previously highlighted as diagnostic for *Ichthyornis* by *Clarke (2004)*. These included features like amphicoelous cervical vertebrae, the shape of the distal ulna, and the presence of an internal index process on the II:1 manual phalanx or the unique prezygapophyses of the caudal vertebreae, but also include several features of the skull and lower jaws, the presence of crossed coracoid sulci in the sternum, a furcula bearing an hypocleideum and with pointed omal tips, the hooked acrocoracoid process, the elongated scapula, the shape of the humeral deltopectoral crest and the short femoral trochanteric crest (see Supplemental Information for the complete list of synapomorphies).

All of our phylogenetic analyses recovered a similar topology for the crownward portion of the tree, regardless of the dataset or method used (see Figs. 30 and 31 for the main results from Bayesian and Parsimony analyses, and Supplemental Information for additional results). In all cases, *Ichthyornis* was recovered in a position stemward of Hesperornithes, a position previously inferred on the basis of iterations of the *Wang et al. (2020c)* dataset (*O'Connor, Chiappe & Bell, 2011*, *O'Connor et al., 2020*; *Wang et al., 2017*, *2019*; *Atterholt, Hutchison & O'Connor, 2018*; *Field et al., 2018b*), but never previously recovered from analyses using previous versions of the *Torres, Norell & Clarke (2021)* dataset, which have always recovered *Ichthyornis* closer to the avian crown group (*Chiappe, 2002*; *Clarke, 2004*; *You et al., 2006*; *Huang et al., 2016*; *Torres, Norell & Clarke, 2021*). Notably, two recent iterations of the Wang et al. dataset recovered *Ichthyornis* crownward to Hesperornithes (*Wang et al., 2020c*) or in a polytomy with Hesperornithes and the crown bird group (*Wang et al., 2021*). The more crownward position of Hesperornithes recovered in our analyses appears to be well supported by several synapomorphies absent in *Ichthyornis*, including completely heterocoelous cervical and thoracic vertebrae, pneumatic foramina piercing the centra of the mid-cranial cervicals, the narrow shape of the sternal rostrum, non-tapering tibiotarsal condyles, and several skull and lower jaw characters previously discussed by *Field et al. (2018b)*.

Notably, *Iaceornis* is also recovered crownward to both *Ichthyornis* and Hesperornithes in analyses employing the updated *Torres, Norell & Clarke (2021)* dataset (Fig. 30), despite its remarkable morphological similarity to *Ichthyornis* (*Marsh, 1880*; *Clarke, 2004*). None of the synapomorphies recovered for the Hesperornithes + *Iaceornis* + crown group clade are preserved in *Iaceornis*, from which no cranial or axial material are yet known. Only two synapomorphies are shared between *Iaceornis* and the crown group: the presence of raised intermuscular ridges in the sternum and the development of an ossified supratendinal bridge on the distal tibiotarsus. The crownward position of *Iaceornis* in relation to both

Hesperornithes and *Ichthyornis* highlights the need for a more detailed characterization of its morphology in future work.

The monophyly of Ornithurae (see clade definitions) is well supported by several apomorphies. These include the presence of costal facets on the sternum, clear caudal or caudolateral sternal processes instead of closed fenestrae and lack of a xiphoid process, an ulnar carpal with well-developed dorsal and ventral rami, a relatively elongate extensor process of the carpometacarpus and an intermetacarpal process present as a scar, the presence of a flexor process on the III:1 manual phalanx, the presence of a renal fossa on the postacetabular illium, subparallel pubes and ischia, an ischium less than 1/3 of the pubis length, pubes compressed mediolaterally and not contacting distally, and the presence of two proximal vascular foramina on the tarsometatarsus. Several of these morphological features were previously recovered as synapomorphies of Neornithes, particularly those related to the shape of the sternum and the pelvis (*Clarke, 2004*; *Huang et al., 2016*; *Wang et al., 2017*, *2019*). These structures were previously poorly preserved in *Ichthyornis*, and mostly absent in Hesperornithes due to their extremely derived and specialized anatomy (*Bell & Chiappe, 2016*, *2020*). The presence of these features in *Ichthyornis* therefore pushes the inferred origin of these features to the ancestral lineage subtending Ornithurae.

The topology of the stemward portion of euornithean phylogeny is less stable between alternative analyses using both datasets, although major clades such as Hongshanornithidae are mostly consistently recovered. Notably, the recently defined clade Yanornithidae is not recovered using the Wang et al. dataset despite being supported in recent iterations of this matrix (*Wang et al., 2020c*, *2021*), and instead Songlingornithidae, including *Yixianornis* and *Songlingornis* is recovered. *Iteravis*, traditionally found crownward of these taxa, is recovered as part of Songlingornithidae for the first time in our Bayesian analyses using the *Wang et al. (2020c)* dataset, although the posterior probabilities supporting this clade are low. Despite its exclusion from these analyses due to its unstable position, the inclusion of *Apsaravis* has a notable impact on the tree topologies we recover regardless of the dataset used (see Supplemental Information). When included, *Apsaravis* is recovered in a variable position amongst stemward euornitheans by parsimony analyses (Trees S1, S5, S7, S9 and S13), often forming a clade with Hongshanornithidae (Trees S1 and S9). By contrast, Bayesian inference analyses recover *Apsaravis* very close to crown birds, either slightly stemward of *Ichthyornis* (Trees S7 and S15) or in a polytomy with *Ichthyornis* and more crownward avialans (Trees S3 and S11), due to an unusual combination of character states (*Clarke & Norell, 2002*). We suggest that this taxon is in need of a detailed reinvestigation in order to further understand its unusual morphology, especially in light of its remarkable state of preservation.

The possible stem galloanseran *Asteriornis* was recovered as a potential stem palaeognath by the parsimony phylogenetic analysis of *Torres, Norell & Clarke (2021)*, contrasting with the total-clade galloanseran affinities originally inferred for this taxon (*Field et al., 2020a*). Using the updated version of *Torres, Norell & Clarke (2021)* dataset, we recover *Asteriornis* in the previously reported stem palaeognath position under parsimony (Fig. 30B), but we recover it as a crown anseriform under Bayesian inference

(Fig. 30A), closer to its original interpretation (Field et al., 2020a). However, we urge caution in interpreting these results, since the construction of the Torres, Norell & Clarke (2021) dataset is mainly aimed at reconstructing phylogenetic relationships among non-crown avialans, and the sample of crown birds included in that dataset is very limited.

Although the study of enantiornithine phylogenetic relationships is beyond the scope of this study, it is worth highlighting the extremely variable position of *Falcatakely*, which was originally recovered as an enantiornithine by O'Connor et al. (2020) in a Bayesian analysis using a previous iteration of the Wang et al. (2020c) dataset. Our analyses recover an identical position under Bayesian inference (Fig. 31A), but when our dataset is analyzed under parsimony, *Falcatakely* is recovered as a non-ornithothoracean avialan, just crownward of *Archaeopteryx* (Fig. 31B). Obviously, more complete skeletal material will be necessary to fully resolve the phylogenetic position of this intriguing Maastrichtian taxon (Field, 2020).

CONCLUSION

This study has reevaluated the postcranial morphology of the crownward avialan *Ichthyornis* on the basis of 40 new fossil specimens, making it among the most substantial additions to our knowledge of non-neornithine avialan postcranial morphology. Much of the new material is exceptionally well-preserved, including multiple elements preserved in three-dimensions and illustrating previously unknown impressions of soft tissue attachments. We hope the novel observations and data provided here will help facilitate future insights into the functional morphology of this key near-crown avialan, and a deeper understanding of the functional and anatomical origins of the crown bird skeleton.

Our work has illustrated a substantial range of morphological variation within *Ichthyornis*, including probable evidence of ontogenetic variation. Virtually every element of the postcranial skeleton of *Ichthyornis* is represented among the new specimens, providing an unprecedentedly detailed look into the three-dimensional skeletal morphology of a near-crown avialan. Indeed, the new material illustrates that much of the *Ichthyornis* postcranium falls within the range of anatomical variation of crown birds, and indicates that several features previously considered unique to the bird crown group, such as a cranially deflected deltopectoral crest or the presence of a developed hypotarsus, were present in *Ichthyornis*.

The new material described here should help resolve ongoing uncertainty regarding the relative phylogenetic placement of *Ichthyornis*, Hesperornithes, and Neornithes, with important implications for the crownward-most portion of avialan phylogeny. We illustrate that, irrespective of the phylogenetic dataset used, *Ichthyornis* resolves in a position stemward to Hesperornithes, and our results emphasize the unresolved phylogenetic positions of taxa such as *Apsaravis* and the importance of reevaluating obscure crownward avialans like *Iaceornis*. Additionally, we provide phylogenetic definitions for several key avialan subclades, and hope that these help facilitate unambiguous discourse as future work continues to resolve the systematics of Cretaceous avialans.

In light of this work, as well as previous monographic descriptions by *Clarke (2004)* and *Marsh (1880)*, *Ichthyornis* inarguably ranks among the most completely known fossil avialans of any age. We hope that the new anatomical and phylogenetic information provided for *Ichthyornis* in the present work provides a useful substrate for continued progress on investigations into the biology of the crownward-most portion of the avian stem group.

ACKNOWLEDGEMENTS

We thank L. Rieppel and J. Secord for discussions on the historical significance of *Ichthyornis*, M. Wills for helpful guidance, D. Ehret, J. Ebersole, M. Lowe, D. Brinkman, and V. Rhue for collections assistance, M. Fox, J. Maisano, M. Colbert, and K. Smithson for assistance with CT scanning, J. Watanabe for discussions on skeletal ontogeny, and K. Super for the discovery and donation of FHSM VP-18702. We thank A. Maltese for photographs of recently discovered comparative material. We thank as well R. Olivé for his Mesozoic avialan illustrations. We are indebted to K. van Grouw for assistance with the three-dimensional skeletal reconstruction of *Ichthyornis* and for her stunning skeletal illustration. We also thank H. Hu and C. Torres for helpful reviews that considerably improved this work.

INSTITUTIONAL ABBREVIATIONS

The following abbreviations denote the museum collections where the specimens mentioned in this article are accessioned.

ALMNH	Vertebrate Paleontology Collection, Alabama Museum of Natural History, University of Alabama, Tuscaloosa, AL, USA
BHI	Black Hills Institute of Geological Research, Hill City, SD, USA
FHSM	Sternberg Museum of Natural History, Fort Hays State University, Hays, KS, USA
KUVP	Vertebrate Paleontology Division, University of Kansas Biodiversity Institute & Natural History Museum, Lawrence, KS, USA
NHMUK	National History Museum, London, UK
MSC	McWane Science Center, Birmingham, AL, USA
UMZC	University of Cambridge Museum of Zoology, Cambridge, UK
YPM	Yale Peabody Museum, Yale University, New Haven, NY, USA

Funding

Juan Benito received support from the Palaeontographical Society Richard Owen Research fund, from a Cambridge Philosophical Society Research Studentship, and from the University of Bath University Research Studenshipt Award. Daniel J Field received support from the UKRI Future Leaders Fellowship MR/S032177/1. The funders had no role in study design, data collection and analysis, decision to publish, or preparation of the manuscript.

Grant Disclosures

The following grant information was disclosed by the authors:
Cambridge Philosophical Society Research Studentship.
University of Bath University Research Studenshipt Award.
UKRI Future Leaders Fellowship: MR/S032177/1.

Competing Interests

The authors declare that they have no competing interests.

Author Contributions

- Juan Benito conceived and designed the experiments, performed the experiments, analyzed the data, prepared figures and/or tables, authored or reviewed drafts of the article, and approved the final draft.
- Albert Chen conceived and designed the experiments, analyzed the data, authored or reviewed drafts of the article, and approved the final draft.
- Laura E. Wilson conceived and designed the experiments, authored or reviewed drafts of the article, contributed material, and approved the final draft.
- Bhart-Anjan S. Bhullar conceived and designed the experiments, authored or reviewed drafts of the article, contributed material, and approved the final draft.
- David Burnham conceived and designed the experiments, authored or reviewed drafts of the article, contributed material, and approved the final draft.
- Daniel J. Field conceived and designed the experiments, performed the experiments, analyzed the data, prepared figures and/or tables, authored or reviewed drafts of the article, and approved the final draft.

Data Availability

Phylogenetic datasets in NEXUS and TNT formats are available in the Supplemental Files.

3D surface mesh models of all studied specimens are uploaded to the online repository Morphosource, under Project 'Ichthyornis Postcranial Anatomy' (Project ID: I000405009). DOI links to all the uploaded data (including all osteological elements from all the described specimens) are provided below.

Supplemental Information

Supplemental information for this article can be found online at http://dx.doi.org/10.7717/peerj.13919#supplemental-information.

REFERENCES

Agnolin FL. 2010. An avian coracoid from the Upper Cretaceous of Patagonia, 417 Argentina. *Studia Geologica Salmanticensia* **46**:99–119.

Atterholt J, Hutchison JH, O'Connor JK. 2018. The most complete enantiornithine from North America and a phylogenetic analysis of the Avisauridae. *PeerJ* **6**:e5910 DOI 10.7717/peerj.5910.

Bailleul AM, O'Connor J, Zhang S, Li Z, Wang Q, Lamanna MC, Zhu X, Zhou Z. 2019. An Early Cretaceous enantiornithine (Aves) preserving an unlaid egg and probable medullary bone. *Nature Communications* **10(1)**:1275 DOI 10.1038/s41467-019-09259-x.

Bailleul AM, Scannella JB, Horner JR, Evans DC. 2016. Fusion patterns in the skulls of modern archosaurs reveal that sutures are ambiguous maturity indicators for the Dinosauria. *PLOS ONE* **11(2)**:e0147687 DOI 10.1371/journal.pone.0147687.

Baumel JJ, Raikow RJ. 1993. Arthrologia. In: Baumel JJ, King AS, Breazile JE, Evans HE, Vanden Berge JC, eds. *Handbook of Avian Anatomy: Nomina Anatomica Avium.* Vol. 23. Second edition. Cambridge: Publications of the Nuttall Ornithological Club, 133–188.

Baumel JJ, Witmer LM. 1993. Osteologia. In: Baumel JJ, King AS, Breazile JE, Evans HE, Vanden Berge JC, eds. *Handbook of Avian Anatomy: Nomina Anatomica Avium.* Vol. 23. Second edition. Cambridge: Publications of the Nuttall Ornithological Club, 45–132.

Bell A, Chiappe LM. 2015. Identification of a new hesperornithiform from the Cretaceous Niobrara Chalk and implications for ecologic diversity among early diving birds. *PLOS ONE* **10(11)**:e0141690 DOI 10.1371/journal.pone.0141690.

Bell A, Chiappe LM. 2016. A species-level phylogeny of the Cretaceous Hesperornithiformes (Aves: Ornithuromorpha): implications for body size evolution amongst the earliest diving birds. *Journal of Systematic Palaeontology* **14(3)**:239–251 DOI 10.1080/14772019.2015.1036141.

Bell A, Chiappe LM. 2020. Anatomy of *Parahesperornis*: evolutionary mosaicism in the Cretaceous Hesperornithiformes (Aves). *Life* **10(5)**:62 DOI 10.3390/life10050062.

Bell A, Chiappe LM. 2022. The Hesperornithiformes: A review of the diversity, distribution, and ecology of the earliest diving birds. *Diversity* **14(4)**:p.267 DOI 10.3390/d14040267.

Bell AK, Chiappe LM, Erickson GM, Suzuki S, Watabe M, Barsbold R, Tsogtbaatar K. 2010. Description and ecologic analysis of *Hollanda luceria*, a Late Cretaceous bird from the Gobi Desert (Mongolia). *Cretaceous Research* **31(1)**:16–26 DOI 10.1016/j.cretres.2009.09.001.

Bell A, Everhart MJ. 2011. Remains of small ornithurine birds from a Late Cretaceous (Cenomanian) microsite in Russell County, North-Central Kansas. *Transactions of the Kansas Academy of Science* **114**:115–123 DOI 10.1660/062.114.0111.

Bell AK, Wu Y-H, Chiappe LM. 2019. Morphometric comparison of the Hesperornithiformes and modern diving birds. *Palaeogeography, Palaeoclimatology, Palaeoecology* **513(11)**:196–207 DOI 10.1016/j.palaeo.2017.12.010.

Benito J, Kuo PC, Widrig KE, Jagt JWM, Field DJ. 2022. Cretaceous ornithurine supports a neognathous crown bird ancestor. *Nature* **612(7938)**:100–105 DOI 10.1038/s41586-022-05445-y.

Berger AJ. 1956. Anatomical variation and avian anatomy. *The Condor* **58(6)**:433–441 DOI 10.2307/1365098.

Berv JS, Field DJ. 2018. Genomic signature of an avian Lilliput effect across the K-Pg extinction. *Systematic Biology* **67(1)**:1–13 DOI 10.1093/sysbio/syx064.

Bono RK, Clarke JA, Tarduno JA, Brinkman D. 2016. A large ornithurine bird (*Tingmiatornis arctica*) from the turonian high arctic: climatic and evolutionary implications. *Scientific Reports* **6(1)**:38876 DOI 10.1038/srep38876.

Botelho JF, Ossa-Fuentes L, Soto-Acuña S, Smith-Paredes D, Nuñez-León D, Salinas-Saavedra M, Ruiz-Flores M, Vargas AO. 2014. New developmental evidence clarifies the evolution of wrist bones in the dinosaur-bird transition. *PLOS Biology* **12(9)**:e1001957 DOI 10.1371/journal.pbio.1001957.

Brocklehurst N, Field DJ. 2021. Macroevolutionary dynamics of dentition in Mesozoic birds reveal no long-term selection towards tooth loss. *iScience* **24(3)**:102243 DOI 10.1016/j.isci.2021.102243.

Brocklehurst N, Upchurch P, Mannion PD, O'Connor J. 2012. The completeness of the fossil record of Mesozoic birds: implications for early avian evolution. *PLOS ONE* **7(6)**:e39056 DOI 10.1371/journal.pone.0039056.

Brodkorb P. 1967. Catalogue of fossil birds: part 3 (Ralliformes, Ichthyornithiformes, Charadriiformes). *Bulletin of the Florida State Museum (Biological Sciences)* **11**:99–220.

Buffetaut E, Angst D. 2019. A femur of the Late Cretaceous giant bird *Gargantuavis* from Cruzy (southern France) and its systematic implications. *Palaeovertebrata* **42(1)**:e3 DOI 10.18563/pv.42.1.e3.

Bui HN, Larsson HC. 2021. Development and evolution of regionalization within the avian axial column. *Zoological Journal of the Linnean Society* **191(1)**:302–321 DOI 10.1093/zoolinnean/zlaa038.

Burkhardt F. 2021. *The correspondence of Charles Darwin.* Vol. 28. Cambridge: Cambridge University Press.

Carr TD. 2020. A high-resolution growth series of Tyrannosaurus rex obtained from multiple lines of evidence. *PeerJ* **8(12)**:e9192 DOI 10.7717/peerj.9192.

Carvalho IDS, Agnolin FL, Rozadilla S, Novas FE, Andrade JA, Xavier-Neto J. 2021. A new ornithuromorph bird from the Lower Cretaceous of South America. *Journal of Vertebrate Paleontology* **41(4)**:e1988623 DOI 10.1080/02724634.2021.1988623.

Cau A. 2018. The assembly of the avian body plan: a 160-million-year long process. *Bollettino della Società Paleontologica Italiana* **57**:1–25 DOI 10.4435/BSPI.2018.01.

Cau A, Brougham T, Naish D. 2015. The phylogenetic affinities of the bizarre Late Cretaceous Romanian theropod *Balaur bondoc* (Dinosauria, Maniraptora): dromaeosaurid or flightless bird? *PeerJ* **3(II)**:e1032 DOI 10.7717/peerj.1032.

Cellinese N, Dell C. 2020. RegNum—The international clade names repository. *Available at* https://www.phyloregnum.org (accessed 27 November 2020).

Chapelle KEJ, Botha J, Choiniere JN. 2021. Extreme growth plasticity in the early branching sauropodomorph Massospondylus carinatus. *Biology Letters* **17(5)**:20200843 DOI 10.1098/rsbl.2020.0843.

Chatterjee S. 1989. The oldest Antarctic bird. *Journal of Vertebrate Paleontology* **9(3)**:16A.

Chatterjee S. 2000. The morphology and systematics of *Polarornis*, a Cretaceous loon (Aves: Gaviidae) from Antarctica. In: *Proceedings of the 5th Symposium of the Society of Avian Paleontology and Evolution*, Vol. 1. Beijing125–155.

Chiappe LM. 1991. Cretaceous avian remains from Patagonia shed new light on the early radiation of birds. *Alcheringa* **15(4)**:333–338 DOI 10.1080/03115519108619028.

Chiappe LM. 1996. Late Cretaceous birds of southern South America: anatomy and systematics of Enantiornithes and *Patagopteryx deferrariisi*. *Münchner Geowissenschaftliche Abhandlungen* **30(A)**:203–244.

Chiappe LM. 2001. Phylogenetic relationships among basal birds. In: Gauthier JA, Gall LF, eds. *New Perspectives on the Origin and Early Evolution of Birds: Proceedings of the International Symposium in Honor of John H. Ostrom.* New Haven, CT: Yale Peabody Museum of Natural History, 125–139.

Chiappe LM. 2002. Osteology of the flightless *Patagopteryx deferrariisi* from the Late Cretaceous of Patagonia (Argentina). In: Chiappe LM, Witmer LM, eds. *Mesozoic Birds: Above the Heads of Dinosaurs*. Berkeley: University of California Press, 281–316.

Chiappe LM, Bell A. 2020. Mesozoic birds. *eLS* **1(1)**:549–557 DOI 10.1002/9780470015902.a0029218.

Chiappe LM, Ji SA, Ji Q, Norell MA. 1999. Anatomy and systematics of the Confuciusornithidae (Theropoda, Aves) from the late Mesozoic of northeastern China. *Bulletin of the American Museum of Natural History* **242**:1–89 DOI 10.1642/0004-8038(2000)117[0836:AASOTC]2.0.CO;2.

Chiappe LM, Shu'An J, Qiang JI. 2007. Juvenile birds from the Early Cretaceous of China: implications for enantiornithine ontogeny. *American Museum Novitates* **2007(3594)**:1–46 DOI 10.1206/0003-0082(2007)3594[1:JBFTEC]2.0.CO;2.

Chiappe LM, Zhao B, O'Connor JK, Chunling G, Wang X, Habib M, Marugan-Lobon J, Meng Q, Cheng X. 2014. A new specimen of the Early Cretaceous bird *Hongshanornis longicresta*: insights into the aerodynamics and diet of a basal ornithuromorph. *PeerJ* **2**:e234 DOI 10.7717/peerj.234.

Chinsamy A, Martin LD, Dobson P. 1998. Bone microstructure of the diving *Hesperornis* and the volant *Ichthyornis* from the Niobrara Chalk of western Kansas. *Cretaceous Research* **19(2)**:225–235 DOI 10.1006/cres.1997.0102.

Clarke JA. 2004. Morphology, phylogenetic taxonomy, and systematics of *Ichthyornis* and *Apatornis* (Avialae: Ornithurae). *Bulletin of the American Museum of Natural History* **286**:1–179 DOI 10.1206/0003-0090(2004)286<0001:MPTASO>2.0.CO;2.

Clarke JA, Chatterjee S, Li Z, Riede T, Agnolin F, Goller F, Isasi MP, Martinioni DR, Mussel FJ, Novas FE. 2016. Fossil evidence of the avian vocal organ from the Mesozoic. *Nature* **538(7626)**:502–505 DOI 10.1038/nature19852.

Clarke JA, Chiappe LM. 2001. A new carinate bird from the late Cretaceous of Patagonia (Argentina). *American Museum Novitates* **3323**:1–23 DOI 10.1206/0003-0082(2001)323<0001:ANCBFT>2.0.CO;2.

Clarke JA, Mindell DP, de Queiroz K, Hanson M, Norell MA, Gauthier JA. 2020. Aves. In: de Queiroz K, Cantino PD, Gauthier JA, eds. *Phylonyms: A Companion to the PhyloCode*. Boca Raton, FL: CRC Press, 1247–1253.

Clarke JA, Norell MA. 2002. The morphology and phylogenetic position of *Apsaravis ukhaana* from the Late Cretaceous of Mongolia. *American Museum Novitates* **2002(3387)**:1–46 DOI 10.1206/0003-0082(2002)387<0001:TMAPPO>2.0.CO;2.

Clarke JA, Tambussi CP, Noriega JI, Erickson GM, Ketcham RA. 2005. Definitive fossil evidence for the extant avian radiation in the Cretaceous. *Nature* **433(7023)**:305–308 DOI 10.1038/nature03150.

Clarke JA, Zhou Z, Zhang F. 2006. Insight into the evolution of avian flight from a new clade of Early Cretaceous ornithurines from China and the morphology of *Yixianornis grabaui*. *Journal of Anatomy* **208(3)**:287–308 DOI 10.1111/j.1469-7580.2006.00534.x.

Clifton GT, Carr JA, Biewener AA. 2018. Comparative hindlimb myology of foot-propelled swimming birds. *Journal of Anatomy* **232(1)**:105–123 DOI 10.1111/joa.12710.

Codd JR. 2010. Uncinate processes in birds: morphology, physiology and function. *Comparative Biochemistry and Physiology Part A: Molecular & Integrative Physiology* **156(3)**:303–308 DOI 10.1016/j.cbpa.2009.12.005.

Cordes-Person A, Acosta Hospitaleche C, Case J, Martin J. 2020. An enigmatic bird from the lower Maastrichtian of Vega Island, Antarctica. *Cretaceous Research* **108**:104314 DOI 10.1016/j.cretres.2019.104314.

Cracraft J. 1988. The major clades of birds. In: Benton MJ, ed. *The Phylogeny and Classification of the Tetrapods. Amphibians, Reptiles, Birds.* Vol. 1. Oxford, UK, Oxford: Clarendon Press, 339–361.

Cullen TM, Zanno L, Larson DW, Todd E, Currie PJ, Evans DC. 2021. Anatomical, morphometric, and stratigraphic analyses of theropod biodiversity in the Upper Cretaceous (Campanian) Dinosaur Park Formation. *Canadian Journal of Earth Sciences* **58(2)**:1–15 DOI 10.1139/cjes-2020-0145.

de Queiroz K, Cantino PD. 2020. *International code of phylogenetic nomenclature (PhyloCode).* Boca Raton, FL: CRC Press. *Available at http://phylonames.org/code/* (accessed 27 November 2020).

Dementjev GP. 1940. *Handbook on zoology.* Vol. 6. Moscow: USSR Academy of Sciences.

Demuth OE, Benito J, Tschopp E, Lautenschlager S, Mallison H, Heeb N, Field DJ. 2022. Topology-based three-dimensional reconstruction of delicate skeletal fossil remains and the quantification of their taphonomic deformation. *Frontiers in Ecology and Evolution* **10**:828006 DOI 10.3389/fevo.2022.828006.

Dumont M, Tafforeau P, Bertin T, Bhullar B-A, Field DJ, Schulp A, Strilisky B, Thivichon-Prince B, Viriot L, Louchart A. 2016. Synchrotron imaging of dentition provides insights into the biology of *Hesperornis* and *Ichthyornis*, the last toothed birds. *BMC Evolutionary Biology* **16(1)**:178 DOI 10.1186/s12862-016-0753-6.

Dyke GJ, Dortangs RW, Jagt JWM, Mulder EW, Schulp AS, Chiappe LM. 2002. Europe's last Mesozoic bird. *Naturwissenschaften* **89(9)**:408–411 DOI 10.1007/s00114-002-0352-9.

Elzanowski A, Paul GS, Stidham TA. 2000. An avian quadrate from the late cretaceous lance formation of wyoming. *Journal of Vertebrate Paleontology* **20**:712–719 DOI 10.1671/0272-4634(2000)020[0712:AAQFTL]2.0.CO;2.

Ericson PGP. 1997. Systematic relationships of the Paleogene family Presbyornithidae (Aves: Anseriformes). *Zoological Journal of the Linnaean Society* **121**:429–483 DOI 10.1111/J.1096-3642.1997.TB01286.X.

Field DJ. 2020. The changing face of birds from the age of the dinosaurs. *Nature* **588(7837)**:221–222 DOI 10.1038/d41586-020-03260-x.

Field DJ, Benito J, Chen A, Jagt JWM, Ksepka DT. 2020a. Late Cretaceous neornithine from Europe illuminates the origins of crown birds. *Nature* **579(7799)**:397–401 DOI 10.1038/s41586-020-2096-0.

Field DJ, Bercovici A, Berv JS, Dunn R, Fastovsky DE, Lyson TR, Vajda V, Gauthier JA. 2018a. Early evolution of modern birds structured by global forest collapse at the end-Cretaceous mass extinction. *Current Biology* **28(11)**:1825–1831 DOI 10.1016/j.cub.2018.04.062.

Field DJ, Berv JS, Hsiang AY, Lanfear R, Landis MJ, Dornburg A. 2020b. Timing the extant avian radiation: the rise of modern birds, and the importance of modeling molecular rate variation. In: Pittman M, Xing X, eds. *Pennaraptoran Theropod Dinosaurs: Past Progress and New Frontiers.* Vol. 440. New York: Bulletin of the American Museum of Natural History, 159–181.

Field DJ, Hanson M, Burnham D, Wilson LE, Super K, Ehret D, Ebersole JA, Bhullar B-A. 2018b. Complete Ichthyornis skull illuminates mosaic assembly of the avian head. *Nature* **557**:96–100 DOI 10.1038/s41586-018-0053-y.

Field DJ, Lynner C, Brown C, Darroch SAF. 2013. Skeletal correlates for body mass estimation in modern and fossil flying birds. *PLOS ONE* **8(11)**:e82000 DOI 10.1371/journal.pone.0082000.

Forster CA, Chiappe LM, Krause DW, Sampson SD. 2002. Vorona berivotrensis, a primitive bird from the Late Cretaceous of Madagascar. In: Chiappe LM, Witmer LM, eds. *Mesozoic Birds: Above the Heads of Dinosaurs.* Berkeley: University of California Press, 268–280.

Foth C, Tischlinger H, Rauhut OWM. 2014. New specimen of *Archaeopteryx* provides insights into the evolution of pennaceous feathers. *Nature* **511(7507)**:79–82 DOI 10.1038/nature13467.

Foth C, Wang S, Spindler F, Lin Y, Yang R. 2021. A juvenile specimen of Archaeorhynchus sheds new light on the ontogeny of basal euornithines. *Frontiers in Earth Science* **9**:604520 DOI 10.3389/feart.2021.604520.

Fox RC. 1984. *Ichthyornis* (Aves) from the early Turonian (Late Cretaceous) of Alberta. *Canadian Journal of Earth Sciences* **21(2)**:258–260 DOI 10.1139/e84-026.

Gadow H. 1892. On the classification of birds. *Proceedings of the Zoological Society of London* **60**:229–256.

Gauthier JA. 1986. Saurischian monophyly and the origin of birds. *Memoirs of the California Academy of Sciences* **8**:1–55.

Gauthier JA, de Queiroz K. 2001. Feathered dinosaurs, flying dinosaurs, crown dinosaurs, and the name Aves. In: Gauthier JA, Gall LF, eds. *New Perspectives on the Origin and Early Evolution of Birds: Proceedings of the International Symposium in Honor of John H. Ostrom.* New Haven, CT: Yale Peabody Museum of Natural History, 7–41.

Ghetie V. 1976. *Anatomical atlas of domestic birds.* Bucarest: Editura Academiei Republicii Socialiste Romania.

Gingerich PD. 1972. A new partial mandible of *Ichthyornis*. *The Condor* **74(4)**:471–473 DOI 10.2307/1365900.

Godefroit P, Cau A, Hu D-Y, Escuillié F, Wu W, Dyke G. 2013. A Jurassic avialan dinosaur from China resolves the early phylogenetic history of birds. *Nature* **498(7454)**:359–362 DOI 10.1038/nature12168.

Goloboff PA, Catalano SA. 2016. TNT version 1.5, including a full implementation of phylogenetic morphometrics. *Cladistics* **32(3)**:221–238 DOI 10.1111/cla.12160.

Griffin CT, Nesbitt SJ. 2016. Anomalously high variation in postnatal development is ancestral for dinosaurs but lost in birds. *Proceedings of the National Academy of Sciences of the United States of America* **113(51)**:14757–14762 DOI 10.1073/pnas.1613813113.

Griffin CT, Stocker MR, Colleary C, Stefanic CM, Lessner EJ, Riegler M, Formoso K, Koeller K, Nesbitt SJ. 2021. Assessing ontogenetic maturity in extinct saurian reptiles. *Biological Reviews* **96(2)**:470–525 DOI 10.1111/brv.12666.

Habib M. 2010. The structural mechanics and evolution of aquaflying birds. *Biological Journal of the Linnean Society* **99(4)**:687–698 DOI 10.1111/j.1095-8312.2010.01372.x.

Haeckel E. 1866. *Generelle Morphologie der Organismen: allgemeine Grundzüge der organischen Formen-Wissenschaft mechanisch begründet durch die von Charles Darwin reformierte Deskendenz-Theorie.* Berlin: G. Reimer.

Harrison CJO. 1973. The humerus of Ichthyornis as a taxonomically isolated character. *Bulletin of the British Ornithological Club* **93**:123–126.

Hartman S, Mortimer M, Wahl WR, Lomax DR, Lippincott J, Lovelace DM. 2019. A new paravian dinosaur from the Late Jurassic of North America supports a late acquisition of avian flight. *PeerJ* **7(2)**:e7247 DOI 10.7717/peerj.7247.

Hedrick BP, Schachner ER, Rivera G, Dodson P, Pierce SE. 2019. The effects of skeletal asymmetry on interpreting biologic variation and taphonomy in the fossil record. *Paleobiology* **45(1)**:154–166 DOI 10.1017/pab.2018.42.

Hendrickx C, Hartman SA, Mateus O. 2015. An overview of non-avian theropod discoveries and classification. *PalArch's Journal of Vertebrate Palaeontology* **12**:1–73.

Hieronymus TL. 2015. Qualitative skeletal correlates of wing shape in extant birds (Aves: Neoaves). *BMC Evolutionary Biology* **15(1)**:1–12 DOI 10.1186/s12862-015-0303-7.

Hieronymus TL. 2016. Flight feather attachment in rock pigeons (*Columba livia*): covert feathers and smooth muscle coordinate a morphing wing. *Journal of Anatomy* **229(5)**:631–656 DOI 10.1111/joa.12511.

Hiraga T, Sakamoto H, Nishikawa S, Muneuchi I, Ueda H, Inoue M, Shimura R, Uebayashi A, Yasuda N, Momose K, Masatomi H. 2014. Vertebral formula in red-crowned crane (*Grus japonensis*) and hooded crane (*Grus monacha*). *Journal of Veterinary Medical Science* **76(4)**:503–508 DOI 10.1292/jvms.13-0295.

Hone DW, Farke AA, Wedel M. 2016. Ontogeny and the fossil record: what, if anything, is an adult dinosaur? *Biology Letters* **12(2)**:20150947 DOI 10.1098/rsbl.2015.0947.

Hope S, Chiappe LM, Witmer LM. 2002. The mesozoic radiation of neornithes. In: Chiappe LM, Witmer LM, eds. *Mesozoic Birds: Above the Heads of Dinosaurs*. Berkeley: University of California Press, 339–388.

Houde PW. 1988. *Palaeognathous birds from the early Tertiary of the Northern Hemisphere.* Vol. 22. Cambridge: Publications of the Nuttall Ornithological Club, 1–148.

Houde P, Olson SL. 1992. A radiation of coly-like birds from the Eocene of North America (Aves: Sandcoleiformes new order). In: Campbell KE, ed. *Papers in Avian Paleontology Honoring Pierce Brodkorb, Natural History Museum of Los Angeles County, Science Series*, Vol. 36. 137–160 1992.

Hu H, O'Connor JK, McDonald PG, Wroe S. 2020. Cranial osteology of the Early Cretaceous *Sapeornis chaoyangensis* (Aves: Pygostylia). *Cretaceous Research* **113**:104496 DOI 10.1016/j.cretres.2020.104496.

Huang J, Wang X, Hu Y, Liu J, Peteya JA, Clarke JA. 2016. A new ornithurine from the Early Cretaceous of China sheds light on the evolution of early ecological and cranial diversity in birds. *PeerJ* **4(1)**:e1765 DOI 10.7717/peerj.1765.

Hudson GE, Lanzillotti PJ. 1964. Muscles of the pectoral limb in galliform birds. *American Midland Naturalist* **71(1)**:1–13 DOI 10.2307/2422689.

Hudson GE, Hoff KM, Berge JV, Trivette EC. 1969. A numerical study of the wings and leg muscles of Lari and Alcae. *The Ibis* **111(4)**:459–524 DOI 10.1111/j.1474-919X.1969.tb02565.x.

Hudson GE, Shreiweis DO, Wang SYC. 1972. A numerical study of the wing and leg muscles of tinamous (Tinamidae). *Northwest Science* **46**:207–255.

Hutchinson JR. 2002. The evolution of hindlimb tendons and muscles on the line to crown-group birds. *Comparative Biochemistry and Physiology—Part A: Molecular & Integrative Physiology* **133(4)**:1051–1086 DOI 10.1016/S1095-6433(02)00158-7.

Jarvis ED, Mirarab S, Aberer AJ, Li B, Houde P, Li C, Ho SYW, Faircloth BC, Nabholz B, Howard JT, Suh A, Weber CC, da Fonseca RR, Li J, Zhang F, Li H, Zhou L, Narula N, Liu L, Ganapathy G, Boussau B, Bayzid MS, Zavidovych V, Subramanian S, Gabaldón T, Capella-Gutiérrez S, Huerta-Cepas J, Rekepalli B, Munch K, Schierup M, Lindow B, Warren WC, Ray D, Green RE, Bruford MW, Zhan X, Dixon A, Li S, Li N, Huang Y, Derryberry EP, Bertelsen MF, Sheldon FH, Brumfield RT, Mello CV, Lovell PV, Wirthlin M, Schneider MPC, Prosdocimi F, Samaniego Jé A, Velazquez AMV, Alfaro-Núñez A, Campos PF, Petersen B, Sicheritz-Ponten T, Pas A, Bailey T, Scofield P, Bunce M,

Lambert DM, Zhou Q, Perelman P, Driskell AC, Shapiro B, Xiong Z, Zeng Y, Liu S, Li Z, Liu B, Wu K, Xiao J, Yinqi X, Zheng Q, Zhang Y, Yang H, Wang J, Smeds L, Rheindt FE, Braun M, Fjeldsa J, Orlando L, Barker FK, Jønsson KA, Johnson W, Koepfli K-P, O'Brien S, Haussler D, Ryder OA, Rahbek C, Willerslev E, Graves GR, Glenn TC, McCormack J, Burt D, Ellegren H, Alström P, Edwards SV, Stamatakis A, Mindell DP, Cracraft J, Braun EL, Warnow T, Jun W, Gilbert MTP, Zhang G. 2014. Whole-genome analyses resolve early branches in the tree of life of modern birds. *Science* **346(6215)**:1320–1331 DOI 10.1126/science.1253451.

Karoullas C, Nudds RL. 2021. The link between avian brachial index, flight capability and the neornithine evolutionary radiation. *Journal of Morphology* **282(11)**:1698–1707 DOI 10.1002/jmor.21414.

Knoll F, Chiappe LM, Sanchez S, Garwood RJ, Edwards NP, Wogelius RA, Sellers WI, Manning PL, Ortega F, Serrano FJ, Marugán-Lobón J. 2018. A diminutive perinate European Enantiornithes reveals an asynchronous ossification pattern in early birds. *Nature Communications* **9(1)**:1–9 DOI 10.1038/s41467-018-03295-9.

Kurochkin EN. 1985. A true carinate bird from Lower Cretaceous deposits in Mongolia and other evidence of Early Cretaceous birds in Asia. *Cretaceous Research* **6(3)**:271–278 DOI 10.1016/0195-6671(85)90050-3.

Lefebvre R, Allain R, Houssaye A, Cornette R. 2020. Disentangling biological variability and taphonomy: shape analysis of the limb long bones of the sauropodomorph dinosaur *Plateosaurus*. *PeerJ* **8(1)**:e9359 DOI 10.7717/peerj.9359.

Lewis PO. 2001. A likelihood approach to estimating phylogeny from discrete morphological character data. *Systematic Biology* **50(6)**:913–925 DOI 10.1080/106351501753462876.

Li Y, Zhang Y-G, Zhou Z-H, Li Z-H, Liu D, Wang X-L. 2011. New material of *Gansus* and a discussion on its habit. *Vertebrata Palasiatica* **49(4)**:435–445.

Li Z, Zhou Z, Wang M, Clarke JA. 2014. A new specimen of large-bodied basal enantior-nithine *Bohaiornis* from the Early Cretaceous of China and the inference of feeding ecology in Mesozoic birds. *Journal of Paleontology* **88**:99–108 DOI 10.1666/13-052.

Linnaeus C. 1758. *Caroli Linnæi […] Systema Naturæ per Regna Tria Naturæ, Secundum Classes, Ordines, Genera, Species, cum Characteribus, Differentiis, Synonymis, Locis*. Stockholm: Laurentius Salvius.

Liu D, Chiappe LM, Zhang Y, Bell A, Meng Q, Ji Q, Wang X. 2014. An advanced, new long-legged bird from the Early Cretaceous of the Jehol Group (northeastern China): insights into the temporal divergence of modern birds. *Zootaxa* **3884(3)**:253–266 DOI 10.11646/zootaxa.3884.3.4.

Livezey BC, Zusi RL. 2006. Higher-order phylogeny of modern birds (Theropoda, Aves: Neornithes) based on comparative anatomy: I. – Methods and characters. *Bulletin of the Carnegie Museum of Natural History* **37**:1–556 DOI 10.2992/0145-9058(2006)37[1:PON]2.0.CO;2.

Livezey BC, Zusi RL. 2007. Higher-order phylogeny of modern birds (Theropoda, Aves: Neornithes) based on comparative anatomy. II. Analysis and discussion. *Zoological Journal of the Linnean Society* **149(1)**:1–95 DOI 10.1111/j.1096-3642.2006.00293.x.

Longrich N. 2009. An ornithurine-dominated avifauna from the Belly River Group (Campanian, Upper Cretaceous) of Alberta, Canada. *Cretaceous Research* **30(1)**:161–177 DOI 10.1016/j.cretres.2008.06.007.

Longrich NR, Field DJ. 2012. Torosaurus is not Triceratops: ontogeny in chasmosaurine ceratopsids as a case study in dinosaur taxonomy. *PLOS ONE* 7(2):e32623 DOI 10.1371/journal.pone.0032623.

Longrich NR, Tokaryk T, Field DJ. 2011. Mass extinction of birds at the Cretaceous-Paleogene (K-Pg) boundary. *Proceedings of the National Academy of Sciences of the United States of America* **108(37)**:15253–15257 DOI 10.1073/pnas.1110395108.

Lucas SG, Sullivan RM. 1982. *Ichthyornis* in the Late Cretaceous Mancos Shale (Juana Lopez Member), northwestern New Mexico. *Journal of Paleontology* **56(2)**:545–557.

Marsh OC. 1872a. Notice of a new and remarkable fossil bird. *American Journal of Science* **4(61)**:344–380 DOI 10.1080/00222937308696770.

Marsh OC. 1872b. Description of *Hesperornis regalis*, with notices of four other new species of Cretaceous birds. *American Journal of Science* **3(57)**:359–365 DOI 10.1080/00222937208696680.

Marsh OC. 1873a. Notice of a new species of *Ichthyornis. American Journal of Science* **3(5)**:74.

Marsh OC. 1873b. On a new subclass of fossil birds (Odontornithes). *American Journal of Science* **3(5)**:161–162 DOI 10.1080/00222937308696804.

Marsh OC. 1876. Notice of new Odontornithes. *American Journal of Science* **3(11)**:509–511 DOI 10.2475/AJS.S3-11.66.509.

Marsh OC. 1880. *Odontornithes: a monograph on the extinct toothed birds of North America.* Washington, DC: U.S. Government Printing Office.

Martin LD. 1983. The origin and early radiation of birds. In: Brush AH, Clark GA Jr, eds. *Perspectives in Ornithology: Essays Presented for the Centennial of the American Ornithologists' Union.* Cambridge: Cambridge University Press, 291–338.

Martin LD. 1987. The beginning of the modern avian radiation. *Travaux et Documents des Laboratoires de Géologie de Lyon* **99(1)**:9–19.

Martin LD, Stewart JD. 1977. Teeth in *Ichthyornis* (Class: Aves). *Science* **195(4284)**:1331–1332 DOI 10.1126/science.195.4284.1331.

Maryańska T, Osmólska H, Wolsan M. 2002. Avialan status for Oviraptorosauria. *Acta Palaeontologica Polonica* **47**:97–116.

Matthew WD, Brown B. 1922. The family Deinodontidae, with notice of a new genus from the Cretaceous of Alberta. *Bulletin of the American Museum of Natural History* **46**:367–385.

Mayr G. 2014. Comparative morphology of the radial carpal bone of neornithine birds and the phylogenetic significance of character variation. *Zoomorphology* **133(4)**:425–434 DOI 10.1007/s00435-014-0236-5.

Mayr G. 2016. Variations in the hypotarsus morphology of birds and their evolutionary significance. *Acta Zoologica* **97(2)**:196–210 DOI 10.1111/azo.12117.

Mayr G. 2017a. *Avian evolution: the fossil record of birds and its paleobiological signifcance.* Chichester: Wiley-Blackwell.

Mayr G. 2017b. Evolution of avian breeding strategies and its relation to the habitat preferences of Mesozoic birds. *Evolutionary Ecology* **31(1)**:131–141 DOI 10.1007/s10682-016-9872-1.

Mayr G. 2021. On the occurrence of lateral openings and fossae (pleurocoels) in the thoracic vertebrae of neornithine birds and their functional significance. *Vertebrate Zoology* **71**:453–463 DOI 10.3897/vz.71.e71268.

Mayr G, Clarke J. 2003. The deep divergences of neornithine birds: a phylogenetic analysis of morphological characters. *Cladistics* **6**:527–553 DOI 10.1111/j.1096-0031.2003.tb00387.x.

Miller MA, Pfeiffer W, Schwartz T. 2010. Creating the CIPRES Science Gateway for inference of large phylogenetic trees. In: *Gateway Computing Environments Workshop (GCE 2010).* 45–53.

Mohesn A, Hirayama R, Abdel Gawad M, Sileem A, Aly M. 2020. New record of Testudines and Aves from Bahariya Formation (Cenomanian), Bahariya Depression, Egypt. In: *Society of Vertebrate Paleontology Annual Meeting 2020.*

Mohr SR, Acorn JH, Funston GF, Currie PJ. 2021. An ornithurine bird coracoid from the Late Cretaceous of Alberta, Canada. *Canadian Journal of Earth Sciences* **58(2)**:134–140 DOI 10.1139/cjes-2019-0202.

Musser G, Clarke JA. 2020. An exceptionally preserved specimen from the green river formation elucidates complex phenotypic evolution in gruiformes and charadriiformes. *Frontiers in Ecology and Evolution* **8**:326 DOI 10.3389/fevo.2020.559929.

Necker R. 2006. Specializations in the lumbosacral vertebral canal and spinal cord of birds: evidence of a function as a sense organ which is involved in the control of walking. *Journal of Comparative Physiology A* **192(5)**:439–448 DOI 10.1007/s00359-006-0105-x.

Nesbitt SJ, Turner AH, Spaulding M, Conrad JL, Norell MA. 2009. The theropod furcula. *Journal of Morphology* **270(7)**:56–79 DOI 10.1002/jmor.10724.

Nesbitt SJ, Clarke JA. 2016. The anatomy and taxonomy of the exquisitely preserved Green River formation (early Eocene) Lithornithids (Aves) and the relationships of Lithornithidae. *Bulletin of the American Museum of Natural History* **2016(406)**:1–91 DOI 10.1206/0003-0090-406.1.1.

Nessov LA. 1992. Mesozoic and Paleogene birds of the USSR and their paleoenvironments. *Natural History Museum of Los Angeles County, Science Series* **36**:465–478.

Nudds RL, Atterholt J, Wang X, You H-L, Dyke GJ. 2013. Locomotory abilities and habitat of the Cretaceous bird *Gansus yumenensis* inferred from limb length proportions. *Journal of Evolutionary Biology* **26(1)**:150–154 DOI 10.1111/jeb.12036.

Nudds RL, Dyke GK, Rayner JMV. 2006. Avian brachial index and wing kinematics: putting movement back into bones. *Journal of Zoology* **272(2007)**:218–226 DOI 10.1111/j.1469-7998.2006.00261.x.

Olson SL. 1975. *Ichthyornis* in the Cretaceous of Alabama. *The Wilson Bulletin* **87(1)**:103–105.

Osborn HF. 1924. Three new Theropoda, *Protoceratops* zone, central Mongolia. *American Museum Novitates* **144**:1–12.

O'Connor PM. 2006. Postcranial pneumaticity: an evaluation of soft-tissue influences on the postcranial skeleton and the reconstruction of pulmonary anatomy in archosaurs. *Journal of Morphology* **267(10)**:1199–1226 DOI 10.1002/jmor.10470.

O'Connor JK. 2019. The trophic habits of early birds. *Palaeogeography, palaeoclimatology, palaeoecology* **513**:178–195 DOI 10.1016/j.palaeo.2018.03.006.

O'Connor JK, Chiappe LM, Bell A. 2011. Pre-modern birds: avian divergences in the Mesozoic. In: Dyke G, Kaiser G, eds. *Living Dinosaurs: The Evolutionary History of Modern Birds.* Chichester: Wiley-Blackwell, 39–114.

O'Connor PM, Forster CA. 2010. A Late Cretaceous (Maastrichtian) avifauna from the Maevarano Formation, Madagascar. *Journal of Vertebrate Paleontology* **30(4)**:1178–1201 DOI 10.1080/02724634.2010.483544.

O'Connor JK, Gao KQ, Chiappe LM. 2010. A new ornithuromorph (Aves: Ornithothoraces) bird from the Jehol Group indicative of higher-level diversity. *Journal of Vertebrate Paleontology* **30(2)**:311–321 DOI 10.1080/02724631003617498.

O'Connor PM, Turner AH, Groenke JR, Felice RN, Rogers RR, Krause DW, Rahantarisoa LJ. 2020. Late Cretaceous bird from Madagascar reveals unique development of beaks. *Nature* **588(7837)**:272–276 DOI 10.1038/s41586-020-2945-x.

O'Connor JK, Wang M, Hu H. 2016. A new ornithuromorph (Aves) with an elongate rostrum from the Jehol Biota, and the early evolution of rostralization in birds. *Journal of Systematic Palaeontology* **14(11)**:939–948 DOI 10.1080/14772019.2015.1129518.

O'Connor JK, Wang M, Zhou S, Zhou Z. 2015. Osteohistology of the Lower Cretaceous Yixian Formation ornithuromorph (Aves) *Iteravis huchzermeyeri*. *Palaeontologia Electronica* **18**:35 DOI 10.26879/520.

O'Connor JK, Zelenkov NV. 2013. The phylogenetic position of *Ambiortus*: comparison with other Mesozoic birds from Asia. *Paleontological Journal* **47(11)**:1270–1281 DOI 10.1134/S0031030113110063.

O'Connor JK, Zhou Z. 2013. A redescription of *Chaoyangia beishanensis* (Aves) and a comprehensive phylogeny of Mesozoic birds. *Journal of Systematic Palaeontology* **11(7)**:889–906 DOI 10.1080/14772019.2012.690455.

O'Connor JK, Zhou Z. 2015. Early evolution of the biological bird: perspectives from new fossil discoveries in China. *Journal of Ornithology* **156(1)**:333–342 DOI 10.1007/s10336-015-1222-5.

O'Connor JK, Zhou Z. 2020. The evolution of the modern avian digestive system: insights from paravian fossils from the Yanliao and Jehol biotas. *Palaeontology* **63(1)**:13–27 DOI 10.1111/pala.12453.

Padian K. 2004. Basal Avialae. In: Weishampel DB, Dodson P, Osmólska H, eds. *The Dinosauria*. Second Edition. Berkeley, US: University of California Press, 210–231.

Parris DC, Echols J. 1992. The fossil bird Ichthyornis in the Cretaceous of Texas. *Texas Journal of Science* **44(2)**:201–212.

Pei R, Pittman M, Goloboff PA, Dececchi TA, Habib MB, Kaye TG, Larsson HCE, Norell NA, Brusatte SL, Xu X. 2020. Potential for powered flight neared by most close avialan relatives, but few crossed its thresholds. *Current Biology* **30(20)**:4033–4046 DOI 10.1016/j.cub.2020.06.105.

Pittman M, Heers AM, Serrano FJ, Field DJ, Habib MB, Dececchi TA, Kaye TG, Larsson HCE. 2020c. Methods of studying early theropod flight. In: Pittman M, Xu X, eds. *Pennaraptoran Theropod Dinosaurs: Past Progress and New Frontiers.* Vol. 440. New York: Bulletin of the American Museum of Natural History, 277–294.

Pittman M, O'Connor JK, Field DJ, Turner AH, Ma W, Makovicky P, Xu X. 2020a. Pennaraptoran systematics. In: Pittman M, Xu X, eds. *Pennaraptoran Theropod Dinosaurs: Past Progress and New Frontiers.* Vol. 440. New York: Bulletin of the American Museum of Natural History, 7–36.

Pittman M, O'Connor JK, Tse E, Makovicky P, Field DJ, Ma W, Turner AH, Norell MA, Pei R, Xu X. 2020b. The fossil record of Mesozoic and Paleocene pennaraptorans. In: Pittman M, Xu X, eds. *Pennaraptoran Theropod Dinosaurs: Past Progress and New Frontiers.* Vol. 440. New York: Bulletin of the American Museum of Natural History, 37–95.

Porras-Múzquiz HG, Chatterjee S, Lehman TM. 2014. The carinate bird *Ichthyornis* from the Upper Cretaceous of Mexico. *Cretaceous Research* **51**:148–152 DOI 10.1016/j.cretres.2014.05.018.

Prum RO, Berv JS, Dornburg A, Field DJ, Townsend JP, Lemmon EM, Lemmon AR. 2015. A comprehensive phylogeny of birds (Aves) using targeted next-generation DNA sequencing. *Nature* **526(7574)**:569–573 DOI 10.1038/nature15697.

Raikow RJ. 1970. Evolution of diving adaptations in the stifftail ducks. *University of California Publications in Zoology* **94**:1–52.

Raikow RJ. 1985. Locomotor system. In: King AS, McLelland J, eds. *Form and Function in Birds*. Vol. 3. London, UK: Academic Press, 57–147.
Rieppel L. 2019. *Assembling the dinosaur: fossil hunters, tycoons, and the making of a spectacle.* Cambridge, London: Harvard University Press.

Ronquist F, Teslenko M, Van Der Mark P, Ayres DL, Darling A, Höhna S, Larget B, Liu L, Suchard MA, Huelsenbeck JP. 2012. MrBayes 3.2: efficient Bayesian phylogenetic inference and model choice across a large model space. *Systematic Biology* **61(3)**:539–542 DOI 10.1093/sysbio/sys029.

Sanchez J. 2010. Late Cretaceous (Cenomanian) Hesperornithiformes from the Pasquia Hills, Saskatchewan, Canada. Doctoral dissertation, Carleton University.

Sander PM, Klein N. 2005. Developmental plasticity in the life history of a prosauropod dinosaur. *Science* **310(5755)**:1800–1802 DOI 10.1126/science.1120125.

Sanz JL, Buscalioni AD. 1992. A new bird from the Early Cretaceous of Las Hoyas, Spain, and the early radiation of birds. *Palaeontology* **35**:829–845.

Senter P. 2006. Scapular orientation in theropods and basal birds, and the origin of flapping flight. *Acta Palaeontologica Polonica* **51**:305–313.

Sereno PC. 1998. A rationale for phylogenetic definitions, with application to the higher-level taxonomy of Dinosauria. *Neues Jahrbuch für Geologie und Paläontologie—Abhandlungen* **210(1)**:41–83 DOI 10.1127/njgpa/210/1998/41.

Sereno PC. 2005. Stem Archosauria—TaxonSearch. *Available at* http://taxonsearch.uchicago.edu/?exe=browse (accessed 27 November 2020).

Serrano FJ, Costa-Pérez M, Navalón G, Martín-Serra A. 2020. Morphological disparity of the humerus in modern birds. *Diversity* **12(5)**:173 DOI 10.3390/d12050173.

Shimada K, Fernandes MV. 2006. *Ichthyornis sp.* (Aves: Ichthyornithiformes) from the lower Turonian (Upper Cretaceous) of western Kansas. *Transactions of the Kansas Academy of Science* **109(1)**:21–26 DOI 10.1660/0022-8443(2006)109[21:ISAIFT]2.0.CO;2.

Shimada TR, Wilson LE. 2016. A new specimen of the Late Cretaceous bird, cf. *Ichthyornis sp.*, from the Cenomanian of central Kansas, with comments on the size distribution of *Ichthyornis* in North America. *Transactions of the Kansas Academy of Science* **119(2)**:231–237 DOI 10.1660/062.119.0215.

Smith-Paredes D, Núñez-León D, Soto-Acuña S, O'Connor JK, Botelho JF, Vargas AO. 2018. Dinosaur ossification centres in embryonic birds uncover developmental evolution of the skull. *Nature Ecology and Evolution* **2(12)**:1966–1973 DOI 10.1038/s41559-018-0713-1.

Stegmann BC. 1963. Der Processus internus indicis im Skelett des Vogelflügels. *Journal für Ornithologie* **104(3–4)**:413–423 DOI 10.1007/BF01671057.

Stegmann BC. 1978. *Relationship of the superorders Alectoromorphae and Charadriomorphae (Aves): a comparative study of the avian hand.* Vol. 17. Cambridge: Publications of the Nuttall Ornithological Club, 1–199.

Stejneger L. 1885. Super-order III—euornithes. In: Kingsley JS, ed. *Natural History of Birds.* Boston: S. E. Cassino and Company, 64.

Tanaka K, Zelenitsky DK, Therrien F. 2015. Eggshell porosity provides insight on evolution of nesting in dinosaurs. *PLOS ONE* **10(11)**:e0142829 DOI 10.1371/journal.pone.0142829.

Tickle PG, Ennos AR, Lennox LE, Perry SF, Codd JR. 2007. Functional significance of the uncinate processes in birds. *Journal of Experimental Biology* **210(22)**:3955–3961 DOI 10.1242/jeb.008953.

Tokaryk TT, Cumbaa SL, Storer JE. 1997. Early Late Cretaceous birds from Saskatchewan, Canada: the oldest diverse avifauna known from North America. *Journal of Vertebrate Paleontology* **17(1)**:172–176 DOI 10.1080/02724634.1997.10010961.

Torres CR, Norell MA, Clarke JA. 2021. Bird neurocranial and body mass evolution across the end-Cretaceous mass extinction: the avian brain shape left other dinosaurs behind. *Science Advances* **7(31)**:eabg7099 DOI 10.1126/sciadv.abg7099.

Turner AH, Makovicky PJ, Norell MA. 2012. A review of dromaeosaurid systematics and paravian phylogeny. *Bulletin of the American Museum of Natural History* **371(3)**:1–206 DOI 10.1206/748.1.

van der Reest AJ, Currie PJ. 2017. Troodontids (Theropoda) from the Dinosaur Park Formation, Alberta, with a description of a unique new taxon: implications for deinonychosaur diversity in North America. *Canadian Journal of Earth Sciences* **54(9)**:919–935 DOI 10.1139/cjes-2017-0031.

Vanden Berge JC, Zweers GA. 1993. Myologia. In: Baumel JJ, King AS, Breazile JE, Evans HE, Vanden Berge JC, eds. *Handbook of Avian Anatomy: Nomina Anatomicaavium.* Vol. 23. Second Edition. Cambridge: Publications of the Nuttall Ornithological Club, 189–247.

Vazquez RJ. 1995. Functional anatomy of the pigeon hand (*Columba livia*): a muscle stimulation study. *Journal of Morphology* **226(1)**:33–45 DOI 10.1002/jmor.1052260104.

Verheyen R. 1955. La systématique des Ansériformes basée sur l'ostéologie comparée. *Bulletin de l'Institut royal des sciences naturelles de Belgique* **31(35)**:1–18.

Wagner GP, Gauthier JA. 1999. 1,2,3 = 2,3,4: a solution to the problem of the homology of the digits in the avian hand. *Proceedings of the National Academy of Sciences of the United States of America* **96(9)**:5111–5116 DOI 10.1073/pnas.96.9.5111.

Walker CA. 1981. New subclass of birds from the Cretaceous of South America. *Nature* **292(5818)**:51–52 DOI 10.1038/292051a0.

Walker CA, Dyke GJ. 2009. Euenantiornithine birds from the Late Cretaceous of El Brete (Argentina). *Irish Journal of Earth Sciences* **27**:15–62 DOI 10.3318/ijes.2010.27.15.

Wang X, Cau A, Kundrát M, Chiappe LM, Ji Q, Wang Y, Li T, Wu W. 2020a. A new advanced ornithuromorph bird from Inner Mongolia documents the northernmost geographic distribution of the Jehol paleornithofauna in China. *Historical Biology* **33(9)**:1705–1717 DOI 10.1080/08912963.2020.1731805.

Wang J, Hao X, Kundrát M, Liu Z, Uesugi K, Jurašeková Z, Guo B, Hoshino M, Li Y, Monfroy Q, Zhou B. 2019. Bone tissue histology of the Early Cretaceous bird *Yanornis*: evidence for a diphyletic origin of modern avian growth strategies within Ornithuromorpha. *Historical Biology* **32(10)**:1422–1434 DOI 10.1080/08912963.2019.1593405.

Wang X, Huang J, Hu Y, Liu X, Peteya J, Clarke JA. 2018. The earliest evidence for a supraorbital salt gland in dinosaurs in new Early Cretaceous ornithurines. *Scientific Reports* **8(1)**:1–12 DOI 10.1038/s41598-018-22412-8.

Wang X, Huang J, Kundrát M, Cau A, Liu X, Wang Y, Ju S. 2020b. A new jeholornithiform exhibits the earliest appearance of the fused sternum and pelvis in the evolution of avialan dinosaurs. *Journal of Asian Earth Sciences* **199(1)**:104401 DOI 10.1016/j.jseaes.2020.104401.

Wang X, Ji Q, Teng F, Jin K. 2013a. A new species of *Yanornis* (Aves: Ornithurae) from the Lower Cretaceous strata of Yixian, Liaoning Province. *Geological Bulletin of China* **32**:601–606.

Wang M, Li Z, Liu Q, Zhou Z. 2020c. Two new Early Cretaceous ornithuromorph birds provide insights into the taxonomy and divergence of Yanornithidae (Aves: Ornithothoraces). *Journal of Systematic Palaeontology* **18(21)**:1805–1827 DOI 10.1080/14772019.2020.1836050.

Wang M, Lloyd GT, Zhang C, Zhou Z. 2021. The patterns and modes of the evolution of disparity in Mesozoic birds. *Proceedings of the Royal Society B* **288(1944)**:20203105 DOI 10.1098/rspb.2020.3105.

Wang YM, O'Connor JK, Li DQ, You HL. 2013b. Previously unrecognized ornithuromorph bird diversity in the Early Cretaceous Changma Basin, Gansu Province, northwestern China. *PLOS ONE* **8(10)**:e77693 DOI 10.1371/journal.pone.0077693.

Wang YM, O'Connor JK, Li DQ, You HL. 2016. New information on postcranial skeleton of the Early Cretaceous *Gansus yumenensis* (Aves: Ornithuromorpha). *Historical Biology* **28(5)**:666–679 DOI 10.1080/08912963.2015.1006217.

Wang M, O'Connor JK, Pan Y, Zhou Z. 2017. A bizarre Early Cretaceous enantiornithine bird with unique crural feathers and an ornithuromorph plough-shaped pygostyle. *Nature Communications* **8(1)**:14141 DOI 10.1038/ncomms14141.

Wang M, O'Connor JK, Zhou S, Zhou Z. 2020d. New toothed Early Cretaceous ornithuromorph bird reveals intraclade diversity in pattern of tooth loss. *Journal of Systematic Palaeontology* **18(8)**:631–645 DOI 10.1080/14772019.2019.1682696.

Wang RF, Wang Y, Hu DY. 2015. Discovery of a new ornithuromorph genus *Juehuaornis* gen. nov. from Lower Cretaceous of western Liaoning, China. *Global Geology* **34(1)**:7–11.

Wang M, Zhou Z. 2020. Anatomy of a new specimen of *Piscivorenantiornis inusitatus* (Aves: Enantiornithes) from the Lower Cretaceous Jehol Biota. *Journal of Vertebrate Paleontology* **40(3)**:e1783278 DOI 10.1080/02724634.2020.1783278.

Wang M, Zhou Z, Zhou S. 2016. A new basal ornithuromorph bird (Aves: Ornithothoraces) from the Early Cretaceous of China with implication for morphology of early Ornithuromorpha. *Zoological Journal of the Linnean Society* **176(1)**:207–223 DOI 10.1111/zoj.12302.

Watanabe J. 2017. Quantitative discrimination of flightlessness in fossil Anatidae from skeletal proportions. *The Auk* **134(3)**:672–695 DOI 10.1642/AUK-17-23.1.

Watanabe J. 2018. Clade-specific evolutionary diversification along ontogenetic major axes in avian limb skeleton. *Evolution* **72(12)**:2632–2652 DOI 10.1111/evo.13627.

Watanabe J, Field DJ, Matsuoka H. 2021. Wing musculature reconstruction in extinct flightless auks (*Pinguinus* and *Mancalla*) reveals incomplete convergence with penguins (Spheniscidae) due to differing ancestral states. *Integrative Organismal Biology* **3(1)**:obaa040 DOI 10.1093/iob/obaa040.

Wetmore A. 1962. Notes on fossil and subfossil birds. *Smithsonian Miscellaneous Collections* **145**:1–17.

Woolfenden GE. 1960. Osteology of the Waterfowl. D. Phil. Thesis, University of Florida.

Xu X, You H, Du K, Han F. 2011. An *Archaeopteryx*-like theropod from China and the origin of Avialae. *Nature* **475(7357)**:465–470 DOI 10.1038/nature10288.

Xu X, Zhou Z, Wang Y, Wang M. 2020. Study on the Jehol Biota: recent advances and future prospects. *Science China Earth Sciences* **63(6)**:757–773 DOI 10.1007/s11430-019-9509-3.

You HL, Lamanna MC, Harris JD, Chiappe LM, O'Connor J, Ji SA, Lü JC, Yuan CX, Li DQ, Zhang X, Lacovara KJ. 2006. A nearly modern amphibious bird from the Early Cretaceous of northwestern China. *Science* **312(5780)**:1640–1643 DOI 10.1126/science.1126377.

Zelenkov NV, Averianov AO, Popov EV. 2017. An *Ichthyornis*-like bird from the earliest Late Cretaceous (Cenomanian) of European Russia. *Cretaceous Research* **75(1)**:94–100 DOI 10.1016/j.cretres.2017.03.011.

Zheng X, O'Connor JK, Huchzermeyer F, Wang X, Wang Y, Zhang X, Zhou Z. 2014. New specimens of *Yanornis* indicate a piscivorous diet and modern alimentary canal. *PLOS ONE* **9(4)**:e95036 DOI 10.1371/journal.pone.0095036.

Zheng X, O'Connor JK, Wang X, Wang Y, Zhou Z. 2018. Reinterpretation of a previously described Jehol bird clarifies early trophic evolution in the Ornithuromorpha. *Proceedings of the Royal Society B: Biological Sciences* **285(1871)**:20172494 DOI 10.1098/rspb.2017.2494.

Zhou Z, Jin F, Zhang J. 1992. Preliminary report on a Mesozoic bird from Liaoning, China. *Chinese Science Bulletin* **37**:1365–1368 DOI 10.1360/sb1992-37-16-1365.

Zhou Z, Li FZZ. 2010. A new Lower Cretaceous bird from China and tooth reduction in early avian evolution. *Proceedings of the Royal Society B: Biological Sciences* **277(1679)**:219–227 DOI 10.1098/rspb.2009.0885.

Zhou S, O'Connor JK, Wang M. 2014. A new species from an ornithuromorph (Aves: Ornithothoraces) dominated locality of the Jehol Biota. *Chinese Science Bulletin* **59(36)**:5366–5378 DOI 10.1007/s11434-014-0669-8.

Zhou Z, Zhang F. 2001. Two new ornithurine birds from the Early Cretaceous of western Liaoning, China. *Chinese Science Bulletin* **46(15)**:1258–1264 DOI 10.1007/BF03184320.

Zhou Z, Zhang F. 2005. Discovery of an ornithurine bird and its implication for Early Cretaceous avian radiation. *Proceedings of the National Academy of Sciences of the United States of America* **102(52)**:18998–19002 DOI 10.1073/pnas.0507106102.

Zhou Z, Zhang F. 2006. A beaked basal ornithurine bird (Aves, Ornithurae) from the Lower Cretaceous of China. *Zoologica Scripta* **35(4)**:363–373 DOI 10.1111/j.1463-6409.2006.00234.x.

Zhou S, Zhou ZH, O'Connor JK. 2012. A new toothless ornithurine bird (*Schizooura lii* gen. et sp. nov.) from the Lower Cretaceous of China. *Vertebrata Palasiatica* **50(1)**:9–24.

Zhou S, Zhou Z, O'Connor JK. 2013. Anatomy of the basal ornithuromorph bird *Archaeorhynchus spathula* from the Early Cretaceous of Liaoning, China. *Journal of Vertebrate Paleontology* **33(1)**:141–152 DOI 10.1080/02724634.2012.714431.

Zinoviev AV. 2011. Notes on the hindlimb myology and syndesmology of the Mesozoic toothed bird Hesperornis regalis (Aves: Hesperornithiformes). *Journal of Systematic Palaeontology* **9(1)**:65–84 DOI 10.1080/14772019.2010.512615.

Zusi RL, Bentz GD. 1978. The appendicular myology of the Labrador Duck (*Camptorhynchus labradorius*). *The Condor* **80(4)**:407–418 DOI 10.2307/1367191.